ProQuest LLC.
789 East Eisenhower Parkway
P.O. Box 1346
Ann Arbor, MI 48106 – 1346

Development and validation of cellular models for studying amyloid precursor protein isoforms

Natruedee Potiwat

A thesis submitted in partial fulfilment of the requirements of
Sheffield Hallam University
for the degree of Doctor of Philosophy

September 2015

Abstract

The development and validation of cellular model for studying amyloid precursor protein isoforms

Amyloid β peptide (Aβ) is the major constituent of neuritic plaques in the brains of patients with Alzheimer's disease (AD). Aβ is a small insoluble 39–43 amino acid peptide derived from the Amyloid Precursor Protein (APP) by proteolytic cleavage. Different gene splicing produces variant isoforms ranging from 365 to 770 amino acids in length. The main three isoforms are: APP695, APP751 and APP770 and all are potentially sources of Aβ.

The project aimed to investigate the hypothesis that one of these APP isoforms (APP695, APP751 and APP770) is more likely to be the source of Aβ in Alzheimer's disease under normal and stress-induced conditions. The clones of HEK293 cells stably expressing human APP695, APP751 and APP770 at comparable levels were put under stress inducing conditions: Serum alteration and energy deprivation.

By altering FBS concentration in culture medium, more APP751 was secreted than APP695 and APP770 at all concentrations of FBS. The serum alteration in culture medium had no significant effect on cell number, secreted APP and APP gene expression. Energy deprivation was achieved using 2-deoxy-D-glucose (2DG). There was a significant reduction in cell number to a similar level for all three clones while the level of secreted APP and APP gene expression increased significantly. Also, the trend of APP secretion from each clone under the same concentration of 2DG was the same: more APP751 was secreted than APP695 and APP770.

In summary, this project has suggested that serum in culture medium has no effect on cell number, APP secretion and APP gene expression between isoforms while energy deprivation using 2DG affected cell number, APP gene expression and APP production significantly. Not only does this confirm the importance of glucose as a source of energy but has also revealed the potential relationship between glucose metabolism and pathogenesis of AD. Ultimately, glucose metabolism could be the predominant factor in relation to Aβ peptide production.

Table of contents

Table of Figures

Personal statement

First of all, I would like to thank **my parents** for their support both mentally and financially, and for allowing me to become who I am today.

Secondly, I would like to thank my Director of studies, **Professor David Parkinson** who gave me the PhD opportunity and for being so patient with me while I was adapting to scientific research from my pharmacy background. Thirdly, I would like to thank my BMRC colleagues for being helpful and sharing their thoughts and suggestions throughout the PhD experience

Fourthly, I would like to thank:

Yu-Su Chen for creating the fun and crazy environment to keep me sane.

Umarat Srisawat for giving me academia and moral support (especially when things were too difficult to explain in English).

Rachel Smith for the sneaky coffee break and moaning session.

Finally, I would like to personally thank **Dr. Malcolm Lock** for being so tolerant and understanding while I was trying to understand molecular biology.

Chapter 1: Introduction

1.1 Alzheimer's disease

Alzheimer's disease (AD) is a major neurodegenerative disease of the elderly. AD accounts for at least 60% of dementia cases which makes AD the most common form of dementia (Causevic et al. 2011; Xu, Ferrari and Wang 2013). AD was fully described in 1906 by German psychiatrist and pathologist, Alois Alzheimer. However, Alzheimer published his finding which became public knowledge in 1907. In his publication, he mentioned the case of a 51 years old female patient, Auguste Deter whom at the time experienced memory loss and disorientation to places and time. Her condition deteriorated rapidly, she became bed-bound and passed away four and a half years after the onset of her condition. At post-mortem examination of Auguste Deter's brain, Alzheimer discovered two major pathological hallmarks of AD: neurofibrillary tangles and amyloid plaques (Small, Klaver and Foa 2010).

1.1.1 Epidemiology

According to a consensus study in 2005 on the prevalence and incidence of dementia, there were 24.3 million people in the world who have dementia and there were 4.5 million new cases per year (Ferri et al. 2005). However, the estimation of the number of people with dementia around the globe was changed to 44.4 million in 2013 and this number was predicted to double every 20 years. It was estimated that there will be 75.6 million people living with dementia in 2030 and 135.5 million in 2050. Among these numbers more than two thirds are associated with AD and almost 62% of the cases live in developing countries such as China and India (Alzheimer's disease international 2014). In addition, there are more than 850,000 people in the UK currently living with dementia (Alzheimer's Society 2015).

The prevalence of AD correlates with age which means the prevalence doubles every 5 years after the age of 65 and the prevalence increases from 3% in 65-74 year old the elderly to 50% in the elderly older than 85. Due to prevalence rates of AD consistently increasing until the age of 85, it has been implied that AD results from the ageing

process (Castellani, Rolston and Smith 2010; Xu, Ferrari and Wang 2013). Moreover, the world population age structure has been undergoing significant changes from high birth and mortality rates to low birth and mortality rates coupled with advances in health care which increases life expectancy. As a consequence, while the total number of population has stopped growing, the ageing population is increasing markedly and there has been sharp increase in the incidence of chronic diseases (Prince, Prina and Guerchet 2013).

As a result of rapid growth of the ageing population, the demand in healthcare and social services has also increased, which has caused significant impacts on national economies. The total worldwide estimated cost of dementia in 2010 was 604 billion US Dollars and 23 billion pounds in the UK alone in 2012 (Alzheimer's Society 2015; Wimo and Prince 2010). It is claimed that the changes in demography and its impact on economies have turned dementia into one of many great challenges for the world (Alzheimer's disease international 2014).

1.1.2 Clinical features

AD affects each individual in different ways however there are some common patterns. The clinical manifestation of AD typically begins with short-term memory loss, disorientation to places and time, cognitive decline including not able to judge or reason, having language difficulties, long-term memory loss and, finally, patients become bed-bound due to motor function activities impairment. At the same time, patients might develop behavioral symptoms such as depression, anti-social behavior, delusions or hallucinations (Forstl and Kurz 1999; Yiannopoulou and Papageorgiou 2013).

There are many possible causes of dementia such as Alzheimer's disease, vascular disease or Parkinson's disease therefore the National Institute of Neurological and Communicative Disorders and Stroke (NINCDS) and the Alzheimer' Disease and Related Disorder Association (ADRDA) has established the criteria for staging the clinical diagnosis of AD to distinguish AD causing dementia from others. These criteria were described in 1984 and it has been known as NINCDS-ADRDA criteria until 2011. In 2011, the NINCDS and ADRDA revised and updated the criteria to take into account and in keeping with advance records and better understanding in clinical manifestation

of AD. The latest criteria can not only be used as criteria for dementia caused by AD but also all possible causes of dementia. Also it includes brain imaging, genetic and biochemical understanding of AD and neuropsychological assessment (Mayeux and Stern 2012; McKhann et al. 2011).

According to the criteria from NINDCA-ADRDA in 2011, the AD dementia is classified into one of three categories: (1) Probable AD dementia, (2) Possible AD dementia and (3) Probable or possible AD with pathological evidence. There are two sub-categories in main criteria for probable AD dementia:

(1) "Probable AD dementia" is used when a patient meets main dementia criteria and has one of the following scenarios: long-onset symptoms, pronounced signs of cognitive function deterioration, demonstration of cognitive deficiency by either amnestic or non-amnestic presentations and absence of medical history containing diseases which might possibly involve dementia AD.

(2) Probable AD dementia couples with document represented reduction in cognitive functions or a causative genetic mutation of AD.

The "possible AD dementia" is classified into either atypical course or etiologically mixed presentations. In order to be diagnosed as atypical course possible AD dementia, a patient has to meet the main criteria set for probable AD dementia but instead of long-onset of cognitive impairment, the patient has fast-onset of impairment. If the patient has a medical history containing causative disease of AD, the patient is classified as etiologically mixed presentation of possible AD dementia. Finally, the probable or possible AD dementia with pathological evidence is currently reserved for research purposes (McKhann et al. 2011).

1.2 Neuropathological hallmarks

The outstanding neuropathological changes in the brain of AD patients are amyloid plaques and neurofibrillary tangles (see Figure 1.2.1) as first described by Alois Alzheimer (Small and Cappai 2006). Also, there are other changes in the brain which are considered to be minor lesions namely cerebral amyloid angiopathy, synaptic deficit and neuronal loss.

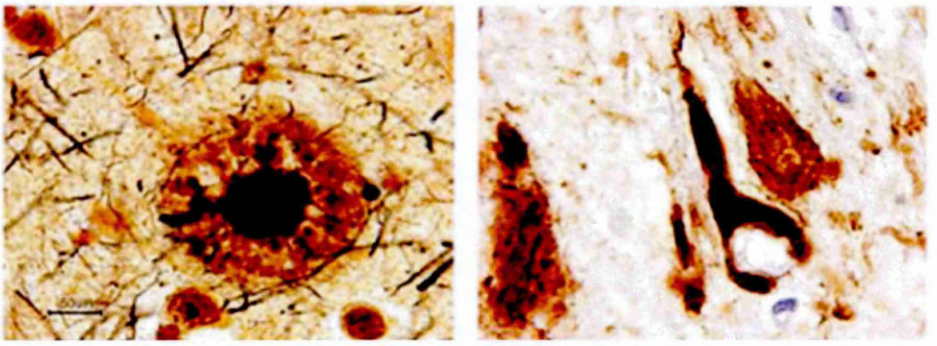

Amyloid plaque Neurofibrillary Tangle

Figure 1.2.1 The main classical pathological hallmarks of Alzheimer's disease; amyloid plaque and neurofibrillary tangle (adapted from Colorado's Dementia News and Resource Center 2014).

1.2.1 Amyloid plaques

Amyloid means a starch-like protein which is deposited in the liver, kidneys, spleen, or other tissues in certain diseases and Plaque means a small, distinct, typically raised patch or region on or within the body resulting from local damage or deposition of material. Therefore amyloid plaque means a deposition of amyloid protein in the organs and tissues in the body. Also, amyloid plaque, which is also known as senile plaque, is one of the major pathological hallmarks of AD (Ng and Chan 1993; Perl 2010). As shown in Figure 1.2.1, amyloid plaques are globular-like complex extracellular structures which vary from 10- 200 μm in diameter. The plaque core consists of 4 kDa protein which is known as Aβ peptide. The amyloid plaques are classified practically into diffuse plaques, neuritic plaques and burnt-out plaques (Castellani, Rolston and Smith 2010; Perl 2010). The types of amyloid plaque are shown in Figure 1.2.2.

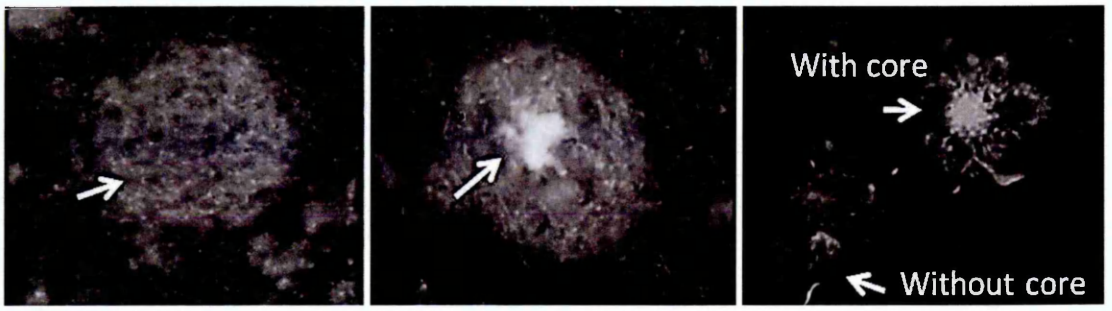

Diffuse plaque Burnt-out plaque Neuritic plaque

Figure 1.2.2 Different types of amyloid plaque; diffuse plaque, burnt-out plaque and neuritic plaque (Murray et al. 2011).

The diffuse plaques are commonly found in the cerebral cortex region of the brain without the presence of dystrophic neurites and it is usually found in the brains of normal aged individuals. It was reported that the number of diffuse plaques corresponded to the severity of cognitive impairment (Perl 2010). Also, diffuse plaques are believed to occur early on in the progression of AD before turning into neuritic plaques and this type of plaque exhibits no correlation to inflammation. The diffuse plaques are highly varied in size with the inversion to the distribution. For example, the smaller diffuse plaques tended to have higher distribution areas. The silver based staining method is routinely used to identify the diffuse plaques (Castellani, Rolston and Smith 2010).

The classical compact form of amyloid plaques is commonly known as a neuritic plaque. The neuritic plaques vary from 10-50 μm in diameter (Castellani, Rolston and Smith 2010). Similarly to other amyloid plaques, the core of neuritic plaques is composed of Aβ peptide. The Aβ peptide in the core of neuritic plaques are arranged in a spiral form and surrounded by dystrophic neurites. Structurally, the neuritic plaques exhibit a dense core, alteration of membrane and paired helical filaments. Also neuritic plaques are positively stained by silver stain procedure (Perl 2010). Unlike diffuse plaques, neuritic plaques showed a great relation to inflammatory process due to the presence of active microglia and astrocyte (Castellani, Rolston and Smith 2010).

The other type of amyloid plaque is called burnt-out plaques. The outstanding feature of this type of plaques is a solely dense core with an absence of dystrophic neurites. It was suggested that the burn-out plaques are the end-stage neuritic plaques.

1.2.2 Neurofibrillary tangles

Apart from amyloid plaques in the brains of patients with Alzheimer's disease, another crucial neuropathological hallmark of AD is neurofibrillary tangles (NFTs) which are often found mainly in the cerebral cortex and large pyramidal neurons of Ammon's horn in the hippocampus (Castellani, Rolston and Smith 2010; Causevic et al. 2011). The NFT is an intracellular aggregation of hyperphosphorylated microtubule-related protein (MAP) tau. NFTs start to develop inside neurons which slowly and eventually fill the intracellular space causing neuronal cell death. However, these dead neuronal cells still maintain their external and internal morphology and they are called ghost tangles (Bhatia and Hall 2013; Yates and McLoughlin 2007). The main component of NFTs is several 80 nm diameter paired helical filament. Although tau protein is the main component of NFTs, there are several other proteins involved in NTFs formation including Aβ peptide and ubiquitin (Yen et al. 1995). Under normal conditions tau plays roles in microtubule structural stabilization and functional maintenance. As microtubules are responsible for neuronal and axonal transportation, therefore tau is indirectly responsible for those functions (Brunden et al. 2010). The proline directed serine-threonine protein kinase and non-proline directed protein kinase are the two main kinases involved in tau phosphorylation. The glycogen synthase kinase (GSK3) and cyclin dependent kinase 5 (cdk5) are the most frequently mentioned proline directed serine-threonine protein kinase and the protein kinase A, B and C are the most common non-proline directed protein kinases. The balance between the phosphorylation and dephosphorylation of tau designates the normal physiological functions of tau. Therefore, the aberrant and unusual phosphorylation of tau results in increased paired helical filaments formation and self-aggregation, indirect disruption of microtubule functions and biological activity impairment including an ability to bind to microtubules, as shown in Figure 1.2.3 (Iqbal et al. 2010; Obulesu, Venu and Somashekhar 2011). Also, it was reported that phosphorylated tau showed higher potential for fibril formation (Brunden et al. 2010). In addition, NFTs can be visualized using silver-based staining procedure (Castellani, Rolston and Smith 2010).

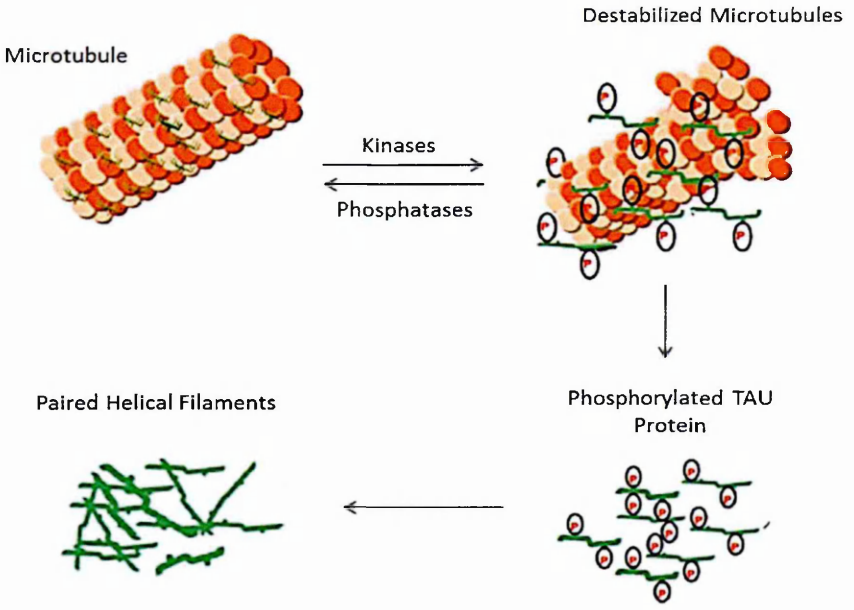

Figure 1.2.3 The relationship between microtubule and tau protein. Under the normal conditions, tau protein stabilises microtubule which facilitates axonal transportation. Once tau protein is phosphorylated, the microtubule is destabilised. The phosphorylated tau proteins start to aggregate and form Paired Helical Filament (PHF) which is the main component of neurofibrillary tangle (NTF) (adapted from de Paula et al. 2009).

The longest form of tau protein could potentially carry up to 80 phosphorylation sites (Kolarova et al. 2012). It was observed that the NFTs in the brain of AD patient contained almost nine phosphates per molecule of protein which is approximately three times higher than the healthy brains of the control subjects (Wang et al. 2013). Also, it was reported that cdk5 and GSK3 phosphorylated of Thr231 and Ser235 were the starting point in paired helical filament formation in AD (Obulesu, Venu and Somashekhar 2011). The work by Eva Braak and co-workers has pioneered the relationship between tau and AD pathogenesis by showing the strong correlation between the clinical manifestation of AD and NFTs lesions (Bhatia and Hall 2013).

Although the development of NFTs found strictly correlated to the severity of cognitive impairment, it is not limited only to AD as it was also found in other neurodegenerative disease including Parkinson's disease, Down's syndrome and Pick's Disease (Castellani, Rolston and Smith 2010; Iqbal et al. 2005).

1.2.3 Cerebral amyloid angiopathy

The Cerebral Amyloid Angiopathy (CAA) was first described by Gustav Oppenheim in 1909. At the time he discovered necrosis in the brain parenchyma and capillary walls at the post-mortem examination of AD patients with clinical manifestations which later established CAA: the complex diversity of biochemical and genetic disorders in the central nervous system (Biffi and Greenberg 2011). The term CAA is also used to describe amyloid deposition in the walls of small and medium sized cerebral blood vessels, especially arteries and arterioles (Ghiso et al. 2010; Resink et al. 2003). Practically, CAA is characterized by a positive staining with Congo-red dye which gave rise to an alternative name of CAA; Congophilic Angiopathy. Like neurofibrillary tangles, the CAA is common among aged-individuals. It is found in both familial and sporadic cases and it is not specific to AD (Attems et al. 2011). However, the researchers paid little to no attention to CAA in the pathogenesis of AD. More recently, CAA is considered to be one of the main contributors to AD pathogenesis (Arvanitakis et al. 2011).

In general, the main component of CAA is the short form of Aβ peptide; Aβ40 and the Aβ40/ Aβ42 ratio obtained from CAA is greater than the one obtained from amyloid plaques (Attems et al. 2011). Although CAA is found in both cerebral blood vessels and brain parenchyma, they can be distinguished by the distribution pattern and the Aβ peptide form. For example, the deposition in the brain parenchyma composes mainly of Aβ42 and the cerebrovascular deposition consists of Aβ40 as the main component (Ghiso et al. 2010). Pathologically, the CAA begins with the small amount of Aβ peptide deposition on the wall of blood vessels in the brain and at this stage the deposition neither blocks vessels lumen nor interferes with its biological functions (Perl 2010). Once the degree of deposition increases to moderate or severe, the blood vessel walls are thickening or thinning and the lumen of the vessels are either bigger or smaller, depending on severity of deposition. For instance, the moderate deposition, the blood vessel wall was thickened and the lumen appears smaller due to the blockage, while the wall was thinned and the lumen appeared bigger in severe deposition (Attems et al. 2011). In brief, the beginning of Aβ deposition causes the thickening of vessel walls which causes the size reduction of vessel lumen, whereas the continuous deposition of Aβ degenerates smooth muscles hence the thinning vessel wall and dilated vessel

lumen (Attems et al. 2011). The histochemistry procedure using Congo-red or Thioflavin S, or the immunhistochemistry procedure using Aβ peptide antibody are required to visualize the CAA (Attems et al. 2011; Perl 2010). In addition, it was reported that around 30% of individuals age over 60 years old have CAA while up to 90% of diagnosed AD patients exhibited CAA.

1.2.4 Synaptic deficits and neuron loss

Neuronal cell death and synaptic loss were found throughout the area where the deposition of amyloid β peptide (Aβ) and neurofibrillary tangles were observed (Yates and McLoughlin 2007). It has been reported that patients with AD showed an exaggeration of Aβ related to intricate neuronal dysfunction. For example, amyloid plaque reduced the strength and plasticity of glutamatergic synaptic transmission (Palop and Mucke 2010). Moreover, the previous study on APP transgenic mice showed that the magnitude of neuronal loss is correlated to the number of amyloid plaques in the brain. (Bayer and Wirths 2010).

Learning and memorising functions require long-term potentiation of transmission (LTP) at synapses which mainly takes place in hippocampal area. In mouse model-Aβ-induced Alzheimer's disease showed an impairment of hippocampal long-term potentiation transmission. The recent study revealed that NMDA receptor is responsible for the loss of an essential protein which is involved in the synaptic process. Under normal conditions, NMDA receptor is responsible for inducing LTP and memory development. Also an increased Aβ level suggested intercellular synaptic loss which corresponded to the severity of cognitive impairment in humans (Malenka and Manilow 2011).

1.3 Amyloid precursor protein

1.3.1 Amyloid precursor protein

The amyloid precursor protein (APP) is a type 1 transmembrane protein comprised of a large extracellular N-terminal domain, a hydrophobic transmembrane domain and a small intracellular C-terminal domain. APP is transported from the endoplasmic

reticulum to the cell surface to be modified either by glycosylations or phosphorylations before being proteolysed by secretase or re-internalised into the endosomal compartment (O'Brien and Wong 2011).

Amyloid precursor protein (APP) expresses in several organs and tissues (Nalivaeva and Turner 2013). Several isoforms of APP ranging from 365 to 770 amino acid remnants result from the alternative splicing within 18 exons of amyloid precursor protein (APP) by secretases, three of which are the most common in Alzheimer's disease; APP695, APP751 and APP770, as shown in Figure 1.3.1. The APP isoforms are distinguished by both expression and structure (Zheng and Koo 2011).

Although the expression level of APP in the brain varies between regions, the expression level of APP695 is significantly higher in comparison to APP751 and APP770. The mRNA ratio between different isoforms of APP is APP695: APP751: APP770 = 20: 10: 1 (Nalivaeva and Turner 2013). Also, the APP695 is mainly expressed in the CNS while the APP751 and APP770 are mainly expressed in non-neuronal tissues. (Cappai 2014; Nalivaeva and Turner 2013; O'Brien and Wong 2011; de Silva et al. 1997).

All three main isoforms of APP contain Aβ domain at exon 16 and 17. Structurally, they are distinguished by the presence and/or the absence of exon encoding a 56-amino acid Kunitz protease inhibitor (KPI domain) and/or exon 8 encoding a 19-amino acid OX2 domain, which shares the similar sequence to thymus-derived lymphoid cells (Belyaev et al. 2010; Preece et al. 2004; de Silva et al. 1997). The APP770 contains both KPI and OX2 domains while the APP751 contains only KPI domain. Both KPI and OX2 domains are absence in APP695 (Zhang et al. 2012). The KPI domain has been suggested to play role in blood coagulation and wound repair based on the highly expressed of APP751 and APP770 in platelets (Dawkins and Small 2014). Also, the KPI domain has been suggested to play role in dimerization and processing of APP (Khalifa et al. 2012). The OX2 domain has been suggested to play role in cell-surface binding and recognition since it contains immunoglobulin loops which are commonly found in cell surface receptor (Dawkins and Small 2014).

APP is a member of a family of related proteins including amyloid precursor-like proteins 1 and 2 (APLP1 and APLP2) in mammals and amyloid precursor protein-like (APPL) in Drosophilia. Also members of this protein family share the same conserved

domains among them such as E1 and E2 which are located in extracellular N-terminal part of APP. The E1 domain is believed to be involved in the dimerisation of APP and APLPs but there has been no solid evidence to suggest the function of E2 domain. However, APP is the only member of this protein family that contains the amyloidogenic Aβ sequence (O'Brien and Wong 2011; Zheng and Koo 2011; Zhang et al. 2012).

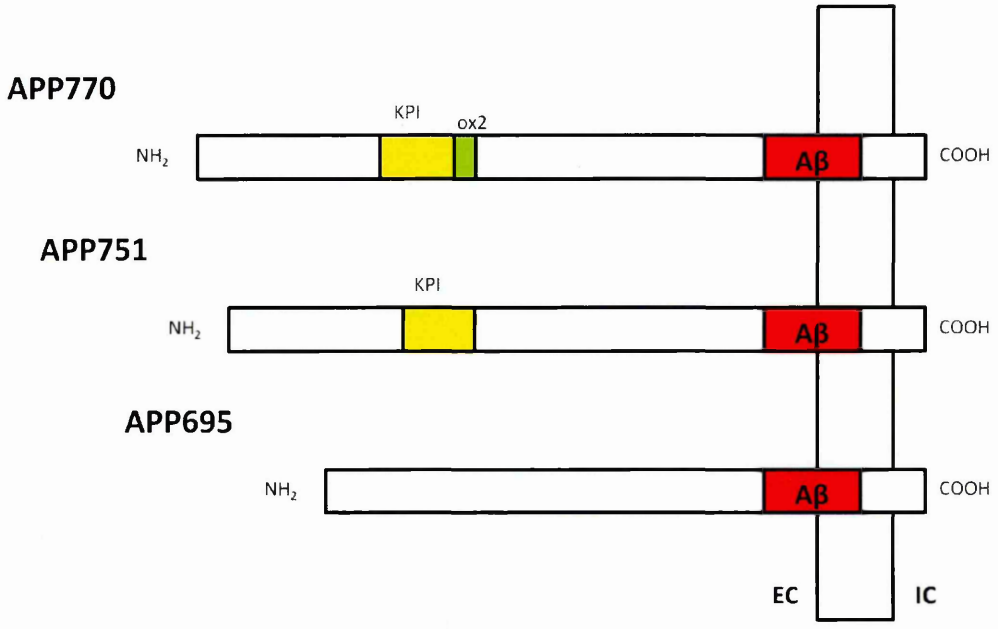

Figure 1.3.1 The three main isoforms of amyloid precursor protein; APP696, APP751 and APP770. The APP770 contains two additional domains which are Kunitz-type serine protease inhibitor (KPI) and OX2 domains while APP751 only contains one additional domain; the KPI domain and there is no additional domain found in APP695.

1.3.2 Proteolytic processing of APP

Neurons do not only have a large capacity when it comes to producing APP but have the ability to metabolize APP promptly as well (Lee et al. 2008). Once APP is produced, it is categorized in the endoplasmic reticulum and Golgi before being packed and distributed to axon and synaptic terminal via fast axonal transport. The two main vital steps in APP processing take place at the cell surface and in the trans-Golgi network (TGN). In brief, APP on the cell surface is either cleaved by α-secretase then γ-secretase, which does not result in Aβ fragment formation, or reinternalised into an endosomal compartment which contains β- and γ-secretase, which generates the Aβ fragment. The Aβ fragment is then transported to the extracellular space. On the other

hand, APP processing which occurs at the TGN is simpler than the process at the cell surface. APP from TGN is either transported directly to the cell surface or to an endosomal compartment; the latter is mediated by retromers (O'Brien and Wong 2011).

Amyloid β peptide (Aβ) is the major constituent of amyloid plaques in the brains of AD patients. Aβ consists of 39-43 amino acids and the most common form is Aβ40 but Aβ42 is considered to play a crucial role in plaque development. Also there are a number of studies which suggested that Aβ42 is the most abundant in plaques and it also has greater potential to aggregate, oligomerise and form fibrils in comparison to Aβ40. These accumulations may cause deleterious effects to neurons (Vetrivel and Thinakaran 2010; Zheng and Koo 2011).

As already mentioned, APP is metabolically processed by different secretases, mainly α-, β- and γ-secreatase (see Figure 1.3.2), at different subcellular sites via either amyloidogenic or non-amyloidogenic pathways as shown in Figure 1.3.3.

The non-amyloidogenic pathway mainly occurs at the cell surface due to the availability of the secretases. In this pathway, APP is initially cleaved by α-secretase at Aβ sequence (between lysine 16 and leucine 17) resulting in the release of the soluble APPα (sAPPα) fragment into the extracellular matrix (Anderson et al. 1991; Sisodia et al. 1990). Cleavage of APP by α-secretase is the main and universal pathway of APP metabolism in most cells (Ling, Morgan and Kalsheker 2003). The α-secretase is a membrane bound enzyme and mainly works at the cell surface (Sisodia 1992). Also it has been reported that several zinc metalloproteinases share similar functions to α-secretase. In other words, the enzymatic activity of α-secretase is being shared by a group of the disintegrin and metalloproteinase (ADAM) family such as ADAM 9, ADAM 10 and ADAM 17 (Allinson et al. 2003; Haass et al. 2012). The remaining membrane-associated C-terminal fragment, which contains 83 amino acids (so called C83), is then cleaved by γ-secretase in the transmembrane region of APP resulting in 3 kDa p3 fragment and APP intracellular domain (AICD). Moreover, 3 kDa p3 fragment does not play role in pathogenesis of AD (Cao and Sudhof 2001; Haass et al. 1993; Hartmann 1999).

In the amyloidogenic pathway, APP is initially cleaved at the extracellular domain of the N-terminal of the Aβ sequence, at amino acid +1 or +11 sites, by β-secretase resulting in the release of soluble APPβ into the extracellular matrix (Vassar et al. 1999). The remaining membrane-associated C-terminal fragment, which contains 99 amino acids (so called C99), is then cleaved by γ-secretase generating Aβ fragment and AICD (Annaert and De Strooper 2002).

Unlike the non-amyloidogenic pathway that mainly occurs at the cell surface, the amyloidogenic pathway involves trafficking APP through endosomal compartment which contains β- and γ- secretase (Thinakaran and Koo 2008). Even though the majority of APP is believed to go to the cell surface, there is only a limited number of APP molecules detected on the cell surface despite its very fast processing (O'Brien and Wong 2011). Also, increased α-secretase activity significantly reduces Aβ fragment generation hence plaque formation both *in vivo* and *in vitro*, which suggests that APP processing is a competitive process (Nitsch et al. 1992; Postina et al. 2004). After all, the balancing of APP processing might play an important role in the development and progression of AD.

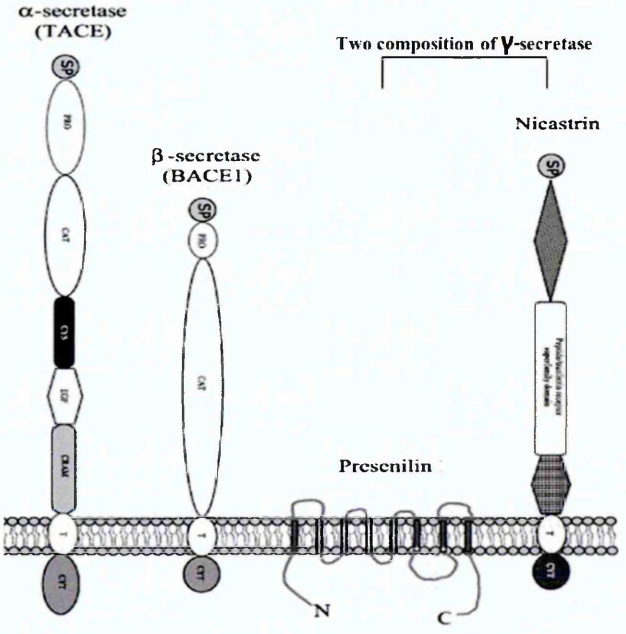

Figure 1.3.2 The organisation of secretases including α-secretase, β-secretase and part of γ-secretase; Presenilin and Nicastrin (adapted from Ling, Morgan and Kalsheker 2003).

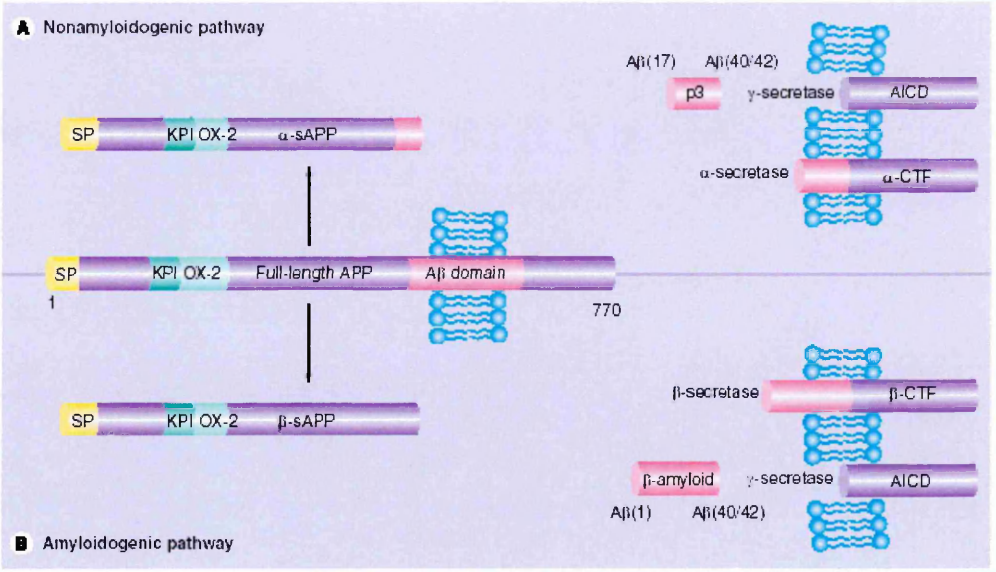

Figure 1.3.3 The processing pathway of amyloid precursor protein (APP). (A) Non-amyloidogenic pathway, the APP is cleaved by α- and γ-secretase, respectively which generates soluble APPα and a small non-toxic fragment; p3. (B) Amyloidogenic pathway, the APP is cleaved by β- and γ-secretase, respectively which generates soluble APPβ and Aβ peptides (Portelius et al. 2008).

1.3.2.1 α-secretase

Several proteins have been identified to have α-secretase-like activity and they belong to a disintegrin and metalloproteinase (ADAM) family including ADAM9, ADAM10 and ADAM17 (Zhang et al. 2012). Also, the ADAMs family of integral membrane protein belongs to the zinc protease super family which means members of this family are characterized by a metalloproteinase domain, integrin receptor binding activity and a cytoplasmic domain. The ADAMs family has been suggested to play several roles such as control of cell migration, membrane fusion, growth factor and cytokine shedding (Seals and Courtneidge 2003). Fundamentally, as previously mentioned, the majority of α-secretase activity occurs at the cell surface whereas the regulated activity is mainly located inside the Golgi (Ling, Morgan and Kalsheker 2003). The activity of α-secretase in the Golgi is rather important since there is evidence suggesting a significant increase in α-cleavage after the activation of protein kinase C; including an increase in APP being transported to the cell surface, an increase in α-cleavage in TGN and an inhibition of re-uptake of cell surface APP into the endosomal compartment (O'Brien and Wong 2011).

ADAM9 is universally expressed in human tissues. Evidently, COS cells co-expressed ADAM9 and APP then treated with phorbol ester have shown that ADAM9 cleaved APP, specifically at the α-secretase site. Also, overexpression of ADAM9 in COS cells increased sAPPα production which strongly suggested that ADAM9 has α-secretase activity (Ling, Morgan and Kalsheker 2003; Seals and Courtneidge 2003).

ADAM10 is mainly localised to Golgi and TGN. However it was first isolated during bovine myelin membrane preparation which later showed the ability to cleave APP at α-cleavage site (Ling, Morgan and Kalsheker 2003). Moreover, HEK293 cells overexpressed ADAM10 also showed a sharp increase in sAPPα production which suggested the role of ADAM10 in α-secretase processing of APP. Also, increasing the expression of SIRT1 (the ADAM10 gene expression regulator) in mice models has shown a significant reduction of Aβ fragment deposition alongside reduced cognitive decline (O'Brien and Wong 2011).

ADAM17 is found in most tissues and is typically expressed in neurons, vascular cells and leukocytes (Schlondorff, Becherer and Blobel 2000). It was originally identified as the enzyme responsible for cleavage of the membrane-bound pro-protein of tumor necrosis factor α (TNF- α) hence it is also called tumor necrosis factor alpha converting enzyme (TACE) (Ling, Morgan and Kalsheker 2003). Also a mouse model with ADAM17 deficit which showed signs of EGF signalling defect confirming the role of ADAM17 in cleavage of EGF family member (Peschon et al. 1998)

1.3.2.2 β- secretase

β-secretase is a 501 amino acid type1 transmembrane aspartyl protease containing an extracellular membrane active site (Zhang et al. 2012). Currently, there are two enzymes which have been identified to act as β-secretase; β-site APP-cleavage enzyme1 and 2 (BACE1 and BACE2, respectively) (Ling, Morgan and Kalsheker 2003). Both BACEs require low pH conditions for its activity and are mainly expressed within endosome, TGN as well as on the cell surface (Vassar et al. 2009).

BACE1 cleaves APP at the aspartic acid 1 and glutamic acid 11 sites on the extracellular domain suggesting it is a site specific protease. However, cleaving APP by BACE1 is both general and specific. For example, human APP can be cleaved by murine BACE1 at

position 1, or vice versa, but human APP cannot be cleaved by murine BACE1 at position 11 (Ling, Morgan and Kalsheker 2003). Moreover, the studies on BACE1 knockout mice showed that BACE1 is a neuronal β-secretase since neurons obtained from mice do not produce Aβ fragment but glia cells do. Although BACE1 is able to cleave various substrates, its preferential substrate site would be acidic or contain polar residues. It was suggested that BACE1 is a membrane bound protease and only cleaves APP that is bound to membrane (Venugopal et al. 2008).

BACE2 is another enzyme which has been identified as a β-secretase. As a counterpart enzyme of BACE1, BACE2 share 71% homology and 45% identity with BACE1, but BACE2 has much lower expression levels in the brain and it is mainly expressed in glia cells (Zhang et al. 2012). Interestingly, instead of cleaving APP at amino acid position 1 or 11, BACE2 cleaves APP at amino acid position 19 or 20 which is in the middle of the Aβ sequence, resulting in a 79 amino acids C-terminal fragment, which does not contribute to Aβ generation (Venugopal et al. 2008).

1.3.2.3 γ-secretase

γ-secretase is a multiple-protein complex consisting of several units of transmembrane protein (see Figure 1.3.4); presenilin 1 (PS1) or presenilin 2 (PS2), nicastrin (Nct), anterior pharynx defective 1 (Aph-1) and presenilin enhancer protein 2 (Pen-2). Essentially, in order to enable γ-secretase activity, all four compartments are required to act together (Small, Klaver and Foa 2010).

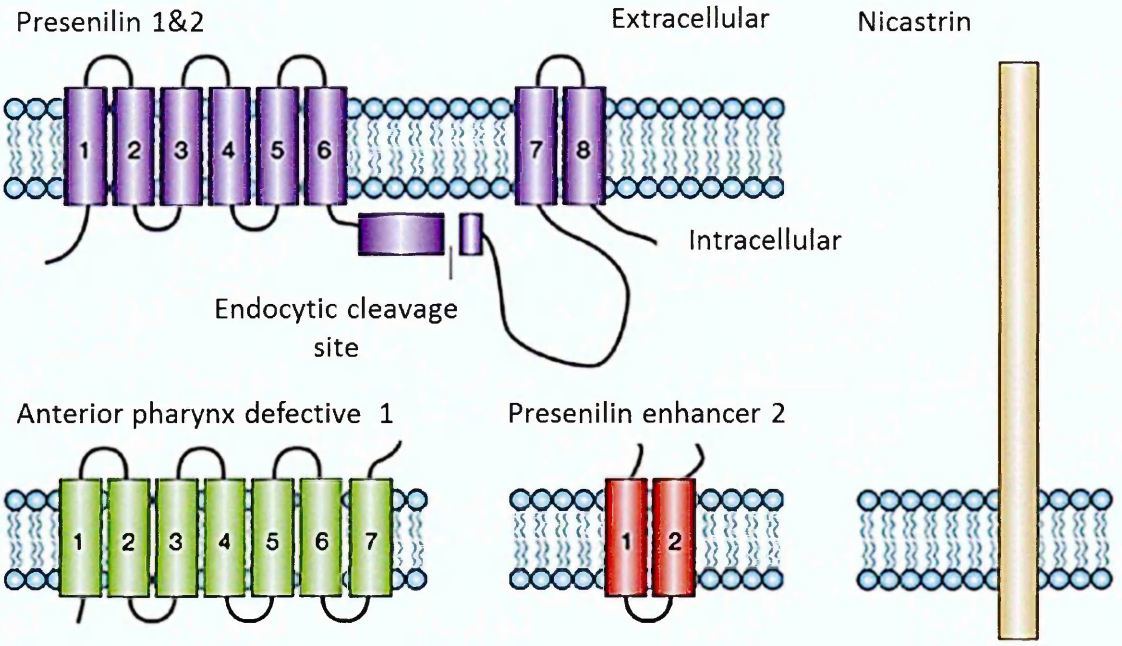

Figure 1.3.4 The γ-secretase complex; presenilin 1 & 2, anterior pharynx defective 1, presenilin enhancer 2 and nicastrin (Kopan and Ilagan 2004).

PS1 and PS2, which consist of 463 and 448 amino acids respectively, are comprised of nine transmembrane units and intracellular N- and C- terminal (De Strooper, Iwatsubo and Wolfe 2012; Ling, Morgan and Kalsheker 2003). Not only do PS1 and PS2 share 76% homology but they both also have a big cytoplasmic loop between transmembrane unit 6 and 7, which is cleaved during the post-translational process to generate the N- and C-terminal fragments. Each of these fragments contain aspartyl residues required to activate the γ-secretase activity (Small, Klaver and Foa 2010; Zhang et al. 2012). Also both PSs are mainly detected in ER and Golgi.

Nicastrin (Nct) is described as a type 1 transmembrane glycoprotein with a large extracellular domain. After glycosylation, which is a part of maturation of Nct recognises and binds to the C-terminal fragment of APP after either α- or β- cleavage (O'Brien and Wong 2011).

Anterior pharynx defective 1 (Aph-1) consists of seven transmembrane units with cytoplasmic C-terminal. The main function of Aph-1 is to assemble preliminary structure γ-secretase multiple-protein complex by interacting with immature nicastrin and PSs. The complex is then transported from the ER to the TGN (O'Brien and Wong 2011; Zhang et al. 2012).

Presenilin enhancer protein 2 (Pen-2) consists of 2 transmembrane units and it has a hairpin-like shape with both N- and C- termini in the extracellular space. The function of Pen-2 in the complex is to facilitate the cleavage of PSs which generate essential N- and C-terminal fragments required to initiate γ-secretase activity activation process (Zhang et al. 2012).

1.3.3 Function of APP and its derivatives

To date, the exact function of APP is still unclear but as its structure is significantly similar to Notch, therefore one of its proposed functions is as a cell surface receptor. Besides, it has been reported that APP has effects on both health and growth in transgenic mice, overexpressed wild-type APP and transient transfected cell lines. According to the structure of APP, the extracellular part contains two heparin-binding domains which were suggested to be responsible for its bioactivity. Several proteins, such as Aβ fragment or F-spondin, bind to extracellular part of APP resulting in APP processing and downstream signalling modulation (O'Brien and Wong 2011; Zhang et al. 2012). In 2004, Wang and Ha suggested that APP plays role in cell adhesion by forming parallel dimers facilitated neurite outgrowth and synaptogenesis. Also it was shown that the expression of APP is not only different during the neuronal maturation and differentiation but also during traumatic brain injury (Corrigan et al. 2010; Wang and Ha 2004).

It has been suggested that the soluble APPα (sAPPα) fragment, a product from non-amyloidogenic processing pathway, has neuroprotective and neurotrophic properties as well as the ability to regulate cell excitability and synaptoplasticity (Zhang et al. 2012). In 2007, the study showed that abnormalities occurred with mice caused by APP deficiency were rescued using sAPPα alone, which suggested that nearly all of APP functions are initiated by its extracellular part (Ring et al. 2007). Not only are there 17 amino acid differences between sAPPβ and sAPPα but they also function contradictorily. Generally, sAPPβ seems to lack the neuroprotective property. Furthermore, it can act as a precursor of an N-terminal fragment which is able to bind to Death Receptor 6 and activate caspase 6, causing axonal pruning and neuronal cell death (O'Brien and Wong 2011; Zhang et al. 2012).

Since the discovery of relationship between Aβ and AD, Aβ has been the centre of attention in pathological study of AD. So far, it has been reported that excessive amount of Aβ promotes cause neurotoxicity, neuronal tangle formation, synaptic damage and neuronal death (Zhang et al. 2012). Indeed, the combination of low levels of APP fragments and the accumulation of Aβ may be an explanation for cognitive decline in early onset AD (Turner et al. 2003). On the other hand, the recent studies reported that by applying low concentrations of Aβ fragments showed positive effects on synaptic plasticity and memory.

As APP intracellular domain (AICD) degrades rapidly, it is virtually impossible to conduct a physiological investigation *in vivo,* hence the majority of information on AICD obtained from experiments based on exogenous system. AICD is a consequence of γ-cleavage and its size could vary from 50 to 59 amino acids. It has two proposed functions; transcriptional regulator and self-intracellular sorting regulator. There are three conserved domains on AICD; YTSI, VTPEER and YENPTY. Each domain is responsible in binding to different binding partners. For example, to become the binding partner of YENPTY requires the existence of phosphotyrosine interacting domain (PID): the two best candidate binding partners of YENPTY are Fe65 and X11 (O'Brien and Wong 2011; Zhang et al. 2012). On its own, Fe65 induces transportation of APP to cell surface but together with AICD and Tip60, it facilitates the formation of transcriptional active complex (Slomnicki and Lesniak 2008). The X11 binding partner is found to reduce Aβ production by interacting with AICD. Also both Fe65 and X11 are strongly expressed in the brain.

1.4 Other pathologies associated in AD

Besides amyloid plaques and neurofibrillary tangles formation, cerebral amyloid angiopathy, synaptic and neuronal loss, neuronal inflammation, oxidative stress and metallobiology are suggested to have significant contribution for AD pathogenesis.

1.4.1 Inflammation and AD

Inflammation is a biological process responding to self and non-self antigens. The aim of an inflammatory process is to eliminate the antigen and the damage it has caused to

cells and tissues. The unsuccessful attempt to get rid of the antigen and restore healthy cells and tissues could turn the inflammation into a chronic condition which results in further deterioration of the surrounding area (Rubio-Perez and Morillas-Ruiz 2012). The inflammatory process occurs in two phases; (1) acute inflammation where the response to an antigen is short and aggressive, and (2) chronic inflammation where there is a mild and continuous response to an antigen (Zotova et al. 2010). Moreover, the acute phase clinically manifests with pain, swelling, redness and heat where monocytes, macrophages in PNS or glia cells and astrocytes in CNS are the inflammatory features of chronic phase.

Evidently, the immune response involved in AD pathogenesis was observed since the 1980s when immune related molecules were found surrounding amyloid plaques in the brains of AD patients. Ten years later, the view on inflammation in CNS or neuroinflammation was prompted by the additional findings about the molecules involved in the inflammatory process. These molecules include compliment factors, chemokine and cytokines (Zotova et al. 2010). As a result, the inflammation within the brain is classified as one of the pathological hall mark of AD. However, the clinical sign of acute inflammation phase is absent therefore the neuroinflammation is usually referred to as chronic inflammation (Rubio-Perez and Morillas-Ruiz 2012).

It was believed that inflammation alone is more likely to contribute to the progression of AD rather than being the cause of AD itself. The inflammation is a response to the insults, including infection which causes cell injury and necrosis (Rubio-Perez and Morillas-Ruiz 2012). It was proposed that the inflammation participates in the progression of the AD by (1) immediately acting in response to the changes and (2) later persisting in response to the low-level of inflammatory stimuli, such as Aβ plaques and NFTs, in the brain (Zotova et al. 2010). This concept is supported by several studies. For example short-term infection initiated inflammation as a response which in the AD patients, resulted in a rapid decline in cognitive functions which hardly recovered to the point before infection had occurred, even after the infection was treated (Perry, Cunningham and Holmes 2007). It was also reported that the level of inflammatory proteins increased prior to the onset of clinical manifestation of AD; or inflammatory features were mainly found in the AD affected area of the brain (Overmyer et al. 1999). Also microglia, astrocytes and neurons are accountable for the

inflammatory process in the brain and by activating these cells the pro-inflammatory molecules are produced (Rubio-Perez and Morillas-Ruiz 2012).

Microglia contribute approximately 10% of the total cell number in the nervous system (Rubio-Perez and Morillas-Ruiz 2012; Wyss-Coray and Rogers 2012). One of the crucial roles of microglia is removing debris and dead neurons which results in brain remodelling. The recent studies have shown that microglia repeat the housekeeping routine every few hours. Also, microglia act as the first port of call towards the pathogens, cellular and tissue injury in order to maintain healthy brain condition. As the activated microglia are able to remove detritus, it is often referred to as brain's macrophage (Wyss-Coray and Rogers 2012). A reduction in microglia activation was observed when the APP gene and APP processing were interfered with and the binding of Aβ peptide to microglia promotes chemokine and cytokine production (Rubio-Perez and Morillas-Ruiz 2012). The microglia are able to produce several inflammatory factors including; cytokines, chemokines, reactive oxygen species, growth factors and complement factors and an increased level of these factors usually results in neurodegeneration in cellular and animal models. It was reported, in the cell culture of microglia and histochemistry of sections of the AD brain, that microglia were attracted to Aβ peptide as well as attempting to remove it. The study of the relationship of Aβ peptide and microglia using two-photon microscope suggested that microglia reached neurons at the same time as the damage was done to adjacent neurons. Despite the observation, it is still not conclusive whether microglia are responsible for neuronal damage during their recruitment to the plaques (Wyss-Coray and Rogers 2012).

In the nervous system, the number of astrocytes is five times higher than the neuron. The astrocytes are also often known as neuroprotective cells in the brain. Not only do astrocytes play numerous roles in the brain including; providing optimal condition for the neurons in the brain, supporting neuronal structure, regulating metabolism and modulating neuronal development but also act primarily in the synaptic transmission process; recycling neurotransmitters, remodelling synapses, maintaining the balance of ion and regulating oxidative stress levels (Molofsky et al. 2012; Wyss-Coray and Rogers 2012). It was reported that an exposure of Aβ peptide to the astrocytes evidently interfered astrocytes' homeostasis which eventually resulted in neuronal degradation. Also, the astrocytes play role in the defensive system similar to microglia. For example,

it was reported that one of the functions of astrocytes was to attack and remove Aβ peptide deposition as well as providing defensive construct between Aβ peptide deposition and healthy neurons. This example was further supported by the observation in the brains of AD patients and animal models showing that astrocytes migrated around the Aβ peptide deposition to provide a protective barrier in the damage control manner (Rubio-Perez and Morillas-Ruiz 2012; Wyss-Coray and Rogers 2012).

It was believed that neurons only acted as witnesses while the changes in the brain occurred. However, recently it was reported that neurons are capable of producing inflammatory factors such as fractalkine and complement protein CD59. It was observed in the AD animal model that there was a reduction of fractalkine level in the hippocampus and cortex. Also, the expression level of CD59 in brains of AD patients partially decreased in the affected areas (Beech et al. 2007; Singhrao et al. 1999).

1.4.2 Oxidative stress and AD

The term oxidative stress has been used to describe the condition resulting from an alteration of oxidative homeostasis. In other words, oxidative stress is an imbalanced condition between free radicals and antioxidants. The major form of free radicals derived from oxygen is called reactive oxygen species (ROS) which includes superoxide radical anion (O2–·), hydrogen peroxide (H_2O_2) and hydroxyl radical (·OH). These ROS are generated under normal conditions and are kept in a minimal state by various antioxidants. However the excess amount of free radicals from both self-produced and environmental sources are able to overwhelm the elimination process provided by antioxidants, which results in molecular damage. There are several ways to address the molecular damage caused by ROS, depending on the targets. For example, protein or DNA/RNA oxidation describes the condition where protein or DNA/RNA is damaged by ROS. The condition where the ROS caused damage to lipids is addressed as lipid peroxidation. In the brains of AD patients, the damage caused by ROS during the development of the disease is exhibited (Pratico 2008; Swomley et al. 2013). Moreover, overexpression of Aβ peptide in animal models and cell cultures exhibit an increase in oxidative stress biomarkers (Axelsen, Komatsu and Murray 2011).

The oxidation of protein occurs at both the backbone and the side chain of the amino acid within the protein. Also, protein oxidation commonly refers to the oxidation of the protein at its side chain. The breakage of the polypeptide chain and protein-protein crosslinking is ultimately the most common results of protein oxidation (Pratico 2008). Chemically, the oxidation of protein by ROS via the carbonylation process occurs both directly and indirectly. The direct carbonylation of protein occurs where carbonyl groups are directly introduced to amino acid residues such as lysine, arginine, proline and threonine, whereas indirect carbonylation is where the hydroxyl group at the side chain of the amino acid is oxidized and turned into either ketone or aldehyde derivatives. However, there are several other oxidative pathways which cause protein carbonylation including the oxidation of glutamyl and the α-amidation pathway (Gella and Durany 2009). Evidently, there was an increase in carbonylized protein in the frontal and parietal lobe in the brains of AD patients in comparison to same age controls (Pratico 2008). Other studies also supported the fact that there was an increase in protein carbonylation in the hippocampus and parietal cortex; the common brain regions which are usually affected by the progression of AD (Axelsen, Komatsu and Murray 2011; Sultana and Butterfield 2010).

Lipid peroxidation is the process where the hydrogen atom at the side chain of the methylene carbon is removed as a consequence of ROS action. Also, the susceptibility to lipid peroxidation depends on the number of double bonds in the lipid molecule. For example, the poly-unsaturated fatty acids (PUFAs) are more prone to lipid peroxidation by ROS in comparison to saturated fatty acids. As the brain has high oxygen demands and contains a vast quantity of peroxidizable fatty acids, the brain is highly susceptible to lipid peroxidation. In addition, arachidonic acid and docosahexaenoic acid are the main component of lipid bilayers in the brain and the oxidation of these lipids results in aldehyde productions (Pratico 2008). Besides an observation that Aβ peptide promoted peroxidation of lipid, it was also reported that the products gained from the lipid peroxidation process, including 4-hydroxynonenal (HNE), acrolein, melondialdehyde and F2-isoprostanes, increased in comparison to controls at the same age. The HNE is a product resulting from lipid peroxidation of arachidonic acid and is able to bind to protein causing several dysfunctions including inhibition of glucose and glutamate transporters in neurons, inhibition of Na-K ATPases, disruption

of intracellular calcium signalling and eventually initiating apoptosis. Furthermore, one of the AD neuropathological hallmarks; NFTs was found to be enriched with HNE and melondialdehyde which indicated lipid peroxidation process (Gella and Durany 2009). It was reported that Aβ peptide continued to promote peroxidation of lipid compounds such as cholesterol and phospholipids as long as the methionine side chain is not damaged (Axelsen, Komatsu and Murray 2011). Although these are only a few examples of HNE involved in oxidative stress, it is enough to conclude that HNE is toxic and one of the causes of AD pathogenesis via oxidative stress. Besides HNE, F2-isoprostane is able to induce the oxidation of arachidonic acid and it can be used as a marker due to its high accuracy against lipid peroxidation (Milne, Musiek and Morrow 2005). F2-isopropanes belong to a prostaglandin-like compound family and it is formed as a consequence of ROS-mediated lipid peroxidation in the absence of enzymatic reactions. The increasing level of F2-isopropanes was found in the brain regions which are usually affected by AD pathogenesis such as the frontal lobe and hippocampus, as well as in CSF (Pratico 2008).

The ROS induced oxidation of DNA results in DNA-protein crosslinking, fragmentation of DNA strands and, ultimately, DNA mutations due to direct modification at purine and pyrimidine bases. The DNA fragmentation also generates free carbonyl groups within neurons and glia cells (Pratico 2008). The 8-hydroxy-2-deoxyguanosine (8OHdG), 8-hydroxyguanine (8OHG) and 8-hydroxyadenine (8OHA) were typical markers against DNA damage. It was reported that the level of 8OHdG, 8OHG and 8OHA were increased in the AD patient at the affected brain regions such as temporal, parietal and frontal lobes. Also, 8OHdG and 8OHG were found to restrict to amyloid plaque and NFT (Pratico 2008; Sultana and Butterfield 2010). The elevation of 8OHdG was increased in CSF of the AD patient as well as in the brain. Due to the lack of protection by histones or hydrogen bonds and being a single strand nucleic acid, it makes RNA more prone to oxidation by ROS in comparison to DNA (Sultana and Butterfield 2010). Also, the number of RNA molecules is greater than DNA and RNA tends to locate in the proximity of mitochondria which is the main origin of ROS production. The susceptibility to oxidative damage of RNA was supported by studies in both cell culture and human tissues including human leukocytes and skin fibroblasts as well as in the brains of AD patients (Nunomura et al. 2009). The 8-hydroxyguanine (8-

OHG) and 8-hydroxyuracil (8-OHU) are accounted as RNA oxidation markers. Both 8-OHG and 8-OHU were increased in the brains of AD patients; particularly frontal, temporal and parietal lobes (Sultana and Butterfield 2010). Whereas the increased level of 8-OHG was decreased inversely to the development of amyloid plaque and NFT formations (Pratico 2008).

It was found that both DNA and RNA markers could be detected prior to plaque formation.

Another substrate which is related to oxidative stress is sugar. The oxidation process of sugar requires either protein or lipid molecules. The oxidation of protein or lipid related sugar can be addressed with different terminology; non-enzymatic glycosylation, glycation or the Maillard reaction (Srikanth et al. 2011). The Advance Glycation end products (AGEs) are believed to be involved in pathogenesis of many diseases including diabetes, vascular disease, renal failure and Alzheimer's disease (Goldin et al. 2006; Singh et al. 2001; Srikanth et al. 2011). The mechanism of AGEs is induced by the reaction between the carbonyl group obtained from oxidized sugar and lipids or protein molecules which produced Schiff bases and Amadori products. The denatured protein forms an aggregation which yellow-brown is the common result from the reaction (Goldin et al. 2006; Srikanth et al. 2011). It was suggested that the presence of either high turnover rates of suitable proteins for glycation or the considerate level of oxidative stress are the main controlling factors of AGEs.

1.4.3 Metallobiology in AD

Metal ions play a crucial part and are responsible for several biological functions and cellular processes in living organisms, both prokaryotes and eukaryotes (Jomova and Valko 2011; Jomova, Baros and Valko 2012). The levels of metal ions are regulated by the system called "ion homeostasis" based on the balance between the absorption and elimination or excretion of metal ions of the cells. As metal ions are essential for normal enzymatic and catalytic functions, stability of cellular structure, oxygen transportation and cellular signaling, and by disrupting the balance of the metal ions can become toxic causing oxidative deterioration to the target molecules. The most common transition metal ions found in eukaryotic cells are iron (Fe), zinc (Zn) and copper (Cu) (Robert et al. 2012). In addition, it was found that the level of Fe, Zn and

Cu were higher in the brains of mammals in comparison to other tissues which corresponded to the fact that there are several ion-dependent enzymes and metabolic pathways within the brain. The levels of these metals in the brain are strictly controlled by the blood brain barrier (BBB). It was reported that the total concentrations of each of these metals were greater in AD patients in comparison to the same age controls. In the post-mortem examination of the brains of AD patients, it was found that the centre of amyloid plaques contained excessive amounts of Fe, Zn and Cu (Tabner, Mayes and Allsop 2011). As well as an increased total concentration of each metal, these metals were found localized strictly within the same location of amyloid plaques in both AD patients and animal models (Greenough, Camakaris and Bush 2013). Also, Fe, Zn and Cu are able to cause Aβ peptide precipitation (Robert et al. 2012).

Iron (Fe) is essential for many biological processes including oxygen transportation, electron transfer and the production of both neurotransmitters and myelin (Robert et al. 2012). Although Fe is important for maintaining normal biological activity, the excessive amount of Fe in the system can become toxic. The toxicity of Fe is due to its catalytic ability in the Fenton reaction which produces free radicals causing damage to the affected organ. Fe has two major oxidation states; Fe (II) and Fe (III) in the biological system (Jomova, Baros and Valko 2012). It was shown that Fe was involved in downstream processes after NMDA (N-methyl-D-aspartate) receptor activation such as ryanodine-mediated calcium release. The NMDA receptor involves in cholinergic hypothesis of AD. It was believed that the level of Fe in the brain increases according to age. The mild acidity condition is the preferred condition for Fe binding to Aβ. It was also suggested that the mild acidic condition facilitated Fe entry into neurons, which was the cause for toxicity of Aβ peptide in animal models of AD (Robert et al. 2012).

Zinc (Zn) plays roles in cell metabolic processes of protein, lipid and carbohydrate molecules as it is involved in more than 70 metabolic enzymes. Zn also plays a role in maintaining insulin, blood glucose levels, and immune system (Jomova and Valko 2011). A high concentration of Zn is found in the nerve terminals of glutamatergic neurons. Once it is released from synaptic clefts, Zn binds to receptors including the NMDA receptor. The overall concentration of Zn does not change despite aging condition. It has been a well-known fact that the core amyloid plaques from AD patients contain high concentrations of Zn compared to the same age controls.

Therefore it was suggested that the accumulation of Zn in amyloid plaques may potentially cause dysfunction of Zn in the brain (Robert et al. 2012).

Copper (Cu) acts as a co-factor of several redox-related enzymes including cytochrome C oxidase, ascorbate oxidase and superoxide dismutase. Also, azurin and plastocyanin are examples of copper proteins which play roles in electron transportation. Cu is normally obtained from food and stored in the liver. The serum albumin and histidine facilitate the transportation of Cu either to the target organ or to be removed from the system (Jomova and Valko 2011). The Cu level in the brain is varying depending on brain region. Also, the level of Cu in the brain was found increasing up until adulthood then the level started to decline (Robert et al. 2012). The most common oxidation state of copper in biological system are Cu (I) and Cu (II) (Jomova and Valko 2011; Jomova, Baros and Valko 2012). One of several ways to facilitate amyloid plaque formation is by reactive oxygen species which requires the presence of a transition metal; especially Cu. It was reported that Cu was able to bind strongly to Aβ peptide as long as histidine and tyrosine were present (Jomova, Baros and Valko 2012). In the brains of AD patients, the level of Cu was decreased in the brain tissue while the high concentration of Cu was found within the amyloid plaques. As a consequence, it was suggested that Cu was drawn toward the plaques and accumulated there which left the rest of the brain with low concentration of Cu (Robert et al. 2012).

1.5 Genetics aspects of AD

Alzheimer's disease is an intricate and genetically different neurodegenerative disease. The estimation of an inherited rate has been presumed to be less than 30% of all patients with Alzheimer's disease. As a result, genetic mutations are considered as a small factor which influenced the increasing risk of developing Alzheimer's disease. Until now there are four mutated genes which have been clearly verified to be involved in causing Alzheimer's disease. The mutations occur in amyloid precursor protein gene (APP) located on chromosome 21, Presenilin 1 (PSEN1) located on chromosome 14, Presenilin 2 (PSEN2) located on chromosome 1 and ApolipoproteinE (APOE) located on chromosome 9 (Guerreiro, Gustafson and Hardy 2012). Moreover, there are studies which have suggested that since the clinical manifestation of the

disease are similar in both sporadic and familial types; most of patients with Alzheimer's disease must carry hidden genetic causes (Castellani, Rolston and Smith 2010). In 1996, Lautenschlager and co-workers did a study on the age-specific incidence of Alzheimer's disease; it was suggested that the first degree relative of a patient with Alzheimer's disease had developed a significant risk of the disease. Also, the offspring of Alzheimer's disease carrier couples had developed five times the risk of having Alzheimer's disease in comparison to offspring of non-carrier couples (Crentsil 2004). The APP, PSEN1 and PSEN2 are believed to be involved in early-onset Alzheimer's disease (EOAD) which is mainly familial type Alzheimer's disease (FAD), while APOE and SORL1 are seen as risk factors of late-onset Alzheimer's disease (LOAD) which is mainly sporadic type Alzheimer's disease (SAD) (Guerreiro, Gustafson and Hardy 2012). Surprisingly, the three genes; APP, PSEN1 and PSEN2 which have incomparable mutations, give the same outcome after the mutation process which is an increase in amyloid β peptide (Aβ) production. In addition, APOE decreases Aβ production but increases its aggregation resulting in an increase in plaque formation (Crentsil 2004).

1.5.1 Amyloid Precursor Protein (APP) mutations

The APP gene is located on chromosome 21, more accurately on the long arm of chromosome 21 at position 21 (21q21) (Guerreiro, Gustafson and Hardy 2012). The identification of a mutation in APP, the so called autosomal dominant mutation, was the first contribution to initiate a study of the genetic aspects of AD. So far there are 24 single nucleotide mutations on APP. All mutations occur either around or inside the Aβ sequences specifically within 54 amino acids (Brouwers, Sleegers and Van Broeckhoven 2008; Schellenberg and Montine 2012). The mutation in APP associated AD has affected more than 80 families with age-at-onset ranging between 30 and 65 years (Cruts, Theuns and Van Broeckhoven 2012). The first example of APP mutation is the Swedish mutation. Swedish mutation involves two amino acid replacements close to the beginning of Aβ sequence; lysine to asparagine and methionine to leucine at positions 670 and 671, respectively. As Swedish mutation does not occur within the Aβ sequence and the consequence of mutation is a double or triple increase in Aβ production in comparison to non-mutated APP, this suggested that the mutation affects β-secretase activity. In addition, it is believed that an excessive production of

Aβ is enough to cause AD which was supported by the observation made on Down syndrome (DS) patients (trisomy 21) who have developed neuropathological hallmarks since an early age (Goate and Hardy 2012; Schellenberg and Montine 2012). It was proposed that the location of APP gene possibly provides the pathological aspects correlating between Down syndrome (DS) and Alzheimer's disease (AD) based on reports showing that the lack of APP coding sequence on the third chromosome in DS patients resulted in AD pathological hallmarks abolishment (Castellani, Rolston and Smith 2010). Another common example of APP mutation is the mutation that occurs after Aβ sequence; substitution of valine with isoleucine at amino acid position 717 (Val717Ile). Under normal conditions, the C-terminal fragment is cleaved by γ-secretase and mainly generates Aβ40 resulting in low ratios of Aβ42/Aβ40. However, after mutation, γ-cleavage tends to generate more of Aβ42 and higher Aβ42/Aβ40 ratios, but it does not necessarily suggest that the process generates smaller amounts of Aβ40 (Schellenberg and Montine 2012). Most studies on neuropathological effects of APP mutations have been carried out in a small sample group hence the data might not be appropriate to be used to represent global population. Nonetheless one of many interesting aspects of APP mutation on neuropathological hallmarks is the variety of Aβ aggregation structures. For instance, the substitution of alanine with glycine at amino acid position 692, the so called Flemish mutation, results in compressed plaques (Kumar-Singh et al. 2002) whereas replacing glutamic acid with glycine at position 693, the so called Arctic mutation, results in circular shaped plaques (Basun et al. 2008).

1.5.2 Presenilin mutations

Presenilin 1 (PS1) and presenilin 2 (PS2) are located on chromosomes 14 and 1, respectively, and they encode proteins which are the major components of γ-secretase (Guerreiro, Gustafson and Hardy 2012; Small, Klaver and Foa 2010). Up to date, there are approximately 185 mutations in the PS1 gene and 13 mutations on the PS2 gene (Cruts, Theuns and Van Broeckhoven 2012). These mutations predominantly occur within the transmembrane domain of PSs (Li and Greenwald 1998). Normally, a consequence of γ-secretase activity is the generation AICD and p3 or Aβ fragment, mainly Aβ40. However mutated PSs genes seemed to produce more Aβ42 than Aβ40 (Schellenberg and Montine 2012). Even though, the final outcome of both PSs

mutation are the same but mutations in PS1 and PS2 affect Aβ42/ Aβ40 in a different way. PS1 mutations result in an increased amount of Aβ42 while Aβ40 remains the same (Jankowsky et al. 2004). In contrast, mutations in PS2 resulted in the same amount of Aβ42 with decreased amount of Aβ40 (Walker et al. 2005).

Furthermore, a single amino acid replacement is a consequence of the majority of mutations in PS1; missense mutations. Although there are other kinds of mutation occurring in PS1, the most serious one has to be a double amino acids replacement with in-frame deletion of exon 9; donor-acceptor splice mutation (De Strooper 2007). Also, PS1 mutations affect the Aβ aggregation structure by generating a cotton wool shape plaque which, again, consisted more of Aβ42 (Schellenberg and Montine 2012).

According to brain autopsy reports of EOAD patients caused by PS1 or PS2 mutations, not only did the number of amyloid plaques increase but also the Aβ42/ Aβ40. Despite PSs mutation effects on neurofibrillary tangles, there is no significance different in term of numbers of NFT presented in FAD and SAD. Another neuropathological hallmark associated with PSs mutation, the less common one, is Lewy's body (Schellenberg and Montine 2012).

1.5.3 Apolipoprotein E (ApoE) alleles

Originally, ApoE was discovered to be involved in lipid metabolism but, with more advanced technologies, it has been suggested that ApoE also plays roles in lipid transport, synaptic function, intracellular signalling, immune regulation and, very importantly, Aβ trafficking (Schellenberg and Montine 2012). ApoE is also responsible for glycoprotein synthesis in the brain and liver. ApoE is located on chromosome 19 and it encodes Apolipoprotein E. ApoE acts as a binding component of lipoprotein to cell surface receptors and it is the majority of apolipoprotein in HDL complexes, especially in the brain. As the majority of Alzheimer's disease cases are SAD and the high susceptibility of ApoE as a genetic risk factor for SAD have made ApoE a centre of attention in the genetic contribution of Alzheimer's disease. Unlike other mammals, humans have three main alleles of ApoE; ϵ2, ϵ3 and ϵ4. These alleles are encoded by one genetic locus and are distinguished by two amino acid differences; at positions 112 and 158. For example, ϵ2 encodes cysteine at both position 112 and 158, ϵ3 encodes cysteine at position 112 and arginine at position 158, and ϵ4 encodes arginine at both

positions. In addition, ϵ3 is a dominant allele found and ϵ2 is a minor allele among all alleles. Each allele of ApoE has played a different role in AD. ϵ2 has a neuroprotective property against AD development and ϵ3 has a neutral effect against AD while ϵ4 has a great ability to increase the risks of AD development (Guerreiro, Gustafson and Hardy 2012). In other words, the onset age of AD associated with the ApoE allele is ϵ4> ϵ3> ϵ2 to early> middle> late, respectively. Homozygous allele such as ϵ4/ ϵ4 tends to have higher risk than heterozygous ϵ4/ ϵ3 or ϵ4/ ϵ2. Also ϵ4/ ϵ4 is more aggressive than ϵ2/ ϵ2. Interestingly, an individual carrying a single copy of ϵ4 has three times higher chance to develop AD than carrying zero copies, but if an individual was carrying two copies of ϵ4, homozygous, a chance of developing AD increased up to 15 times (O'Brien and Wong 2011). Nevertheless, ApoE only acts as an additive to AD development as a risk or disposable factor but not a causative factor on its own (Schellenberg and Montine 2012), and there is a possibility that ApoE contributes to AD development through its cellular ability on the uptake and clearance of Aβ (O'Brien and Wong 2011).

1.5.4 SORLA

SORLA or sorting protein-related receptor is a type 1 membrane protein which is mainly expressed in the brain. It belongs to a low density lipoprotein superfamily and its function as a shuttle transporting vesicles to the cell surface, endosome, Golgi and ER. It has been suggested to play an important part in APP processing and producing Aβ fragment as a result. SORLA operates vesicle transportation by using its N-terminal to bind to APP and its vacuolar protein-sorting region to bind to the retromer complex; the retromer complex mediates the connection between endosomal compartments and TGN (Anderson et al. 2005; O'Brien and Wong 2011). The function of SORLA as an APP shuttle is supported by studies which have shown that SORLA is able to deliver APP for γ-cleavage. It was also discovered that the expression of SORLA in the brain of AD patient has declined and suppression of SORLA gene expression in animal models induced Aβ aggregation. Apart from binding to APP, SORLA also plays role as an ApoE receptor (Schellenberg and Montine 2012).

1.6 Hypotheses proposed to account for AD

1.6.1 Cholinergic hypothesis

The cholinergic neurons are responsible for several brain functions including neuronal plasticity sleep regulation, depression, delirium, learning ability and cognitive function. The cholinergic neurons are categorised into; (1) projection neurons which are mainly located in the upper brain stem and prosencephalon and (2) interneurons which are found in the spinal cord, cortex, cerebellum and striatum. The principal function of cholinergic neuron is to produce neurotransmitters; acetylcholine and its enzyme; choline acetyltransferase (ChAT). Since acetylcholine was identified and characterised by Henry Dale and Otto Loewi in 1936, many researchers have been influenced to investigate its properties in detail. One of several findings of acetylcholine, and indeed the most well-known one, is the cholinergic hypothesis in relation to cognitive imparment and dementia; the so called "cholinergic hypothesis in AD" (Contestabile 2011).

The cholinergic hypothesis was originally proposed in the 1970s (Francis et al. 1999) based on the post-mortem examination that a loss of cholinergic neurons was often observed in the brains of AD patients (Craig, Hong and McDonald 2011). As a consequence of losing cholinergic neurons, a significant reduction in choline acetyltransferase was also observed. During the development of the cholinergic hypothesis, it was observed that the loss of cholinergic neurons mainly appeared in the brain areas associated with cognitive and memory functions such as the hippocampus and frontal lobe area. Also, pyruvate dehydrogenase which is a crucial enzyme in acetylcholine synthesis was found to be significantly decreased in the brains of AD patients. However, it was reported that cholinergic neuronal loss was more likely to be a consequence of the ageing process and it was not specified to AD, but other neurodegenerative disease as well (Contestabile 2011). It has been suggested that a single factor theory of the cholinergic hypothesis was not sufficient to be used solely as an explanation of clinical and pathological manifestations of AD. Consequently the multiple co-factor theory has been proposed whereby cholinergic depletion, for example, when enhanced by an episode of stroke becomes sufficient to be used as an explanation for AD related manifestations (Craig, Hong and McDonald 2011; Parent et

al. 2013). It was shown that the damage done to the brains with pre-acquired cholinergic depletion by a stroke attack was worse than the damage done to the healthy brains (Craig, Hong and McDonald 2011).

Regardless of the diversity of evidence, cholinergic drugs which were based on the cholinergic hypothesis still remain the most effective available symptomatic treatment drugs for AD.

1.6.2 Tau hypothesis

The principal of tau hypothesis is based on the fact that aberrant phosphorylation of tau protein leads to pair helical filament (PHF) formation which eventually turns into neurofibrillary tangles (NFTs) (Mohandas, Rajmohan and Raghunath 2009). Under the normal conditions, the binding ability of tau protein to microtubule or tubulin assembly promotion is regulated by the phosphorylation process. However the hyperphosphorylation condition compromises tau protein biological activity, causing the conformational changes and structural misfolding which leads to excessive aggregation within neurons (Kolarova et al. 2012). Also, it was suggested that neuronal cell death as a consequence of continuous modification of tau protein initiated neuro-inflammatory process by releasing oligomerised and filament forms of tau into extracellular spaces which led to neurodegeneration (Maccioni et al. 2010).

Tau protein belongs to the microtubule-associate protein (MAP) family and it is the main component of MAP in mature neurons. The size of tau protein ranges from 352-441 amino acids. The alternative splicing of tau protein generates six different isoforms which are mainly distinguished by the repetition of tubulin binding domain at the C-terminal and the number of inserts at the N-terminal (Maccioni et al. 2010). For example, the longest tau protein containing 441 amino acid residues has four repeats of tubulin binding protein and two 29-amino acid residue inserts while the shortest isoform of tau protein has three repeats of tubulin binding protein with an absence of 29-amino acid residue inserts (Mohandas, Rajmohan and Raghunath 2009). Tau protein does not only play a crucial role in microtubule stabilisation but is also able to promote tubulin assembly (Maccioni et al. 2010).

There are several reasons which have suggested the accuracy of the tau hypothesis and clinical manifestation including; (1) an increase of NFT in the brain corresponds to stage of AD, (2) there is a strong connection between hyperphosphorylated tau in CSF and severity of cognitive impairment and (3) using drugs to reduce tau oligomerisation results in improvement of cognitive functions.

1.6.3 Amyloid hypothesis

The amyloid hypothesis was established in 1992 by Hardy and Higgins, based on a study in the biochemical effects of the amyloid precursor protein processing and the discovery of an amino acid sequence called amyloid β peptide (Aβ). Aβ is a 4 kilo Dalton peptide which is the major element of amyloid plaques. The amyloid hypothesis has been postulated as a main influence in the causation of Alzheimer's disease which was determined by the imbalance in production and elimination of Aβ in the brain (Glenner and Wong 1984; Hardy and Higgins 1992). In 2002, Chechler and Vincent described that the neurodegenerative process in the brains of patients of Alzheimer's disease pathology was induced by an abnormal process of the amyloid precursor protein resulting in over production, aggregation and deposition (Checler and Vincent 2002). The order of events occurring in amyloid hypothesis was shown in Figure 1.6.1. Also, the principal of amyloid hypothesis has been modified over time due to the better understanding of the pathogenic nature of Aβ (Pimplikar 2008).

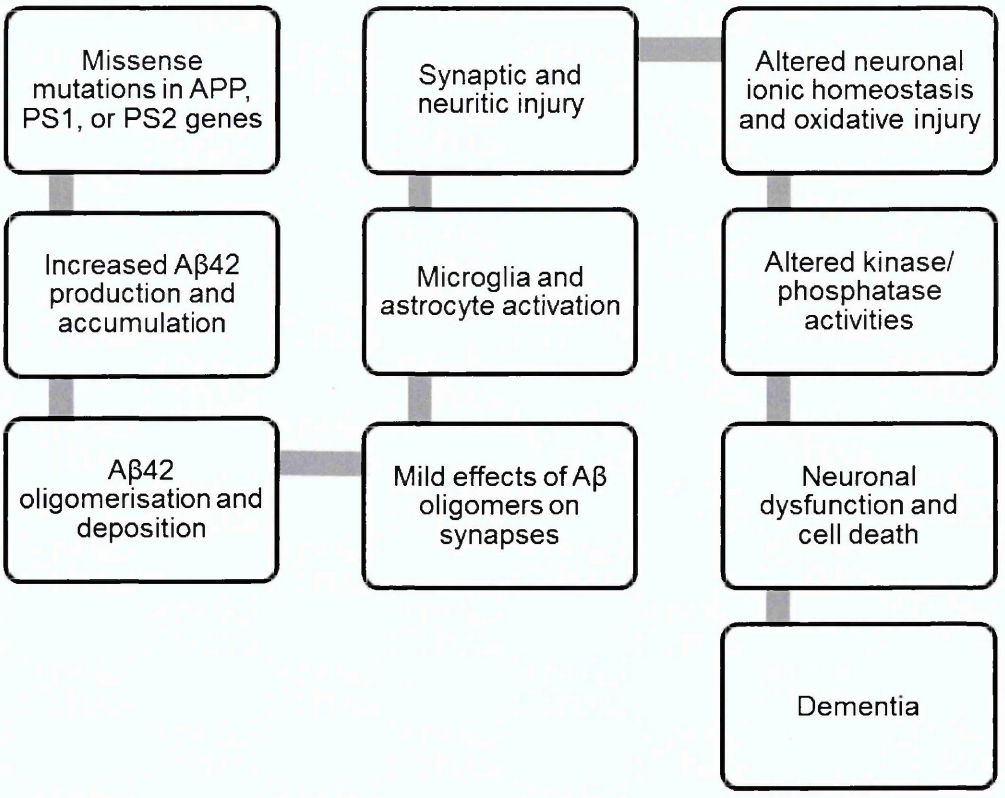

Figure 1.6.1 The order of events occurring in amyloid hypothesis (Hardy and Selkoe 2002).

Later, the amyloid hypothesis was partially questioned mainly due to the discrepancy of the severity of cognitive impairment and the number of plaques, including the presence of high numbers of plaques in cognitively healthy people (Pimplikar 2008). Also, there were four crucial debatable aspects which contributed to the amyloid hypothesis. Firstly, Alzheimer's disease pathogenesis was a result of the generation and elimination of Aβ peptide. Although this was supported by the confirmation of the direct correlation between presenilins and amyloid production which resulted in an increase in production of $A\beta_{42}$ in cell culture, transgenic mice models of AD and AD patients, however, the same could not be said for the apolipoprotein E4 since there has been no evidence suggesting the mechanism of this relationship. Secondly, Aβ peptide is toxic. Although the Aβ oligomers were proved to have an effect at the synapses, it was not a toxic effect and it only created minimal synaptic changes. It was reported that the behavioural improvement in APP transgenic mice was a consequence of Aβ immunisation. Thirdly, Aβ triggered neurofibrillary tangle dysfunction. This aspect presents a large area which required further investigation

since there has been no convincing evidence available. Finally, neuronal cell death is more likely to be caused by neurofibrillary tangle formation rather than amyloid deposition (Hardy 2009).

The most recent idea of amyloid hypothesis is the aggregation of soluble Aβ oligomers. This idea was supported by the fact that Aβ peptide is amphiphilic and the first 28 amino acid residues of Aβ are polar, while the latter 12-14 amino acid residues are non-polar. At neutral pH, the polarity of both termini of Aβ is enhanced resulting in Aβ aggregation and formation (Pimplikar 2008). Also, there were studies suggesting that there is a strong relationship between soluble Aβ, including soluble Aβ oligomers, and the severity of cognitive impairment (Yates and McLoughlin 2007).

Nevertheless, the post-mortem examination of the brains of AD patients unveiled great neuronal damage including dead neuronal cells and synaptic loss which has been postulated as a result of Aβ peptide (Yates and McLoughlin 2007). On the other hand, the neuronal cell death and synaptic loss could be the results of reactive oxygen species and nitric oxide production, decreased membrane fluidity, redox-active iron, inflammatory process and intracellular calcium accumulation (Kayed et al. 2003; Salminen et al. 2009; Vetrivel and Thinakaran 2010).

1.7 Current treatments

It was previously mentioned in Section 1.1.1 Epidemiology of AD, that global demography has changed because of low birth rates and longer life expectancies. As a consequence of the changes the total world population has been maintained, if not declined, and there has been a significant increase in the proportion of the ageing population; consequently the mean number of population having AD is higher. Also, the higher number of AD patients results in higher demand for health care and social services. These consequences have a huge impact on the global economy (Prince, Prina and Guerchet 2013).

At the present, there are four drugs; donepezil, rivastigmine, galantamine and memantine which were approved by the Food and Drug Administration (FDA) to be used as a symptomatic treatment of AD. These four drugs are classified into two

different groups according to mechanism of action; (1) acetylcholinesterase inhibitor (AChEI); donepezil, rivastigmine and galantamine and (2) N-methyl-D-aspartate (NMDA) receptor antagonist; memantine. Cholinesterase inhibitors are commonly used in AD patients with mild and moderate symptoms while the NMDA receptor antagonist is used in AD patients with moderate to severe symptoms (Salomone et al. 2011; Yiannopoulou and Papageorgiou 2013).

1.7.1.1 Acetylcholinesterase Inhibitors (AChEIs)

The usage of acetylcholinesterase inhibitor (AChEI) is mainly based on the cholinergic hypothesis of AD (see Section 1.6.1). The mechanism of action of AChEI is to inhibit acetylcholinesterase activity resulting in prolonged half-life of acetylcholine. In other words, by using AChEI the level of acetylcholine is increased. It was proposed in the cholinergic hypothesis that there was impairment in the cholinergic system during the early stage of AD. The impairment included a deficit in cholinergic activities due to a loss of cholinergic neurons which caused memory loss and cognitive functions declined. The AChEIs are often referred as an empirical treatment of AD. Interestingly, it was reported that there was no significant difference among each cholinesterase inhibitor and adverse reactions of these drugs is dose-dependent. Moreover, there was another drug which belonged to this group and it was the first of AChEI which was approved by the FDA; tacrine. However, tacrine was withdrawn from the market by the FDA due to acute hepatotoxicity (Lukiw 2012; Yiannopoulou and Papageorgiou 2013).

1.7.1.2 N-methyl-D-aspartate (NMDA) receptor antagonist

The neuronal excitotoxicity caused by excess glutamate has often been linked to the pathogenesis of AD (Yiannopoulou and Papageorgiou 2013) and it was supported by observations made in the brains of AD patients; the majority of dead neurons were glutamatergic neurons (Hynd, Scott and Dodd 2004). Under normal conditions, glutamate acts as a mediator in fast excitatory synaptic responses and involves in learning ability and memory function (Butterfield and Pocernich 2003). The excess glutamate is believed to cause continuous stimulation of NMDA receptors which eventually resulted in cell death. The mechanism of action of memantine is to bind to NMDA receptor and inhibit usual physiological activities of the receptor (Johnson and

Kotermanski 2006). Once memantine binds to NMDA receptors, it is able to inhibit continuous Ca^{2+} influx into neurons, hence preventing neuronal excitotoxicity (Parson, Stoffler and Danysz 2007). Therefore, memantine which is a NMDA receptor antagonist has been used in order to prevent the effect of excess glutamate and as a consequence the neurons regain normal functions (Lukiw 2012).

1.7.1.3 Other treatments

Despite the fact that at the present there is no effective treatment for AD which would be able to treat AD at its causes, prevent symptoms from worsening and restore the lost cognitive functions, the existing drugs are able to improve the quality of life of the AD patients, mostly up to 12 months (Alzheimer's Society 2014; Lukiw 2012). Besides symptomatic treatment drugs for AD, most patients usually require additional drugs; such as antidepressants to treat depression and apathy, and antipsychotics to treat hallucinations and delusions. The commonly prescribed antidepressants are selective serotonin reuptake inhibitors (SSRIs) such as fluoxatine, sertraline and citalopram; serotonin-norepinephrine reuptake inhibitors (SNRIs) such as mirtazapine and duloxatine; and non-tricyclic antidepressants (non-TCA) such as bupropion. The antipsychotics of choice are second generation antipsychotics (so called atypical antipsychotics) such as olanzapine and risperidone because of the weaker parkinsonian effect. Benzodiazepine acts on gamma-aminobutyric acid A ($GABA_A$) receptors and is often used in anxiety and agitation management. However, it was reported that benzodiazepines increased cognitive impairment (Alzheimer's Society 2014; Yiannopoulou and Papageorgiou 2013).

1.8 Background of the project

It has been over two decades since the amyloid cascade hypothesis was established (Hardy and Higgins 1992). The amyloid cascade hypothesis has provided the fundamental concept for understanding the pathogenesis of the Alzheimer's disease; the deposition of Aβ peptide, derived from APP, is the cause of Alzheimer's disease (Hardy and Higgins 1992; Nalivaeva and Turner 2013; Preece et al. 2004). Although several aspects related to APP: regulation of the expression, trafficking, post-

translational modification and proteolytic process are intensively studied and well understood (Dawkins and Small 2014), yet there are many questions remaining to be answered including the normal function of APP, the functional differences between different isoforms of APP and the physiological role of the APP metabolites (Belyaev et al. 2010; Nalivaeva and Turner 2013).

Moreover, effort has been made in order to gain a better understanding of the differences between the three main isoforms of APP; APP695, APP751 and APP770 using both animal and cellular models. Despite clear structural differences between the three APP isoforms; the presence and the absence of KPI and OX2 domains, few studies studied and directly compared these three isoforms of APP:

- *Belyaev et al.* (2010) reported that the APP695 was a preferred isoform, in comparison to APP751 and APP770, for proteolytic processing via the amyloidogenic pathway in neuronal cells. The experiment was carried out using neuronal cells transfected with expression vectors containing human APP isoforms (Belyaev et al. 2010). However, this proposal needs to be accepted with caution since there are some concerns regarding the experimental protocols such as the two different types of expression systems: pIREShyg containing human APP770 and pIREShyg2 containing human APP751 and APP695 used to generate stable clones, the absence of the standardisation of the clones and the changes in culture condition prior to the actual experiments.
- *Qiao Qui et al.* (1995) reported that the Aβ peptide produced from APP751 and APP770 strongly promoted neurite outgrowth of hippocampal neurons, in comparison to Aβ peptide produced from APP695. The experiment was carried out by co-culturing hippocampal neurons and CHO cells transfected with expression vectors containing human APP isoforms (Qiao Qiu et al. 1995).

Some studies categorised the experimental subjects into KPI^+ APP or KPI containing APP isoform (APP751 and APP770) and KPI^- APP or non-KPI containing APP isoform (APP695):

- *Chua, Lim and Wong* (2013) reported that the KPI^+ APP (i.e. APP751) lowered the expression of major mitochondrial enzymes significantly in comparison to KPI^- APP (i.e. APP695). The mitochondrial dysfunction associated with the

abnormal expression and function of mitochondrial enzymes along with an increase in KPI^+ APP are important features in the AD brain. This observation has confirmed the importance of KPI^+ APP isoform as a potential pharmacological target for the treatment of AD. The experiment was carried out using APP knock-out cell line transfected with expression vectors containing human APP695 representing KPI^- APP and APP751 representing KPI^+ APP (Chua, Lim and Wong 2013).

- *Khalifa et al.* (2012) reported that the KPI domain of APP751 facilitated APP dimerization. The native fold of the KPI domain is involved in the trafficking and processing of the APP to favour the non-amyloidogenic pathway. These observations have provided information regarding the functional differences between the isoforms of APP. The experiments were carried out using cell lines transfected with expression vectors containing APP isoforms where APP695 represented the KPI^-APP and APP751 represented KPI^+APP (Khalifa et al. 2012).
- *Matsui et al.* (2007) reported an increased expression of KPI^+ APP mRNA in the temporal neocortex which correlated to the protein level of KPI^+ APP. The study was carried out by examining temporal cortex tissue of the AD patients and the measurement values were reported as a total APP, KPI^+APP and KPI^+ APP ratio (KPI^+ APP divided by total APP) (Matsui et al. 2007).
- *Preece et al.* (2004) reported that the increased ratio of KPI^+ APP mRNA to KPI^- APP mRNA was the result of change in the cell population. These observations have further confirmed that KPI^+ APP isoforms are non-neuronal isoforms and suggested that a small change in the relative level of KPI^+ APP mRNA could significantly contribute to pathogenesis of AD. The experiment was carried out by examining the APP mRNA level in the brain tissue of AD patients and reported as an individual isoform such as APP695 and a combination of several isoforms such as APP C (695/714/751/770) (Preece et al. 2004).
- *Panegyres, Zafiris-Toufexis and Kakulas* (2000) reported an increase ratio of APP751 to APP695 in frontal and temporal regions. Since the KPI^+ APP isoforms were reported to be more amyloidogenic *in vitro*, this observation suggested the possibility that the progression of AD could be initiated as a consequence. The study was carried out by examining the brain tissue of AD patients to determine the relationship of the APP695 (KPI^- APP) and APP751 (KPI^+ APP).

Since the number of samples used in this study was small, the results obtained might not represent the general population (Panegyres, Zafiris-Toufexis and Kakulas 2000).

- *Moir et al.* (1998) reported the relative increase of the soluble form cerebral Aβ as APP695 and APP751 representing KPI^- APP and KPI^+ APP, respectively. The study was carried out by examining the brain tissue of the AD patients (Moir et al. 1998).
- *Brugg et al.* (1995) reported that the experimentally-induced inflammation causes a shift in APP isoforms, from APP695 to KPI^+ APP. This observation has suggested that inflammatory processes play a role in APP processing in relation to AD pathogenesis. The experiment was carried out using transgenic mice and reported the measurement values as APP695 and KPI^+ APP isoform (APP751 and APP770) (Brugg et al. 1995).

Some studies either studied one isoform of APP or made comparisons between wild-type APP and mutated APP:

- *Chasseigneaux et al.* (2011) reported that sAPPα was more efficient in enhancing the elongation of axons in comparison to sAPPβ and the elongation of axons related to a decrease in cell adhesion. The experiment was carried out using primary cortical neurons growing in the culture medium containing either sAPPβ or sAPPα generating from APP695 (Chasseigneaux et al. 2011).
- *De Strooper et al.* (1995) reported that the Swedish and Flemish mutation caused an increase in all APP metabolites while there was a significant reduction of APP metabolites produce from mouse APP. The experiment was carried out using rat hippocampal neuron transfected with mouse APP, human APP and human APP with mutations; Swedish and Flemish (De Strooper et al. 1995).
- *Haass et al.* (1993) reported that the APP which matures in the late Golgi and/or cell surface was predetermined to produce Aβ peptide without being processed in the lysosome. The experiment was carried out using HEK293 cells transfected with APP695 (Haass et al. 1993).
- *Liu et al.* (2003) reported that APP expression and secretion were enhanced by hepatocyte growth factor leading to an increase in Aβ peptide secretion in both

normal and Swedish mutation. The experiment was carried out using HEK293 cells transfected with wild-type human APP751 and human APP751 containing Swedish mutation. (Liu et al. 2003).

So far, there have been numerous animal and cellular models which have been created and used in AD studies. However they do have some limitations including an inability to completely reflect the AD pathology. For example, the Aβ peptide-obtained from rodents is less prone to the aggregation due to three amino acid differences within the Aβ domain (Fraser et al. 1992; Nalivaeva and Turner 2013). Despite the overexpression of human APP in transgenic mice, it was reported that the human APP is proteolytically cleaved differently in mice due to the lack of secretases specifically for human APP and the mouse models do not reflect the advanced stage of disease when a patient is diagnosed (Chow et al. 2010). Also, the treatments which are available for Alzheimer's disease either treat the symptoms or slow down the progression of the disease for a period of time. The treatments could not reverse the damage that has been done to the brain. Therefore, it is necessary to establish a suitable model to allow researchers to attain a better understanding of pathogenesis of the Alzheimer's disease in order to prevent or prolong the onset of the disease. Also, the model could also be used to develop the effective treatment or, even, a cure.

1.9 Aim and objectives

The aim of this project is to develop and validate the cellular model for studying amyloid precursor protein (APP) isoforms.

The objectives of the project are as follows:

- Develop an appropriate cell model of Alzheimer's disease using genetic manipulation of existing cell lines to secrete APP695, APP751 and APP770
- Investigate the effects of nutritional stress, using altered FBS concentration on APP isoforms expression and secretion
- Investigate the effects of energy deprivation, using 2DG on APP isoforms expression and secretion

Chapter 2: Materials and methods

2.1 Bacterial culture

Bacteria were grown two ways: agar-based cultures and liquid cultures performed according to different experimental requirements. The agar-based bacterial cultures were performed with the purpose of single colony identification and selection, carried out in petri dishes containing 25 ml of sterile LB broth agar and selective antibiotic. The LB agar plates were incubated overnight at 37 °C.

The liquid bacterial cultures were performed with the purpose of increasing the bacterial biomass to prepare for the further experiments such as plasmid DNA extraction (minipreparation). The liquid bacterial cultures were carried out in sterile 50 ml plastic tubes containing 10 ml of liquid LB broth and selective antibiotic. Once bacteria were suspended in the prepared liquid mixture, the tube was incubated overnight at 37 °C in a shaker at 200 rpm.

Negative control plates and tubes were always carried out alongside each of the bacterial culture procedures.

The amplicillin was used as the selective antibiotic in the bacterial culture and the concentration was 50-150 µg/ml. The bacteria used in this project were NEB 5-α competent *E.coli*.

2.2 Cryopreservation and recovery of bacteria

In order to cryopreserve bacteria, bacteria containing the expression vector were cultured at 37°C overnight in liquid culture and shaken at 200 rpm. 850 µl of the culture was transferred to a sterile tube before addition of 300 µl of 50% v/v sterile glycerol, which acted as cryopreservative agent. The culture was dispersed evenly by vortexting and stored as aliquots at -80°C.

In order to recover bacteria from cryopreservation, a sterile plastic loop was used to scrape the surface of frozen bacteria then immediately streaked onto LB agar plates containing selective antibiotic. LB agar plates were incubated overnight at 37°C and the cryopreserved bacteria tube was returned to be stored at -80°C.

2.3 Polymerase Chain Reaction (PCR)

The polymerase chain reaction (PCR) was developed during the 1980s for the purpose of DNA or RNA amplification. There are 3 main steps in the PCR process: (1) denaturation where double-strand DNA is separated, (2) annealing where primers bind to single-stranded DNA and (3) extension where the new complementary strand of DNA is synthesized by polymerase enzyme. However, in case of amplification of RNA, RNA is required to be transcribed into cDNA before the three-step PCR can begin (Schochetman, Ou and Jones 1988).

Polymerase chain reaction was generally performed as 50 µl reactions composed of 1 unit of Phusion® DNA polymerase (NEB), sterile water, 5x Phusion® HF buffer (NEB), 10 mM dNTPs mixture (NEB), 10 µM forward primer (Invitrogen), 10 µM reverse primer (Invitrogen) and 2 µl of template DNA. The primers are listed in Figure 3.2.1 in Chapter 3. Reaction was carried out using a Primus 96 ^{plus} PCR machine (MWG-Biotech). The standard amplification was performed with an initial denaturation at 98 °C for 2 minutes following by 30 cycles of denaturation at 98°C for 45 seconds, annealing at 54°C for 45 seconds and extension at 72°C for 2 minutes and 30 seconds, then final extension at 72°C for 5 minutes.

The other forms of PCR were also performed: Touchdown PCR (TD-PCR), Overlap Extension PCR (OE-PCR), Reverse Transcriptase PCR (RT-PCT) and quantitative Real-Time PCR. The last two types of PCR; Reverse Transcriptase PCR (RT-PCT) and quantitative Real-Time PCR are explained in Section 2.22.

TD-PCR is a well-known solution to reduce non-specific amplification and to avoid the need for extensive optimization of PCR reactions. The main concept of TD-PCR is to start the reaction with a high annealing temperature, usually higher than melting temperature (T_m) of the primers, and over 10-15 cycle period the annealing

temperature is decreased gradually; 0.5°C per cycle until the T_m of the primers is reached. Then the reaction continues with 20-25 cycles using the final touchdown temperature (Korbie and Mattick 2008). In other words, decreasing an annealing temperature over 10-15 cycles allows primers to bind to the template DNA at various temperatures which generates both correct and incorrect PCR products. Then over the last 20-25 cycles allows the correct product to be amplified. In this project TD-PCR reaction started with an initial denaturation at 95°C for 3 minutes following by 10 and 25 cycles step. The first 10 cycles began with denaturation at 95°C for 1 minute, annealing at 54°C for 45 seconds (temperature decreased by 0.5°C every cycle) and extension at 72°C for 2 minutes. The next 25 cycles started with a denaturation at 95°C for 1 minute, annealing at 50°C for 45 seconds and extension at 72°C for 2 minutes. The final step of this reaction was the final extension which was carried out at 72°C for 10 minutes.

OE-PCR was proposed as an alternative way to create mutations at a specific site within a DNA fragment and it has usually been the method of choice for genetic engineering (An et al. 2005; Bryksin and Matsumura 2010; Urban, Neukirchen and Jaeger 1997). The principal of OE-PCR is that two separated typical PCR reactions generated two DNA fragments which contained mutated overlapping regions introduced by the primers. When the two fragments are combined and extended by DNA polymerase, the strand serves as a template DNA for further amplification (Higuchi, Krummel and Saiki 1988). In this project, the two DNA fragments were generated by TD-PCR. The two fragments were assembled by preparation of 50 µl of reaction containing sterile water, 5x Phusion® HF buffer (NEB), 10 mM dNTPs mixture (NEB) and approximately 10 ng of each fragment. The assembled reaction was carried out in a Primus 96 ^{plus} PCR machine (MWG-Biotech). The OE-PCR reaction began at 97 °C for 4 minutes followed by 75 cycles at 95 °C for 15 seconds with 0.5 °C decrease in temperature every cycle. The reaction was then placed on ice before an addition of 1 unit of Phusion® DNA polymerase (NEB) and heated at 72 °C for 3 minutes and placed on ice. The 10 µM of forward and reverse primer from 5' end and 3' end of the full length PCR product were added to the reaction following by the standard PCR steps.

2.4 Restriction enzyme digestion

Restriction enzyme digestion is the method used to obtain the DNA fragments which suitable for further analysis or experiments. This method allows the enzyme to cleave DNA at specific sites to produce DNA fragments of interest (Goodsell 2002; Hartl and Jones 2005). In this project, both single and double restriction digestions were carried out as 50 µl reactions containing 10 units of each restriction enzyme, 1 µg of plasmid DNA, 5 µl of 10x NEBuffer 4, 5 µl of 1 mg/ml BSA, with the volume adjusted to 50 µl with deionized water. Single restriction digestion was incubated at 37 °C for 2 hours then inactivated at 80 °C for 20 minutes. Whereas double restriction digestion was performed using two restriction enzymes; AflII and BstBI that have different working temperature, so the first enzyme was added to the reaction and incubated at 37 °C for 2 hours then the second enzyme was added. Once the second enzyme was added, the reaction was incubated at 65 °C for 2 hours before 20 minutes of inactivation of the restriction enzymes at 80 °C. The vector map containing restriction sites can be found in Figure 3.5.1.

2.5 Ligation

The selected method for joining DNA fragments and linearised plasmids together was ligation using T4 DNA Ligase (NEB). The 20 µl ligation reaction contained 1 µl T4 DNA Ligase, 2 µl of 10x ligase buffer, 0.02 pmol of linearised vector, 0.06 pmol of DNA fragment and the final volume was adjusted to 20 µl with deionized water. The amount of DNA fragment was usually three times of the amount of linearized DNA (in molar terms) and the T4 DNA Ligase was added last. Ligation reaction was carried out at 16 °C for 4 hours (adapted from Sambrook and Russell 2001).

2.6 Agarose gel electrophoresis

Agarose gel electrophoresis is used to separate DNA fragments using a property of DNA: the negative charge. DNA has a negative charge due to the presence of

phosphate groups on its backbone therefore the DNA migrates toward the anode during electrophoresis when an electric field is applied across an agarose gel. The agarose has pores which allow the DNA to be separated according to its size and shape as well as its charge. The smaller molecules of DNA have higher mobility rate hence migrating through the porous matrix faster in comparison to the larger molecules, thus using agarose gel also allows approximate size measurement for DNA.

In order to detect the DNA on agarose gel, ethidium bromide (EtBr) was used. Also EtBr does not require a de-staining step and can be added to the gel prior to setting. Ethidium bromide intercalates itself between the base pairs of DNA to enable fluorescence visualization.

Throughout the project 1% agarose gels were used. The Tris acetate EDTA (TAE) buffer was prepared as 10x stock solution by dissolving 48.4 g Trizma base in 750 ml de-ionized water, adding 11.42 ml glacial acetic acid and 20 ml of 0.5 M EDTA (pH 8.0) solution, and brought the final volume up to 1 L with de-ionized water. The final pH of TAE buffer was adjusted to 8.3 and the buffer was stored at room temperature. Preparation of a 1% agarose gel was carried out by dissolving 0.5 g agarose powder (Bio-Rad) in 50 ml of 1x TAE buffer; 5 ml of 10x TAE buffer diluted in 45 ml de-ionized water. Before pouring the gel, 2 µl of 10 mg/ml ethidium bromide was added and mixed thoroughly. Once the gel was poured the plastic comb was placed in order to create loading wells. The agarose gel was allowed to set for at least 15 minutes at room temperature. DNA loading buffer (6x) was prepared by dissolving 25 mg bromophenol blue in 1 ml de-ionized water, adding 3 ml glycerol and making up the final volume to 10 ml using de-ionized water.

Prior to running the agarose gel, 1 µl of 6x DNA loading buffer was added to 5µl of each DNA sample and mixed thoroughly by pipetting before loading onto each well of the gel. A 1,000 base-pair (bp) DNA ladder (Sigma-Aldrich and NEB) was prepared by adding 1 µl of 6x DNA loading buffer to 5 µl DNA ladder and mix thoroughly by pipetting. The agarose gel was run at 100 volt for 60 minutes before being visualized using a UV light box at 302 nm and captured on UVP camera with LabWorks software.

2.7 Gel extraction

Gel extraction procedure was used to isolate the DNA fragments of interest from agarose gels after electrophoresis. The procedure was carried out using a spin column of Qiaquick gel extraction kits (Qiagen). The 500 µl of QG buffer was added to the gel piece in microcentrifuge tubes and heated at 60 °C for at least 10 minutes or until the gel piece was completely melted. The QG buffer facilitated the binding of DNA fragments to the silica membrane of the spin column at high salt conditions. Also, the QG buffer contained a pH indicator which allowed the optimal pH ≤ 7.5 to be maintained to maximise DNA binding. After an additional of 100 µl of isopropanol, the melted gel was transferred to the Qiaquick spin column where DNA fragments were then absorbed to silica membrane by centrifugation at 13,000 rpm for 1 minute. The flow-through was discarded before another 500 µl of QG buffer was added to the spin column in order to remove the trace of agarose gel on the silica membrane. The flow-through from 1 minute centrifugation at 13,000 rpm was discarded. The remained high salt on the silica membrane was removed by adding 750 µl of PE buffer (10 mM Tris-HCl, pH7.5 and 80% v/v ethanol). The PE buffer and existing ethanol in the PE buffer were removed by centrifugation twice for 1 minute each time at 13,000 rpm. In short, the impurities, including agarose gel, ethidium bromide and ethanol, did not bind to silica membrane of spin column therefore impurities flowed through the membrane after centrifugation step. The DNA fragment was eluted into 1.5 ml Eppendorf tubes from the spin column by adding 50 µl of EB buffer (Tris-Cl, pH 8.5) following by centrifugation at 13,000 for 1 minute.

2.8 Plasmid preparation

The purpose of plasmid preparations is to prepare plasmid DNA for further experiments. In this project the plasmid preparation was carried out at small scales which will be referred to as minipreparation. Minipreparation was carried out using QIAprep Spin Miniprep Kit (Qiagen) according to the manufacturer's standard protocol. The principle of this method is to extract plasmid DNA from bacteria by using alkaline lysis with SDS. In details, 24 hours before starting the minipreparation procedure, a

selected colony was inoculated into 2 ml LB broth containing 50 µg/ml ampicillin and inoculated overnight at 37 °C in a shaker at 200 rpm. Minipreparation was carried out at room temperature. The next day, bacterial cells pellet were harvested by centrifuged 1.5 ml of overnight culture at 13,000 rpm for 2 minutes. Then the pelleted bacteria were resuspended completely with 250 µl of P1 buffer by vortexing. Then the 250 µl P2 of buffer was added to suspended bacterial to lyse the cells and mixed by inverting tube four times. The bacterial cell lysate was then neutralized and adjusted to high-salt by adding 350 µl of N3 buffer, the high salt aiding DNA-column binding. At this point, protein, chromosomal DNA and cellular debris were degraded and precipitated while small plasmid DNA was still intact and retained in solution. The solution after adding N3 buffer was transferred onto Qiaprep spin column and centrifuged at 13,000 rpm for 1 minute and the flow through was discarded. The silica membrane of spin column was washed by adding 500 µl and 750 µl of PB and PE buffer respectively before centrifugation at 13,000 rpm for 1 minute. The flow through obtained from each centrifugation step was discarded. Although, both, PB and PE buffers are wash buffers, the PB buffer was used to inhibit the activity of nuclease from host strain and PE was used to precipitate any leftover acid residue from the membrane. Finally, the plasmid DNA was eluted from the silica membrane by adding 50 µl of EB buffer (Tris-Cl, pH 8.5) before centrifugation at 13,000 rpm for 1 minute (Qiagen).

2.9 Transformation of NEB 5-α competent *E.coli*

The transformation method for NEB 5-α competent *E.coli* recommended by the manufacturer (NEB) was the heat shock method. In short, a tube of competent cells was thawed on ice for 10 minutes then 100 ng of plasmid DNA was added. The tube was agitated four times to mix plasmid DNA and competent cells. The tube was placed on ice for 10 minutes and heat shocked at 42 °C for exactly 30 second before placing the tube back on ice for 5 minutes. Next, 950 µl of SOC (2% Vegetable Peptone 0.5% Yeast Extract, 10 mM NaCl, 2.5 mM KCl, 10 mM MgCl2, 10 mM MgSO4 20 mM Glucose) medium at room temperature was added to the transformation reaction tube. The SOC medium allowed NEB 5-α competent *E.coli* to recover from the

heat shock procedure. The transformation reaction tube was incubated for 60 minutes at 37 °C in a vigorous shaker at 200 rpm. Finally, 100 µl of transformed cells was transferred onto warm LB agar plate containing 50 µg/ml ampicillin and incubated overnight at 37 °C.

2.10 Sequencing

DNA sequencing was performed by Eurofins MWG Operon. The plasmid DNA samples were sent at 50-100 ng/µl. Purified PCR products were sent at 100 ng/µl due to its size being greater than 1,000 bp. Along with samples, primers were sent at 15 pmol per primer. Generally, sequencing was carried out on strands of DNA that were no longer than 1,000 base pairs otherwise the sequencing result was not reliable. Therefore, throughout the study, sequencing was carried out as a two-step process. The first step, the DNA was sequenced from both ends of the PCR products. The results obtained from the first sequencing then were used to design another pair of primers. These pair of primers was then used in sequencing process in order to complete the full sequence.

2.11 Cell culture

Cell culture media, antibiotics and cell counting equipments were obtained from Gibco™ Invitrogen UK unless stated otherwise. All cell culture methods and procedures were carried out under sterile conditions in a class II lamina air flow cabinet.

2.11.1 Cell line stock

Chinese Hamster Ovary (CHO) cells and Human Embryonic Kidney (HEK293) cells were preserved in 1 ml of heat-inactivated fetal bovine serum (HI-FBS) (Biosera) containing 10% (v/v) dimethyl sulfoxide (DMSO) (Sigma-Aldrich). Cells were stored in cryovials in a liquid nitrogen Dewar until required for use.

2.11.2 CHO culture

The CHO cell stock in a cryovial was thawed quickly at 32 °C and grown in a cell culture incubator at 37°C and 5% CO_2 in a 25 cm^2 flask containing 6 ml complete media. The complete medium consisted of Dulbecco's Modified Eagle's medium (DMEM) Glutamax II which contained 10% (v/v) HI-FBS, 1% penicillin-streptomycin (100 units/ml and 0.1 mg/ml, respectively). Once cells were determined to be more than 80% confluence, cells were passaged into new 25 cm^2 flasks by removing culture media and washing cells using 5 ml of 1x Dulbecco's Phosphate Buffer Saline (PBS) solution. The cells were incubated in 3 ml of Dulbecco's Trypsin-EDTA solution (containing 0.25% (v/v) trypsin and 0.38 g/l EDTA) at 37°C for 5 minutes. The flask was tapped gently if the cells were not completely detached from the flask. The reaction of Trypsin-EDTA was stopped by adding 3 ml of complete medium and the cell suspensions were transferred to 50 ml Falcon tubes. Cell suspensions were centrifuged at 1,000 rpm for 5 minutes and supernatant was discarded. The cell pellet was re-suspended in 10 ml of complete medium and 1 ml of cell suspension was dispensed into a new 25 cm^2 flask to make up 1:10 passage ratio; adding 1 ml of cell suspension to 5 ml of complete medium. In order to allow cells to grow, flasks were incubated at 37 °C and 5% CO_2.

2.11.3 HEK293 culture

HEK293 cells were cultured in a similar procedure to that used to culture CHO cells.

2.11.4 Cell counting

Cells were counted by combining 10 µl of cell suspension to 10 µl of 0.4 % Trypan blue and mixed thoroughly. 10 µl of the cell's mixture was then transferred onto Countess® Cell Counting Chamber Slides. The cells were counted using the Countess® Automated Cell Counter which determined the number of cell in total/ml, the number of live cells/ml, the number of dead cells/ml and the percentage of cell viability. The principle of Trypan blue stain is that the live (viable) cells with the intact cell membrane are able to prevent the dye entering the cells whereas dead cells with compromised cell membrane do not have that ability, therefore being stained by the dye.

2.12 Cryopreservation and resurrection of mammalian cells

In order to cryopreserve mammalian cells, cells were cultured according to methods described in Section 2.11. After centrifugation, the cell pellet was re-suspended in 1 ml of cryopreservative solution; 90% HI-FBS and 10% DMSO before being transferred to cryo-vial. The vial was kept in -80 °C freezer for 24 hours before transferring to a liquid nitrogen Dewar for long-term storage purpose.

In order to resurrect mammalian cells from cryopreservation, the cryo-vial was removed from liquid nitrogen Dewar and thawed quickly. The vial was wiped using 70% Ethanol. Cells were transferred to 15 ml tubes before adding 3 ml of warm complete medium drop wise. Cells were centrifuged at 1,000 rpm for 5 minutes and re-suspended with 6 ml of fresh complete medium.

2.13 Antibiotic kill curve

The antibiotic kill curve procedure was used to determine the optimal concentration of a selective antibiotic for transfection. The optimal concentration of a selective antibiotic is just enough to kill all the host cells after 4-7 days and this optimal concentration is used in transfected colony selection after the transfection procedure. The general idea of antibiotic selection is that the host cells taking up the expression vector benefit from an antibiotic resistance gene carried in the vector therefore the host cells are able to survive in the presence of the antibiotic. The concentration of the antibiotic for colony selection was twice the concentration used for maintenance.

The selection of stably transfected cell line was carried out using two antibiotic selectable markers on two different expression vectors; hygromycin resistant gene in pIREShyg2 and neomycin resistant gene in pcDNA3.1. Throughout this project, hygromycin B (Sigma-Aldrich) and geneticin (G418) (Sigma-Aldrich) were used as selective antibiotics. The suggested concentration of Hygromycin B for CHO cells ranges from 50-600 μg/ml therefore the five chosen concentrations for selection were 50, 100, 200, 400 and 600 μg/ml and the control concentration was 0 μg/ml. The suggested concentrations of G418 are 200-400 μg/ml for CHO cells and 400-1000

μg/ml for HEK293 cells, therefore the five chosen concentrations and a controlled concentration for CHO selection were 0, 100, 200, 300, 400 and 500 μg/ml. Whereas concentrations for HEK293 selection were 0, 200, 400, 600, 800, 1000 μg/ml. In brief, 2.5 x 10^5 cells/well were dispensed onto each well of six-well plate and allowed to adhere at least 6 hours before adding selective medium containing varied concentrations of the selective antibiotic. Cells were observed and photographed with camera attached to the microscope and the XLI cap program, every day for 7 days.

2.14 Transfection

Due to the properties of the phospholipid bilayer of cell membranes, water soluble molecules such as nucleic acid are prevented from entering mammalian cells. Therefore, a transfection agent is an ideal solution for gene delivery into mammalian cells. Transfection can be carried out in different ways such as particle bombardment (micro particle, such as gold is loaded with nucleic acid, was then directly injected into cell nucleus), electroporation (applying the short-term electric field to the cells resulting in an increased permeability of the cell membrane) or lipid formulation (liposome vesicle containing nucleic acid fuse to cell membranes and allowed nucleic acid to transfer) (Hahn and Scanlan 2010). In this project, plasmid DNA was introduced into nuclei of the host cells to allow the expression of recombinant genes by using Lipofectamine® LTX with Plus™ Reagent (Invitrogen).

Lipofectamine® LTX with Plus™ Reagent is a transfection agent which is classified as a lipid formulation forming cationic liposome vesicles. Plasmid DNA can be delivered by liposomes in two ways; plasmid DNA is carried within the enclosed vesicle of the liposome or plasmid DNA was integrated into the phospholipid bilayer of the liposome. The cationic lipid forming liposome is usually comprised of cationic and zwitterionic lipids which allowed liposomes to interact and fuse to cell membranes, respectively, in order to deliver plasmid DNA into host cells (Hahn and Scanlan 2010).

The transfection procedure was carried out in 24-well plates according to the manufacturer's standard protocol. The preparation of cells was done one day before starting the transfection procedure. For each well, CHO 4 x 10^4 cells and HEK293 1.25 x

10^5 cells were plated in 500 µl of complete medium and allowed to adhere overnight or grow up to 80% confluence. The DNA-Lipofectamine complex was prepared for each well by diluting 500 µg of plasmid DNA with 100 µl of DMEM-Glutamax I® without FBS, then add 1 µl of PLUS™ Reagent and the mixture was then incubated for 5 minutes at room temperature. The 3 µl of Lipofectamine® LTX was added to the diluted DNA solution and DNA-Lipofectamine® LTX complexes to form by incubating the mixture for 25 minutes at room temperature. The complete medium was removed from each well and replaced with 500 µl of fresh DMEM-Glutamax I® without FBS and 100 µl of DNA-Lipofectamine® LTX complexes. The 24-well plate was incubated at 37 °C with 5% CO_2 incubator for 24 hours before selection with antibiotic for 4-7 days and then processing limited dilution cloning.

2.15 Limited dilution cloning

Limited dilution cloning is a technique used in molecular cell biology experiments to obtain single cells which can then be expanded into a clone. The main principle of this technique is that a heterogeneous population is separated in order to generate a homogeneous population by carrying out a series of dilutions in a 96-well plate (Figure 2.15.1). The limited dilution cloning was carried out twice before the selective culture medium was screened for protein expression.

Cells were cultured, trypsinised and resuspended according to cell culture procedure in Section 2.11. A 100 µl of selective medium was dispensed to every well of 96-well plate, apart from A1 well. The cell suspension was prepared at 2 x 10^4 cells/ml and 200 µl of prepared cell suspension was dispensed to well A1. Then 100 µl of cell suspension in A1 well was transferred vertically down the column; from B1 well to H1 well. The final 100 µl was discarded. Also, during the transfer, the cell suspension was mixed thoroughly by pipetting gently to avoid creating bubbles. Another 100 µl of selective medium was added to the first column of the 96-well plate and mixed gently using multi-channel pipette. The 100 µl of cell suspension in the first column was then transferred horizontally across the plate; from column 1 to 12. Again, the final eight of 100 µl from each row was discarded and during the transfer the cells suspension was

mixed thoroughly but gently to avoid bubble formation. The final volume of each well was adjusted to 200 µl by adding 100 µl of selective culture medium. The plate was incubated at 37 °C with 5% CO_2 for at least a week until required, and at the same time the plate was observed under phase microscopy for wells containing single colonies. The plate set up diagram is shown in Figure 2.15.1. The chosen wells containing single colonies were then expanded into 12-well plates and then 6-well plates. The cells were allowed to grow to at least 50% confluency in 12-well plates before transfer to 6-well-plates. Once the cells in the 6-well plate grew at least to 50% confluence, they were proceeded with the repeat of limited dilution cloning procedure. At the end of the second limited dilution cloning procedure, cells were grown in complete medium with additions of antibiotic at concentrations one half of that obtained from the kill curve, and cells were allowed to grow until 80% confluence before culture medium was collected for protein expression screening.

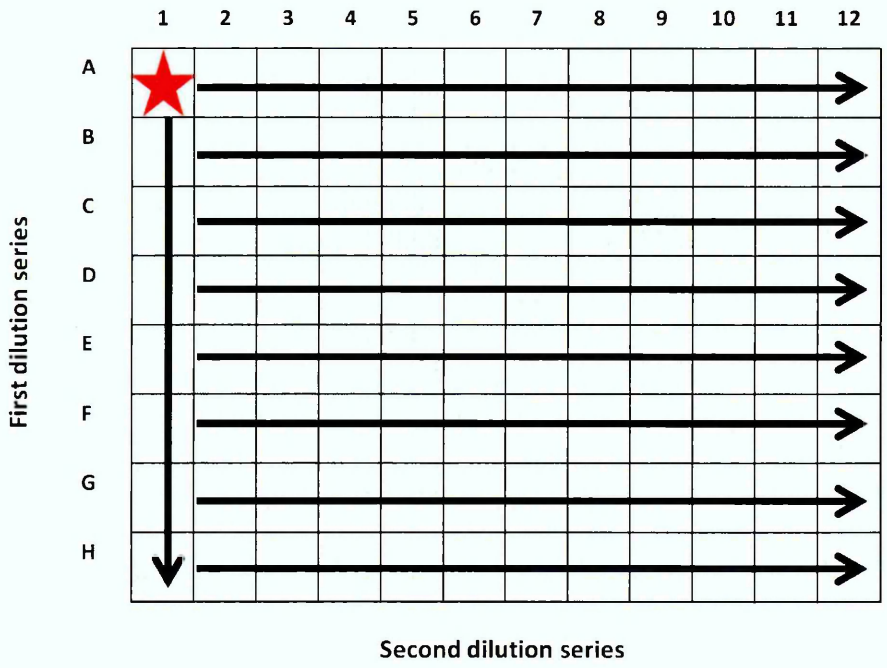

Figure 2.15.1 A plate set up for limited dilution cloning procedure in a 96-well plate. The plate was prepared as described in Section 2.15. The cells were transferred and mixed thoroughly but gently using pipette. The dilution of the cells was carried out from the well A1 to H1 first before it was carried out horizontally. The cell suspension from well H1 and column 12 were discarded. The plate was then put back in the incubator.

2.16 Immunoprecipitation

Immunoprecipitation is the method used to isolate proteins of interest from a complex solution by using a specific antibody. Cell culture medium was collected at various points of time throughout this project dependent on the nature of experiment. The immunoprecipitation procedure was carried out in 1.5 ml Eppendorf tubes. Each reaction contained 1 ml of cell culture medium, 250 µl of anti-Aβ DE2 (mouse monoclonal supernatant), 100 µl of 10x Tris Buffer Saline (TBS; 0.2 M Tris, 1.5 M NaCl) pH 7.5 and 50 µl of 50% slurry anti-mouse IgG agarose beads (Sigma-Aldrich). Sample was mixed by rotating for 1 hour at room temperature then centrifuged at 13,000 rpm for 1 minute and the supernatant was discarded. For double immunoprecipitation; additional 1.0 ml of cell culture media and 100 µl of 10x TBS were added to the precipitated agarose beads and mixed by rotation for 1 hour at room temperature. The samples were centrifuged at 13,000 rpm for 1 minute and the supernatant was discarded. The beads were washed three times with 1.0 ml of 1x TBS, centrifuged at 13,000 rpm and the supernatant was discarded. In order to dissociate samples from the beads, 100 µl of 2x SDS-PAGE sample buffer containing 30.8 mg/ml of DTT was added and heated at 60 °C for 10 minutes. The 2x sample buffer was prepared by dissolving 308 mg of DTT in 10 ml of 0.5 M Tris-HCl pH 6.8 following by addition of 2 ml of 10% SDS, 3 ml of 60% glycerol and 0.5 ml of 2 mg/ml bromophenol blue.

2.17 Reduction and alkylation of disulphide bonds

In order to facilitate the binding of antibodies which were used in the project, especially 993 and 1151, the disulphide bonds within the target protein molecules must be broken. After the sample was dissociated from the beads with SDS-PAGE sample buffer, sample was allowed to cool down for 15 minutes at room temperature before adding fresh 5 µl of 400 mM iodoacetamide then the sample was mixed by rotation for 1 hour at room temperature. The sample was centrifuged at 13,000 rpm for 1 minute before loading onto SDS-PAGE gel.

2.18 Sodium Dodecyl Sulfate polyacrylamide gel electrophoresis

The sodium dodecyl sulfate polyacrylamide gel electrophoresis (SDS-PAGE) is a method used to separate macromolecules such as protein based mainly on molecular weight. The typical gel electrophoresis procedure cannot be used to determine the molecular weight of biological molecules because the mobility of a molecule in the gel depends on both its charge and size. Therefore, it is necessary to treat the protein in order to obtain the uniform charge to mass ratio by using 2x SDS-PAGE sample buffer containing 30.8 mg/ml of DTT). At this point, the separation on the gel is primarily based on the polypeptide size.

The gel consists of 2 parts: stacking and resolving gels. The stacking gel is located at the upper part of the gel and usually contains a large pore size with low pH (pH 6.8) whereas the resolving gel is located at the bottom part of the gel and usually contains smaller pore size with higher pH (pH 8.8)

Throughout this project 5% stacking gel were used with 6% and 8% resolving gel. SDS-PAGE gels were prepared using the following stacking and resolving gel mixes:

Resolving gel

	6%	8%
Deionised water	2.6 ml	2.3 ml
30% Acrylamide/Bis	1.0 ml	1.3 ml
1.5M Tris-HCl pH 8.6	1.3 ml	1.3 ml
10% (w/v) SDS	0.05 ml	0.05 ml
10% (w/v) ammonium persulphate	0.05 ml	0.05 ml
TEMED	0.004 ml	0.003 ml
Total solution volume (per gel)	5 ml	5 ml

Stacking gel

	5%
Deionised water	1.4 ml
Acrylamide/Bis	0.33 ml
0.5M Tris-HCl pH 6.6	0.25 ml
10% (w/v) SDS	0.05 ml
10% (w/v) ammonium persulphate	0.05 ml
TEMED	0.002 ml
Total solution volume (per gel)	2 ml

2.19 SDS-PAGE running conditions and immunoblotting

SDS-PAGE gels were run typically at room temperature at 0.4A for 1 hour and then transferred onto nitrocellulose membranes. SDS-PAGE running buffer was prepared as 10x stocking concentration consisted of 250mM Tris, 1.92 mM Glycine and 1% SDS. Prior to transfer, the nitrocellulose membrane was wetted in transfer buffer (25mM Tris, 192mM glycine and 10% methanol, pH 8.3). The transfer process was carried out at 0.4 A for 1 hour.

The immunoblotting procedure was carried out at room temperature on the rocking rack. To start the procedure, the nitrocellulose membrane was blocked in 5% W/V non-fat dry milk in TBST for 30 minutes (0.05% V/V Tween 20 (Sigma-Aldrich) in 1x TBS). Then, the membrane was incubated in primary antibody solution for 90 minutes at room temperature followed by two washes with 25 ml TBST for 5 minutes on the rocking rack. The antibodies used in this project are listed and shown in Figure 2.19.1. The membrane was then incubated in secondary antibody solution for 45 minutes. The secondary antibody was selected according to origin of primary antibody; DE2 primary antibody paired with anti-mouse secondary antibody while 23/2, 993, 1151 primary antibody paired with anti-rabbit secondary antibody. The membrane was washed twice with 25 ml TBST for 5 minutes and once with 10 ml deionised water for 10 minutes. Both washes were carried out on the rocking rack. If the secondary antibody solution was either IRDye 680RD Goat anti-Mouse IgG or IRDye 680RD Goat anti-

Rabbit, the membrane was visualised using an infrared fluorescent imaging system (Li-Cor Odyssey, Li-Cor) whereas using AP conjugated secondary antibody, the membrane was developed in 10 ml reconstituted BCIP/NBT solution (Sigma-Aldrich) for 30 minutes.

Antibody	Description		Dilution
	Function	Binding	
DE2 (mouse)	Immunoprecipitation	Aβ domain on APP	1:5.6
	Primary antibody solution	Aβ domain on APP	1:10
23/2 (rabbit)	Primary antibody solution	OX2 domain on APP	1:250
993 (rabbit)	Primary antibody solution	KPI domain on APP	1:250
1151 (rabbit)	Primary antibody solution	N-terminal of APP	1:250
Anti-mouse AP-linked	Secondary antibody solution	DE2 antibody	1:1000
Anti-rabbit AP-linked	Secondary antibody solution	23/2, 993 and 1151 antibody	1:1000
IRDye 680RD Goat anti-Mouse IgG	Secondary antibody solution	DE2 antibody	1:20000
IRDye 680RD Goat anti-Rabbit IgG	Secondary antibody solution	23/2, 993 and 1151 antibody	1:20000

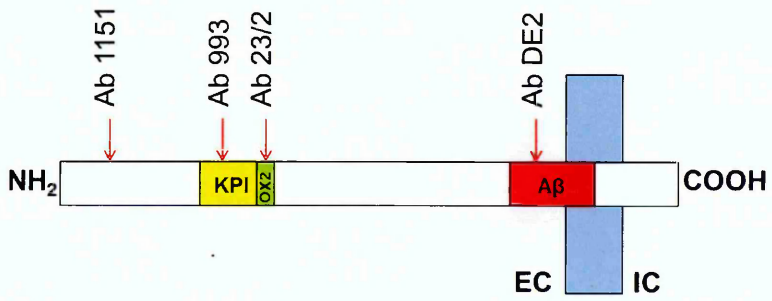

Figure 2.19.1 (top) antibodies used in immunoprecipitation and immmunoblotting procedure. (bottom) antibodies recognition of APP.

2.20 RNA extraction

RNA extractions from cell culture were carried out using RNeasy Mini Kit (Qiagen) which uses spin technology to obtain total RNA from cultured cells. The RNA extraction from HEK293 cells was carried out according to the manufacturer's standard protocol. In brief, $1x10^6$ HEK293 cells were harvested and prepared as cell pellets in 1.5 ml microcentrifuge tubes by centrifugation at 10,000 rpm for 1 minute. The lysis buffer (RLT; containing guanidinium salt), originally prepared by manufacturer, was added 10 µl of β-mercaptoethanol (β -ME) per 1 ml of RLT buffer. 600 µl of β -ME/RLT buffer was added to each cell pellet and the pellets loosened by agitating the tube. The β-ME/RLT buffer inactivated RNases therefore providing intact RNA. The cell lysate was homogenised thoroughly by passing through a 20 gauge needle before adding 600 µl of 70% ethanol. The homogenised lysate including precipitates was transferred to an RNeasy spin column placed in a 2 ml collection tube and centrifuged at 13,000 rpm for 15 seconds. The flow-through was discarded and the spin column contained bound total RNA was saved.

The bound total RNA on the membrane of spin column placed in collection tube was washed by adding 700 µl of washing buffer 1 (RW1) then centrifuged at 13,000 rpm for 15 seconds. After the flow-through was discarded, the spin column was washed twice with 500 µl of washing buffer 2 (RPE) by centrifugation at 13,000 rpm firstly for 15 seconds then 2 minutes. The purpose of the 2 minute centrifugation was to dry the spin column ensuring that the spin column was dry and ethanol free before eluting the total RNA, the spin column was placed on a new 2 ml collection tube and centrifuged at 13,000 rpm for 2 minute. The spin column was placed on a new 1.5 collection tube and 50 µl of RNase-free water was added directly to the spin column membrane followed by centrifugation at 13,000 rpm for 1 minute. The purified total RNA was stored at -80°C.

2.21 Quantification of RNA samples using NanoDrop ND-1000 UV-VIS Spectrophotometer

The precise quantity of total RNA was quantified using a NanoDrop ND-1000 UV-VIS Spectrophotometer in the RNA nucleic function (RNA40) where the concentration was determined at 260 nm. RNase/DNase free water was used to initialise the spectrophotometer and was used as a blank. In order to obtain the total RNA concentration value, 1 µl of each total RNA sample was loaded onto machine. Moreover, the acceptable purity of RNA was determined by OD 260/OD 280 ratios: 1.8-2.0.

2.22 The principle of Reverse Transcriptase PCR (RT-PCR) and quantitative Real-Time RT-PCR

Quantitative real-time RT-PCR is a procedure used to detect and quantify the expression of a gene of interest. In order to begin quantitative real-time RT-PCR, mRNA is converted to complementary DNA (cDNA) using reverse transcriptase enzyme. Next, the cDNA undergoes repetitive amplification steps or the thermal cycle of quantitative real-time RT-PCR resulting in the synthesis of numerous copies of DNA of interest exponentially. The amplified product was measured after every cycle via the use of fluorescence labelled molecules which accumulate after each amplification cycle. Figure 2.22.1 shows the mechanism of action of taqman probe. The fluorescence intensity was reported as a semi-log graph between the variations of log (ΔRn) with PCR cycle number; where ΔRn is the difference between the fluorescence signal from the reporter and the background fluorescence. The example of the semi-log graph obtained from quantitative real-time RT-PCR was shown in Figure 2.22.2.

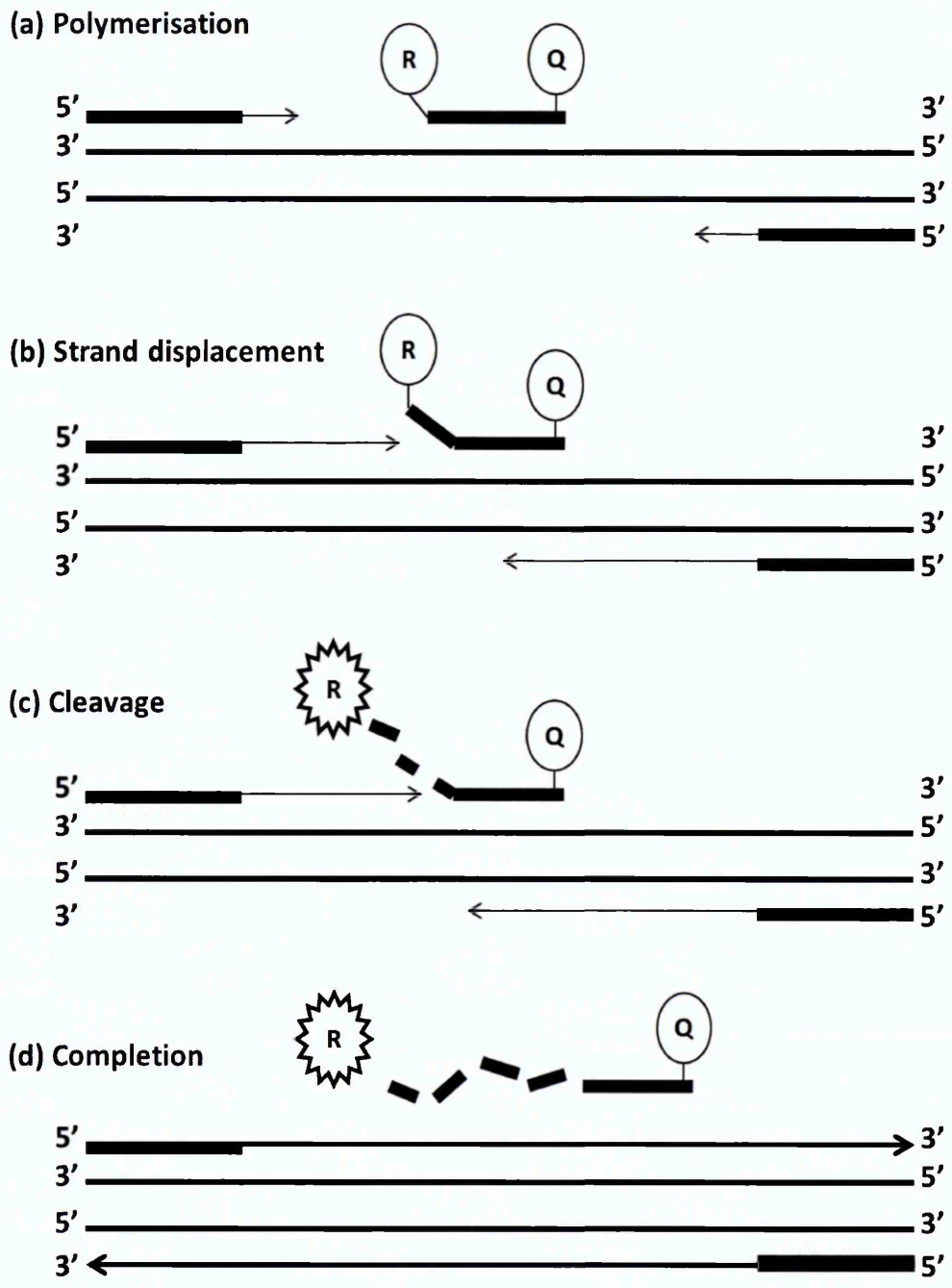

Figure 2.22.1 The mechanism of action of Taqman probe in real-time RT-PCR. The TaqMan probe contains a fluorophore at the 5' end and a quencher on the 3' end, rendering the molecule non-fluorescent. During the real-time RT-PCR amplification, the probe binds to the template. When the polymerase encounters the probe at the 5' end, it starts the cleaving process and releasing the fluorophore into solution (Applied Biosystems 2014).

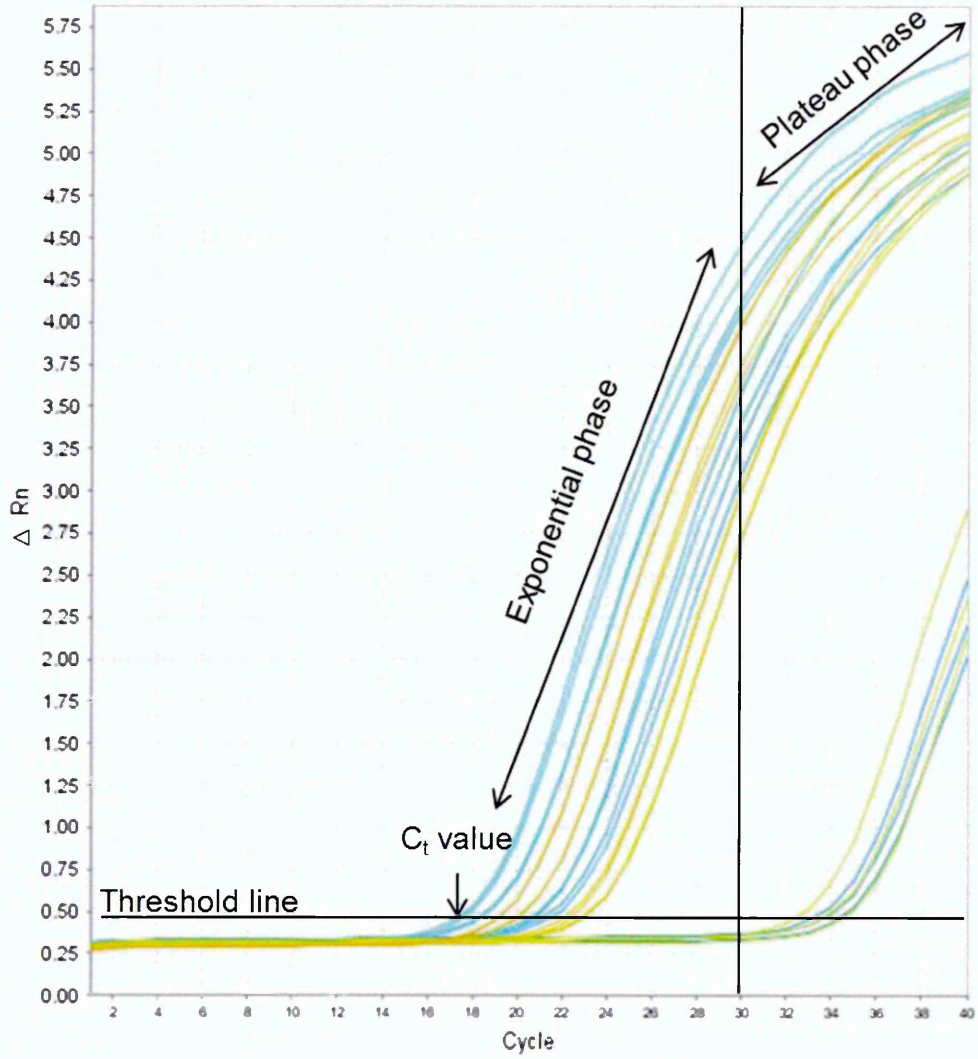

Figure 2.22.2 Quantitative real-time RT-PCR semi-log graph consisted of exponential phase and plateau phase. In the exponential phase, there were plenty amounts of reagents for the PCR reactions therefore the PCR products were doubled every cycle. These PCR reagents, however, decreased as the PCR reactions moving toward the end of exponential phase which slowing down the PCR products amplification. In the plateau phase, all the reagents were used up and eventually the PCR reactions stopped.

Key: C_t value; Cycle threshold value

2.23 Complementary DNA synthesis from RNA sample for real-time RT-PCR

The complementary DNA synthesis was carried out using QuantiTect Reverse Transcription Kit (Qiagen). Total RNA (1µg) was transferred to 0.2ml microcentrifuge tube before adding 2 µl gDNA Wipeout buffer. The tube was incubated at 42 °C for 2 minutes in Primus 96 plus PCR machine (MWG-Biotech). This step allowed contaminating genomic DNA to be removed which enhances the accuracy of real-time RT-PCR result. Then, RNA was reversed transcribed to cDNA by adding 6 µl of reverse-transcription master mix; 1 µl Quantiscript Reverse Transcriptase, 1 µl RT Primer mix and 4 µl of 5x Quantiscript RT Buffer. The final volume was adjusted to 20 µl using RNase/DNase free water. The tube was incubated at 42 °C for 15 minutes to activate the reverse transcriptase following with inactivation of the enzyme at 95 °C for 3 minutes.

The negative controls for cDNA synthesis were carried out using the same protocol as mentioned above but without RNA as one negative control and replacing 1 µl Quantiscript Reverse Transcriptase with 1µl of RNase/DNase free water.

2.24 Reference gene assessment for use in real-time RT-PCR

A reference gene is also known as a housekeeping gene. Also, it is acknowledged that the expression of a reference gene does not change under various experimental conditions in order to maintain cellular functions. Determination of suitable reference genes for real-time RT-PCR is crucial since all of gene expression measurements are normalised against the value of reference genes. In this project, the geNorm™ PLUS Reference Gene Selection kit (PrimerDesign), which is a set of primers of twelve candidates reference genes, was used to obtain the reference gene expression value which was analysed using geNorm software. The details of twelve reference gene candidates are shown in Figure 2.24.1.

The twelve candidate reference genes were obtained in lyophilised form and the tubes were centrifuged briefly at 10,000 rpm for 15 second to avoid spillage when opening.

Each primer was prepared by addition of 220 µl RNAse/DNAse free water before re-suspending completely by vortexing.

The reference genes assessment was carried out using MicroAmp® Optical 96-Well Reaction Plate (Applied Biosystem) and StepOnePlus™ Real-Time PCR Systems. Each real-time PCR reaction consisted of 1 µl of 5 ng/µl cDNA, 1 µl of re-suspended primer mix, 10 µl of PrimerDesign Precision™ 2x qPCR Mastermix and RNAse/DNAse free water. The negative control reactions were carried out using 1 µl of no reverse transcriptase enzyme cDNA, 1 µl of no RNA cDNA and replacing cDNA with 1 µl of RNAse/DNAse free water. The real-time PCR reaction began with enzyme activation at 95 °C for 10 minutes followed by 50 cycles of 15 seconds denaturation at 95 °C and 1 minute data collection at 60 °C. The thermocycle of real-time RT-PCR using SYBR green® is shown in Figure 2.24.2.

Gene symbol	Description and functions	Anchor nucleotide	Context length sequence (bp)	Amplicon length (bp)
ERCC6	Homo sapiens excision repair cross-complementing rodent repair deficiency, complementation group 6. Encoding DNA-binding protein for transition and excision repair.	2170	160	121
UBE2D2	Homo sapiens ubiquitin-conjugating enzyme E2D 2. Regulated degradation of misfolded, damaged or short-live protein.	952	168	127
UBE4A	Homo sapiens ubiquitination factor E4A (UFD2 homolog, yeast). Encoded ubiquitin ligase family involving in chromosome condensation and separation.	2764	94	88
ENOX2	Homo sapiens ecto-NOX disulfide-thiol exchanger 2. Encoded cell surface NADH oxidase.	879	148	114
PRDM4	Homo sapiens PR domain containing 4. Transcription factor of the PR-domain protein family.	2346	174	128
SCLY	Homo sapiens selenocysteine lyase. Catalyzed the pyridoxal 5-prime phosphate-dependent conversion of L-selenocysteine to L-alanine and elemental selenium.	928	138	111
TYW1	Homo sapiens tRNA-yW synthesizing protein 1 homolog (S. cerevisiae). Stabilized codon-anticodon interaction in the ribosome.	1186	163	126
RNF20	Homo sapiens ring finger protein 20. Regulated chromosome structure.	2735	175	129
CHO14ORF	Homo sapiens chromosome 14 open reading frame 133. Involved in the sorting of lysosomal proteins.	448	166	122
ACTB	Homo sapiens actin, beta. Encoded actin proteins.	1195	106	92
GAPDH	Homo sapiens glyceraldehyde-3-phosphate dehydrogenase. Encoded glyceraldehyde-3-phosphate dehydrogenase protein family.	1087	142	110
18S	Homo sapiens 18S rRNA gene.	235	99	93

Figure 2.24.1 Table reference genes analyzed for expression stability in gene expression experiments. Twelve human reference genes in geNorm™ PLUS Reference Gene Selection kit were assessed for expression stability between non-transfected HEK293 and selected clone of HEK293 transfected APP isoforms, also the stability of reference genes in experimental conditions.

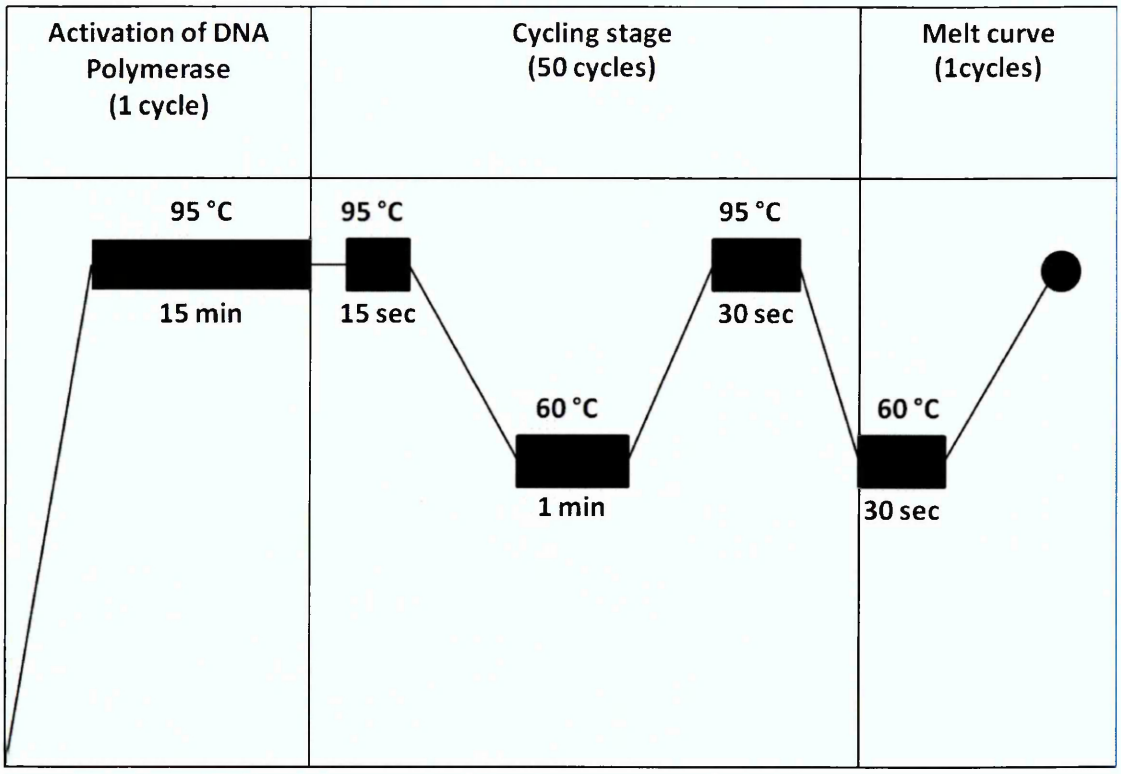

Figure 2.24.2 SYBR green® real-time RT-PCR thermocycler protocol. The reference genes stability assessment was carried out using real-time RT-PCR mastermix containing SYBR green and subjected to the thermocycle shown above. The thermocycler protocol for SYBR green composed of 3 main steps: (1) a cycle of DNA polymerase activation at 95 °C for 15 minutes. (2) 40 cycles of amplification of target gene and (3) melt curve. The melt curve was carried out due to the possible non-specific binding which may occur. The melt curve was used to distinguish specific PCR product from non-specific one. Also, the melt curve initially started at 60 °C with an increase of 0.5 °C per cycle until the final temperature reached 95 °C.

2.25 Reference gene stability assessment

The reference gene transcript stability of non-transfected and transfected HEK293 was determined using the following method. Each 15 µl SYBR Green real-time RT-PCR reaction (Section 2.24) was prepared in triplicate for each of the individual 12 reference genes (Figure 2.24.1) in order to compare between non-transfected HEK293 and selected clone of HEK293 transfected APP isoforms, and the stability of reference genes under experimental conditions; variation in FCS and an additional of 2-Deoxy-D-glucose. The three negative control reactions were carried out using 1 µl of no reverse transcriptase enzyme cDNA, 1 µl of no RNA cDNA and replacing cDNA with 1 µl of RNAse/DNAse free water. The samples were assessed by carrying out real-time RT-PCR reaction in the StepOnePlus™ Real-Time PCR Systems according to standard thermal protocol showed in Figure 2.24.2.

The result of the real-time RT-PCR performance was obtained as the cycle threshold (C_t) value of each sample. These values were later exported from the PCR system and analysed using GeNorm software (Biogazelle). The software processed C_t values and analysed the stability of the reference genes by sequential removal of these gene after calculation of the pair-wise correlations of all probabilities which eventually left a pair of the most stable reference genes represented with expression stability values (M) (Pfaffl et al. 2004; Vandesompele et al. 2002). The most stably expressed reference genes were then used as gene transcript quantification references to quantify the relative expression of the genes of interest throughout the gene expression experiments.

The GeNorm software (Biogazelle) not only analyzed the stability of reference genes (M-value) but it also generated a pair-wise variation value (V). The V-value was used as a guideline to determine the minimum number of reference gene required for normalization in gene expression experiments and the V-value at 0.15 was used as a cut-off point. The V-value was given as $V_{n/n+1}$ and If V_n has V-value less than 0.15, then it was not necessary to introduce an additional reference gene in that gene expression experiment.

2.26 Conditions and components of TaqMan® real-time RT-PCR reaction

The TaqMan® real-time RT-PCR master mix consisted of 5 µl of TaqMan® Fast Universal Master Mix (Applied Biosystems), 0.5 µl of TaqMan® assay probe (Applied Biosystems) and 3.5 µl of RNAse/DNAse free water. Master Mix was prepared for the total number of reactions plus 10 % for potential pipetting errors. Each individual reaction contained 1 µl of cDNA sample and 9 µl of master mix. 1 µl of cDNA sample obtained from reaction in the absence of reverse transcriptase, no RNA reaction and RNAse/DNAse free water were used as negative controls. The MicroAmp® Optical 96-Well Reaction Plate (Applied Biosystems) was set up according to the nature of each experiment and then sealed with MicroAmp® Optical Adhesive Film (Applied Biosystems). The reaction plate was placed in the StepOnePlus™ Real-Time PCR Systems and subjected to the amplification.

The amplification condition consisted of two main steps which started with enzyme activation, at 95 °C for 10 minutes followed by 40 cycles of denaturation and data collection. The denaturation was carried out at 95 °C for 15 seconds and data collection was carried out at 60 °C for 1 minute. The thermocycle of real-time RT-PCR using TaqMan is shown in Figure 2.26.1.

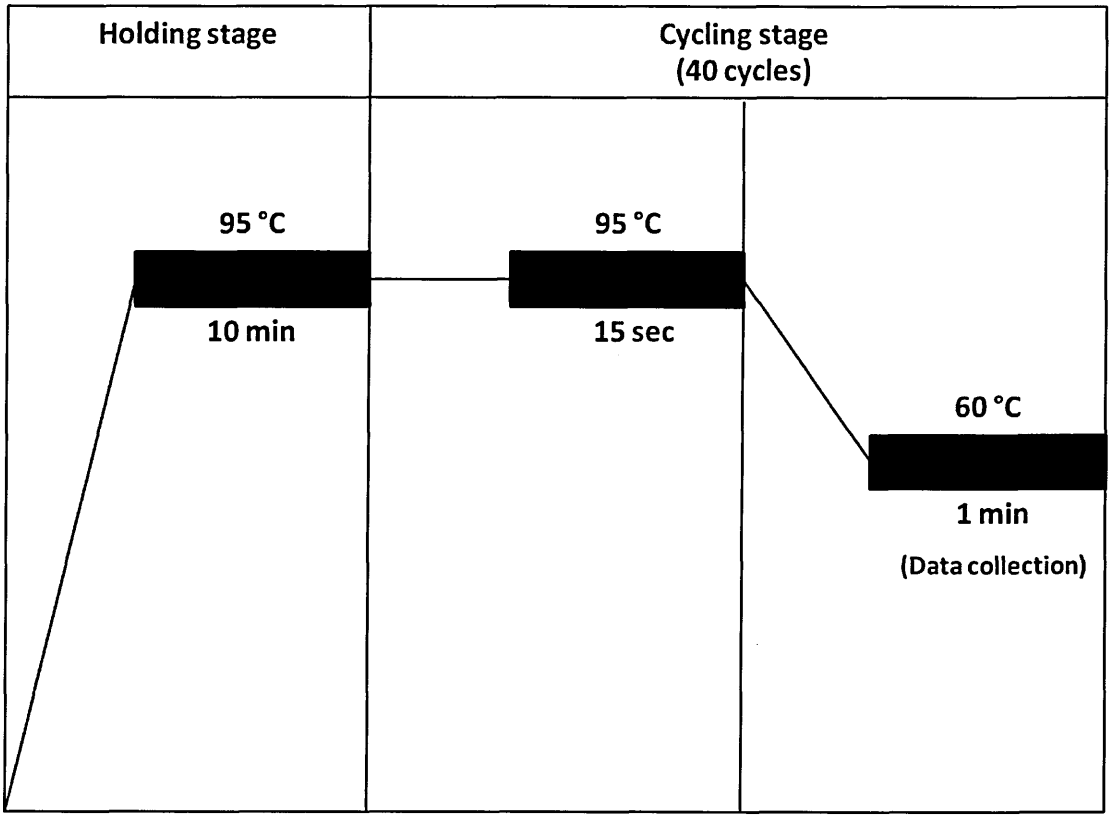

Figure 2.26.1 The thermocycle used for TaqMan® real-time RT-PCR. The thermocycle of TaqMan® real-time RT-PCR began with a cycle of holding stage at 95 °C for 10 minutes following by 40 cycles of the cycling stage where cDNA of interest was amplified. Each cycle of the cycling stage consisted of an amplification step at 95 °C for 15 second and data collection step at 60 °C for 1 minute where the cycle threshold (C_t) value was obtained.

2.27 Primer efficiency assessment

The efficiency of primers used in real-time RT-PCR experiments was determined to ensure that they were effective and reliable. The cDNA obtained from a conversion of total extracted RNA from cell pellets was diluted into four dilutions: 1:5, 1:10, 1:50 and 1:100 by adding appropriated volume of RNAse/DNAse free water. Each dilution was prepared in triplicate in the MicroAmp® Optical 96-Well Reaction Plate by adding 1 µl of each diluted cDNA sample and 9 µl of TaqMan® real-time RT-PCR master mix of each set of primers. The reaction plate was placed in the StepOnePlus™ Real-Time PCR Systems and amplified according to standard procedure stated in Section 2.26.

According to the method described in "A *new mathematical model for relative quantification in real-time RT–PCR*" by Michael W. Pfaffl in 2001, the C_t values gained from each sample and each set of primers were plotted into an individual semi-log graph between dilution of cDNA and C_t values (X-axis and Y-axis, respectively). The slope was generated using linear regression analysis. Then the slope of each graph was used in the followed formula to determine efficiency of each primer: Efficiency = $10^{-(1/slope)}$ (Pfaffl 2001). In addition, efficiency (E) is obtained as a number such that value of 1 means there is no PCR product in each cycle or a value of 2 which means PCR product was amplified doubly in every cycle. In addition to the slope of the graph the function also generated the linear correlation coefficient (R^2). The R^2 value generally represents the strength of relationship between two values or how close the data is to the trend line and normally ranges from -1 to +1, and an R^2 value of higher than 0.99 was considered as acceptable.

2.28 Real-time RT-PCR data analysis

There are two ways to analyse data obtained from real-time RT-PCR experiments: (1) absolute quantification which determines definite copy numbers of gene of interest based on an absolute standard curve and (2) relative quantification which determines approximate amount of fold difference of gene of interest either based on differences between C_t value of gene of interest and control and reference genes or a standard curve. The first quantification method is normally used for viral copy number

determination. The second quantification method is typically used in gene expression studies (Applied Biosystems 2014).

The reference gene in relative quantification was used as a normalizer in order to monitor changes of other genes during transcription. Although, this method of analysing real-time RT-PCR data does not require highly precise standard curves due to the use of normalizer and controls but it is essential that the expression of the reference genes is highly stable across samples. Also, results obtained from this method are easily interpreted. For example, value of 1 is given when an expression of gene of interest is equal to the expression of the reference gene; a value of less than 1 is given when the expression of the gene of interest is less than the expression of reference gene and a value of more than 1 is given if the expression of the gene of interest is higher than the expression of the reference gene.

To date, there are two available and commonly used relative quantification models. The first model is:

$$\text{Fold difference} = 2^{-\Delta\Delta Ct}$$

Where $\Delta\Delta C_t = \Delta C_{t\ sample} - \Delta C_{t\ control}$; $\Delta C_{t\ sample}$ is the difference of mean of C_t between the gene of interest and the reference gene of the sample; $\Delta C_{t\ control}$ is the difference of mean of C_t between control and reference gene of control. The fold difference in gene expression can be determined using this model assuming that primer efficiency of the sample (gene of interest) and the reference genes are 2: $E_{sample} = E_{reference} = 2$. Therefore, this model was used only for general assessment of relative expressions of the gene of interest. Also, this model is used when percentage of primer efficiency (E) is within the acceptable range of 90-110%.

The second model takes the actual primer efficiency into account which makes this model more complicated than the first model:

$$\text{Fold difference} = E_{sample}^{\Delta Ct\ sample} / E_{reference}^{\Delta Ct\ reference}$$

Where E_{sample} is the primer efficiency of gene of interest; $E_{reference}$ is the primer efficiency of a reference gene; $\Delta C_{t\ sample}$ is the difference of the mean of C_t between the

control and the gene of interest; $\Delta C_{t\ reference}$ is the difference of the mean of C_t between the reference gene of control and the reference gene of the sample.

2.29 Statistics

Statistical analysis was performed using the program Prism (GraphPad Software Inc.). Two-way ANOVA and the Bonferroni's multiple comparison test were performed in order to determine the possible effects of independent factors; isoforms of APP and concentration of foetal calf serum (FCS) or 2-deoxy-D-glucose (2DG) in the culture media.

Chapter 3: Confirmation of APP770 construct and generation of APP751 and APP695 constructs (pIREShyg2)

3.1 Introduction

As stated in the introduction Chapter (Chapter1, Section 1.3.1), there are three main isoforms of APP: APP695, APP751 and APP770, which may be involved in the pathogenesis of Alzheimer's disease (AD). In order to determine which isoform of APP might be more likely to be involved in AD pathogenesis, the first objective was to obtain separate expression vectors containing each of the three isoforms of APP. Once the expression vectors containing three human APP isoforms were generated, the next objective was to stably express the expression vectors in mammalian cells using a transfection procedure, and selecting the clone from each APP isoform which expressed each APP isoform at a similar level.

3.2 Method for confirmation of APP770 construct

An expression vector, pIREShyg2 encoding APP770 (shown in Figure 3.5.1), was kindly provided by Professor Nigel Hooper (University of Leeds) as an *E.coli* stab culture. However, to confirm the presence of APP770 and its location in the multiple cloning sites of the vector, the multiple cloning site of pIREShyg2 required sequencing as the expression plasmid was to be used as a basis to generate APP751 and APP695 constructs.

3.2.1 Primer design

The sequence of pIREShyg2 was obtained as well as sequences of AflII and BstBI restriction sites via Addgene online database (http://www.addgene.org/browse/sequence_vdb/3180/) and the pIREShyg2 vector information provided by Clontech Laboratories. Every pair of primers used in this experiment was designed using online

software; Primer3 Input v.0.4.0 (http://bioinfo.ut.ee/primer3-0.4.0/primer3/). The first pair of primers was designed to bind to the multiple cloning site of pIREShyg2 outside AflII and BstBI restriction sites for the purposes of amplification and then sequencing APP770. The pair of primers consisted of a forward primer APP770_Lf and a reverse primer APP770_Rt. The detail of these primers is shown in Figure 3.2.1.

In order to obtain a significant amount of pIREShyg2 expressing APP770, *E.coli* from the stab culture was streaked onto LB-agar plates containing 50 µg/ml amplicillin to obtain single colonies which were then used as an inoculum for an overnight growth in 5 ml liquid medium. Subsequently, plasmid DNA was extracted using the QIAprep Spin Miniprep Kit and its presence was confirmed by agarose gel electrophoresis (as shown in Figure 3.2.2). Once purified and confirmed, the integrity of the plasmid was primarily verified by double restriction enzyme digestion analysis; at the AflII and BstBI restriction sites in the plasmid DNA and gel electrophoresis before sequencing. The result obtained from double restriction enzyme digestion is shown in Figure 3.2.3. Each sequencing process was only able to generate a limited number of sequences. Therefore, after obtaining the sequencing results, another pair of primers was designed in order to complete the APP770 sequence.

3.2.2 Sequence alignment

Each sequencing result was aligned against the human APP770 (huAPP770) sequence obtained from the online database of European Molecular Biology Laboratory (EMBL) using online software; BLAST 2 Sequences (Bl2seq) via National Centre for Biotechnology Information (NCBI) webpage which allowed the obtained nucleotide sequence alignments to be compared to known reference sequences without searching the whole online database. The alignment results are shown in Figure 3.2.4 (a) to (d) and Figure 3.2.4 (e) represents the alignment to the complete APP770 sequence.

No.	Primer		
	Name	Sequence (5'-3')	Purposes
1.	APP770_Lt	TCACTATAGGGAGACCCAAGC	Amplifying and sequencing APP770
2.	APP770_Rt	GAGGGAGTACTCACCCCAAC	Amplifying and sequencing APP770
3.	APP770A_Lt	AATTCTTACACCAGGAGAGGAT	Sequencing APP770
4.	APP770A_Rt	CCAAGACGTCATCTGAATAGTT	Sequencing APP770
5.	APP751_Rt_Front	TGTTGTAGGAATGGCGCTGCCACACACG	Amplifying and sequencing APP751
6.	APP751_Lt_Back	CCATTCCTACAACAGCAGCCAGT	Amplifying and sequencing APP751
7.	APP695_Rt_Front	TGCTGTTGTAGGAACGAACCACCTCTTCCACAG	Amplifying and sequencing APP695
8.	APP695_Rt_Back	AAGAGGTGGTTCGTTCCTACAACAGCAGCCAGT	Amplifying and sequencing APP695

Figure 3.2.1 Table stating primer names, sequences and purposes.

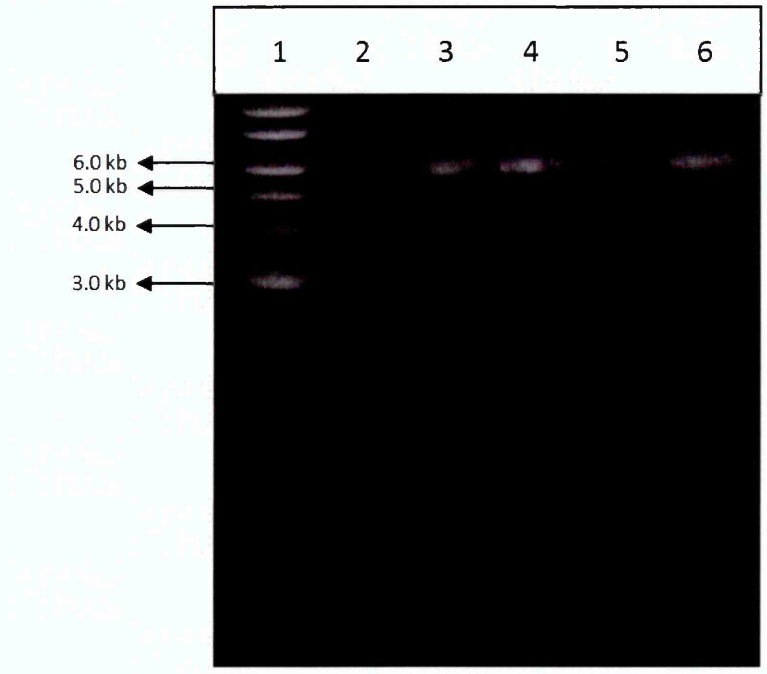

(a)

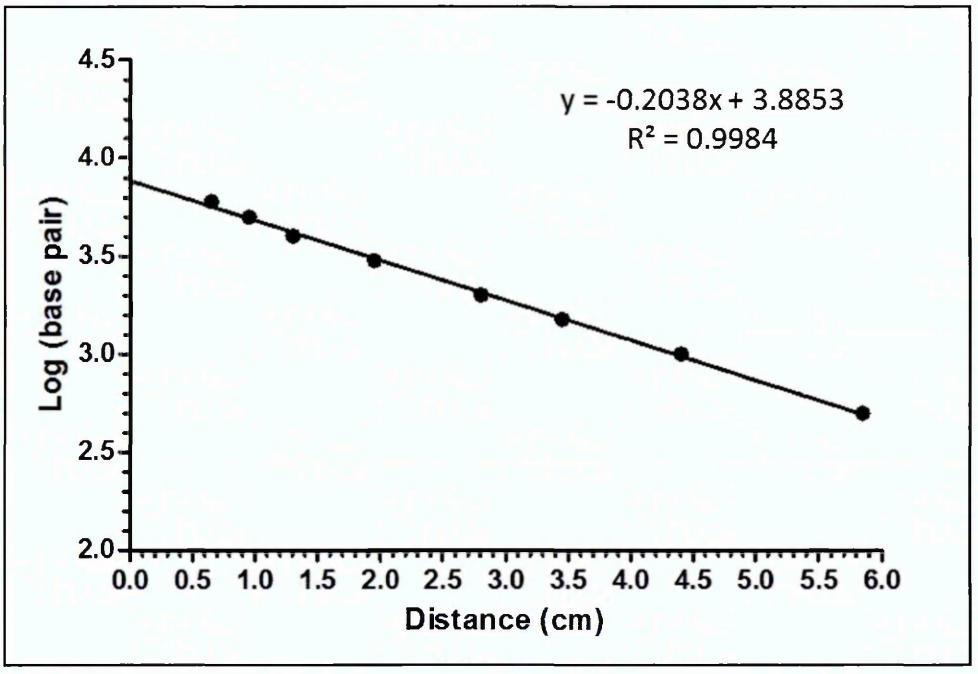

(b)

Figure 3.2.2 The purified plasmid using QIAprep Spin Miniprep Kit® on 1% agarose gel. Lane 1, 1 kb DNA Ladder; lane 2, negative control (without plasmid); lanes 3 to 6, purified plasmid obtained from minipreparation procedure, its size was approximately 6.0 kb. (b) The graph illustrated the distance of the bands and the number of base pair of DNA ladder and as average distance of the plasmid DNA was 0.7 cm which was predicted to be 5.8 kb.

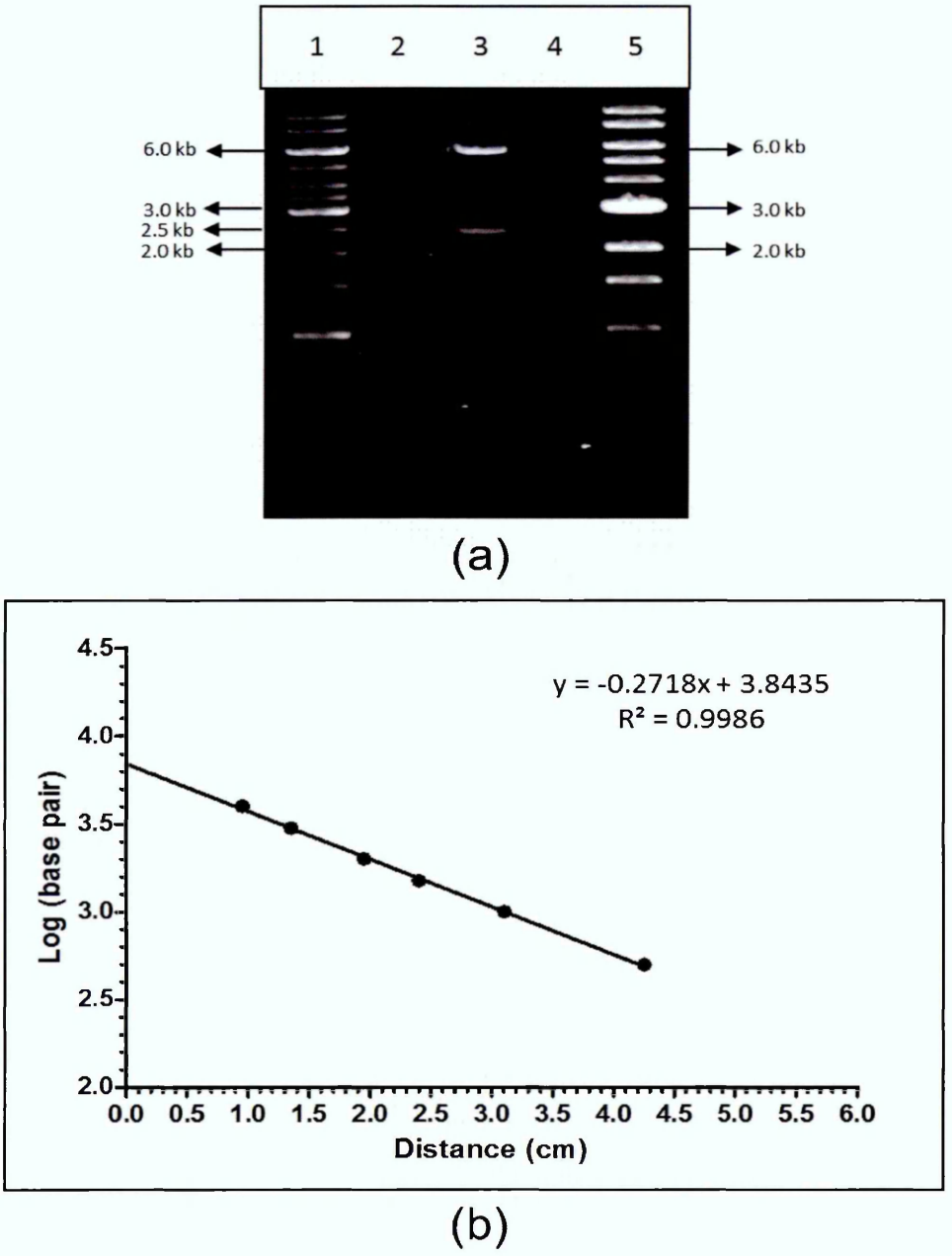

Figure 3.2.3 The restriction enzyme digestion of plasmid DNA containing APP770 sequence. (a) Plasmid DNA digested with restriction enzymes, AflII and BstBI, and analysed on a 1% agarose gel. Lane 1, GeneRuler™ 1 kb DNA Ladder used as a size marker; lane 2 and 4 are negative controls (without plasmid DNA); lane 3, plasmid DNA digest with AflII and BstBI - upper band is approximately 6.0 kb and lower band is approximately 2.5 kb; lane 5, 1kb DNA Ladder. The upper band was linearized pIREShyg2 and the lower band was APP770 sequence as an insertion. (b) The graph illustrates the migration distance of the bands and the number of base pairs of DNA ladder and as the migration distance of the digested product was 1.75 cm which was predicted to be 2.5 kb.

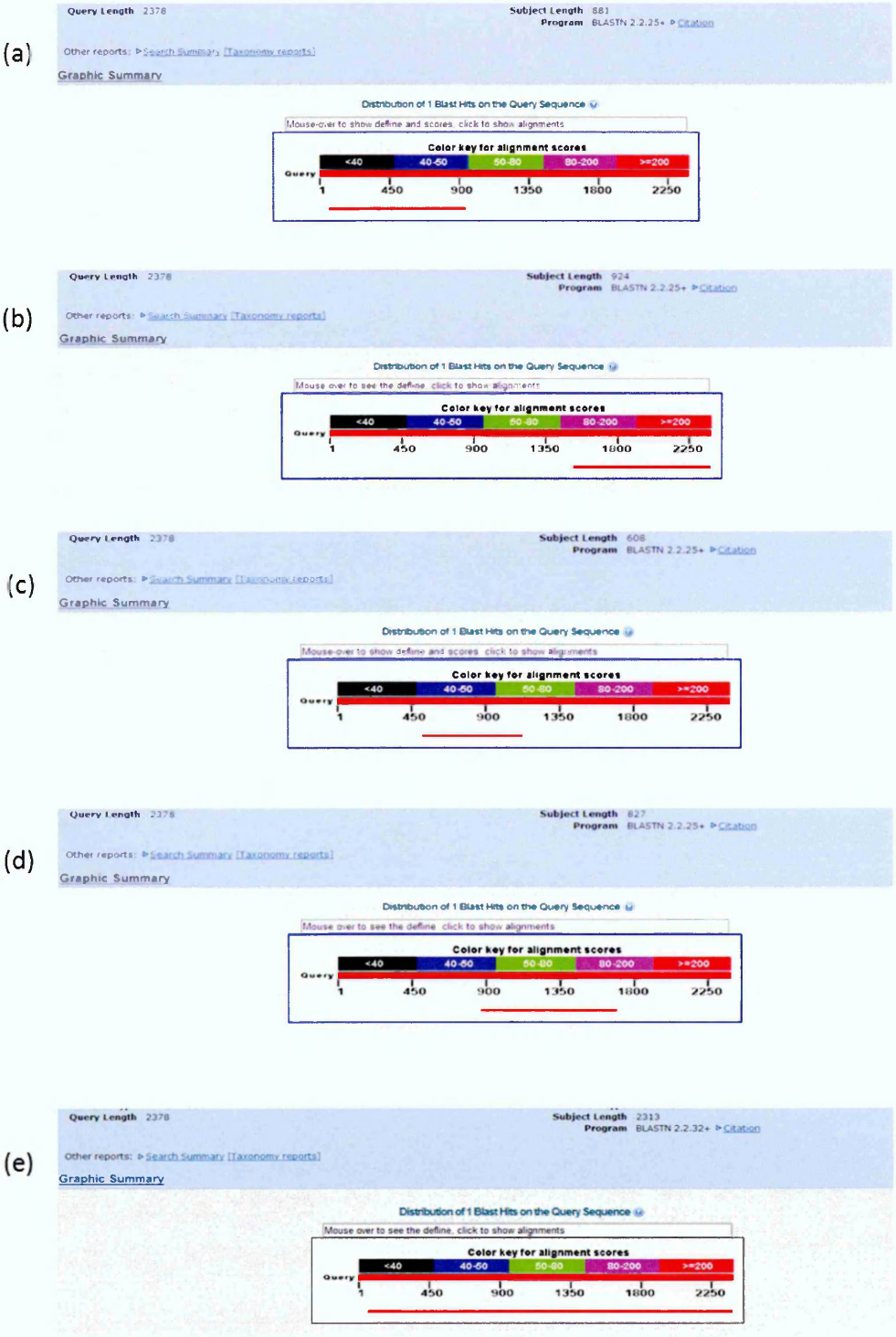

Figure 3.2.4 The alignments of the reference human APP770 obtained from EMBL online database and the results obtained from sequencing. (a) and (b) were the alignments of sequences obtained from the first reading using APP770_Lt and APP770_Rt; base 1-881 and 1518-2378, respectively. (c) and (d) were the alignments of sequences obtained from the second reading using APP770A_Lt and APP770A_Rt; base 521- 1129 and 870-1694, respectively. (e) the alignment of complete sequence of APP770 obtained from sequencing process against reference human APP770.

3.3 Expression vector expressing APP751 construct

The complete sequence of APP770 was used as a basis to generate APP751 using molecular biology techniques; namely touchdown and overlap extension PCR (TD-PCR and OE-PCR, respectively). APP770 contains two domains; KPI and OX2 domains while APP751 only contains the KPI domain which means the OX2 domain needs to be deleted. Once the complete APP751 cDNA fragment was obtained, it was then ligated into pIREShyg2 and transformed into competent cells. The plasmid DNA was extracted from transformed competent cells and sent for sequencing. The APP751 was confirmed by aligning against reference human APP751 sequence from EMBL.

3.3.1 Primer Design

According to the alignment between the reference human APP770 sequence and the human APP751 sequence obtained from EMBL online database using ClustalW software, it revealed the sequence and location of the missing additional domain; OX2 domain on APP751. The online software called Primer3 Input v.0.4.0 (http://bioinfo.ut.ee/primer3-0.4.0/primer3/) was used in order to design a pair of internal primers; APP751_Rt_Front and APP751_Lt_Back in order to amplify the sequence outward from the OX2 domain of APP770. The sequences and functions of the primers are listed in Figure 3.2.1.

3.3.2 Generation of APP751 cDNA and expression vector

As a result of the TD-PCR procedure, two DNA fragments on each side of the OX2 domain were generated as shown in Figure 3.3.1 (a). By using the standard curve in Figure 3.3.1 (b), the size of fragments A and B were approximately 1.05 kb and 1.25 kb, respectively. These fragments were extracted using Qiaquick gel extraction kits (see Section 2.7 for the complete procedure) before assembly into a single DNA fragment containing the complete sequence APP751 using the OE-PCR procedure. The complete APP751 cDNA was initially analysed by agarose gel electrophoresis (Figure 3.3.2 (a)). The standard curve showed that the size of APP751 cDNA was 2.5 kb. The complete descriptions of TD-PCR and OE-PCR are described in Section 2.3.

The complete APP751 DNA fragment was then ligated into the multiple cloning sites of empty pIREShyg2 vector; at AflII and BstBI restriction sites, generating the expression vector expressing human APP751. The ligation procedure was carried out using the T4 DNA Ligase standard protocol obtained from New England Biolabs (NEB) which is described in Section 2.5. The transformation of expression vectors into competent cells; NEB 5-α was carried out according to the standard high efficiency transformation protocol from New England Biolabs (NEB) which is described in Section 2.9. The transformed competent cells were inoculated overnight in the LB containing ampicillin followed by plasmid preparation before dispatch to MWG Eurofins for sequencing.

3.3.3 Sequence alignment

As a limitation of the sequencing process is the limited number of bases per read, the complete APP751 sequence was obtained in two steps (see Section 2.10). Each sequencing result was aligned against the human APP751 (huAPP751) sequence obtained from the online database of European Molecular Biology Laboratory (EMBL) using online software; BLAST 2 Sequences (Bl2seq) via National Centre for Biotechnology Information (NCBI) webpage which allowed the obtained nucleotide sequence to be aligned to known reference sequences without searching the whole online database. The alignment results are shown in Figure 3.3.3 (a) to (d) and Figure 3.3.3 (e) represented the alignment to the complete APP751 sequence.

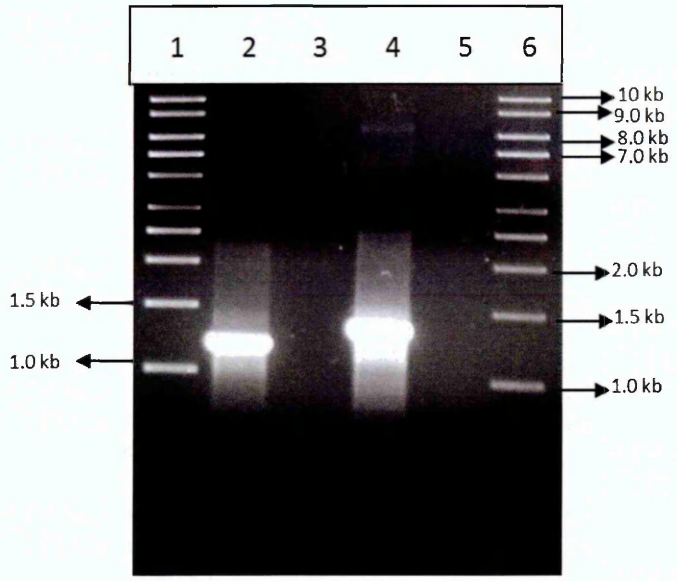

(a)

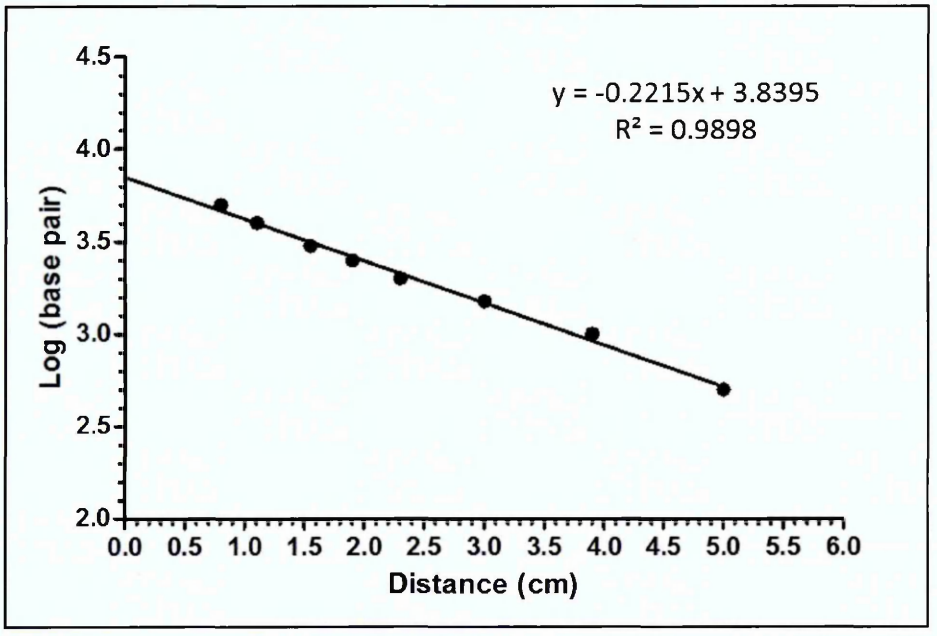

(b)

Figure 3.3.1 APP751 fragments generated by Touchdown PCR. (a) Fragments obtained from touchdown PCR were analysed on a 1% agarose gel. Lane 1 and 6, DNA 1 kb Ladder; Lane 2, fragment A is approximately 1.1 kb; lane 3, fragment A negative control (without template DNA); lane 4, fragment B is approximately 1.3 kb and lane 5, fragment B negative control (without DNA template). (b) The graph illustrates the distance of the bands and the number of base pair of DNA ladder. The size of fragments A and B were approximately 3.35 and 3.2 cm which were 1.05 and 1.25 kb, respectively.

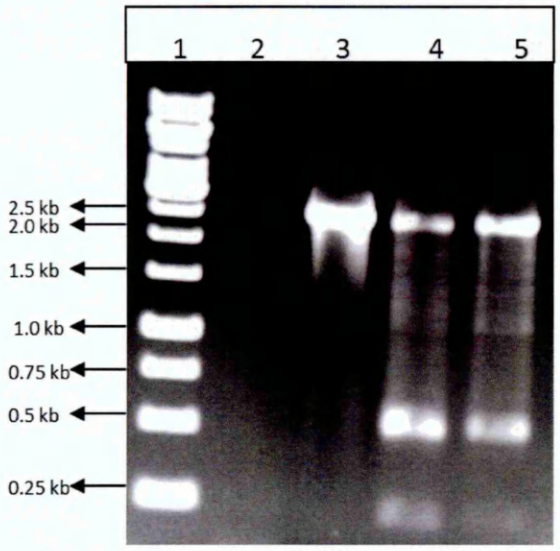

(a)

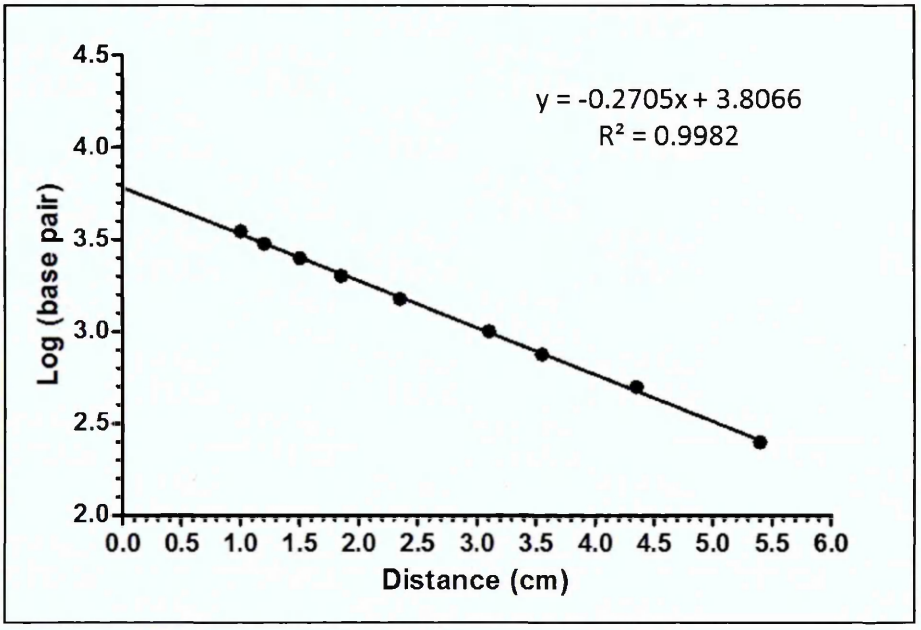

(b)

Figure 3.3.2 The assembly of two APP751 fragments by Overlap Extension PCR. (a) Assembling fragment A and B using Overlap Extension PCR analysed on 1% agarose gel. Lane 1, GeneRuler™ 1 kb DNA Ladder; lane 2, fragments A and B assembly negative control (without fragment A and B); lane 3, APP770 is approximately 2.5 kb and lane 4 and 5,assembled fragment A and B (APP751) is approximately 2.4 kb. (b) The graph illustrates the migration distance of the bands and the number of base pair of DNA ladder. The migrating distance of APP770 was 3.4 cm which was approximately 2.6 kb and distance of APP751 was 3.41 cm which was approximately 2.5 kb.

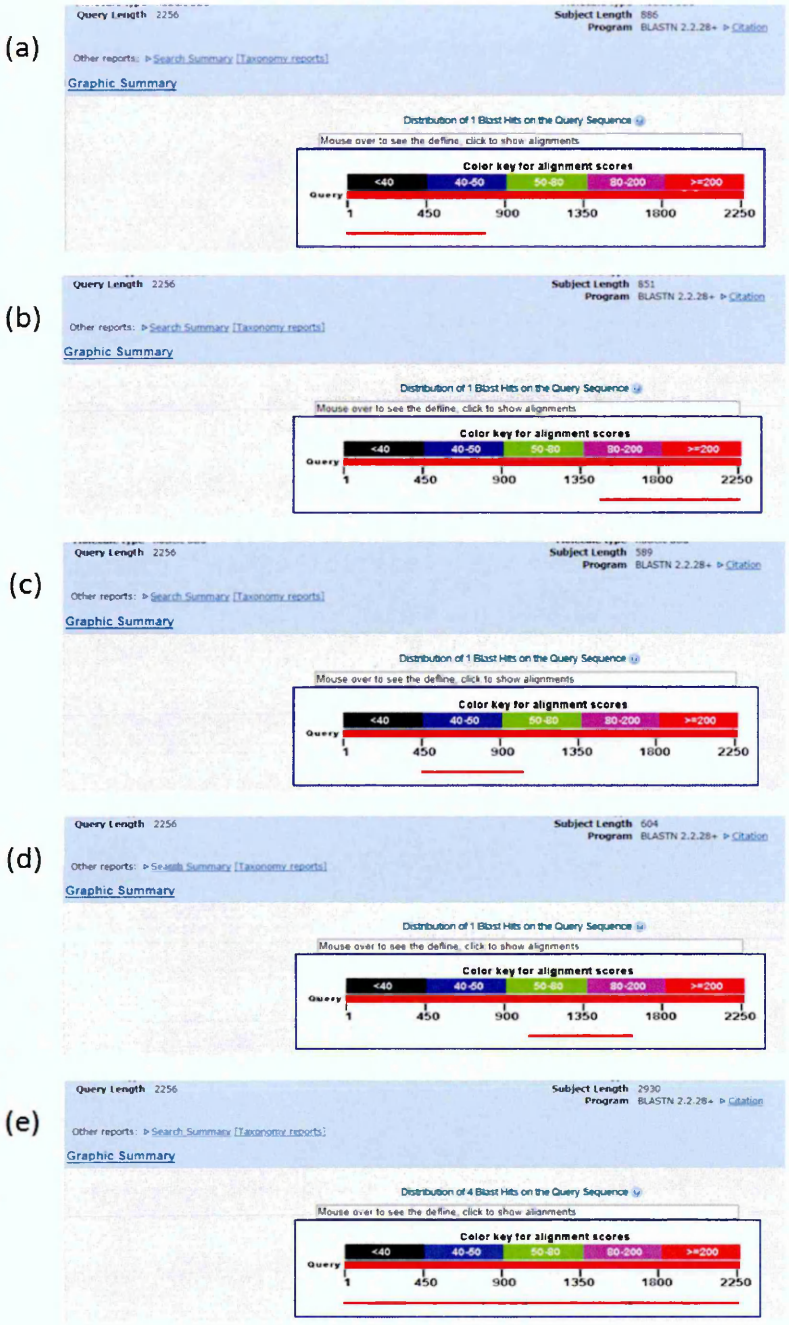

Figure 3.3.3 The alignments of the reference human APP751 obtained from the EMBL online database and the sequencing results. (a) and (b) were the alignments of sequences obtained from the first read using APP770_Lt and APP770_Rt; bases 1-886 and 1485-2256, respectively. (c) and (d) were the alignments of sequences obtained from the second reading using APP751_Rt_Front and APP751_Lt_Back; bases 448-1037 and 1020-1624, respectively. (e) the alignment of combined sequence of APP751 obtained from sequencing process against reference human APP751.

3.4 Expression vector expressing APP695 construct

In a similar method to the construction of the expression vector expressing APP751, the complete sequence of APP770 was used as a basis to generate an expression vector containing APP695 using touchdown PCR (TD-PCR) and overlap-extension PCR (OE-PCR). The APP695 does not contain either the KPI or the OX2 domains. Therefore, both additional domains need to be deleted. Once the complete APP695 cDNA fragment was generated, it was ligated into pIREShyg2 and generated an expression vector expressing APP695. The expression vector was confirmed by sequencing and alignment of the obtained sequence against the human APP695 sequence obtained from the EMBL database.

3.4.1 Primer design

The ClustalW software was used as an alignment tool between the reference human APP770 sequence and APP695 sequence obtained from the EMBL online database which showed the locations and sequences of the KPI and OX2 domains on APP770. As these two domains need to be deleted, the pair of internal primers; APP695_Rt_Front and APP695_Lt_Back were designed using online software called Primer3 Input v.0.4.0 (http://bioinfo.ut.ee/primer3-0.4.0/primer3/). As the KPI and OX2 domains are located next to each other, these primers were designed to amplify the sequence outward from the KPI and OX2 domains of APP770. The sequences and purposes of the primers are listed in Figure 3.2.1.

3.4.2 Generation of APP695 cDNA and expression vector

The two DNA fragments on each side of the KPI and OX2 domains generated through TD-PCR procedure are shown on the Figure 3.4.1 (a) The agarose gel electrophoresis showed that the estimated size of fragment A was 0.63 kb and the size of fragment B was 1.58 kb. These fragments were extracted using Qiaquick gel extraction kits (see Section 2.7 for the complete procedure) before assembly into a DNA fragment containing the complete APP695 sequence using the OE-PCR procedure. The complete APP695 cDNA was initially analysed by agarose gel electrophoresis (Figure 3.4.2 (a)). The size of APP695 cDNA was 2 kb. The complete descriptions of TD-PCR and OE-PCR are described in Section 2.3.

The complete APP695 DNA fragment was then ligated into the multiple cloning sites of empty pIREShyg2 vector at AflII and BstBI restriction sites generating the expression vector containing human APP695. The ligation procedure was carried out using the T4 DNA Ligase standard protocol obtained from New England Biolabs (NEB) which is described in Section 2.5. The transformation of expression vectors into competent cells; NEB 5-α was carried out according to the standard high efficiency transformation protocol from New England Biolabs (NEB) which is described in Section 2.9. The transformed competent cells were inoculated in the LB containing ampicillin overnight followed by plasmid preparation before dispatch to MWG Eurofins for sequencing.

3.4.3 Sequence alignment

As a limitation of the sequencing process is the limited number of bases per read, the complete APP695 sequence was obtained in two steps (see Section 2.10). Each sequencing result was aligned against the human APP695 (huAPP695) sequence obtained from the online database of European Molecular Biology Laboratory (EMBL) using online software; BLAST 2 Sequences (Bl2seq) via National Centre for Biotechnology Information (NCBI) webpage which allowed the obtained nucleotide sequence to be aligned to known reference sequences without searching the whole online database. The alignment results are shown in Figure 3.4.3 (a) to (d) and Figure 3.4.3 (e) represented the alignment of the complete APP695 sequence.

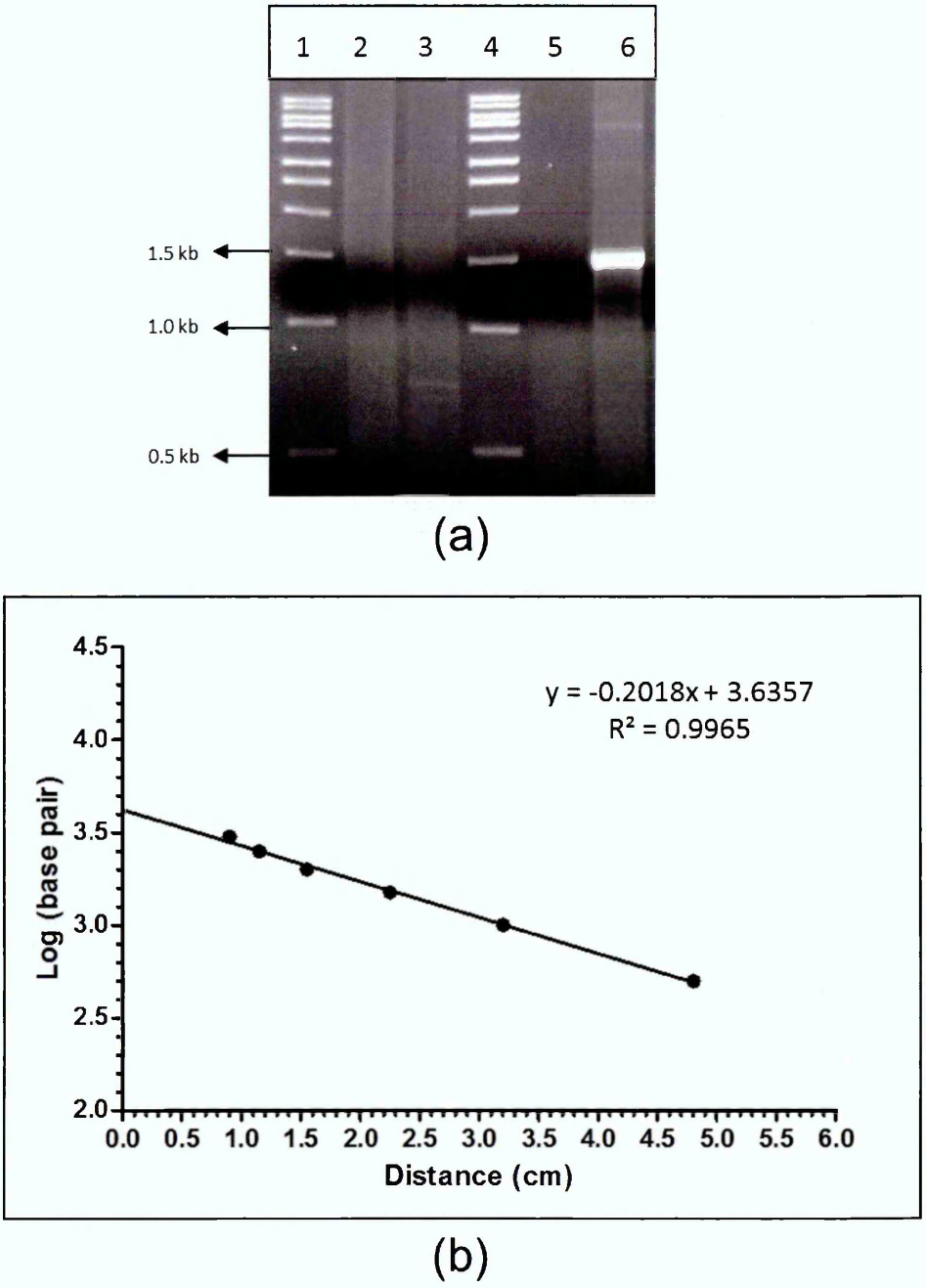

Figure 3.4.1 APP695 fragments generated by Touchdown PCR. (a) Fragment A and B of APP695 obtained from touchdown PCR procedure analysed on a 1% agarose gel. Lane 1 and 4, DNA 1 kb Ladder; Lane 2, fragment A negative control (without template DNA); lane 3, fragment A is approximately 0.55 kb; lane 5, fragment B negative control (without template DNA) and lane 6, fragment B is approximately 1.5 kb. (b) The graph illustrates the migration distance of the bands and the number of base pairs of DNA ladder, migration distance of fragments A and B are 2.8 and 3.2 cm which were predicted to be 0.63 and 1.58 kb in size, respectively.

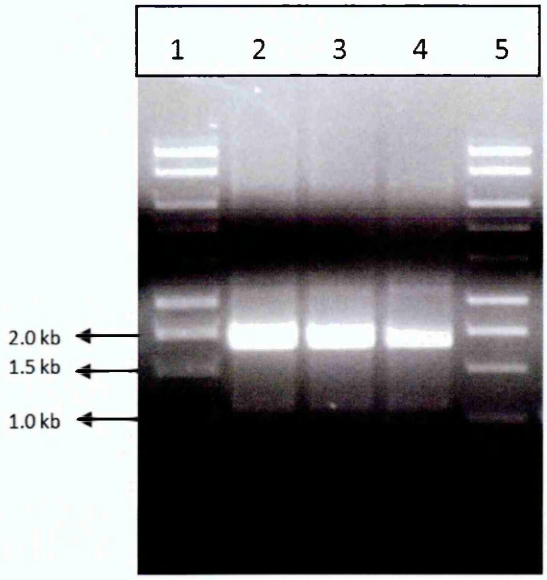

(a)

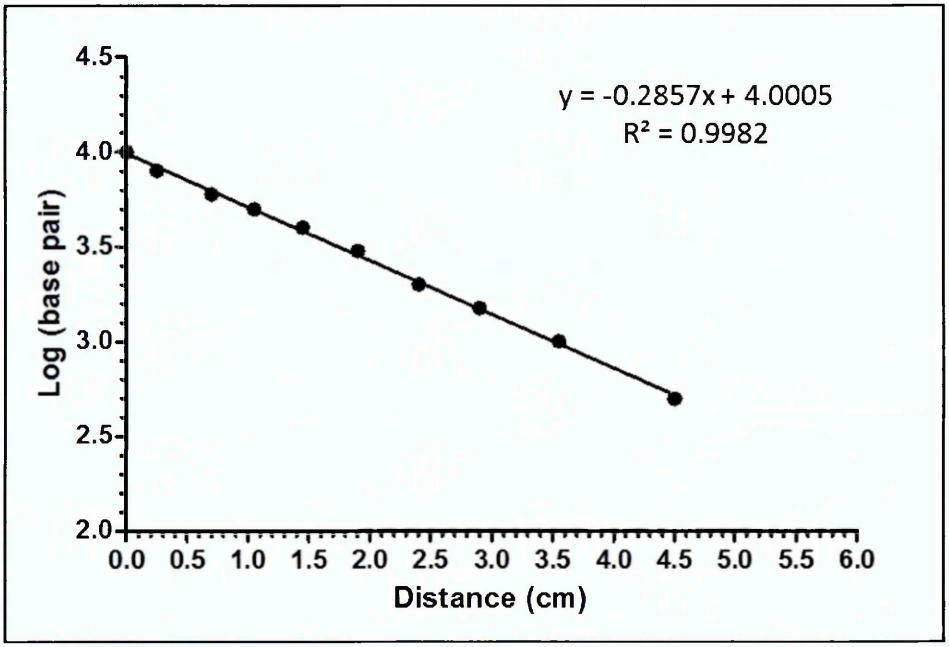

(b)

Figure 3.4.2 The assembly of two of APP695 fragments by Overlap Extension PCR. (a) Assembled fragments A and B of APP695 using Overlap Extension PCR analysed on a 1% agarose gel. Lanes 1 and 5 are 1 kb DNA ladder; lanes 2, 3 and 4 are the product of the assembled fragments A and B of APP695 approximately 2 kb in size. (b) The graph illustrates the migration distance of the bands and the number of base pairs of DNA ladder, APP695 has travelled 2.4 cm which is approximately 2 kb in size.

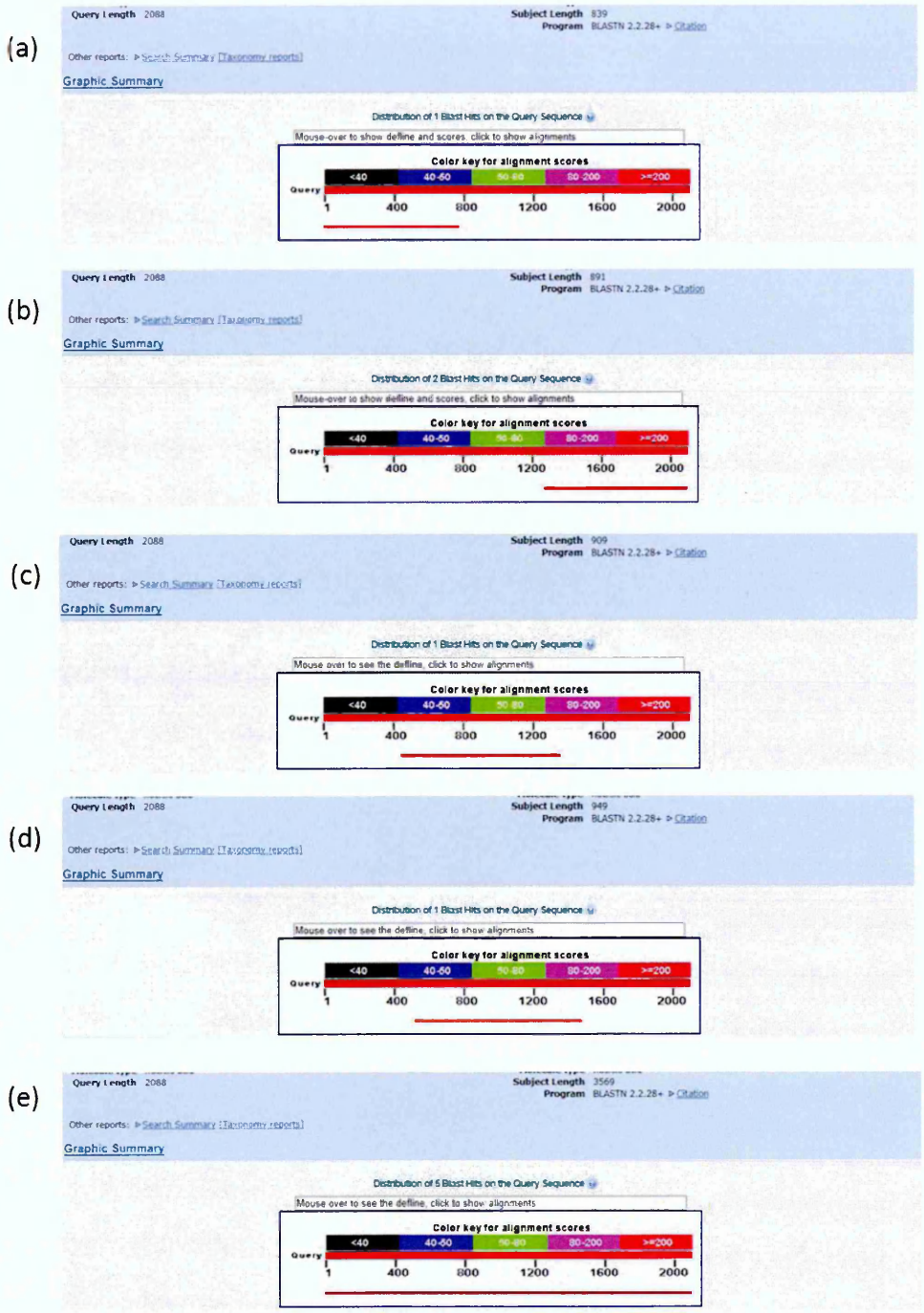

Figure 3.4.3 The alignments between the reference human APP695 obtained from EMBL online database and the sequencing results obtained from sequencing. (a) and (b) were the alignments of sequences obtained from the first read using APP770_Lt and APP770_Rt; bases 1-789 and 1310-2088, respectively. (c) and (d) were the alignments of sequences obtained from the second read using APP695_Rt_Front and APP695_Lt_Back; bases 476-1385 and 552-1501, respectively. (e) the alignment of combined sequence of APP695 obtained from sequencing process against reference human APP695.

3.5 Expression of pIREShyg2 containing APP695, APP751 and APP770 by Chinese Hamster Ovary cells

After completion of the human APP770 expression vector validation and generation of expression vectors encoding human APP695 and APP751, the second objective of the project was to stably express all three isoforms of APP in Chinese Hamster Ovary (CHO) cells by transfection at comparable levels.

3.5.1 Introduction

The CHO cells were originally established in 1956 by Dr. Puck (Wurm and Hacker 2011). Due to their flexibility in *in vitro* cultivation and high reproduction rate, CHO cells have been selected for several different studies such as studying the cell cycle, cancer biology and treatment studies because of their ease to synchronise and anchorage-independent characteristics, respectively (Jayapal et al. 2007; Wurm and Hacker 2011). Also, CHO cells are commonly selected to be used in APP processing study (Khalifa et al. 2012). In this project, the CHO cells were the mammalian cell line of choice due to its low maintenance requirement and ease of transfection and cloning which have made them easy to work with. In the other words, CHO cells were chosen for the initial step because they are relatively easy to transfect and clone.

Transfection is a process to introduce nucleic acids into mammalian cells in order to express proteins of interest in mammalian cells. Also, for stable transfection it is important that prior to the transfection the optimal concentration of a selective antibiotic is determined by kill curve. The optimal concentration is used after transfection in order to select cells that have taken up the expression vector and are capable of expressing the vectoral gene. The general idea of the antibiotic selection is that the host cells taken up expression vector benefit from an antibiotic resistance gene expressed by the vector itself therefore these host cells are able to survive in the presence of antibiotic. In this Chapter the expression vectors encoding APP695, APP751 and APP770 contained hygromycin B resistance gene, therefore the optimal concentration of hygromycin B was determined.

3.5.2 Hygromycin B kill curve

The pIREShyg2 vector contains two antibiotic resistance genes; ampicillin and hygromycin B. The ampicillin resistance gene was used as a selectable marker during transformation procedure in bacterial culture while hygromycin B resistance gene was used as a selective agent in mammalian cell culture. The hygromycin B antibiotic resistance gene encodes Hygromycin B phosphotransferase (Hph), as shown in Figure 3.5.1. Hygromycin B is an aminocyclitol which is a major component of aminoglycoside antibiotic family, and is produced by *Streptomyces hygroscopicus*. The proposed mechanisms of actions are that hygromycin B inhibits transport of mRNA and tRNA on the ribosome, and interrupts the binding affinity of aminoacyl-tRNA (Blochlinger and Diggelmann 1984; Borovinskaya et al. 2008). The recommended concentration of hygromycin B as a selective agent is between 50-1,000 μg/ml which depends on the cell line. The recommended concentration of hygromycin B for CHO cell culture selection ranges between 50 μg/ml to 600 μg/ml.

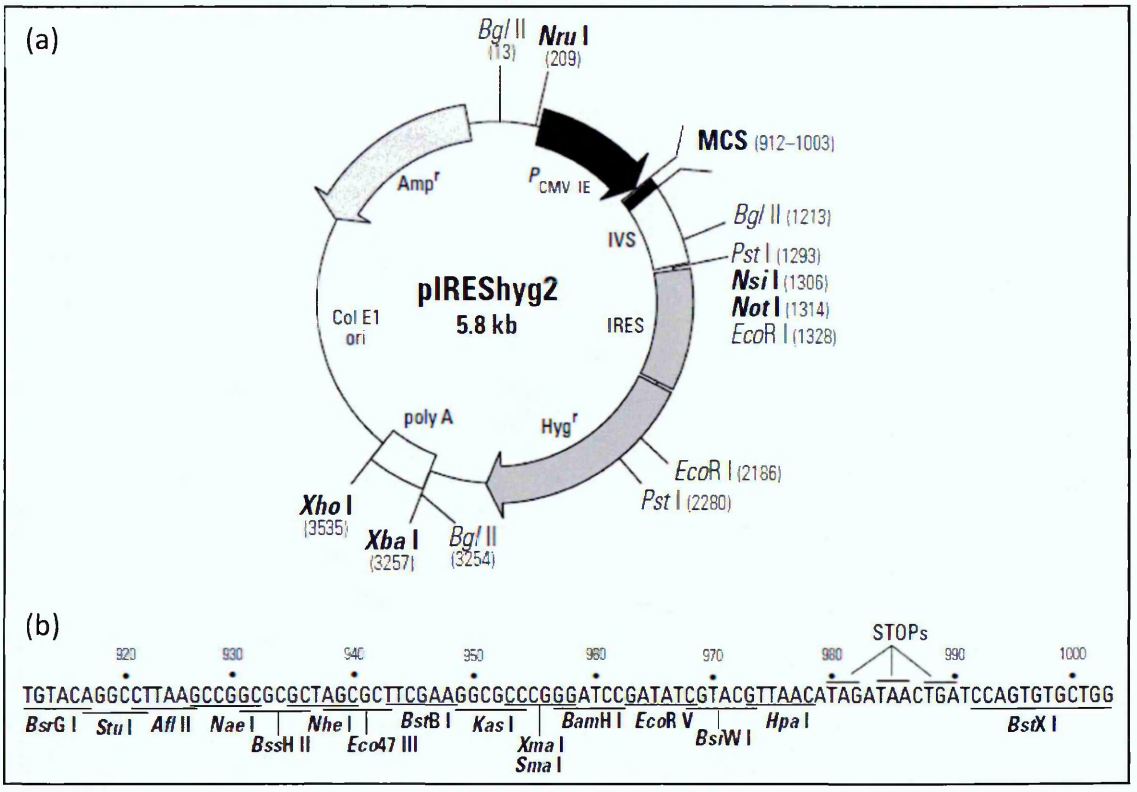

Figure 3.5.1 The pIREShyg2 vector map with restriction sites. (a) The pIREShy2 vector. This is a 5.8 kb vector which contains two antibiotic resistance genes; ampicillin and hygromycin B. Ampicillin is used as a selectable marker in transformation whereas hygromycin B is used transfection. (b) the multiple cloning site (MCS). The DNA of each APP isoform was inserted in the MCS, bases 912 to 1003, of the vector using AflII and BstBI.

Five hygromycin B concentrations were tested and compared to growth in the absence of hygromycin B: 0, 50, 100, 200, 400 and 600 µg/ml. The hygromycin B kill curve experiment was carried out in 6-well plates over a 7-day period. The CHO cells were allowed to adhere in the 6-well plates for at least six hours before adding various concentrations of hygromycin B. The CHO cells were alive and healthy at every concentration up until day 3. On day 4, which was the time CHO cells normally took to become confluence (as seen in the absence of hygromycin B), cells seemed to either stop growing or slowed their growth rate at 200 and 400 µg/ml and there were significant numbers of dead cells at 600 µg/ml, as shown (Figure 3.5.2 (a)). As also shown in Figure 3.5.2, (b) on day 7 that cells were 80% confluence at 200 µg/ml and there were only few cells left at 400 µg/ml while cells were all dead at 600 µg/ml,

which at this point cells were very confluence at controlled concentration (0 μg/ml), 50 and 100 μg/ml.

As a result of the hygromycin B kill curve experiment, the optimal concentration for CHO cells culture selection, after the transfection procedure, was 400 μg/ml and this concentration was used during the first and second limited dilution cloning procedures. The concentration of hygromycin B was reduced to 200 μg/ml in order to maintain the expression vector in the transfected CHO clones.

Figure 3.5.2 CHO cell viability during hygromycin B kill curve. CHO cells were plated at 2.5 x 10^5 cells/well in 6-well plates and allowed to adhere over night before adding hygromycin B at various concentrations. (a) Day 4 of hygromycin B kill curve experiment. At 200 and 400 µg/ml, cells were growing albeit slowly, in comparison to control (0 µg/ml) whereas there were significant numbers of dead cells at 600µg/ml. (b) Day 7 of hygromycin B kill curve experiment. At 200 µg/ml, cells became 80% confluence while at 400µg/ml showed significant numbers of dead cells and at 600 µg/ml all cells were dead. It appeared that the optimal concentration of hygromycin B for CHO cell culture selection was 400 µg/ml. (magnification x200)

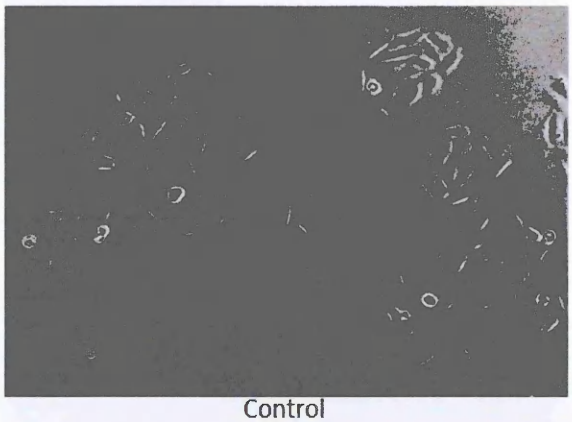

Control

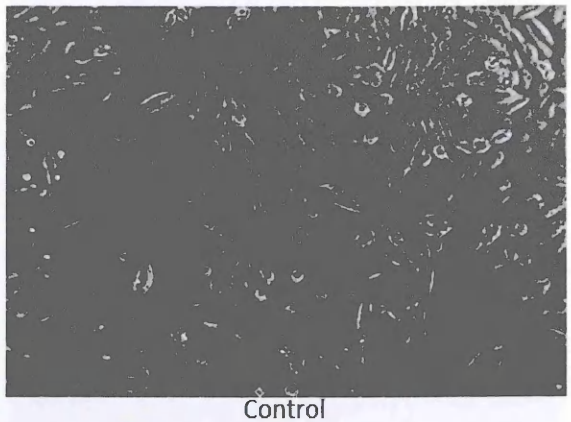

Control

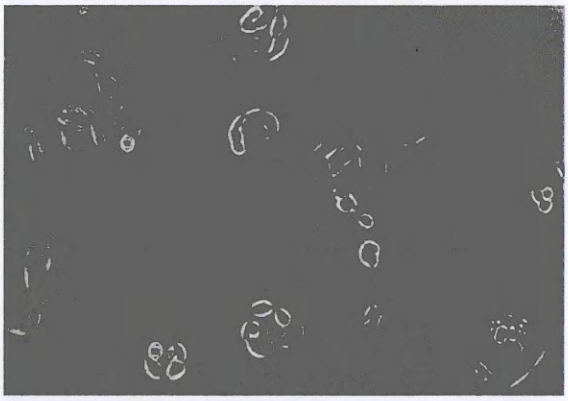

200 µg/ml

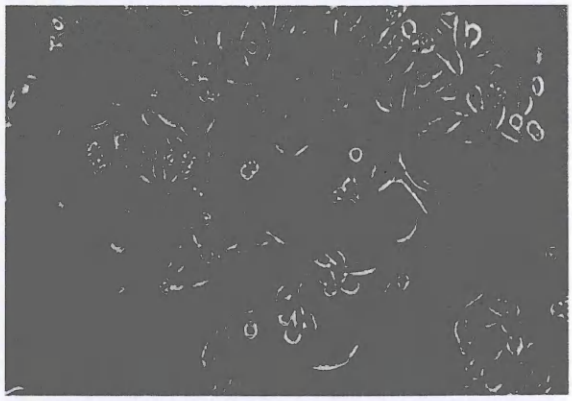

200 µg/ml

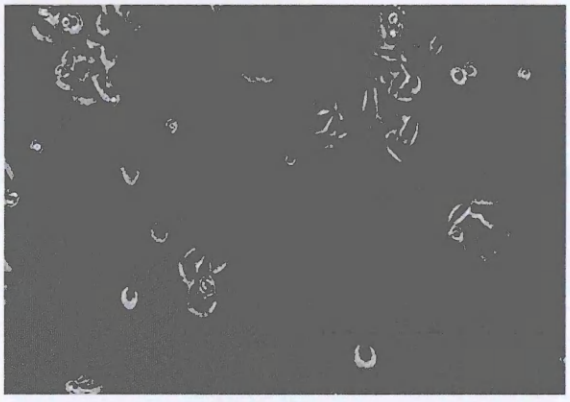

400 µg/ml

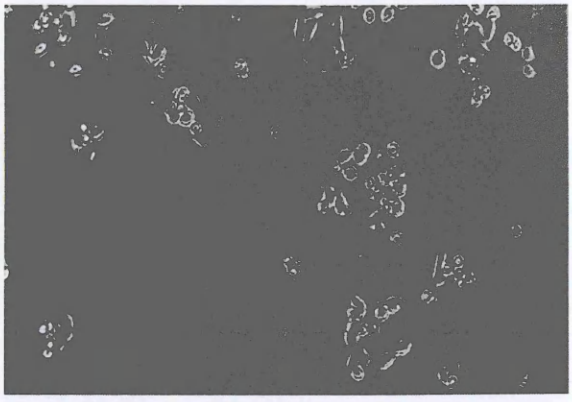

400 µg/ ml

600 µg/ ml

(a) Day 4

600 µg/ ml

(b) Day 7

3.5.3 Generation of CHO cells stably expressing APP695, APP751 and APP770 using pIREShyg2 expression vector

After determining the optimal concentration of antibiotic from the kill curve, the next step was to introduce the expression vector containing human APP constructs into host cells by transfection.

Methods in brief

Prior to the transfection procedure, CHO cells were plated at 4 x 10^4 cells per well in 24-well plates and cells were allowed to adhere overnight or allowed to grow up to 80% confluence before proceeding with the transfection procedure. The transfection reagent used was Lipofectamine® LTX plus Reagent. The preparation and procedure of transfection were described in Section 2.14.

Cells were incubated in transfection reagent at 37 °C with 5% CO_2 for 24 hours before the beginning of limited dilution cloning procedure described in Section 2.15. Four days after the first limited dilution cloning, four wells of a 96-well plate which appeared to have a colony of cell originated from single cells were selected and expanded into 12- and 6-well plates in the selective culture medium containing 400 µg/ml of hygromycin B. Cells were cultured until 50% confluence before proceeding with the second limited dilution cloning. On day 4 of the second limited dilution cloning, four wells of each 96-well plate were selected, trypsinised and transferred to a 12-well plate. Once cell growth had grown to at least 50% confluence, cells were transferred to 6-well plates. Then cells were cultured until 80% confluence in selective culture medium containing 200 µg/ml of hygromycin B. At this stage the selective culture medium was collected for APP secretion analysis.

The conditioned culture medium was immunoprecipitated using DE2 antibody according to procedure described in Section 2.16, followed by reduction and alkylation of disulphide bonds (Section 2.17). Samples were initially run on 8% SDS-PAGE before changing to 6% SDS-PAGE, which was freshly prepared (Section 2.18) followed by protein transfer and immunoblotting (Section 2.19). There were three primary antibodies used in immunoblotting; DE2, 993 and 23/2 (listed in Figure 2.19.1 (top)). Each of the primary antibodies recognizes different epitopes on APP sequence. The

DE2 antibody recognizes Aβ domain which is found in all three isoforms of APP. The 993 antibody recognizes KPI domain which is found in APP751 and APP770 and 23/2 recognizes OX2 domain which only existed on APP770. The DE2 and 993 antibodies not only recognize human APP but also recognize bovine APP present in culture medium while 23/2 antibodies does not. The AP-linked anti-mouse IgG and anti-rabbit IgG were used as secondary antibodies. The estimated concentration and size of protein of the secreted APP was evaluated by a colorimetric detection method using reconstituted of BCIP/NBT solution which converted alkaline phosphatase existing in the secondary antibody to give the intensity of purple band which indicated the approximate size and concentration of APP.

Results

The preliminary transfection data was obtained using the pooled selective culture medium from transfected clones according to the isoform of APP at the end of the first limited dilution cloning stage where CHO cells were allowed to grow in 6-well plates to at least 50% confluence. The medium was immunoprecipitated before proceeding with the immunoblotting procedure where the membrane was incubated in primary antibody solution containing DE2 antibody and secondary antibody solution containing anti-mouse IgG AP-linked before purple bands of protein were developed. The preliminary result of transfection is shown in Figure 3.5.3. The band of protein (arrow) on the membrane suggested that the transfected CHO cells secreted APP into selective culture medium as the band of protein (arrow) was approximately 120 kDa corresponded to molecular weight of secreted APP770.

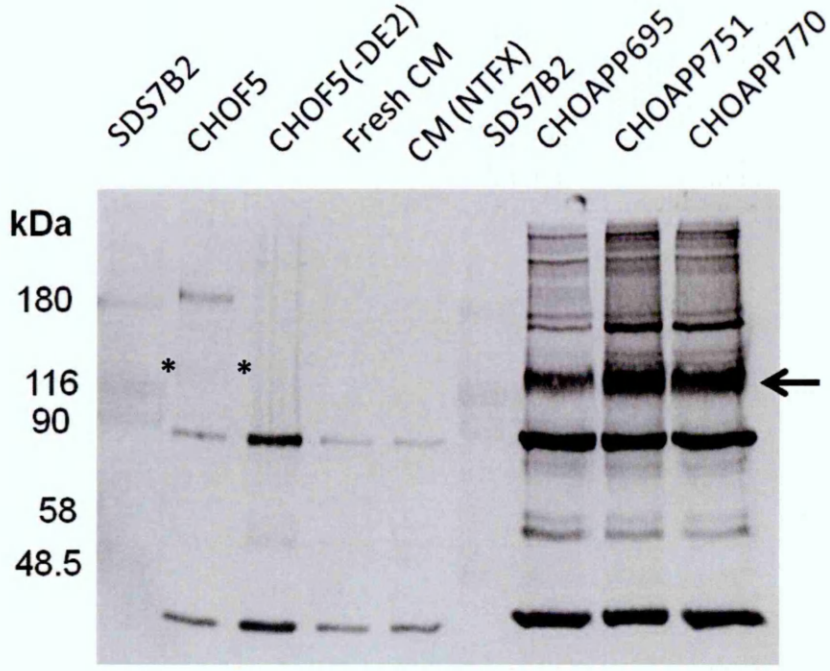

Figure 3.5.3 Protein analysis using DE2 antibody against processed pooled selective media of secreted APP by pIREShyg2 transfected CHO cells over 96-hour incubation period in 6-well plates. Cells were allowed to proliferate for four days in a 6-well plate in 2 ml selective medium containing 400 µg/ml of hygromycin B before the medium was collected. The secreted APP was immuoprecipitated from pooled selective medium before reduction and alkylation of disulphide bonds, and running on 8% SDS-PAGE gel. Protein on SDS-PAGE gel was transferred to nitrocellulose membrane following by immunobloting procedure using DE2 as primary antibody and anti-mouse IgG AP-linked as secondary antibody. The protein bands were detected using reconstituted BCIP/NBT solution. The arrow indicates the protein band produced by transfected CHO. The protein band (arrow) is located above 116 kDa mark and at the same location as CHOF5 (APP positive control, star) which is estimated to be 120 kDa which corresponded to the expected molecular weight of APP.

Key: CM; complete medium, NTFX; non-transfected

As the preliminary data suggested that APP was secreted by transfected clones, the selective culture medium collected at the end of the second limited dilution cloning from each clone APP isoforms was processed individually by immunoprecipitation followed by immunoblotting in order to determine the relative amount of secreted APP from each clone. The DE2 antibody was used as the primary antibody and anti-mouse IgG AP-linked was the secondary antibody. The membrane was developed using colorimetric detection. As it appeared on the membranes shown in Figure 3.5.4, there were two clones which secreted APP; one clone from CHO cells transfected with APP751 (APP751H4) and another from CHO cells transfected with APP770 (APP770H6) as the protein band was located above the 116 kDa mark of protein marker. The estimated size of the bands of protein was 120 kDa which corresponded with the molecular weight of APP770. Since the four selected clones of CHO transfected APP695 did not secrete APP, more clones were selected from the second limited dilution cloning.

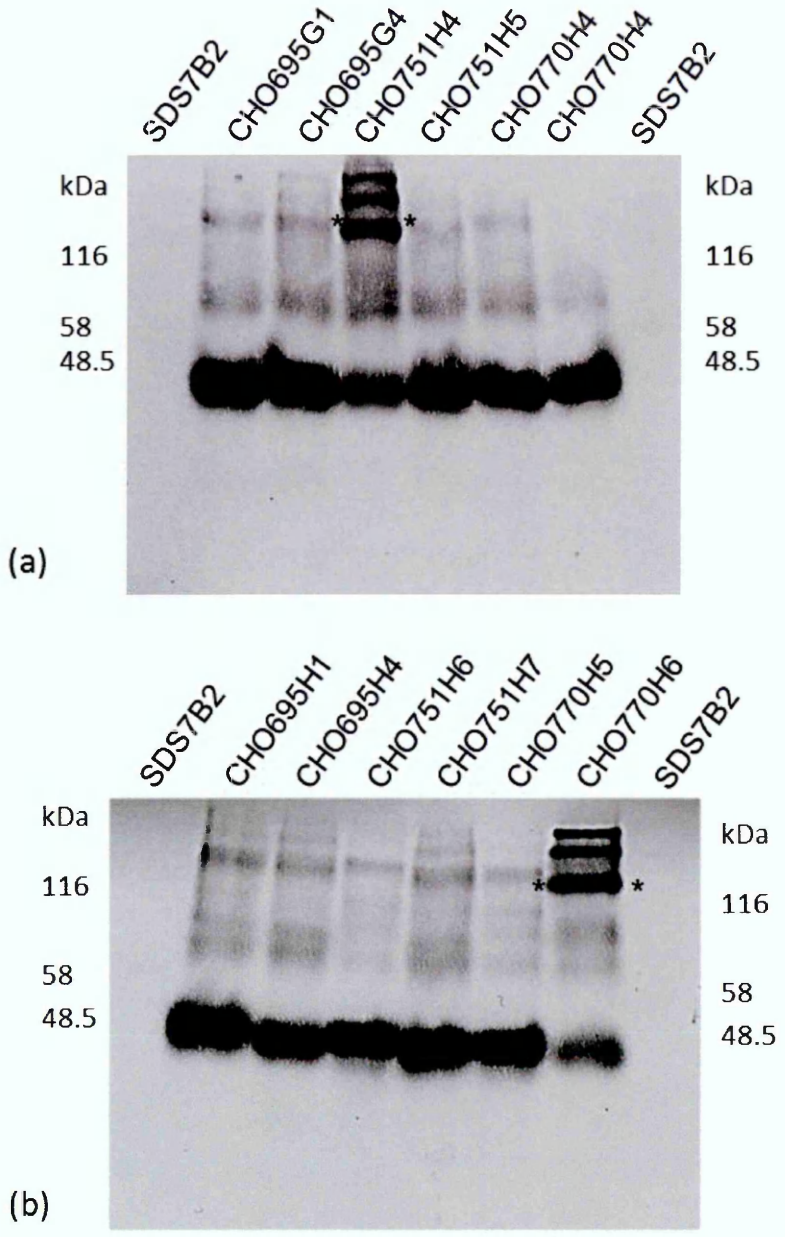

Figure 3.5.4 Protein analysis of secreted APP by pIREShyg2 transfected CHO cells in complete medium with DE2 antibody. Samples were run on 8% SDS-PAGE gel before protein transfer procedure. These samples were processed from medium collected after the second limited dilution cloning and transfected cells were allowed to grow for 4 days. (a) Only clone H4 of CHO transfected APP751 (star) showed a protein band approximately 120 kDa in size which corresponded to the expected molecular weight of APP. (b) Only clone H6 of CHO transfected APP770 (star) showed a protein band approximately 120 kDa in size which corresponded to the expected molecular weight of secreted APP.

The new four selected CHO clones of each isoform of APP were allowed to grow in 6-well plates for 96 hours before the selective culture medium was collected and processed by immunoprecipitation and immunoblotting. In addition, prepared samples from selective culture medium of each new clone were run on three identical sets of SDS-PAGE to allow analysis with three primary antibodies by immunoblotting; DE2, 993 and 23/2. Figure 3.5.5, the membrane was incubated in primary antibody solution containing DE2 antibody and secondary antibody solution containing anti-mouse IgG AP-linked. Of the four new selected clones of each APP isoform, there were only two clones from CHO cells transfected with APP770 that secreted APP while the CHO cells transfected with APP695 and APP751 clones did not secrete APP. The size of purple band of protein produced by APP770 clones was approximately 120 kDa corresponding to molecular weight of APP770 and the existence of Aβ domain. Alongside the DE2 antibody, the other two identical sets of membranes were incubated separately in primary antibody solution containing 993 and 23/2 antibody following by an incubation in secondary antibody solution containing anti-rabbit IgG AP-linked before purple band of protein was detected using the colorimetric detection method as shown in Figures 3.5.6 and 3.5.7, respectively. Figure 3.5.6, as the result of bovine APP770 in culture medium, all the clones produced purple band of protein (approximately 120 kDa). However, the aggregation of bovine APP and secreted APP resulted in a stronger band of protein from APP770 clones. The protein band recognised by 993 antibody also confirmed the presence of the KPI domain. Figure 3.5.7 showed that only APP770 clones produced a 120 kDa protein band recognised by 23/2 antibody. This confirmed the presence of OX2 domain that exists on APP770. The two APP770 clones which shown the protein band at 120 kDa against DE2 antibody also showed protein band of approximately 120 kDa in size recognised by 993 and 23/2 antibodies which verified the presence of APP770 in culture medium. However, the new selective clones did not appear to be transfected with APP695 or APP751.

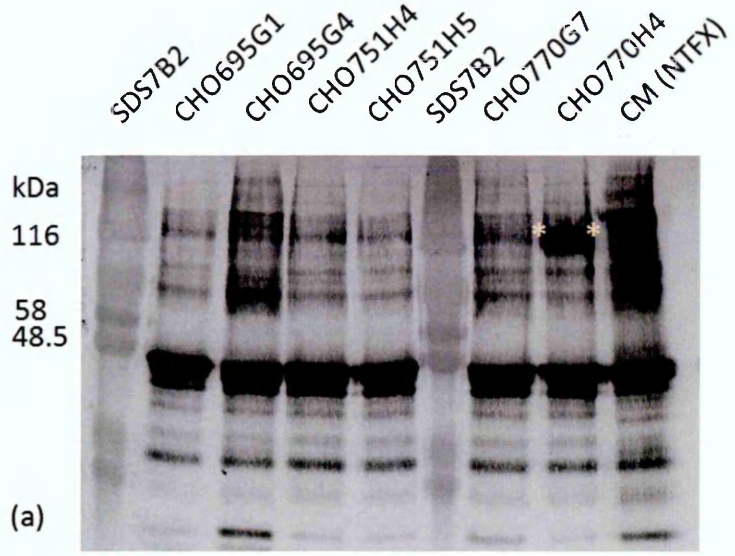

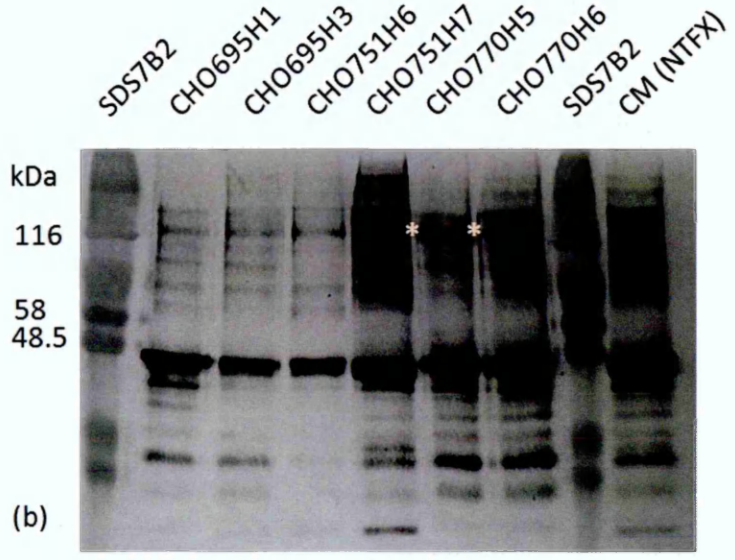

Figure 3.5.5 Protein analysis of secreted APP by pIREShyg2 transfected CHO cells in the complete medium with DE2 antibody. Samples were run on 6% SDS-PAGE gel before transfer. (a) Only clone H4 of CHO transfected APP770 (star) showed a protein band approximately 120 kDa in size which corresponded to the expected molecular weight of APP770. (b) Only clone H5 of CHO transfected APP770 (star) showed a protein band of approximately 120 kDa which corresponded to the expected molecular weight of APP770.

Key: CM; complete medium, NTFX; non-transfected.

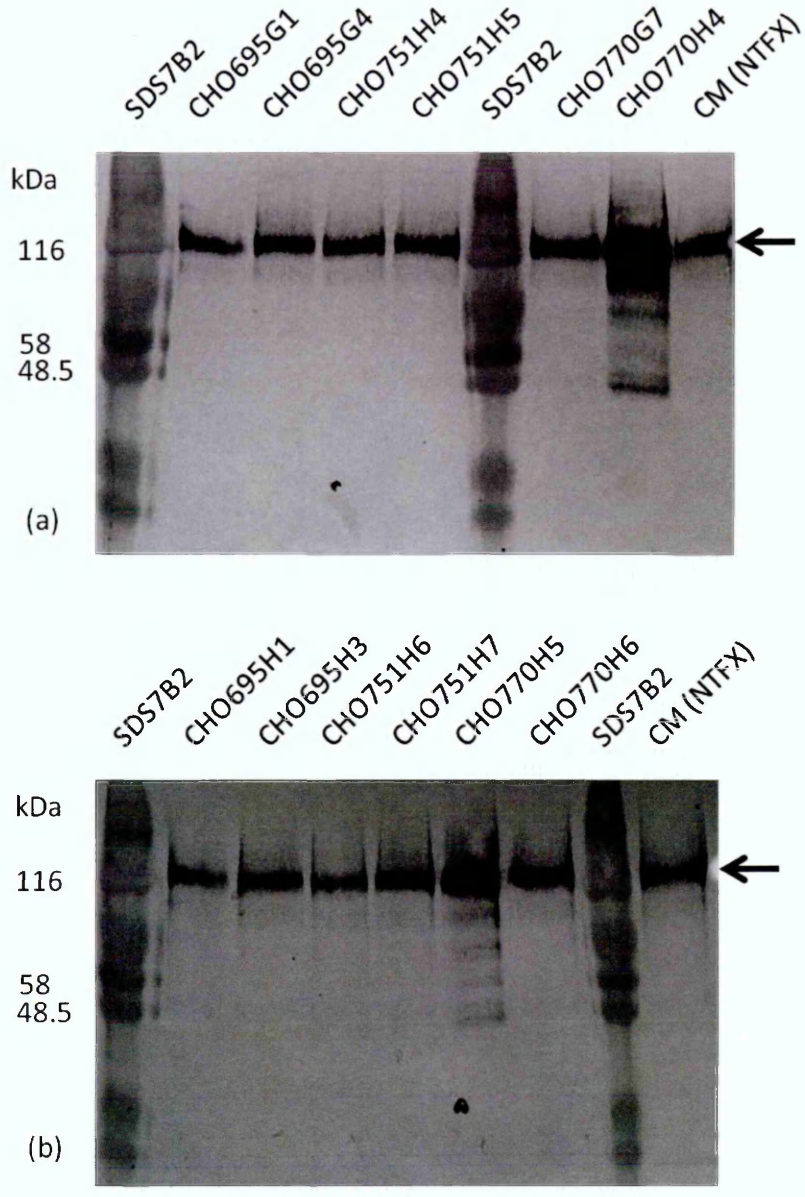

Figure 3.5.6. Protein analysis of secreted APP by pIREShyg2 transfected CHO cells in the complete medium with 993 antibody. Samples were run on 6% SDS-PAGE gel before transfer. Only clone H4 of CHO transfected APP770 (arrow) showed a protein band approximately 120 kDa in size which corresponded to the expected molecular weight of APP770. (b) Only clone H5 of CHO transfected APP770 (arrow) showed a protein band of approximately 120 kDa which corresponded to the expected molecular weight of APP770.

Key: CM; complete medium, NTFX; non-transfected

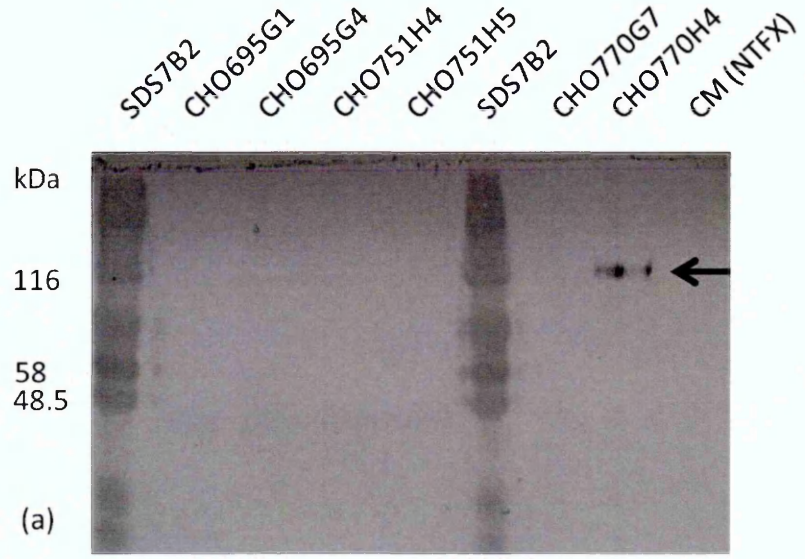

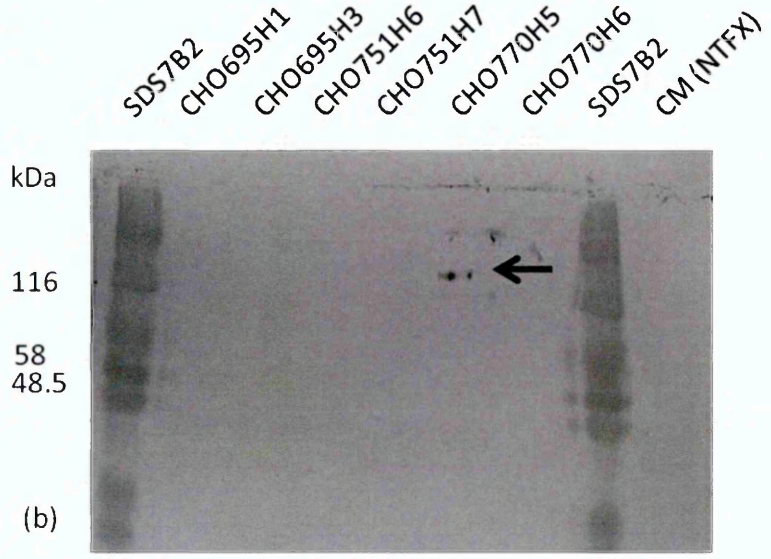

Figure 3.5.7 Protein analysis of secreted APP by pIREShyg2 transfected CHO cells in the complete medium with 23/2 antibody. Samples were run on 6% SDS-PAGE gel before transfer. Only clone H4 of CHO transfected APP770 (arrow) showed a protein band approximately 120 kDa in size which corresponded to the expected molecular weight of APP770. (b) Only clone H5 of CHO transfected APP770 (arrow) showed a protein band of approximately 120 kDa which corresponded to the expected molecular weight of APP770.

Key: CM; complete medium, NTFX; non-transfected

3.6 Quantification of APP secretion

As previously demonstrated in Section 3.5.3, there were two CHO clones which successfully expressed APP770: CHO770H4 and CHO770H5. The CHO770H4 was originally selected as a candidate to assess methods for quantification APP secretion. In this experiment, selective culture medium which contained 200 µg/ml of hygromycin B was collected from CHO770H4 and prepared by immunoprecipitation and reduction and alkylation of disulphide bonds. Figure 3.6.1 (a) shows samples diluted in a series: 0, 10, 20, 30, 40, 50, 60, 70, 80, 90 and 100%, before separation by 6% SDS-PAGE gel. Proteins were transferred onto nitrocellulose membrane followed by immunoblotting. The 1151 antibody was used as primary antibody in immunoblotting for the first time in this project because the 1151 antibody not only recognised a domain at the N-terminal of all three human APP isoforms but also the 1151 antibody does not recognise bovine APP present in the culture medium which made this antibody a suitable antibody in human APP quantification.

So far in this project, the colorimetric detection method was used to estimate the size and approximate amount of protein of interest on the nitrocellulose membrane. The fluorescence detection method (referred to as *LI-COR* system) is a well-established method for protein quantification as it allows the protein of interest to be precisely quantified using the excitable fluorescence emission. Moreover, the fluorescence intensity corresponds to the amount of protein therefore it was used as a detection method to quantify the protein band in the immunoblotting procedure. The dilutions of APP were measured using *LI-COR* system where the fluorescence intensity at 700 nm from the binding of fluorescence labelled anti-rabbit secondary antibody to the APP-1151 protein primary antibody complex. The protein quantification numbers gained from *LI-COR* system were plotted on a graph of fluorescence intensity detection and the relative amount of APP. As it is shown in Figure 3.6.1 (b), the graph generated a standard curve of the APP concentrations against fluorescence intensity.

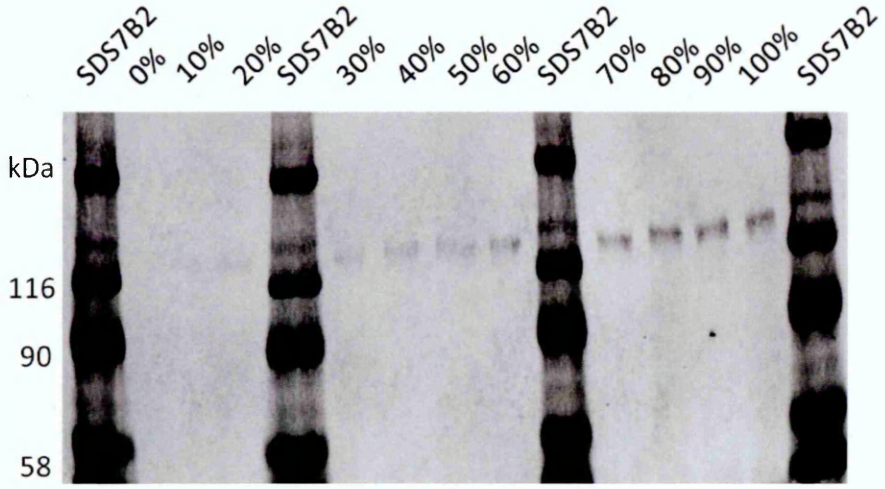

(a)

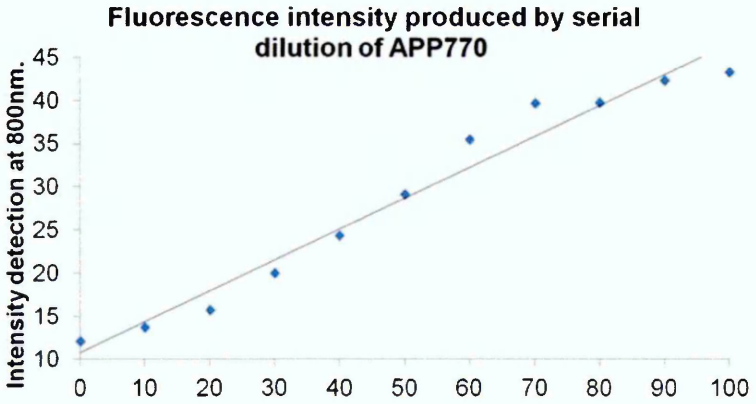

(b)

Figure 3.6.1 Quantification of secreted APP using conditioned culture medium of CHO770H4. Conditioned culture medium from CHO770H4 was prepared by immunoprecipitation, reduction and alkylation of disulphide bonds. (a) Sample was diluted into a series of concentrations: from 0% to 100% before running on 6% SDS-PAGE gel following by protein transferred and immunoblotting using 1151 primary antibody and anti-rabbit IRDye 700 as a secondary antibody. (b) The amount of APP770 were measured by the fluorescence intensity reads of the fluorescence labelled secondary antibody which were then plotted on a graph against the concentration of APP770 which generated standard curve for APP quantification method.

3.7 Discussion

The first objective of the project was to obtain expression vectors containing three different isoforms of human APP; APP695, APP751 and APP770. At the beginning of the project, an expression vector containing human APP770 was provided by Professor Nigel Hooper as *E.coli* stab culture. The vector was sequenced in order to confirm the presence of APP770 and its location within the multiple cloning sites of the vector. The first step in the validation process was designing a pair of primers which bound just outside the restriction sites where APP770 cDNA was inserted. At the same time, an expression vector was prepared by bacterial culture and minipreparation procedures. The expression vector was amplified using a pair of customised primers and the PCR product was purified using a gel extraction procedure before sending off for sequencing along with primers. Due to the sequencing limitations (the number of base pairs returned per read) a pair of internal primers was designed for sequencing purposes. In order to confirm that the complete sequence was obtained, the sequence was aligned against human APP770 reference sequence from EMBL online database. It was confirmed that the expression vector provided by Professor Hooper contained human APP770 cDNA as shown in Figure 3.2.4 and the vector subsequently expressed human APP770 as a consequence. At this point it was safe to continue to the next step to achieve the first objective of the project.

The complete sequence of human APP770 was used as a basis to generate both human APP751 and APP695 cDNA, as all three isoforms shared similarity in most parts of the structure.

In order to generate human APP751 expression vector, a pair of primers was designed to delete the OX2 domain. A pair of internal primers was designed to amplify outward from the deleted region of the APP770 sequence. The two DNA fragments of APP751 were generated using TD-PCR and were then assembled using OE-PCR, before gel extraction and sequencing procedures. The complete sequence of APP751 was aligned against the reference human APP751 sequence obtained from EMBL online database. As it is shown in Figure 3.3.3, the complete sequence of APP751 was confirmed and it was ligated into empty pIREShyg2 in order to generate the complete human APP751 expression vector.

Similarly to APP751 expression vector generation, a new pair of primers was designed due to the need to delete both the KPI and OX2 domains to generate APP695. These primers were designed to amplify outward from the deletion region of APP770 sequence following by TD-PCR and OE-PCR. The complete sequence of APP695 was aligned against a reference human APP695 sequence obtained from EMBL online database and it showed that both sequences had 100% positive match as shown in Figure 3.4.3 hence the fragment was ligated to empty pIREShyg2 vector to generate human APP695 expression vector.

To summarise, at this stage, all three isoforms of APP were obtained as expression vectors and the first objective of this project was achieved.

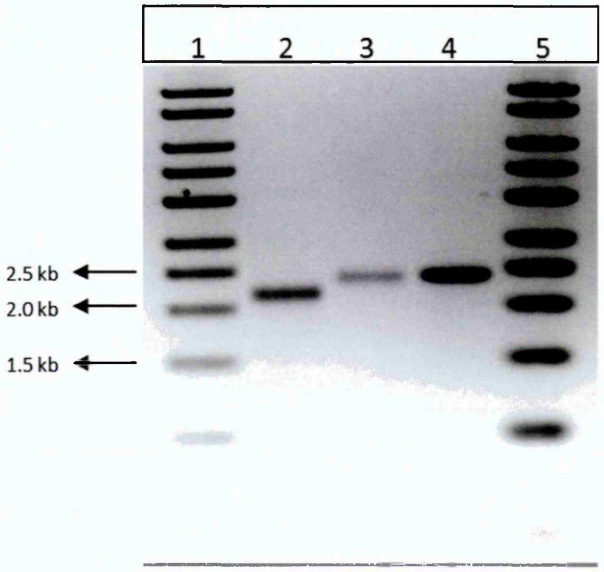

Figure 3.7.1 The confirmation of APP 695, APP751 and APP770 cDNA visualised on 1% agarose gel. Lanes 1 and 5, 1Kb DNA ladder. Lane2, human APP695 cDNA. Lane3, human APP751 cDNA and Lane4, human APP770 cDNA.

The second objective of the project was to generate stably expressing CHO cells using in-house expression vectors containing three different human APP isoforms: APP695, APP751 and APP770.

In eukaryotes, the translation of mRNAs is initiated by the binding of the initiation complex to the 5'-untranslated region (5'-UTR) which contains an attached cap-methylated guanosine. Not only is the cap-methylated guanosine recognised by the ribosome translation initiation complex but also ensures the stability of mRNA (Richter and Sonenberg 2005). The initiation complex consists of a small ribosomal subunit and the initiator Met-tRNAi. Once the initiation complex binds to the cap, it initiates the reading at 5'-UTR to the first starting codon resulting in the complete assembly of ribosomal units and the nascent polypeptide synthesis initiation. This manner of translation is called cap-dependent (Mokrejs et al. 2006; Roux et al. 2007; Sachs 2000).

Some viruses do not contain the cap at the 5'-UTR and consequently have to employ the alternative strategy in protein synthesis initiation which is called cap-independent manner. These viruses contain a long and strongly conserved structure of 5'-UTR mediating the binding of initiation complex and the formation of the ribosome. This 5'-UTR region is called internal ribosome binding site (IRES) (Li and Wang 2012; Mokrejs et al. 2006). The expression of IRES elements varies in size and specificity. For examples, the internal ribosome entry site (IRES) obtained from encephalomyocarditis virus (EMCV) is the most active in the transiently transfected cell lines and less stable in the stably transfected cell (Pierandrei-Amaldi et al. 1999). The size of EMCV IRES ranges from 500-588 (Mokrejs and Pospisek 2015).

The utilisation of IRES elements as IRES-dependent expression vector in bicistronic expression system has been repeatedly reported in the past few decades (Li and Wang 2012). Bicistonic expression vectors allow the protein of interest and selection marker gene to express using a single transcription unit (Hennecke et al. 2001; Ho et al. 2013).

pIREShyg2 used in this Chapter is a bicistronic expression vector and is composed of first cistron located after a promoter, intervening sequence (IVS), an encephalomyocarditis virus (EMCV) internal ribosome entry site (IRES) elements and a second cistron which is the hygromycin resistance gene. The hygromycin resistance gene is used as a selectable marker in antibiotic selection of transfection (Shikama et

al. 2010) and EMCV IRES is one of the commonly used IRES elements in constructing the bicistronic expression system (Hennecke et al. 2001). As a result of the IRES inclusion in the vector, the first cistron is translated in a cap-dependent manner while the second cistron is translated in cap-independent manner (Ho et al. 2013; Shikama et al. 2010). It was suggested that cap-dependent translation is partially influenced by the IRES elements and the first cistron dictates the strength of the second cistron translation. A different position in which the first and second cistron are assembled in the bicistronic expression vector can also affect the strength of translation (Hennecke et al. 2001). Besides the translation in cap-independent manner has lower efficiency in comparison to cap-dependent manner leading to the lower expression of the second cistron (Ho et al. 2013; Kozak 2005). In addition, the EMCV IRES is a non-coding RNA enabling cap-independent protein synthesis (Bochkov and Palmenberg 2006) and belongs to the type 2 family of the IRES (Lindeberg and Ebendal 1999). The type 2 IRES has been suggested to function more efficiently than type 1 and it has been shown to be more sensitive to changes of the sequences (Lindeberg and Ebendal 1999). Therefore the expression vectors pIREShyg2 containing human APP751 and APP695, which were constructed from pIREShyg2 containing human APP770, might be affected. Hence this may explain the failure to stably express APP751 and APP695 with pIREShyg2.

It has been reported that the translational efficiency of IRES elements is not only controlled by several cellular factors but also depends on cell type and the composition of IRES binding factors within the cell (Hennecke et al. 2001). For example, the proteins synthesised from reticulocyte ribosome tend to come from the translation initiation of IRES or the second cistron rather than first cistron (Bochkov and Palmenberg 2006). It has been shown that there are other parameters related to the construct of the vector which greatly influence the translation efficiency of IRES elements. This implies that the protein expression from the bicistronic expression vector is not stable and cannot be predicted (Hennecke et al. 2001). The provided expression vector pIREShyg2 containing human APP770 was originally stably transfected to HEK293 cells (Belyaev et al. 2010). However, when both provided (APP770) and in-house constructed (APP751 and APP695) expression vectors were used to establish the clonal stably transfected CHO cells, it has shown to be more problematic and only transiently transfected CHO

cells were achieved using APP751 and APP695. The expression of APP770 in CHO cells was possible however difficult as was shown in the first and the second sets of selected clones. There was only one out of four APP770 clones in the first set of selected clones which secreted APP770 and there were only two out of another four APP770 clones which secreted APP770 in the second set of selected clones.

Although the bicistronic expression systems have become an important tool in biotechnology, it does not mean the application of IRES elements is always a success (Kozak 2005). Although there is a total decrease in the cellular protein synthesis, the high translational rate of the mRNA is maintained by the internal initiation facilitated by the IRES elements (Kozak 2005; Sachs 2000). The 6A at the bifurcation loop of pIREShyg2 facilitates the strong expression of the second cistron and the translation of the second cistron locating after EMCV IRES was shown to be independent from the translation of the first cistron (Bochkov and Palmenberg 2006). This might explain the survival of the transfected CHO cells under the pressure of hygromycin B in the culture media without secretion of APP located in the first cistron. Also, it was reported that pIREShyg2 affected the stability of the mRNA obtained from the cistrons within the expression vector which led to the poor expression of the carried cistrons (Shikama et al. 2010).

Finally, several successful experiments using bicistronic expression system have been clearly noted whereas the failed applications of bicistronic expression system were usually not reported (Hennecke et al. 2001; Mokrejs and Pospisek 2015)., and as a consequence of the challenges associated with creating stably expressing CHO cells using the pIREShyg2 vector, alternative approaches were explored.

Chapter 4: Generation of CHO and HEK293 stably expressed APP695 APP751 and APP770 (pcDNA3.1)

4.1 Expression of APP695, APP751 and APP770 in CHO cells using the pcDNA3.1 expression vector

It was demonstrated in Chapter 3 that among several transfected CHO clones which had been screened for APP secretion, there were only two successful clones from CHO cells transfected with APP770 which secreted APP. Also, many attempts were made to produce CHO clones which expressed APP695 and APP751 without success. Therefore, expression vectors for APP695, APP751 and APP770 were custom synthesised by Life Technology in order to complete the second objective of this project: CHO cells stably expressing APP isoforms.

4.1.1 Introduction

The new APP695, APP751 and APP770 synthesised vectors were provided in pcDNA3.1 (Figure 4.1.1). It is a general practice that an antibiotic kill curve is carried out when introducing the new expression vector, there is a change in antibiotic batches or when the expression vector is introduced to the new cell line. The pcDNA3.1 expression vector contains neomycin resistance gene which is a different antibiotic resistance gene from the one carried on pIREShyg2. Therefore it was necessary to carry out a new antibiotic kill curve with G418, which neomycin resistance gene protects against.

The antibiotic kill curve procedure is used to determine the optimal concentration of a selective antibiotic of choice in a particular cell line. The optimal concentration of a selective antibiotic is just enough to kill the host cells over 4-7 days period and it is used in transfected colony selection post transfection. The general idea of antibiotic selection is that the host cells taking up the expression vector benefit from an antibiotic resistance gene during expression of the vector by the host cells which are able to survive in the presence of an antibiotic.

4.1.2 Geneticin kill curve for CHO

The synthesized expression vector containing APP695, APP751 and APP770 cDNA were obtained from Life Technologies, UK. Each APP isoform was cloned into the chosen vector; pcDNA 3.1. The pcDNA 3.1 contains two antibiotic resistance genes, it has neomycin gene as shown in Figure 4.1.1 which encodes aminoglycoside 3' phosphotransferase (APH). APH is able to deactivate neomycin, kanamycin and geneticin. However, neomycin and kanamycin are normally used in prokaryotic selection while geneticin is used in eukaryotic selection. The geneticin which is often referred to as G418 was used as a selectable marker in mammalian cell culture due to its specificity to mammalian ribosomes. G418 is classified as an aminoglycoside antibiotic and is produced by *Micromonospora rhodorangea*. The well-understood mechanism of action of G418 is inhibition of protein synthesis through inhibition of peptide elongation (Eustice and Wilhelm 1984).

Methods in brief

The recommended concentration of G418 in CHO cell culture selection is 200-400 µg/ml (Section 2.13). The kill curve experiment was carried out in a 6-well plate over 7-days period. Cells were allowed to adhere for at least six hours before the addition of various concentrations of G418.

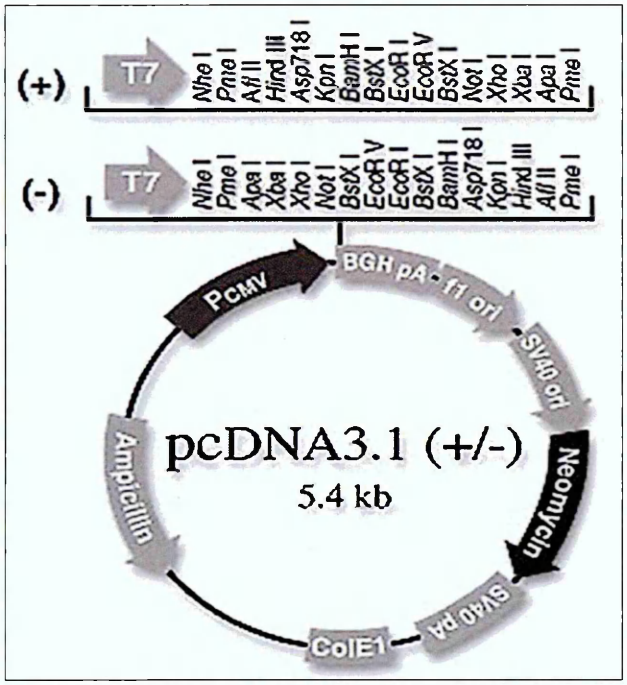

Figure 4.1.1 The vector map of pcDNA3.1 with restriction sites. The pcDNA3.1 is 5.4 kb vector which contains two antibiotic resistance genes; ampicillin and neomycin. Ampicillin is used as a selectable marker in transformation whereas geneticin is used in transfection.

Results

Cells grew but with an inverse relationship between cell growth and concentration of antibiotic: the growth rate decreased as G418 concentration increased. At high concentrations of G418, 400 and 500 µg/ml, cells were all dead on the second day after adding antibiotic. As shown in Figure 4.1.2 (a) on day 4, at 100 µg/ml of G418, cells appeared healthy but did not grow as fast as cells in the controlled well which contained 0 µg/ml of additional G418. Also, at 200 µg/ml of G418 a few cells began to die whereas there were great numbers of dead cells appeared at 300 µg/ml of G418. Furthermore, on day 7 at 100 µg/ml, cells became almost 100% confluence while a significant numbers of dead cells appeared at 200 µg/ml and cells were all dead at 300 µg/ml, as shown in Figure 4.1.2 (b). As a result of this experiment, the optimal concentration determined from the geneticin kill curve experiment was 200 µg/ml and this concentration was used during the limited dilution cloning procedure. Also, in order to retain the expression vector within CHO cells, the presence of G418 in culture medium was required however the concentration of G418 was reduced to 100 µg/ml.

Figure 4.1.2 CHO cells viability during geneticin kill curve. CHO cells were plated at 2.5 x 10^5 cells/well in 6-well plates and allowed to adhere overnight before adding geneticin at various concentrations. (a) Day 4 of geneticin kill curve experiment. At 100 and 200 µg/ml, cells were growing but quite slowly, in comparison to control (0 µg/ml) whereas cells started to die (detach from culture plate) at 300µg/ml. (b) Day 7 of geneticin kill curve experiment. At 100 µg/ml, cells became 80% confluence while at 200µg/ml showed significant numbers of dead cell and at 300 µg/ml all cells were dead. It appeared that the optimal concentration of geneticin for CHO cell culture selection was 200 µg/ml. (magnification 200x)

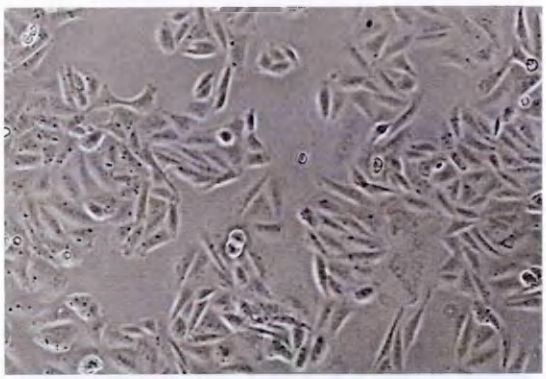

Control

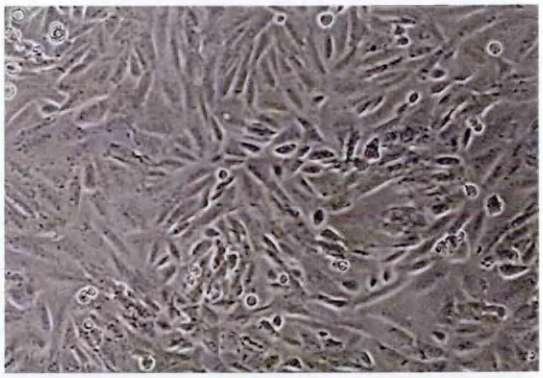

Control

100 µg/ ml

100 µg/ ml

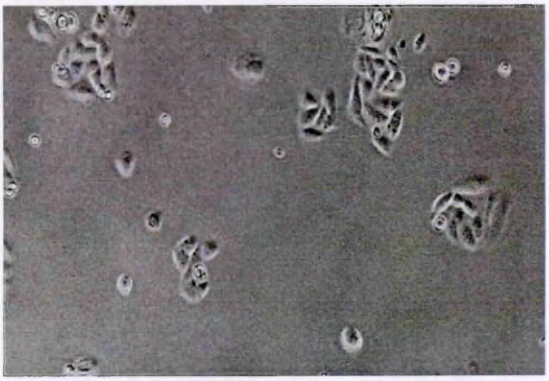

200 µg/ ml

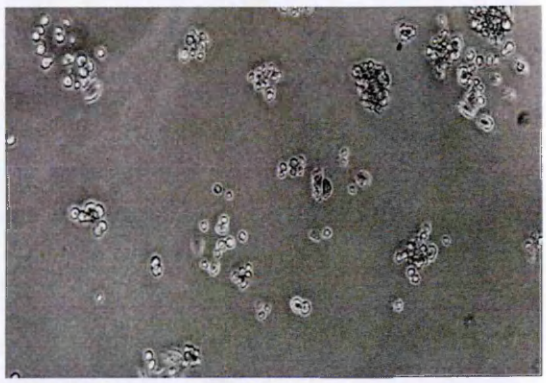

200 µg/ ml

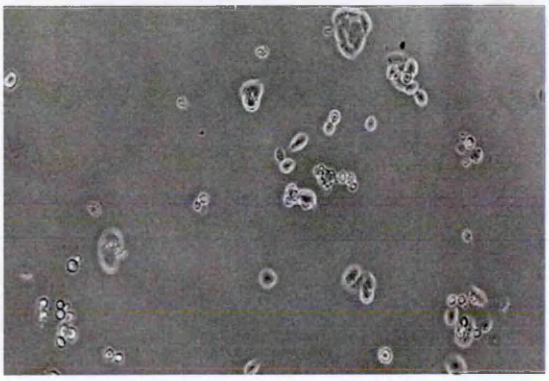

300 µg/ ml

(a) Day 4

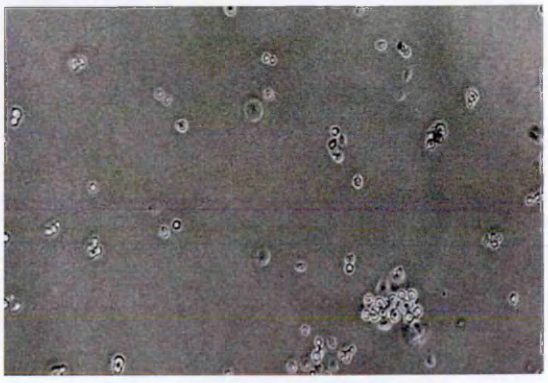

300 µg/ ml

(b) Day 7

4.1.3 Generation of CHO cells stably expressing APP695 and APP751 using pcDNA 3.1 expression vector

Methods in brief

CHO cells were plated at 4 x 10^4 cells per well of a 24-well plate and cells were allowed to adhere overnight or allowed to grow up to 80% confluence before beginning transfection. Transfection was carried out according to the procedure described in Section 2.14. After transfection, cells were then separated in order to obtain colonies which originated from single cells by limited dilution cloning procedure described in Section 2.15. During limited dilution cloning, cells were incubated as well as being selected in selective culture medium which contained 200 µg/ml of G418. Later, the selected 10 wells of a 96-well plate were chosen from the second limited dilution cloning, trypsinised and transferred to a 12 well-plate and a 6-well plate, respectively. In the 12 well-plate, cells were allowed to grow until at least 50% confluence before transferring to a 6-well plate and then cells were allowed to grown up until 80% confluence in 2 ml selective culture medium containing 100 µg/ml G418 in 6-well plate before medium was collected and processed for APP secretion analysis.

In order to analyse the level of APP secretion, selective culture medium was collected from the 6-well plate and prepared by immunoprecipitation, reduction and alkylation of disulphide bonds (Sections 2.16 and 2.17, respectively) before separation on 6% SDS-PAGE gel following by protein transfer and immunoblotting (Sections 2.18 and 2.19, respectively). Four primary antibodies were used during immunoblotting: DE2, 993, 23/2 and 1151. Each primary antibody binds to a different epitope on the APP sequence: DE2 binds to Aβ domain present in all three isoforms, 993 binds to KPI domain existing on APP751 and APP770, 23/2 binds to OX2 domain which is only exists on APP770 and 1151 binds to the N-terminal of all three APP isoforms. The SDS-PAGE gels were produced in a set of four identical gels per a set of samples, and all four gels were run at the same time. Also the protein transfer and immunoblotting procedure of four gels were carried out alongside each other.

4.1.3.1 APP695 secretion

Figure 4.1.3, all ten selected clones showed results with all four primary antibodies as expected. The serum free medium and selective culture medium from CHO770H4 were used as negative and positive controls, respectively. In comparison to both controls, CHO overexpressed APP695 clones showed a strong band of protein recognised by DE2 and 1151 primary antibodies and the molecular weight of the protein band was approximately 115 kDa, which is expected molecular weight of APP695. None of the clones produced any band recognised 23/2 antibody. Also, there were only faint bands of protein appeared at approximately 120 kDa in size against 993 antibody.

4.1.3.2 APP751 secretion

Similarly to Figure 4.1.3, the result of selective culture medium from CHO overexpressed APP751 clones are shown in Figure 4.1.4 with serum free medium and selective culture medium from CHO770H4 were used as controls. All ten clones of CHO overexpressed APP751 produced a strong protein band recognised by the DE2, 1151 and 993 antibodies and the molecular weight of the protein band was approximately 118 kDa which is expected molecular weight of APP751. None of the clones produced a protein band recognised by the 23/2 antibody.

4.1.3.3 APP770 secretion

The result of selective culture medium from CHO overexpressed APP770 clones are shown in Figure 4.1.4 with serum free medium and selective culture medium from CHO770H4 were used as controls. All ten clones produced a protein band approximately 120 kDa in size recognised by all four antibodies.

Figure 4.1.3 Protein expression analysis of secreted APP by APP695 pcDNA3.1 transfected CHO cells in the culture medium with four primary antibodies; DE2, 1151, 993 and 23/2. Samples were run on 6% SDS-PAGE gel before protein transfer. Lane 1, serum free medium (negative control). Lane 2, CHO770H4 clone (positive control) from APP770 pIREShyg2 expression vector. Lanes 3 and 14, SDS7B2. Lanes 4 to 13, clone 1 to 10 of APP695 pcDNA3.1 transfected CHO. Primary antibodies: (a) DE2, (b) 1151, (c) 993 and (d) 23/2. All ten selected clones produced protein band recognised by DE2 and 1151 antibodies located just below 116 kDa which correlated to the molecular weight of APP695; 115 kDa.

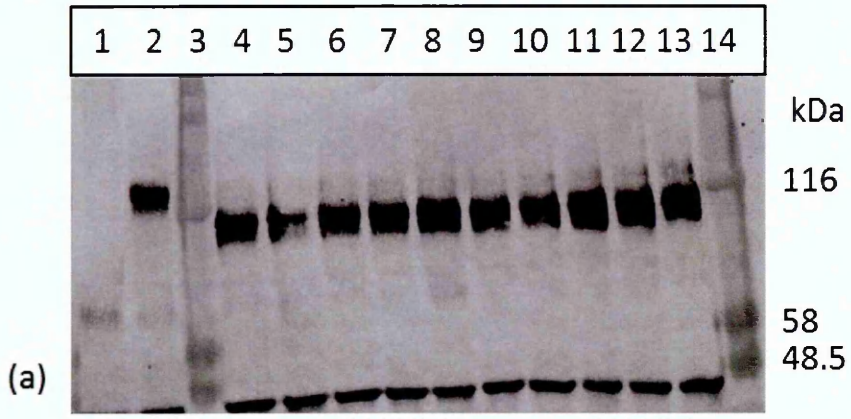
1 2 3 4 5 6 7 8 9 10 11 12 13 14
kDa
116
58
48.5

(a)

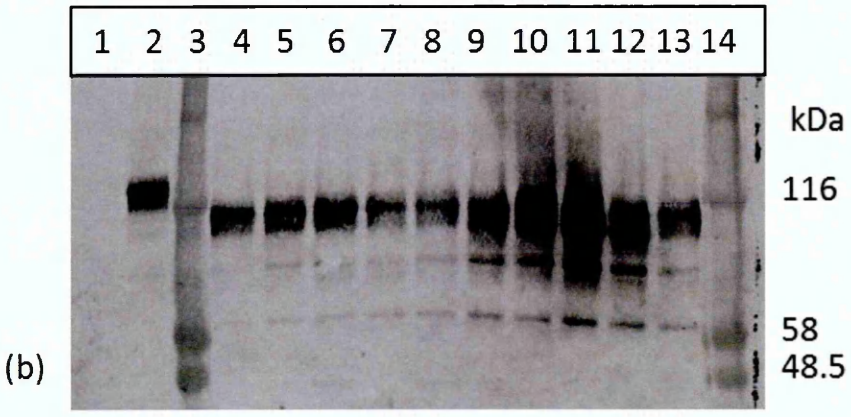
1 2 3 4 5 6 7 8 9 10 11 12 13 14
kDa
116
58
48.5

(b)

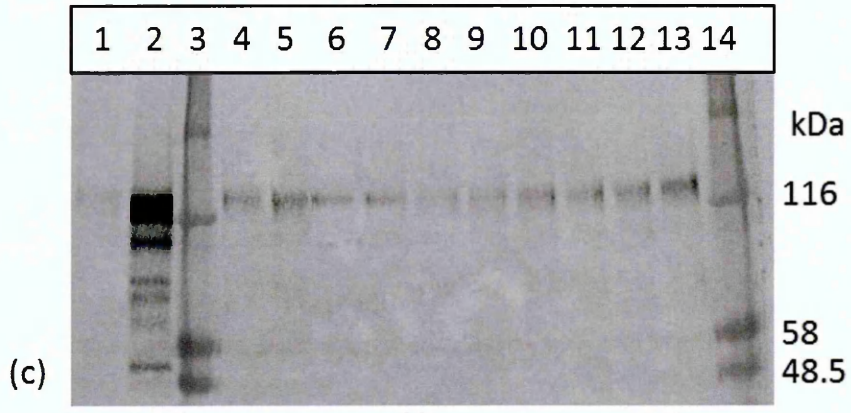
1 2 3 4 5 6 7 8 9 10 11 12 13 14
kDa
116
58
48.5

(c)

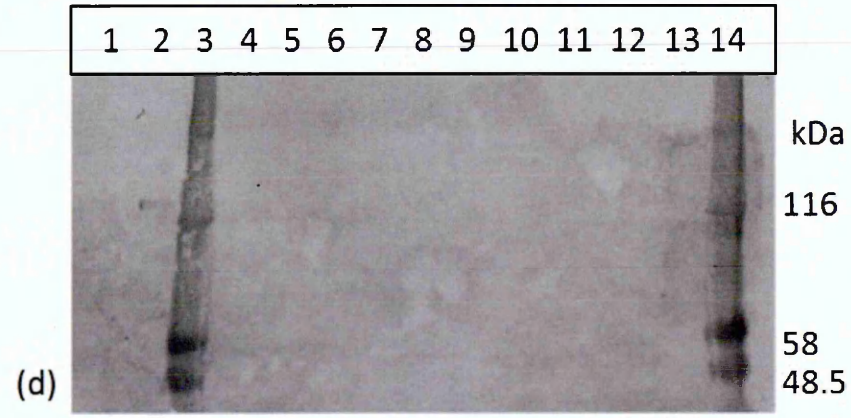
1 2 3 4 5 6 7 8 9 10 11 12 13 14
kDa
116
58
48.5

(d)

Figure 4.1.4 Protein expression analysis of secreted APP by APP751 pcDNA3.1 transfected CHO cells in the culture medium with four primary antibodies; DE2, 1151, 993 and 23/2. Samples were run on 6% SDS-PAGE gel before protein transfer. Lane 1, serum free medium (negative control). Lane 2, CHO770H4 clone (positive control) from APP770 pIREShyg2 expression vector. Lanes 3 and 14, SDS7B2. Lanes 4 to 13, clones 1 to 10 of APP751 pcDNA3.1 transfected CHO. Primary antibodies: (a) DE2, (b) 1151, (c) 993 and (d) 23/2. All ten selected clones produced a protein band recognised by DE2, 1151 and 993 antibodies and approximately 118 kDa in size which correlated to the molecular weight of APP751.

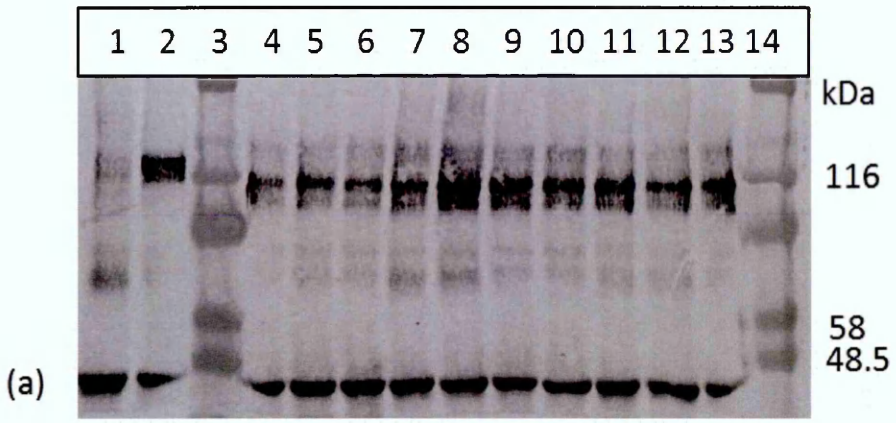
1 2 3 4 5 6 7 8 9 10 11 12 13 14
kDa
116
58
48.5

(a)

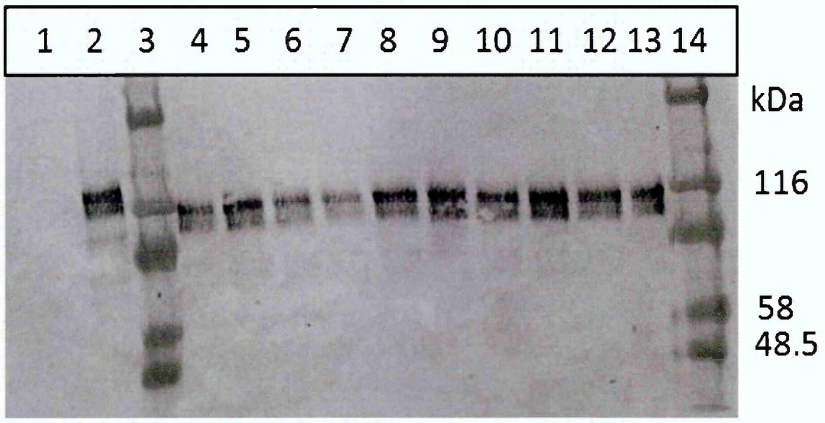
1 2 3 4 5 6 7 8 9 10 11 12 13 14
kDa
116
58
48.5

(b)

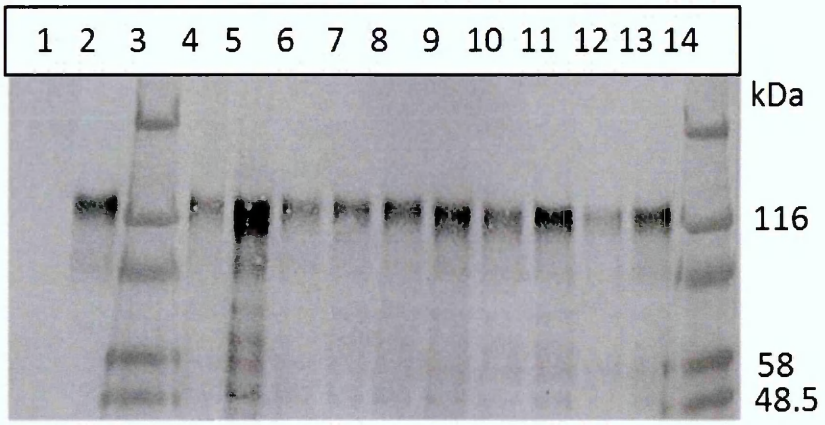
1 2 3 4 5 6 7 8 9 10 11 12 13 14
kDa
116
58
48.5

(c)

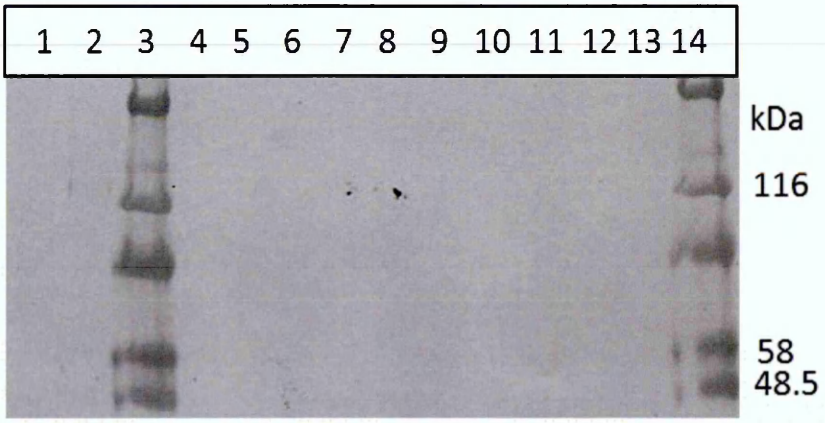
1 2 3 4 5 6 7 8 9 10 11 12 13 14
kDa
116
58
48.5

(d)

Figure 4.1.5 Protein expression analysis of secreted APP by APP770 pcDNA3.1 transfected CHO cells in the culture medium with four primary antibodies; DE2, 1151, 993 and 23/2. Samples were run on 6% SDS-PAGE gel before protein transfer. Lane 1, serum free medium (negative control). Lane 2, CHO770H4 clone (positive control) from APP770 pIREShyg2 expression vector. Lanes 3 and 14, SDS7B2. Lanes 4 to 13, clones 1 to 10 of APP770 pcDNA3.1 transfected CHO. Primary antibodies: (a) DE2, (b) 1151, (c) 993 and (d) 23/2. All ten selected clones produced protein band recognised by all four antibodies and approximately 120 kDa in size which correlated to the molecular weight of APP770.

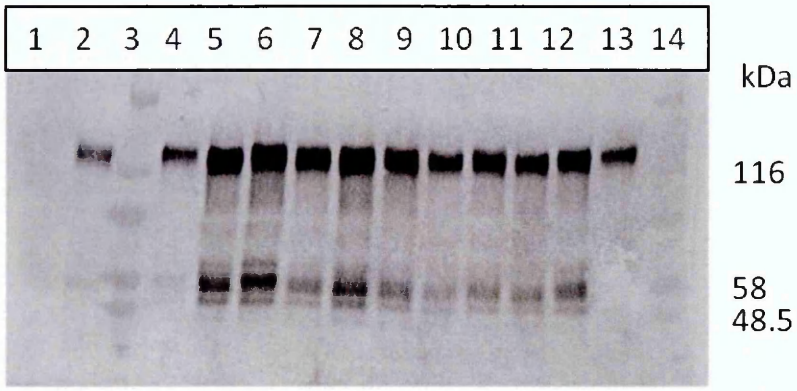
1 2 3 4 5 6 7 8 9 10 11 12 13 14
kDa
116
58
48.5

(a)

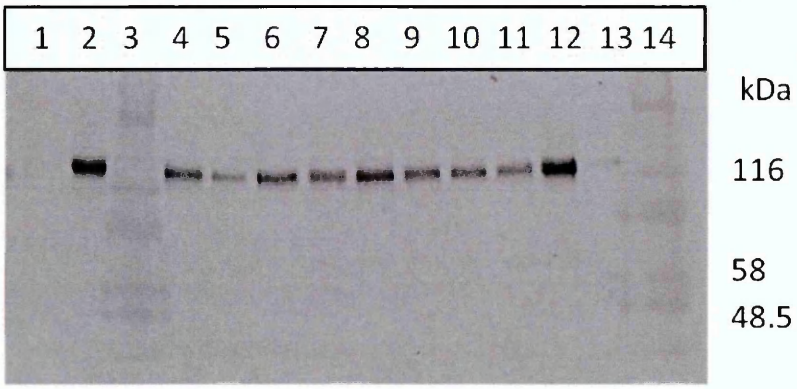
1 2 3 4 5 6 7 8 9 10 11 12 13 14
kDa
116
58
48.5

(b)

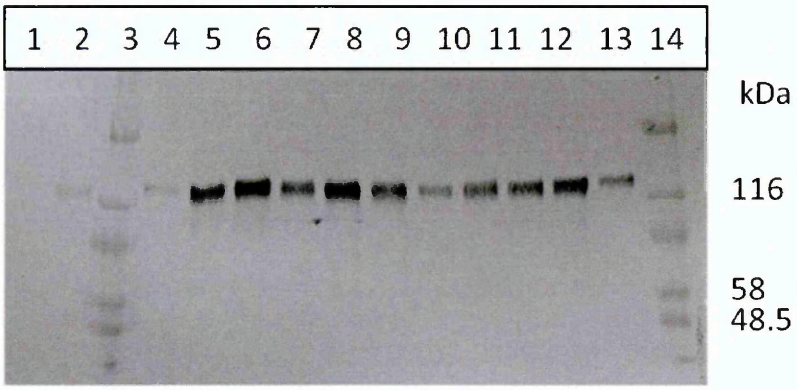
1 2 3 4 5 6 7 8 9 10 11 12 13 14
kDa
116
58
48.5

(c)

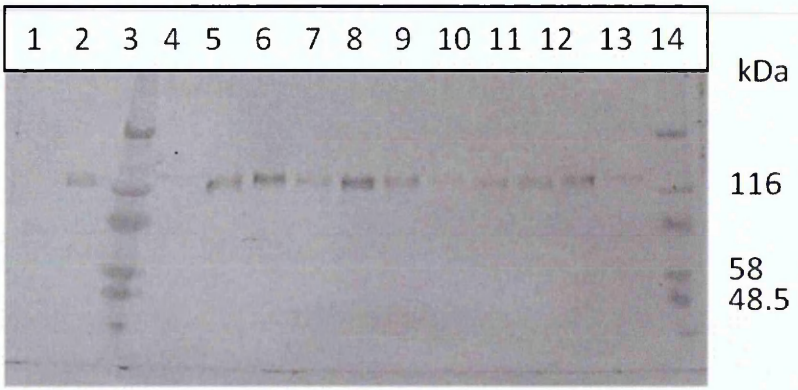
1 2 3 4 5 6 7 8 9 10 11 12 13 14
kDa
116
58
48.5

(d)

4.2 Expression of APP695, APP751 and APP770 by HEK293 cells using pcDNA3.1 expression vector

It was demonstrated earlier in this Chapter that CHO cells stably expressing three APP isoforms could be generated using the pcDNA3.1 synthesised expression vector containing APP695, APP751 and APP770 cDNA. However, in order to closely reflect the situation of Alzheimer's disease, the Human Embryonic Kidney 293 cell line (referred to as HEK293) was selected as a host cell to stably express all three isoforms of APP. Hence the third objective of this project was to stably express APP695, APP751 and APP770 in HEK293 cells.

4.2.1 Introduction

In 1977, a group of scientists; Graham, Smiley, Russell and Nairn carried out a transformation of human embryonic kidney cells by exposure to human adenovirus, which later produced HEK cells and became HEK 293 that are commonly used as a tool in protein expression systems (Graham et al. 1977). There are several reasons suggesting that HEK293 is an ideal candidate as a host cell for studies of APP expression and processing that are related to Alzheimer's disease;

- HEK293 cells allow expression vectors containing the CMV promoter to control protein synthesis and allow genes of interest in expression vectors to integrate into the HEK genome.
- HEK293 cells express several signalling pathways which are similar to neurons.
- HEK293 is a common and useful tool in reproduction various kind of neuronal protein due to its simple structure; both physically and biochemically.
- HEK293, similar to neurons, expresses four neurofilament subunits.
- Specific neuronal mRNAs can be found in HEK293.

Furthermore, HEK293 cells have a higher protein synthesis rate in comparison to CHO cells. For example, HEK293 cells are able to produce 10 mg of protein in few weeks while CHO cells take months (Thomas and Smart 2005).

It is an important prerequisite to determine the optimal concentration of selective antibiotic by determining kill curves (Section 2.13) to be used in transfection. The

optimal concentration of selective antibiotic obtained from the antibiotic kill curve procedure should be just enough to kill non-transfected host cells over a period of 4-7 days. This optimal concentration which is later used in the limited dilution cloning to select the host cells which have been transfected and kill the non-transfected host cells. The use of antibiotic in colony selection permits the host cells that take up the expression vector to benefit from an antibiotic resistance gene encoded by the vector hence the host cells are able to survive. The pcDNA3.1 expression vector contains neomycin resistance gene for mammalian cell culture selection, thus providing resistance to geniticin (G418).

4.2.2 Geneticin kill curve for HEK293

The expression vectors containing APP695, APP751 and APP770 cDNA were obtained from Life Technologies, UK. Each APP isoform was cloned into vector pcDNA 3.1. The pcDNA 3.1 contains two antibiotic resistance genes; ampicillin and neomycin shown in Figure 4.1.1.

Since neomycin is not toxic to mammalian cells, geneticin (G418) was used as a selectable marker in mammalian cell culture due to its specificity for the mammalian ribosome. G418 is classified as an aminoglycoside antibiotic and is produced by *Micromonospora rhodorangea*. G418 kills mammalian cells through the inhibition of protein synthesis by restricting peptide elongation (Eustice and Wilhelm 1984).

Methods in brief

The recommended concentration range of G418 in HEK293 cell culture selection is 400-1000 µg/ml (Section 2.13). The chosen concentrations were 0, 200, 400, 600, 800 and 1000 µg/ml, where 0 µg/ml were used as a controlled concentration. The kill curve experiment was carried out in 6-well plates over a 7-day period. The HEK293 cells were allowed to adhere for at least six hours before the addition of various concentrations of G418.

Results

Cells grew normally with an inverse trend between cell growth and concentration of antibiotic. At concentrations of G418 above 600 µg/ml cells were all dead by the

second day after adding antibiotic. As shown in Figure 4.2.1 (a) on day 4, at 200 µg/ml of G418, cells appeared healthy but did not grow as fast as cells in the control well which contained no G418. Also, at 400 µg/ml of G418 few cells began to die whereas there were great numbers of dead cells at 600 µg/ml of G418. Furthermore, on day 7 at 200 µg/ml, cells became 80% confluence while there were significant numbers of dead cells at 400 µg/ml and cells were all dead at 600 µg/ml, as shown in Figure 4.2.1 (b). Therefore, the optimal concentration determined from G418 kill curve experiment was 400 µg/ml and this concentration was used during limited the dilution cloning procedure. Also, in order to retain expression vector within HEK293 cells, the presence of G418 in culture medium was required but was reduced to 200 µg/ml.

Figure 4.2.1 HEK293 cells viability during geneticin kill curve. HEK293 cells were plated at 2.5 x 10^5 cells/well in 6-well plates and allowed to adhere over night before adding geneticin at various concentrations. (a) Day 4 of geneticin kill curve experiment. At 200 and 400 µg/ml, cells were growing but quite slowly, in comparison to control whereas cells started to die (detach from culture plate) at 600 µg/ml. (b) Day 7 of geneticin kill curve experiment. At 200 µg/ml, cells became 80% confluence while at 400 µg/ml showed significant numbers of dead and at 600 µg/ml all cells were dead. It appeared that the optimal concentration of geneticin for HEK293 cell culture selection was 400 µg/ml. (magnification 200x)

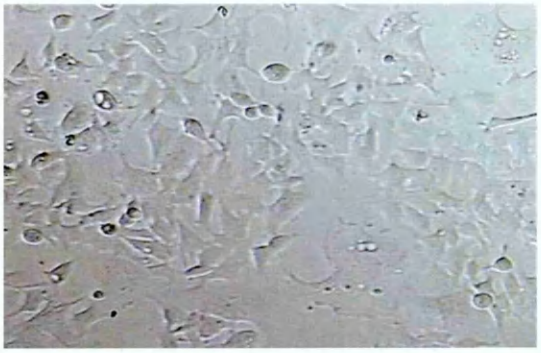

Control

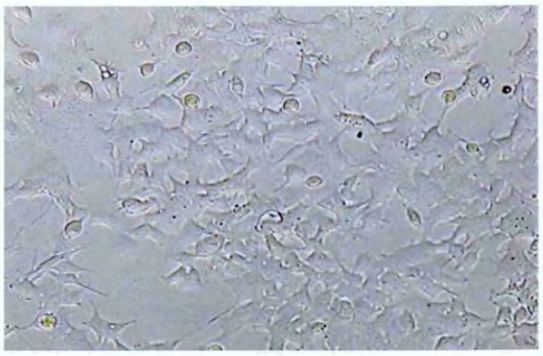

Control

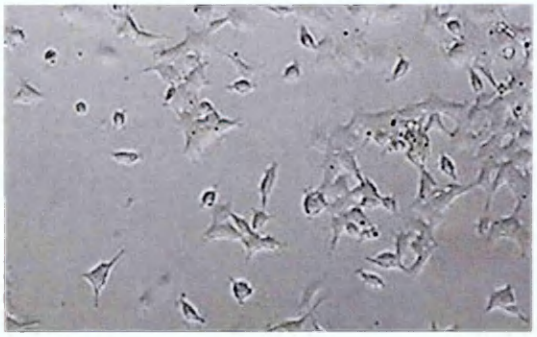

200 µg/ml

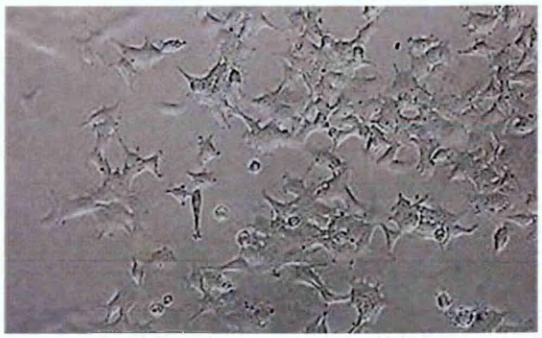

200 µg/ml

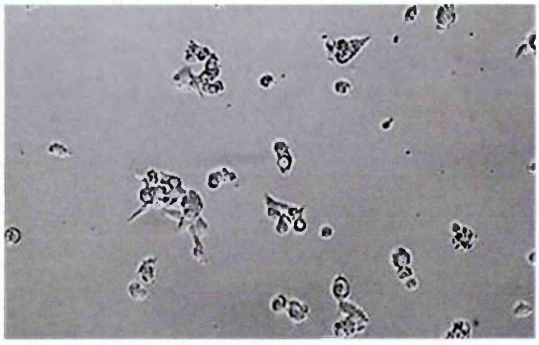

400 µg/ml

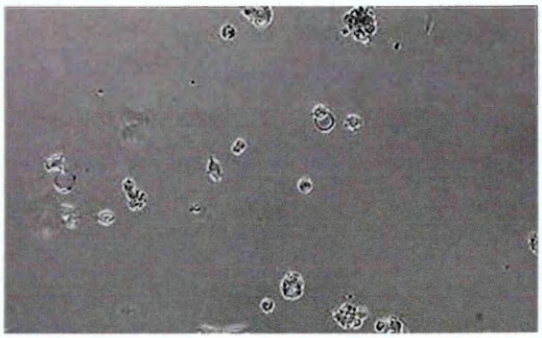

400 µg/ml

600 µg/ml

(a) Day 4

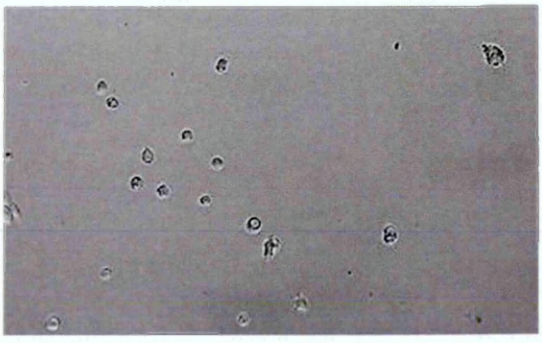

600 µg/ml

(a) Day 7

4.2.3 Generation of HEK293 stably expressed APP695, APP751 and APP770 using pcDNA3.1 expression vector

Methods in brief

HEK293 cells were plated at 1.25 x 10^5 cells per well of a 24-well plate and cells were allowed to adhere overnight or allowed to grow up to 80% confluence before beginning transfection. Transfection was carried out according to the procedure described in Section 2.14. After transfection, cells were then separated in order to obtain colonies which originated from single cells by limited dilution cloning procedure described in Section 2.15. During limited dilution cloning, cells were incubated as well as being selected in selective culture medium which contained 400 µg/ml of G418. Later, the selected 10 wells of a 96-well plate were chosen from the second limited dilution cloning, trypsinised and transferred to a 12 well-plate and a 6-well plate, respectively. In the 12 well-plate, cells were allowed to grow until at least 50% confluence before transferring to a 6-well plate and then cells were allowed to grown up until 80% confluence in 2 ml selective culture medium containing 200 µg/ml G418 in 6-well plate before medium was collected and processed for APP secretion analysis.

In order to analyse the level of APP secretion, selective culture medium was collected from the 6-well plate and prepared by immunoprecipitation, reduction and alkylation of disulphide bonds (Sections 2.16 and 2.17, respectively) before separation on 6% SDS-PAGE gel following by protein transfer and immunoblotting (Sections 2.18 and 2.19, respectively). Four primary antibodies were used during immunoblotting: DE2, 993, 23/2 and 1151. Each primary antibody binds to a different epitope on the APP sequence: DE2 binds to Aβ domain present in all three isoforms, 993 binds to KPI domain existing on APP751 and APP770, 23/2 binds to OX2 domain which is only exists on APP770 and 1151 binds to the N-terminal of all three APP isoforms. The SDS-PAGE gels were produced in a set of four identical gels per a set of samples, and all four gels were run at the same time. Also the protein transfer and immunoblotting procedure of four gels were carried out alongside each other.

4.2.3.1 APP695 secretion

The first set of protein expression results is shown in Figure 4.2.2. Selective culture medium from CHO770H4 was used as the positive control and serum free culture medium were used as negative controls on each immunoblot. All ten clones of APP695 produced strong bands of protein recognised by DE2 and 1151 antibodies and the molecular weight of protein band was approximately 115 kDa which is expected molecular weight of APP695. None of the clones produced any protein band recognised by 23/2 antibody. Also, only faint protein band recognised by 993 antibody being 120 kDa in size.

4.2.3.2 APP751 secretion

The second set of protein expression results is shown in Figure 4.2.3, similar to Figure 4.2.2. Selective culture medium of CHO770H4 was used as the positive control and serum free culture medium was used as negative controls on each immunoblot. All ten clones of APP751 produced strong bands of protein recognised by DE2, 1151 and 993 antibodies and the molecular weight of the protein band was approximately 118 kDa which is expected molecular weight of APP751. In addition, none of the ten selective clones produced any bands recognised by 23/2 primary antibody.

4.2.3.3 APP770 secretion

Figure 4.2.4 showed the final set of protein expression results obtaining from selected clones of HEK293 transfected APP770. The selective culture medium from CHO770H4 and serum free medium was used as positive and negative controls, respectively. All clones showed appropriate protein band recognised by all four primary antibodies and the protein bands was approximately 120 kDa in size which is expected molecular weight of APP770.

4.2.3.4 HEK293 stably expressing APPs selection

The results in Figures 4.2.2 to Figures 4.2.4 showed that each selected clone obtained from each transfection of the different isoforms of APP secreting different amounts of APP in the culture medium. Therefore it was crucial to select a clone from HEK293 transfected with each isoform of APP, which produced the similar amount of APP

before proceeding with further experiments in order to reduce variable results attributable to varying levels of expression.

After several attempts a set of clones consisting of three isoforms of APP, which secrete comparable amounts of APP into culture medium, was established. Figure 4.2.5, each immunoblot consisted of complete medium which was used as the negative control, collected culture medium from clone number 5 of HEK293 overexpressing APP695 (HEK695.C5), collected culture medium from clone number 1 of HEK293 overexpressing APP751 (HEK751.C1) and collected culture medium from clone number 6 of HEK293 overexpressing APP770 (HEK770.C6). All three samples and a negative control produce an appropriate positive result against all four primary antibodies used during the immunoblotting procedure.

Figure 4.2.2 Protein expression analysis of secreted APP by APP695 pcDNA3.1 transfected HEK293 cells in culture medium with four primary antibodies; DE2, 1151, 993 and 23/2. Samples were run on 6% SDS-PAGE gel before the protein transfer procedure. From left to right of each membrane: Lane 1, serum free medium (negative control). Lane 2, CHO770H4 clone (positive control) from APP770 pIREShyg2 expression vector. Lanes 3 and 14, SDS7B2. Lanes 4 to 13, clones 1 to 10 of APP695 pcDNA3.1 transfected HEK293. Primary antibodies: (a) DE2, (b) 1151, (c) 993 and (d) 23/2. All ten selected clones produced a protein band recognised by DE2 and 1151 antibodies located just below 116 kDa which correlated to the molecular weight of APP695.

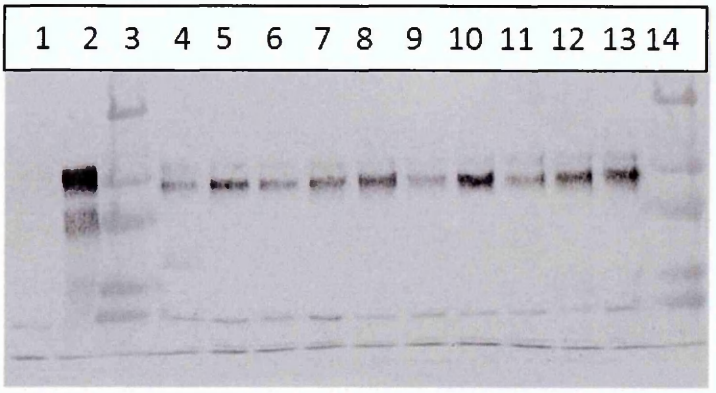
1 2 3 4 5 6 7 8 9 10 11 12 13 14
kDa
116
58
48.5

(a)

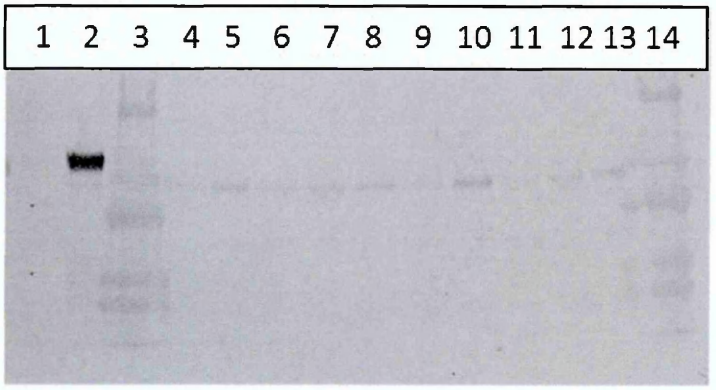
1 2 3 4 5 6 7 8 9 10 11 12 13 14
kDa
116
58
48.5

(b)

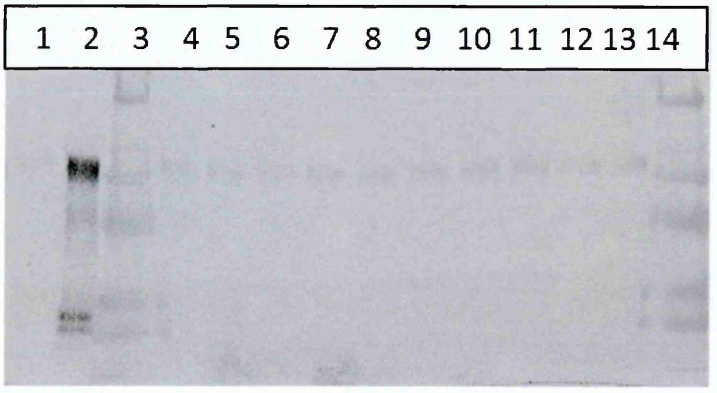
1 2 3 4 5 6 7 8 9 10 11 12 13 14
kDa
116
58
48.5

(c)

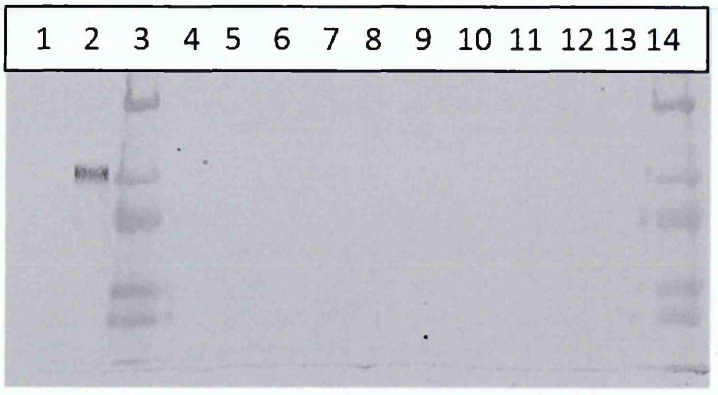
1 2 3 4 5 6 7 8 9 10 11 12 13 14
kDa
116
58
48.5

(d)

Figure 4.2.3 Protein expression analysis of secreted APP by APP751 pcDNA3.1 transfected HEK293 cells in culture medium with four primary antibodies; DE2, 1151, 993 and 23/2. Samples were run on 6% SDS-PAGE gel before the protein transfer procedure. From left to right of each membrane: Lane 1, serum free medium (negative control). Lane 2, CHO770H4 clone (positive control) from APP770 pIREShyg2 expression vector. Lanes 3 and 14, SDS7B2. Lanes 4 to 13, clones 1 to 10 of APP751 pcDNA3.1 transfected HEK293. Primary antibodies: (a) DE2, (b) 1151, (c) 993 and (d) 23/2. All ten selected clones produced a protein band recognised by DE2, 1151 and 993 antibodies and approximately 118 kDa in size which correlated to the molecular weight of APP751.

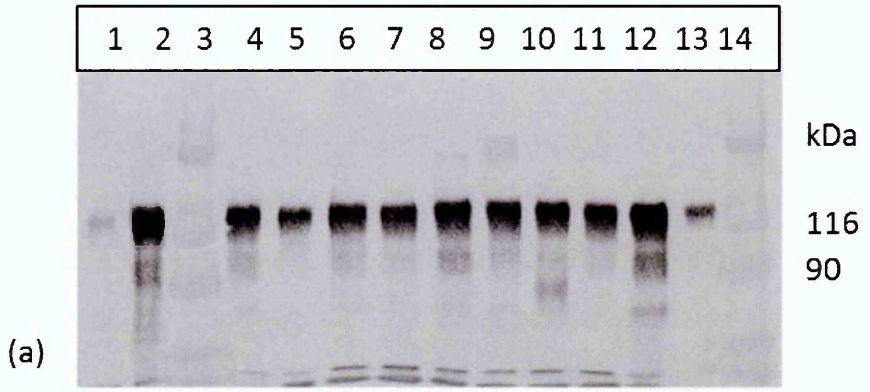
1 2 3 4 5 6 7 8 9 10 11 12 13 14
kDa
116
90

(a)

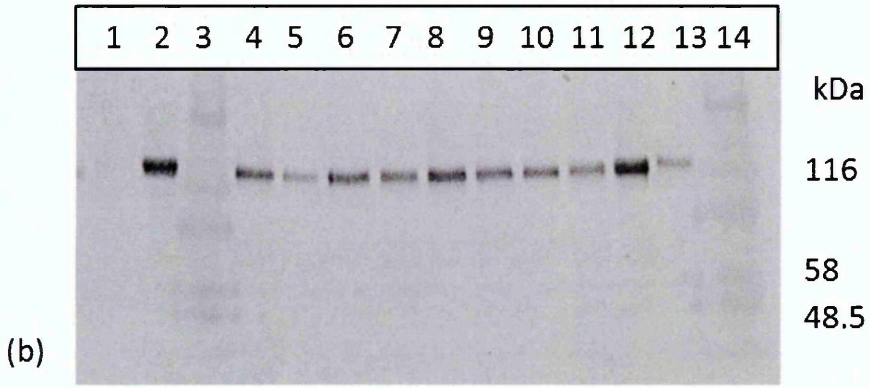
1 2 3 4 5 6 7 8 9 10 11 12 13 14
kDa
116
58
48.5

(b)

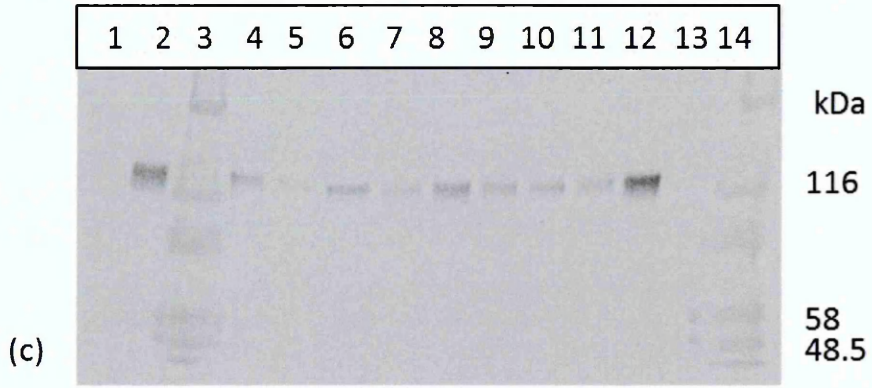
1 2 3 4 5 6 7 8 9 10 11 12 13 14
kDa
116
58
48.5

(c)

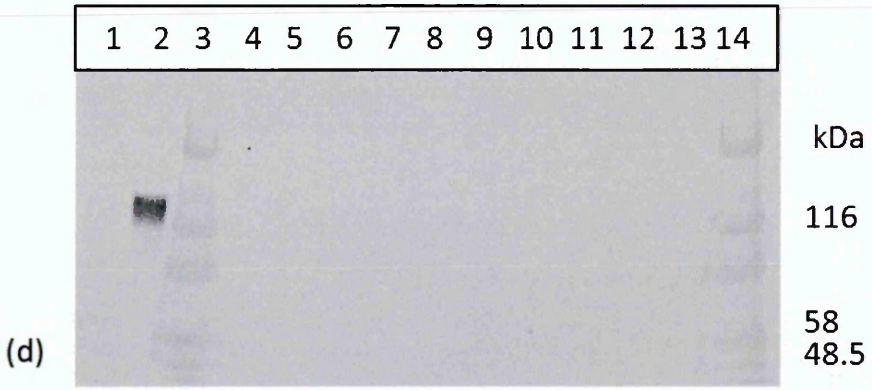
1 2 3 4 5 6 7 8 9 10 11 12 13 14
kDa
116
58
48.5

(d)

Figure 4.2.4 Protein expression analysis of secreted APP by APP770 pcDNA3.1 transfected HEK293 cells in culture medium with four primary antibodies; DE2, 1151, 993 and 23/2. Samples were run on 6% SDS-PAGE gel before protein transferred procedure. From left to right of each membrane: Lane 1, serum free medium (negative control). Lane 2, CHO770H4 clone (positive control) from APP770 pIREShyg2 expression vector. Lanes 3 and 14, SDS7B2. Lanes 4 to 13, clones 1 to 10 of APP770 pcDNA3.1 transfected HEK293. Primary antibodies: (a) DE2, (b) 1151, (c) 993 and (d) 23/2. All ten selected clones produced a protein band recognised by all four antibodies and approximately 120 kDa in size which correlated to the molecular weight of APP770.

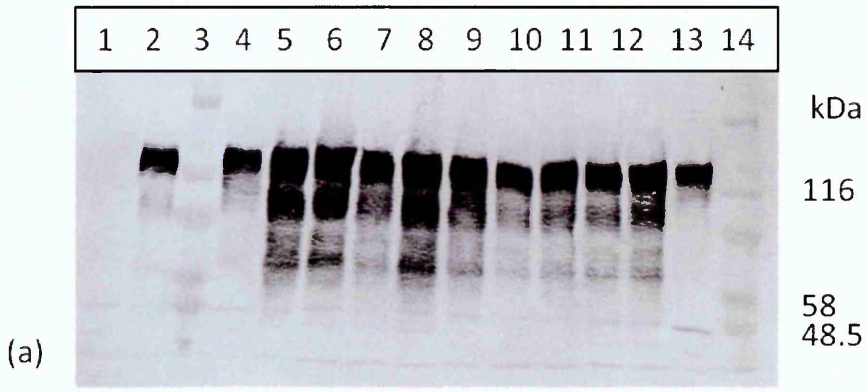
1 2 3 4 5 6 7 8 9 10 11 12 13 14
kDa
116
58
48.5

(a)

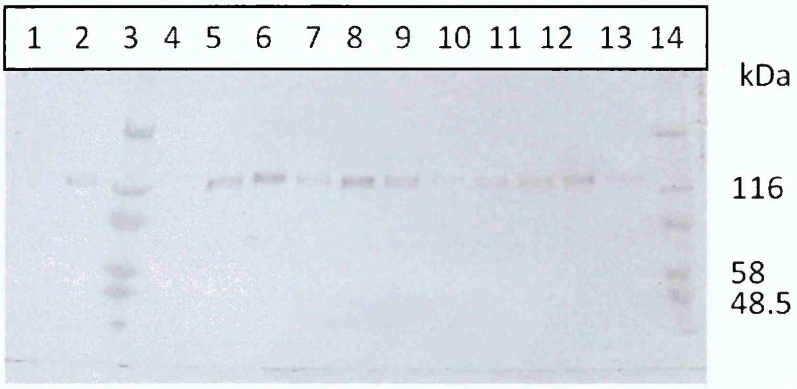
1 2 3 4 5 6 7 8 9 10 11 12 13 14
kDa
116
58
48.5

(b)

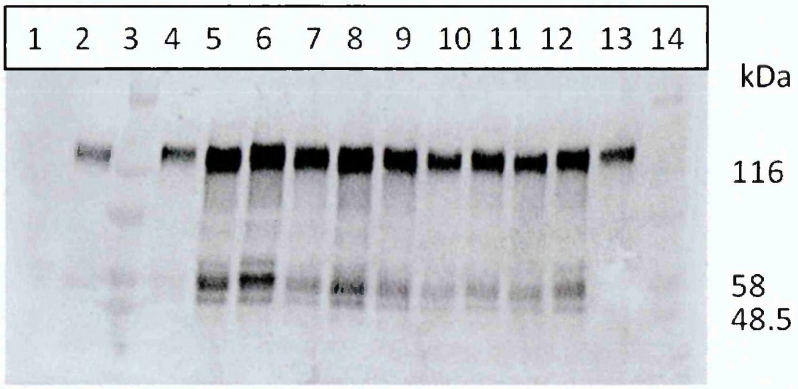
1 2 3 4 5 6 7 8 9 10 11 12 13 14
kDa
116
58
48.5

(c)

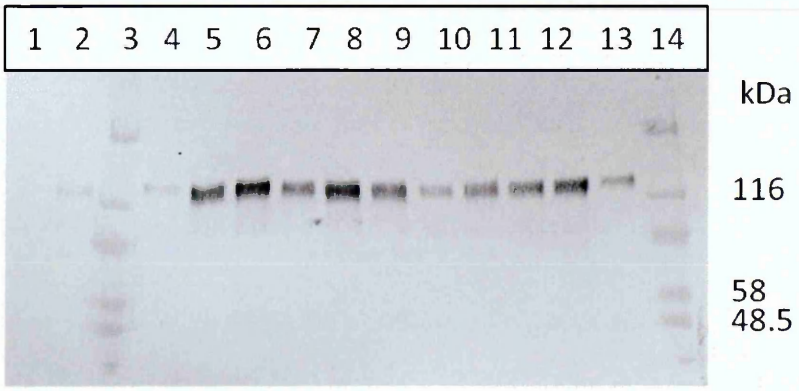
1 2 3 4 5 6 7 8 9 10 11 12 13 14
kDa
116
58
48.5

(d)

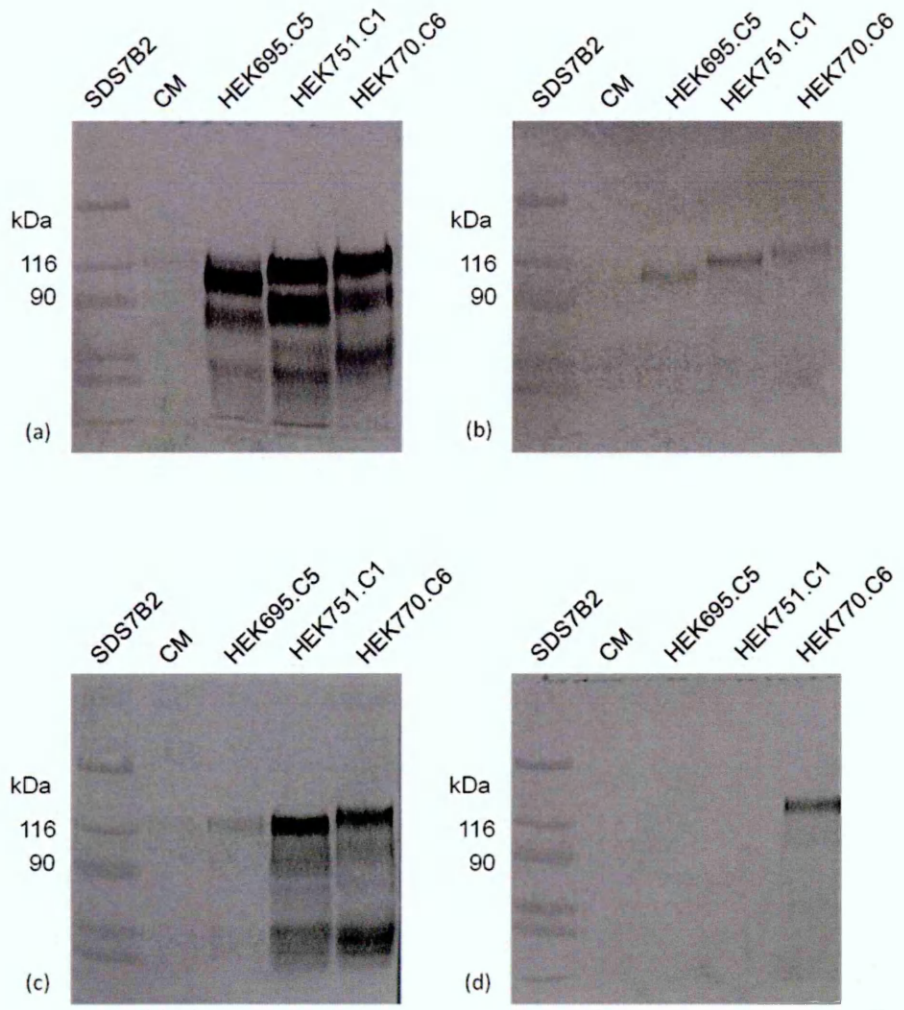

Figure 4.2.5 Protein analysis of secreted APP by HEK293 transfected pcDNA3.1 expression vector containing APP695, APP751 and APP770 cDNA, in selective culture medium over a 24-hour period with four primary antibodies; DE2, 1151, 993 and 23/2. After culture medium was prepared by immunoprecipitation, reduction and alkylation of disulphide bonds, samples were run on 6% SDS-PAGE gel before protein transfer and immunoblotting procedure. Primary antibodies: (a) DE2, (b) 1151, (c) 993 and (d) 23/2. As all three isoforms of APP produced by each clone are slightly different in molecular weight, each isoform produce the protein band at slightly different position. It was expected that APP695 was recognized by 1151 and DE2 primary antibodies and the protein band was just below 116 kDa: 115 kDa, APP751 was recognized by 1151, 993 and DE2 primary antibodies and the protein band was just above 116 kDa: 118 kDa, and APP770 was recognized by all four primary antibodies and the protein band was clearly above 116 kDa: 120 kDa.

4.3 Discussion

After many attempts of trying to establish CHO stably expressed APP695 and APP751 using an in-house constructed expression vector (pIREShyg2 expressing human APP695 and APP751), no success was achieved. The new synthetic expression vector; pcDNA3.1 expressing three isoforms of APP were obtained. Instead of a hygromycin B resistance gene, pcDNA3.1 contains a neomycin resistance gene which was used as a selectable marker in mammalian cell culture selection. The optimal concentration of G418 to be used in limited dilution cloning was 200 μg/ml and the concentration of G418 was reduced to 100 μg/ml to maintain the expression vector within the CHO cells. The DE2, 1151, 993 and 23/2 antibodies were used in immunoblotting because each antibody recognises a different epitope on APP. The DE2 and 1151 antibodies recognise Aβ domain and the N-terminal of all three isoforms of APP, respectively. The 993 antibody recognises the KPI domain on APP751 and APP770 whereas the 23/2 antibody recognises the OX2 domain on APP770. Also, 1151 and 23/2 antibodies do not recognise bovine APP which was present in the culture medium.

The ten selected clones from each isoform of APP produced the expected result towards the four primary antibodies.

Clones 1 to 10 of CHO695 produced a protein band which was approximately 115 kDa in size and recognised by DE2 and 1151 antibodies which corresponded to the molecular weight of human APP695. Also, the protein band of APP which was approximately 120 kDa in size also appeared on the membrane incubated in 993 antibody due to the existence of bovine APP in the medium and no protein band appeared on the membranes incubated in 23/2 antibody. Moreover, these results were supported by the fact that APP695 does not contain additional domains: either the KPI or the OX2 domain therefore the 115 kDa protein band was expected to only appear recognised by DE2 and 1151 antibodies.

The APP751 contain an additional domain; the KPI domain and the molecular weight of human APP751 is approximately 118 kDa. Clones 1 to 10 of CHO751 produced a protein band which was approximately 118 kDa in size and recognised by DE2, 1151 and 993 antibodies while there was no protein band recognised by 23/3 antibody. These results corresponded with APP751 composition and molecular weight.

Clones 1-10 of CHO770 produced a 120 kDa protein band recognised by all antibodies because the estimated molecular weight of APP770 is 120 kDa and APP770 contains two additional domains: the KPI and the OX2 domains hence the protein bands were recognised by all four primary antibodies.

Once the CHO clones stably expressing all three isoforms of APP were established, it was crucial to determine the shortest period of time that APP was secreted into culture medium and could be detected by immunoblotting (data not show). There were four selected time points in which selective culture medium was collected: at 0, 24, 48 and 72 hours and samples were stored at -20 °C until the culture medium was collected at the final time point. Then all collected culture medium was processed at the same time by immunoprecipitation and reduction and alkylation of disulphide bonds before separation on SDS-PAGE and immunoblotting. The secreted APP can be detected as early as 24 hours after cells were plated out. The level of secreted APP in culture medium increased according to the proliferation time. In other words, the longer the cells were allowed to proliferate the more APP they secreted into culture medium.

In order to closely reflect the situation of Alzheimer's disease, HEK293 cells were selected as a host cell to stably express all three isoforms of APP. Therefore the third objective of this project was to establish HEK293 cells stably express APP695, APP751 and APP770 in HEK293. The optimal concentration of G418 to be used in limited dilution cloning was 400 µg/ml and the concentration of G418 was reduced to 200 µg/ml to maintain the expression vector within the HEK293 cells.

Clones 1 to 10 of HEK695 produced a protein band which were approximately 115 kDa in size recognised by DE2 and 1151 antibodies which correlated to the molecular weight of human APP695. Also, the protein band of APP which was approximately 120 kDa in size also appeared on the membrane incubated in 993 antibody due to the existence of bovine APP and no protein band appeared on the membrane incubated against 23/2 antibody. Moreover, these results were supported by the fact that APP695 does not contain additional domains: either the KPI or the OX2 domain therefore the 115 kDa protein band was expected to be recognised by DE2 and 1151 antibodies.

Clones 1 to 10 of HEK751 produced a protein band which were approximately 118 kDa in size and recognised by DE2, 1151 and 993 antibodies while there was no protein band recognised by 23/3 antibody. These results corresponded with APP751 composition and molecular weight that the APP751 contain an additional domain; the KPI domain and the molecular weight of human APP751 is approximately 118 kDa.

Clones 1 to 10 of HEK293 transfected with APP770, as expected, each clone produced the 120 kDa protein band recognised by all four antibodies because the estimate molecular weight of APP770 is 120 kDa and APP770 contains two additional domains: the KPI and the OX2 domains.

Having established a number of clones of HEK293 transfected with each isoform of APP, each clone appeared to produce different amounts of APP into culture medium (Figures 4.2.2 to 4.2.4).

As one clone of each isoform of APP was to be used as a cellular model in further experiments, it was necessary to select the clone from each isoform of APP which secreted relatively similar amounts of APP into culture medium as a way to standardise APP secretion. A set of clones which produced similar amounts of APP into culture medium was found; clone number 5 of HEK293 overexpressing APP695 (HEK695.C5), clone number 1 of HEK293 overexpressing APP751 (HEK751.C1) and clone number 6 of HEK293 overexpressing APP770 (HEK770.C6). The samples were prepared from selective culture medium containing 200 µg/ml of G418 from these clones were resolved on gels following by immunoblotting procedure using all four primary antibodies as shown in Figure 4.2.5. As expected, HEK695.C5 produced a protein band at approximately 115 kDa and was recognised by DE2 and 1151 antibodies because APP695 does not contain either the KPI or the OX2 additional domains. HEK751.C1 produced a protein band at approximately 118 kDa and was recognised by DE2, 1151 and 993 antibodies because APP751 contains a KPI additional domain and finally HEK770.C6 produce a protein band at approximately 120 kDa which was recognised by all four antibodies as APP770 contains both the KPI and the OX2 domains. Also, it appeared that all clones showed anticipated responses against all primary antibodies as well as producing similar amounts of APP.

To conclude, the work in this Chapter showed that it was possible to stably express the three isoforms of APP in HEK293 cells and also to select clones of HEK293 overexpressing each isoform of APP which secreted the comparable amounts of APP into the culture medium. These clones could now be used as a cellular model of APP for further experiments to investigate factors that modulate APP cleavage and secretion.

Chapter 5: Effects of foetal bovine serum on HEK293 cells transfected with APP isoforms

5.1 Introduction

As described in Chapter 4, not only were HEK293 cells stably expressing APP695, APP751 and APP770 established but also an individual clone that expressed each isoform of APP at comparable levels were selected; HEK695.C5, HEK751.C1 and HEK770.C6. These clones could now be used as cellular models in an investigation on the effects of foetal calf serum (FCS) in culture medium on APP production which was the fourth objective of this project.

Foetal bovine serum (FBS) is typically derived from foetal calf blood which is harvested under aseptic conditions to minimize the possibility of contamination. The harvested blood is later centrifuged to separate blood cells (both red and white), platelets and coagulating factors from serum which generally contains basic essential nutrients required for cell metabolism, proliferation and growth; e.g. hormones and growth factors. FBS is a common supplement in cell culture procedures. The FBS plays four principal roles in cell culture medium; (1) provides hormonal factors which induce cell growth, proliferation and differentiation, (2) supplies culture medium with transporter proteins such as transferrin for transporting iron or lipoprotein for transporting lipid, (3) facilitates cell adherence by providing extracellular matrix molecules and (4) helps maintain pH of the culture medium by buffering and neutralising toxic substances both directly and indirectly. Nevertheless, the presence of FBS in culture medium also has disadvantages including; (1) may contain hidden substances or growth inhibitors as it is poorly defined material, (2) compositions are inconsistent due to batch-to-batch variation, (3) could be a source of endotoxins and microbial organisms and therefore it increases the risk of infection. Also, the presence of FBS might interfere with the experimental results; especially with protein purification or isolation studies (Brunner et al. 2010; Gstraunthaler 2003).

Serum deprivation and serum restriction are two of several terms used to describe cell culture procedures involving an alteration in the concentration of FBS. For example, culturing cells in serum-free or reduced serum culture medium and culturing cells in basal medium without bovine serum albumin. To date, there have been numbers of researchers who used FBS concentration alteration as a tool in their studies including protein degradation studies (Epstein, Elias-Bishko and Hershko 1975), cellular stress response studies (Levin et al. 2010), apoptosis studies (Terra et al. 2011) and imitation of pathological condition. For example, the clinical model of the pathological conditions of myocardial infarction and stroke were imitated by low glucose concentration together with FBS restricted condition and hypoxia (Hamabe, Fujita and Ueda 2005; Yu et al. 2008). As components in FBS have not been completely identified, the removal of FBS from culture medium also removes the unknown residues which might cause unknown interferences in the experiment. It was strongly supported by an experiment on skeletal muscle cells where the molecular mechanism of action of insulin was demolished by the presence of FBS in culture medium whereas in the absence of FBS, skeletal muscle cells seemed to have normal responses to insulin (Ching et al. 2010). Furthermore, restriction of FBS in culture medium can also cause the reduction in basal activity which makes cells enter quiescent G_0/G_1 phase. As a result, the population of proliferating cells are more homogenous and this aspect is commonly used in cell cycle or circadian rhythm research (Pirkmajer and Chibalin 2011). Serum deprivation is also commonly used as an apoptotic trigger in neurodegenerative diseases studies as it allows the researchers to study the morphology of the cells under stress or in malnutritious conditions as well as study newly discovered anti-apoptotic agents (Fiorelli, Kirouac and Padmanabhan 2013; Xie et al. 2013).

Although, the alteration of FBS concentrations in culture medium has been a commonly performed procedure, various experimental designs have been adopted. Therefore it was necessary to determine the effect of FBS on APP production prior to further experimentation. The objectives of this investigation were; (1) to determine if the FBS affects the cell number, APP secretion and APP mRNA level at various concentrations, and (2) to determine if the FBS affects each isoform of APP differently at various concentrations. In addition, the investigation of the effects of FBS in culture

medium on APP was carried out in three main parts; cell number, APP secretion into culture medium and APP mRNA level. Also, prior to the cell counting procedure, cells were observed for morphological changes due to the effect of FBS in culture medium.

5.2 Effects of FBS in cell culture medium on cell number

The first part of the investigation of the effects of FBS in culture medium on APP production was to examine the effect of FBS on cell number.

Methods in brief

In general, all three selected clones of HEK293 transfected APP isoforms and non-transfected HEK293 were cultured and maintained according to the cell culture procedures in Section 2.11. The experiments were carried out in 6-well plates and performed independently in triplicate. Also, there were four chosen concentrations of FBS including control: 0%, 1%, 5% and 10%. Each well contained the same original number of live cells: 5×10^5 cells in 2 ml of appropriate medium. Cells were allowed to settle and adhere for at least 6 hours before culture medium was discarded and fresh medium which contained various concentrations of FBS was added. Twenty-four hours after cells were grown in an incubator at 37°C and 5% CO_2 in 2 ml of medium containing different amount of FBS, cells were photographed using XLI cap program and culture medium was collected for APP secretion analysis followed by cell counting and cell pellet harvesting.

The cell counting procedure was carried out three times per concentration of FBS for each transfected HEK293 clone and non-transfected HEK293. Briefly, 10 µl of cell suspension and 10 µl of 0.4 % Trypan blue were combined thoroughly before pipetting 10 µl of the mixture into Countess® Cell Counting Chamber Slides and counting by using the Countess® Automated Cell Counter. Each reading obtained from the cell counting machine measured total cell number, live cell number, dead cell number per ml of cell suspension and percentage of cell viability.

Results

The cell count data are shown in Figure 5.2.1 as mean ± SEM. The two-way ANOVA with 95% confidence interval was coupled with Bonferroni's multiple comparisons test to evaluate any possible effects of the FBS concentration on cell number. These data were analysed based on the two independent factors; (1) the concentration of the FBS in culture medium and (2) the differences in the isoform of APP. The data regarding the effect of FBS concentrations in culture medium on cell number are shown in Figure 5.2.1 (a) and the effect of isoforms of APP on cell number are shown in Figure 5.2.1 (b). Moreover, the statistical analysis revealed that the different concentration of FBS and the isoforms of APP had significant effects on cell number ($p=0.0347$ and $p=0.0237$). However, both independent factors did not have significant statistical interaction on cell number ($p>0.05$) therefore the data gained from the different concentrations of FBS and the different isoforms of APP were interpreted separately.

Firstly, the cell count data was analysed using the same cell type cultured in complete medium (containing 10% FBS) as a control, as shown in Figure 5.2.1 (a). It was shown that the differences in the concentration of FCS did not have a significant effect on the cell number of each transfected clone. However, the non-transfected HEK293 which was cultured in culture medium containing 0% FBS showed significant reduction of cell numbers in comparison to the control ($p<0.05$).

When using non-transfected HEK293 cells cultured in culture medium containing 0%, 1%, 5% and 10% of FBS as controls, as shown in Figure 5.2.1 (b), It was shown that only the HEK751.C1, which was cultured in culture medium containing 1% FCS, showed a significant reduction of cell number in comparison to the control ($p<0.05$).

Each cell type in each culture medium containing varying amounts of FBS was photographed after the 24-hour period ended. The photographs of the cells are shown in Figures 5.2.2 to 5.2.5.

Figure 5.2.2 shows the photographs of non-transfected HEK293 cells which were cultured in culture medium containing various concentration of FBS. It can be seen that the cells started to form clumps more clearly as the concentration of FBS in culture medium reduced. The cells which were cultured in culture medium containing

0% FBS clearly formed clumps linking to each other and tended to have minimal attachment to the bottom of the well.

Figure 5.2.3 shows the photographs of HEK695.C5 which was cultured in culture medium containing various concentrations of FBS. Similarly to non-transfected HEK293 cells, the cells started to form clusters of cells as the concentration of FBS in culture medium reduced. As the cells appeared to grow more slowly in the culture medium containing lesser amount of FBS therefore clusters of cells were clearly visible.

Figure 5.2.4 shows the photographs of HEK751.C1 which was cultured in culture medium containing various amounts of FBS. The cells appeared to grow normally in culture medium containing 1% and 5% FBS while cells grew significantly slower in culture medium containing 0% FBS when comparing to culture medium containing 10% FBS (control). Also, clusters of cells started to appear in culture medium contain FBS lesser than 5%. In the 0% FBS containing medium, cells appeared thinner and elongated as well as forming networks between clumps.

Figure 5.2.5 shows the photographs of HEK770.C6 which was cultured in culture medium containing various amounts of FBS. The cells appeared to grow slowly where there was an alteration in concentration of FBS in culture medium; for example in culture medium containing 0%, 1% and 5%. In the culture medium containing 5% FBS, cells developed a round shape and began to elongate. The elongation of the cytoplasm became clearer and cells appeared thinner as the concentration of FBS in culture medium reduced to 0%.

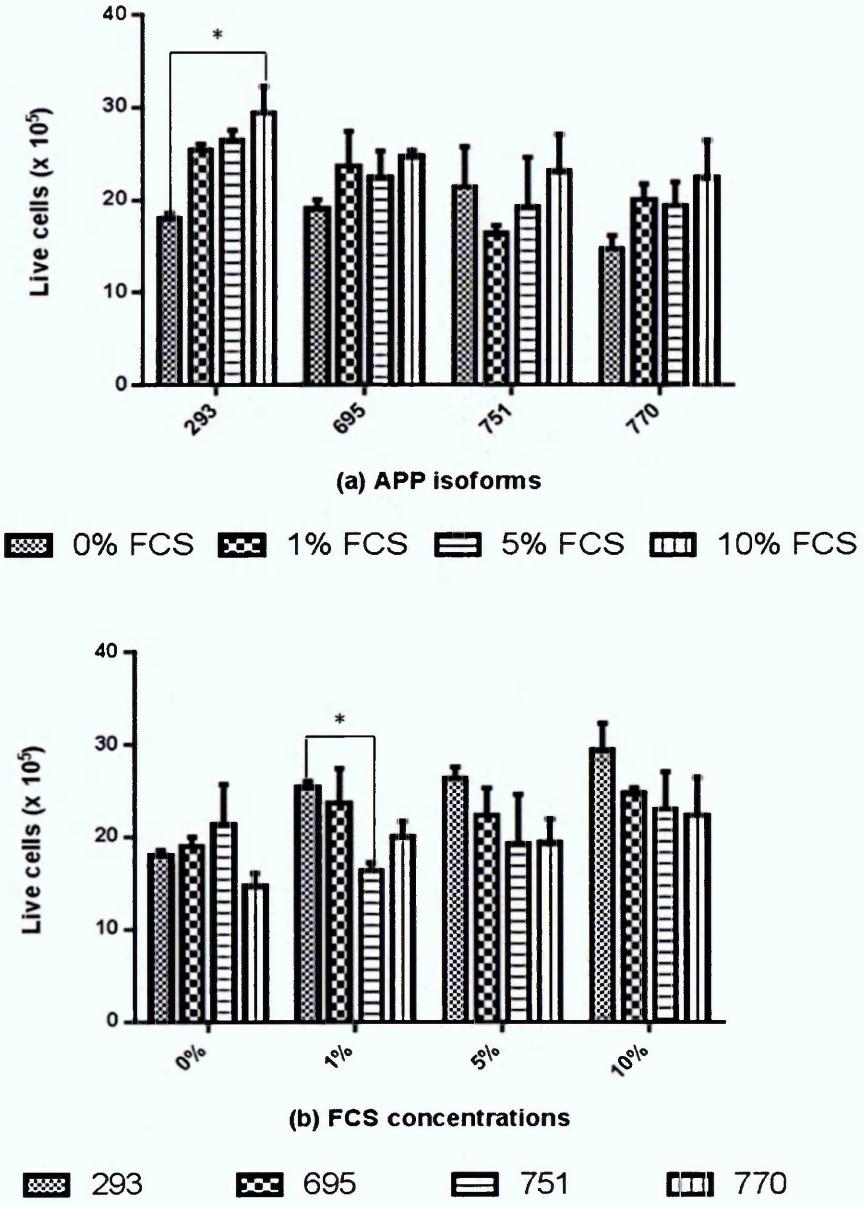

Figure 5.2.1 Overview of cell count data as mean ± SEM which were sub-grouped according to variable factors; cell types and concentration of FBS in culture medium. Both variable factors had a statistically significant effect on cell number independently ($p<0.05$). (a) Cell count data was sub-grouped by cell type and culture medium containing 10% FBS was used as control. There was a significant reduction of cell number of non-transfected HEK293 culturing in the absence of FBS in culture medium in comparison to control ($p<0.05$). (b) Cell count data was sub-grouped by concentration of FBS in culture medium and non-transfected HEK293 was used as a control. There was a significant reduction of cell number of HEK751.C1 in culture medium containing 1% FBS in comparison to control ($p<0.05$).

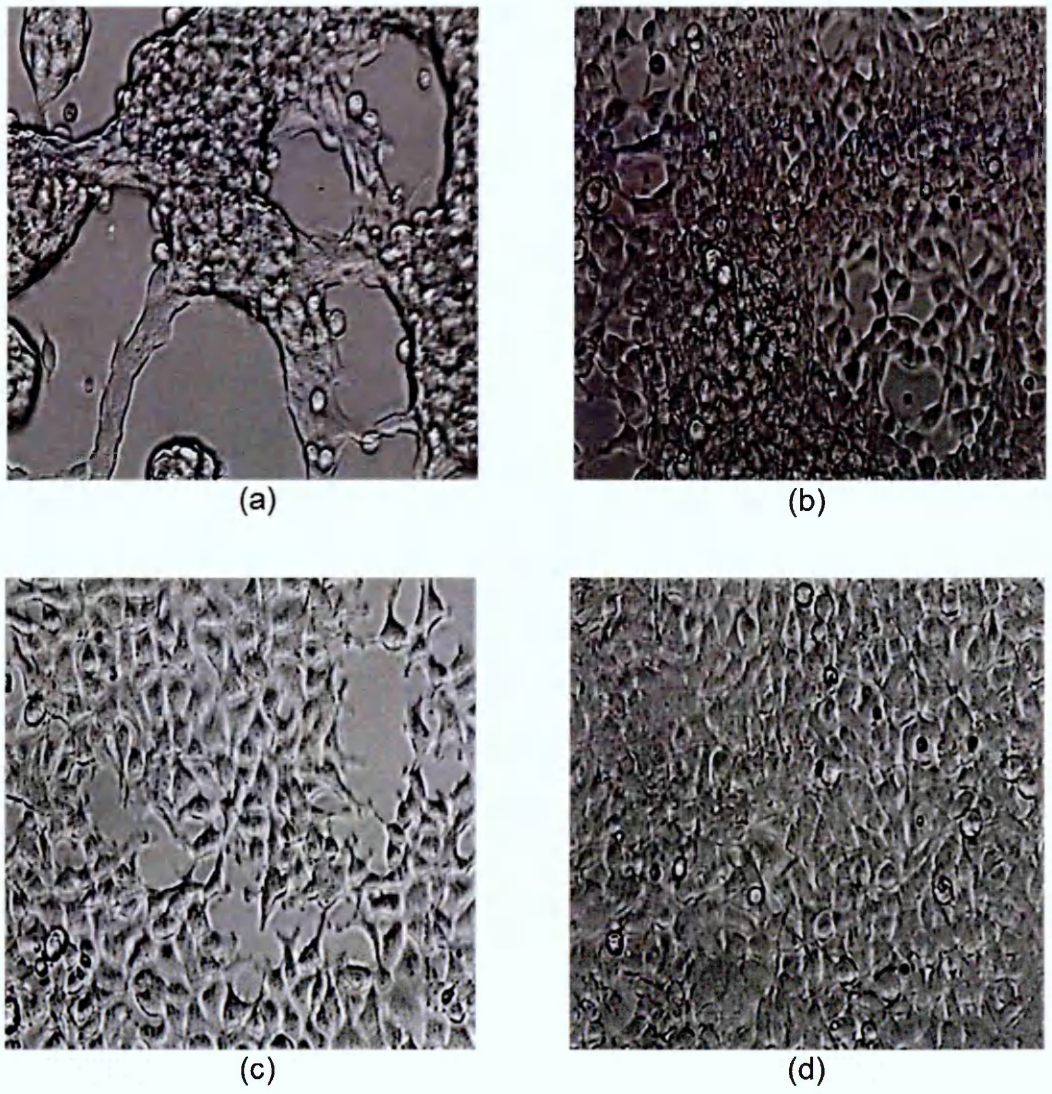

Figure 5.2.2 Non-transfected 293 cells cultured in medium containing various concentrations of FBS: (a) 0%, (b) 1%, (c) 5% and (d) 10%. There were approximately 5 x 10^5 live cells per well at the beginning of the experiment. Cells were allowed to adhere for at least 6 hours before culture medium was discarded and fresh medium containing different concentration of FCS was added. Cells were incubated in conditioned medium for 24 hours before the photographs were taken. The cells start to form clusters more clearly as the concentration of FBS in culture medium decreased. Also, the clusters of cells in culture medium containing 0% of FBS linked to each other and appeared to have minimal attachment to the well. (magnification 200x)

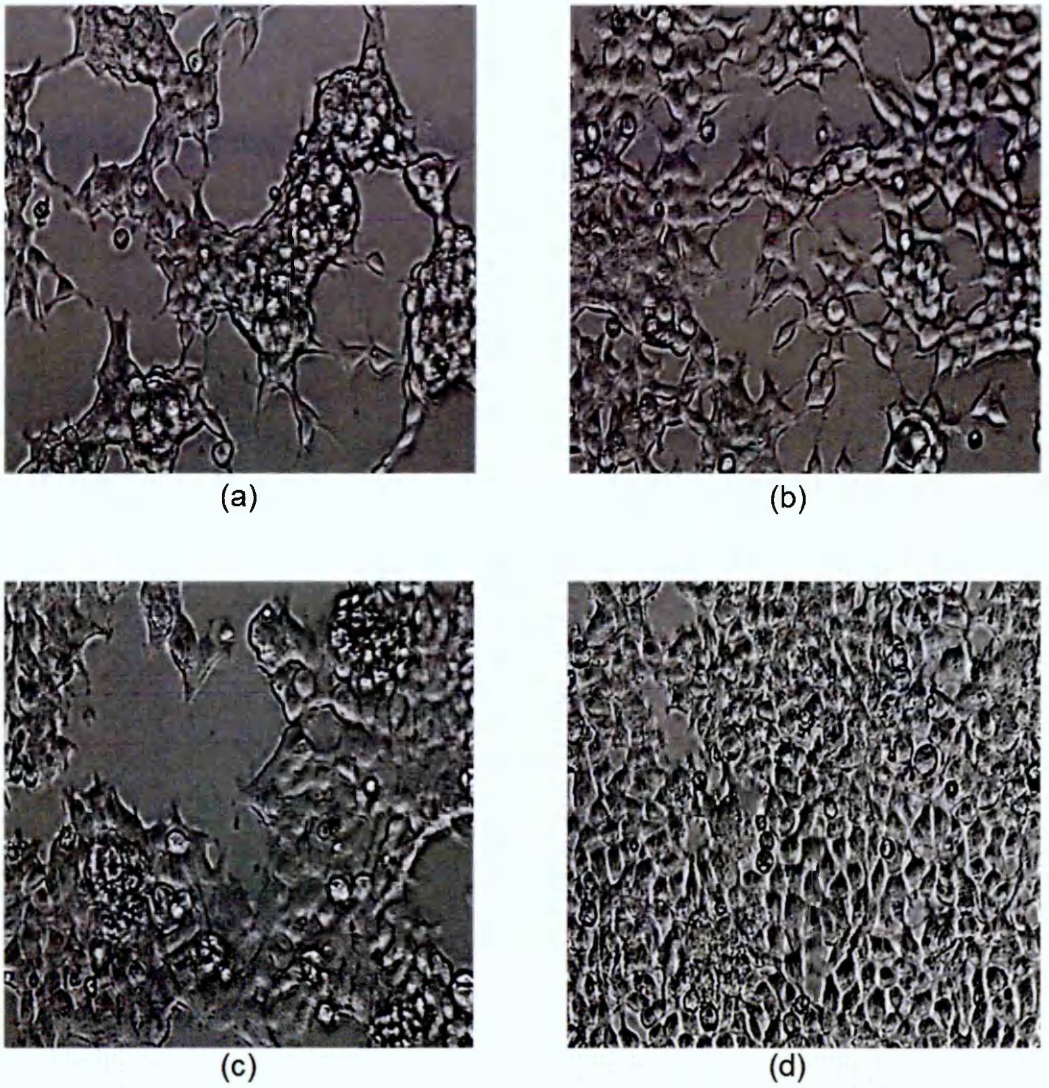

Figure 5.2.3 HEK695.C5 cultured in medium containing various concentrations of FBS: (a) 0%, (b) 1%, (c) 5% and (d) 10%. There were approximately 5 x 10^5 live cells per well at the beginning of the experiment. Cells were allowed to adhere for at least 6 hours before culture medium was discarded and fresh medium containing different concentration of FBS was added. Cells were incubated in conditioned medium for 24 hours before the photographs were taken. The cells start to form clusters more clearly as the concentration of FBS in culture medium decreased. As the cells appeared to grow slower in the culture medium containing lesser amounts of FBS therefore the clusters of cells were clearly seen. (magnification 200x)

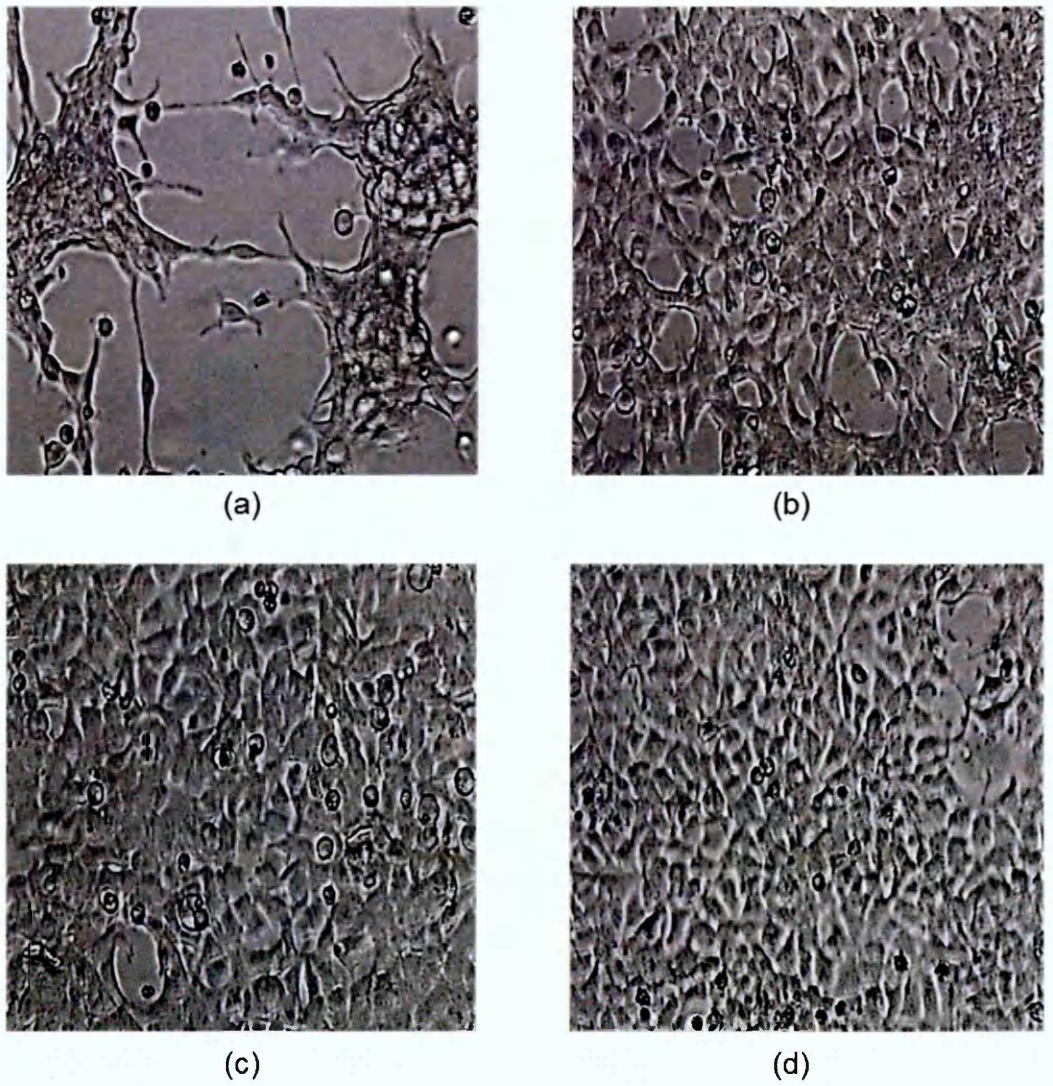

Figure 5.2.4 HEK751.C1 cultured in medium containing various concentrations of FBS: (a) 0%, (b) 1%, (c) 5% and (d) 10%. There were approximately 5 x 10^5 live cells per well at the beginning of the experiment. Cells were allowed to adhere for at least 6 hours before culture medium was discarded and fresh medium containing different concentration of FBS was added. Cells were incubated in conditioned medium for 24 hours before the photographs were taken. The cells appeared to grow normally in culture medium containing 1% and 5% FBS while cells grew significantly slower in culture medium containing 0% FBS when comparing to culture medium containing 10% FBS (control). Also, the clusters of cell started to appear in culture medium contain FBS less than 5%. In the 0% FBS containing medium, cells appeared thinner and elongated as well as forming networks between clumps. (magnification 200x)

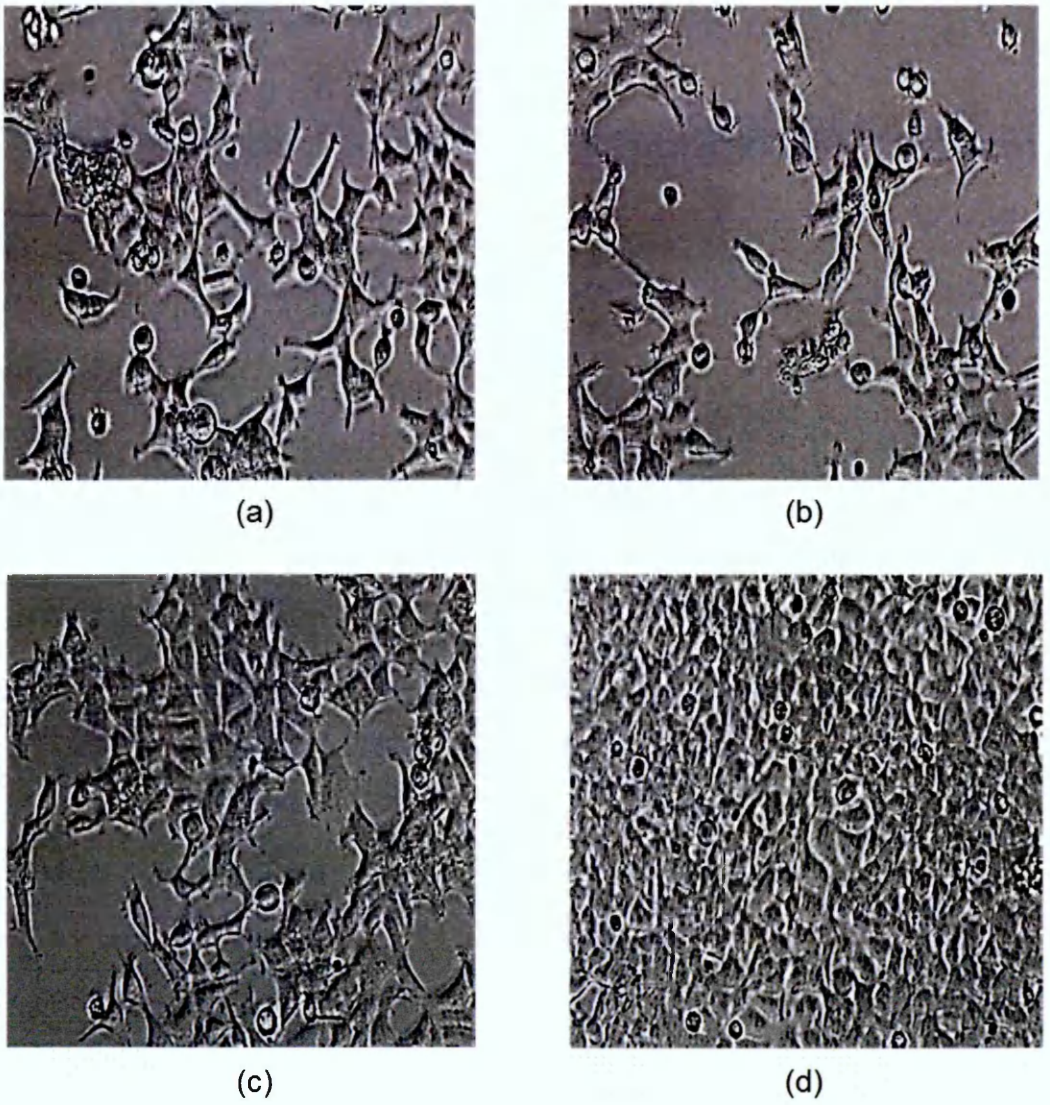

Figure 5.2.5 HEK770.C6 cultured in medium containing various concentrations of FBS: (a) 0%, (b) 1%, (c) 5% and (d) 10%. There were approximately 5 x 10^5 cells per well at the beginning of the experiment. Cells were allowed to adhere for at least 6 hours before culture medium was discarded and fresh medium containing different concentration of FBS was added. Cells were incubated in conditioned medium for 24 hours before the photographs of cells were taken. The cells appeared to grow slowly where there was an alteration in concentration of FBS in culture medium; for example in culture medium containing 0%, 1% and 5%. In the culture medium containing 5% FBS, cells developed the round shape and started to elongate. The elongation of the cytoplasm became clearer and cells appeared thinner as the concentration of FBS in culture medium reduced to 0%. (magnification 200x)

5.3 Effects of FBS in cell culture medium on APP secretion

The second part of the investigation of the effect of FBS in culture medium on APP production was to determine the amount of APP secreted into culture medium. In brief, APP located either at the cell membrane or trans-Golgi network (TGN) is cleaved by one or more of a group of secretases before being released to the extracellular space i.e. culture medium in cell culture.

Methods in brief

The culture medium was collected prior to cell counting and was then immunoprecipitated using DE2 antibody following by reduction and alkylation of disulphide bonds. These samples prepared from collected culture medium were run on 6% SDS-PAGE gel before proceeding with protein expression analysis by immunoblotting (complete procedures see Section 2.16-2.19). Four primary antibodies used during the immunoblotting procedure: DE2, 993, 23/2 and 1151. Each of the primary antibodies recognizes a different epitope on the APP sequence; DE2 recognizes Aβ domain (amino acid 1-14) which is found in all three isoforms of APP after cleavage by α-secretase, 993 recognizes the KPI domain which is found in APP751 and 770, 23/2 recognizes OX2 domain which is only found on APP770 and 1151 recognizes amino acid at the N-terminal of all three APP isoforms. DE2 and 993 primary antibodies also recognize bovine APP presented in culture medium while 1151 and 23/2 primary antibodies do not. Moreover, the fluorescence labelled secondary antibodies: IRDye 680RD Goat anti-Mouse IgG or IRDye 680RD Goat anti-Rabbit were used to detect proteins which were bound to nitrocellulose membrane.

Results

Figure 5.3.1 shows the immunoblotting results obtained from immunoprecipitated culture medium containing various concentrations of FBS collected from non-transfected HEK293. None of the samples produced the protein band recognised by 1151, 993 and 23/2 antibodies however all four samples produced faint protein band against the DE2 antibody. The protein band recognised by DE2 antibody was approximately 120 kDa in size.

The immunoblotting results obtained from immunoprecipitated culture medium containing various concentrations of FBS collected from HEK695.C5 are shown in Figure 5.3.2. All four samples produced protein bands recognised by 1151 and DE2 antibodies and the approximate size of the protein band was 115 kDa. Also, none of the samples produced the protein band against 993 and 23/2 antibodies.

The immunoblotting results obtained from immunoprecipitated culture medium containing various concentrations of FBS collected from HEK751.C1 are shown in Figure 5.3.3. These samples produced clear protein bands recognised by 1151, 993 and DE2 antibodies which was approximately 118 kDa in size. Also, none of the samples produced a protein band against 23/2 antibody.

The final set of immunoblotting results obtained from immunoprecipitated culture medium containing various concentrations of FBS collected from HEK770.C6 was shown in Figure 5.3.4. All four samples produced protein bands against all antibodies and the protein band was approximately 120 kDa in size.

The protein band of APP obtained from each set of immunoblotting was quantified using fluorescence intensity. Figure 5.3.5 (a) shows that the clones shared the same APP secretion trend in each concentration of FBS: APP751 produced more APP than APP695 and APP770. After the number of live cells was taken into account in the determination of the amount of APP secretion per cell, the same trend of APP secretion was also found as shown in Figure 5.3.5 (b). The mean ± S.E.M. of results of APP secretion (a.u.) per cell are expressed as follows:

- 0% FBS: APP751 (61.29±20.08 a.u./cell)> APP695 (60.59±24.34 a.u./cell)> APP770 (46.79±4.49 a.u./cell).
- 1% FBS: APP751 (80.68±18.23 a.u./cell)> APP695 (53.10±22.37 a.u./cell)> APP770 (47.28±8.15 a.u./cell).
- 5% FBS: APP751 (97.83±43.89 a.u./cell)> APP695 (65.21±22.11 a.u./cell)> APP770 (52.54±3.07 a.u./cell).
- 10% FBS: APP751 (63.88±13.51 a.u./cell)> APP695 (54.48±12.54 a.u./cell)> APP770 (49.93±13.28 a.u./cell).

The level of secreted APP per cell was calculated using the following formula: APP secretion level (a.u.) per cell = (fluorescence intensity x 10^6)/ cell number; where a.u. stands for Arbitrary unit.

In order to determine any possible effects of FBS on APP secretion, the amount of secreted APP was statistically analysed using two-way ANOVA with 95% confidence interval and Bonferroni's multiple comparison test. Also, these data were analysed based on two independent factors; (1) the concentrations of FBS in culture medium and (2) the differences in the isoform of APP. The statistical analysis revealed that both factors affected the APP secretion independently ($p>0.05$) but significantly; the type of cell ($p<0.0001$) and the different concentration of FBS ($p=0.0423$). The changes in the APP secretion were presented as mean of fold change ± S.E.M. to the control.

Figure 5.3.6 shows the of APP secretion level (mean of fold change ± S.E.M.) of each cell type compared to the same cells growing in the culture medium containing 10% FBS, in order to compare the APP secretion of each cell type under different concentration of FBS. Each graph in Figure 5.3.6 represents each cell type; non-transfected HEK293 cells, HEK695.C5, HEK751.C1 and HEK770.C6 and consists of four concentrations of FBS; 0%, 1%, 5% and 10%. All cell types, including non-transfected HEK293 cells, shared the same trend of increased APP secretion under various FBS concentrations; APP secretion decreased as the concentration of FBS decreased. The average fold change of APP secretion is as follows:

- Non-transfected HEK293: 5% FBS (0.95±0.02)> 1% FBS (0.93±0.02)> 0% FBS (0.79±0.09).
- APP695.C5: 5% FBS (0.98±0.07)> 1% FBS (0.82±0.13) = 0% FBS (0.82±0.14).
- APP751.C1: 5% FBS (1.02±0.08)> 1% FBS (0.95±0.11)> 0% FBS (0.86±0.11).
- APP770.C6: 5% FBS (1.02±0.14)> 1% FBS (0.99±0.21)> 0% FBS (0.79±0.13).

There were no significant differences in the level of APP secretion within each cell type of non-transfected HEK293 cells, HEK695.C5, HEK751.C1 and HEK770.C6.

Figure 5.3.7 shows the APP secretion level (mean of fold change ± S.E.M) of each clone after subtraction of endogenous APP from non-transfected HEK293 in order to compare the APP secretion between isoform of APP. Each graph in Figure 5.3.7 represents each concentration of FBS; 0%, 1%, 5% and 10% and consists of four cell types; non-transfected HEK293 cells, HEK695.C5, HEK751.C1 and HEK770.C6. In the absence of FBS and the culture medium containing 1% FBS, an increase of APP secretion level from APP695 and APP751 were comparable and lower than APP770. Also, all three isoforms of APP share the same trend of the increased APP secretion level in the culture medium containing 5% and 10% FBS; APP751 had larger increases than APP695 and APP770. The differences in the increase of the APP secretion level between isoforms of APP were not statistically significant. The average results of the increase in APP secretion level are as follows:

- 0% FBS: APP770 (5.67±0.38)> APP695 (5.04±1.72)≥ APP751 (5.03±1.21).
- 1% FBS: APP770 (5.19±0.23)> APP751 (4.55±0.81)> APP695 (4.06±1.26).
- 5% FBS: APP751 (4.75±0.66)> APP695 (4.57±1.1) > APP770 (3.67±0.43).
- 10% FBS: APP751 (4.37±0.32)≥ APP695 (4.32±0.82)> APP770 (3.47±0.12).

The APP secretion of HEK695.C5 increased significantly at all concentrations of FBS (0%: $p<0.01$; 1%, 5% and 10%: $p<0.05$). Also, the APP secretion of HEK751.C1 increased at all concentrations of FBS (0% and 5%: $p<0.01$; 1%, and 10%: $p<0.05$). The APP secretion of HEK770.C6 only showed a significant increase in 0% and 1% FBS ($p<0.001$). However, there were no significant changes in APP secretion between the cell types under the same condition.

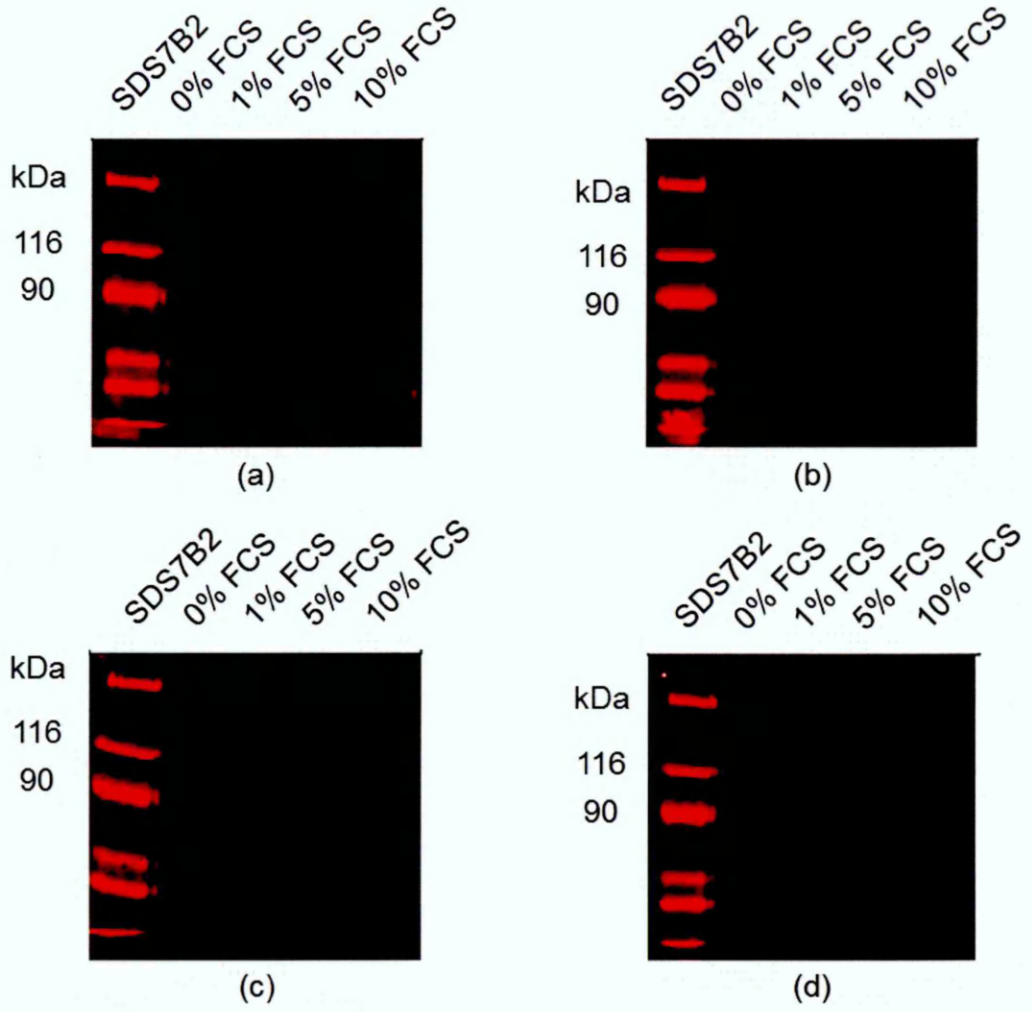

Figure 5.3.1 Protein analysis of APP secretion by non-transfected HEK293 cells which were cultured in medium containing varying concentrations of FBS: 0%, 1%, 5% and 10% over 24-hour period with four primary antibodies; (a) 1151, (b) 993, (c) 23/2 and (d) DE2. None of the samples produced a protein band recognised by 1151, 993 and 23/2 primary antibodies. However, the protein band recognised by DE2 primary antibody was due to bovine APP in FBS and this was confirmed by the sample obtained from collected culture medium which contained 0% FBS.

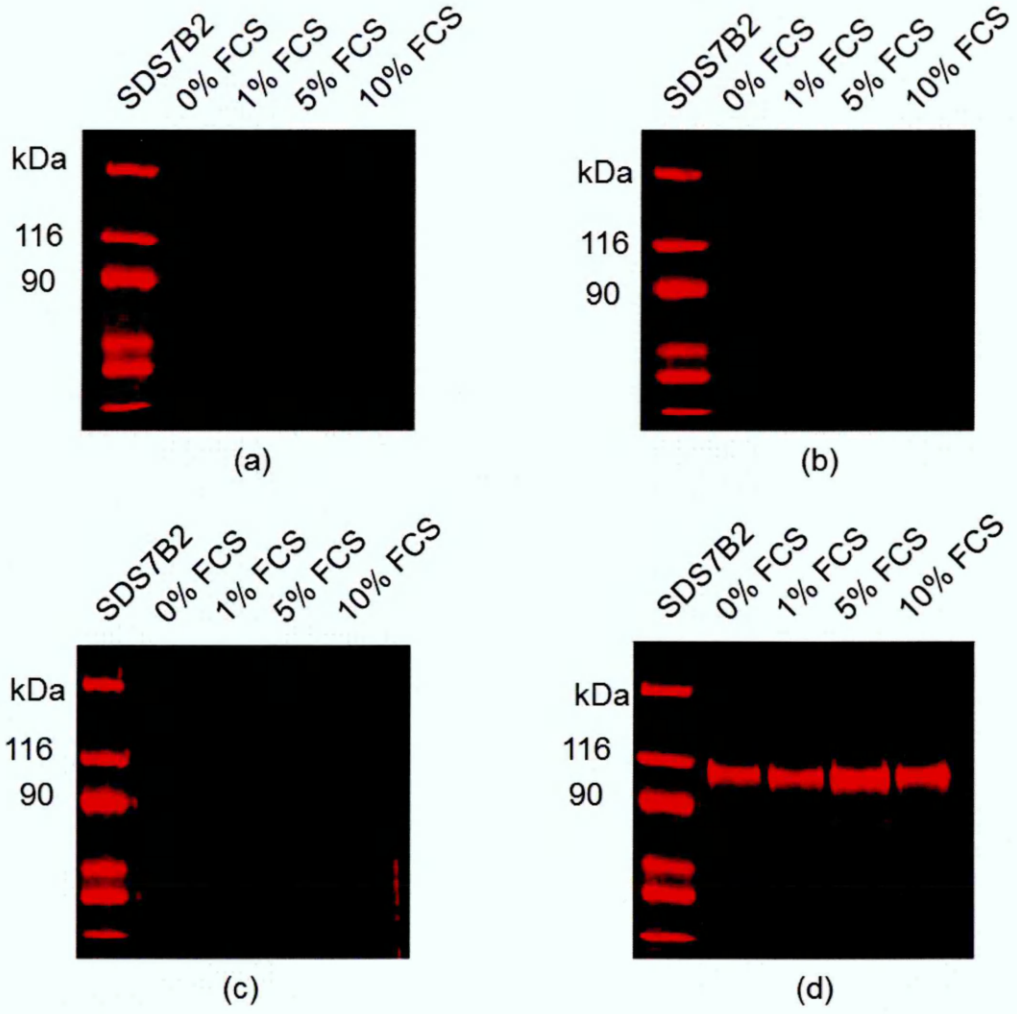

Figure 5.3.2 Protein analysis of APP secretion by HEK695.C5 cells which were cultured in medium containing varying concentrations of FBS: 0%, 1%, 5% and 10% over a 24-hour period with four primary antibodies; (a) 1151, (b) 993, (c) 23/2 and (d) DE2. All culture media containing different amounts of FBS produced positive protein bands recognised by 1151 and DE2 primary antibodies and the approximate size of the protein band was 115 kDa which corresponds to the molecular weight of APP695. The protein band recognised by DE2 antibody was stronger than 1151 antibody possibly due to an additional bovine APP in FBS. Also, none of the samples produced protein bands against 993 and 23/2 antibodies.

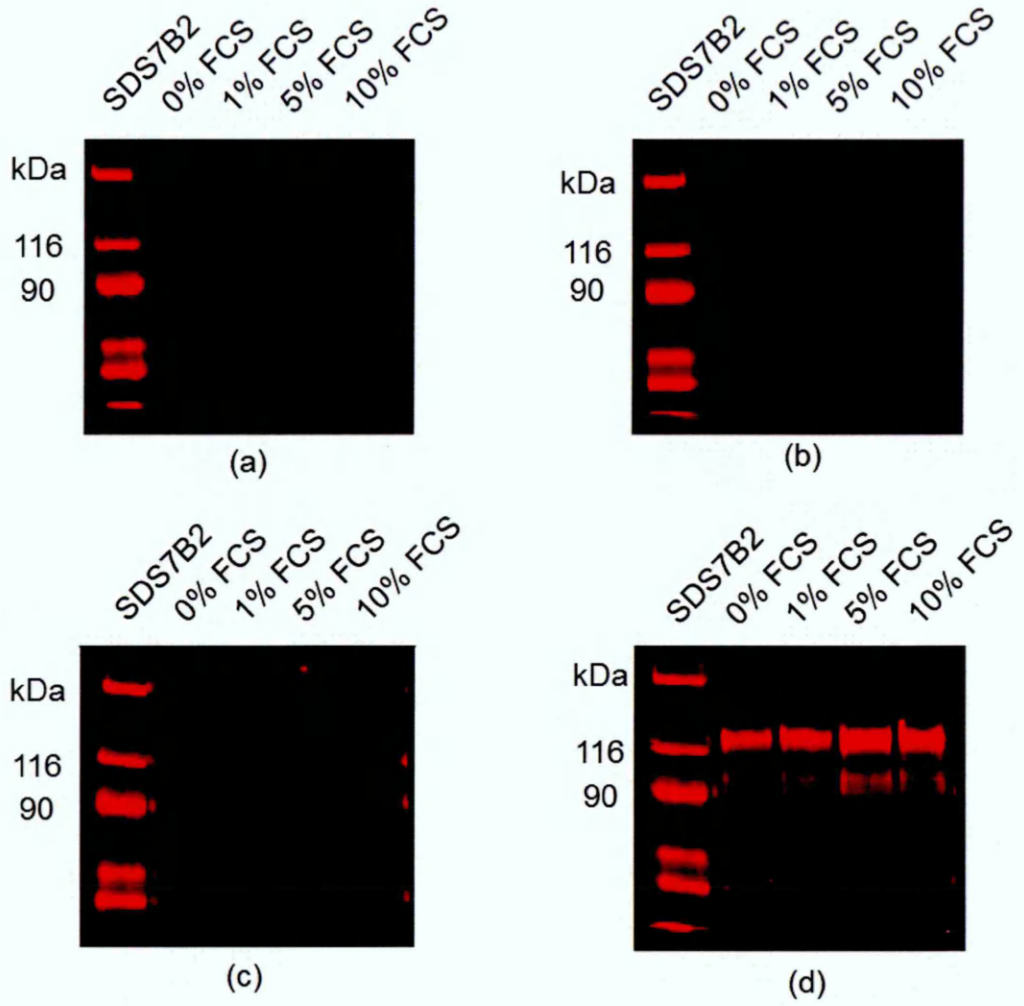

Figure 5.3.3 Protein analysis of APP secretion by HEK751.C1 cells which were cultured in medium containing varying concentrations of FBS: 0%, 1%, 5% and 10% over a 24-hour period with four primary antibodies; (a) 1151, (b) 993, (c) 23/2 and (d) DE2. All culture medium contained different amounts of FBS produced clear protein bands which were recognised by 1151, 993 and DE2 antibodies and was approximately 118 kDa in size corresponding to the molecular weight of APP751. Also, none of the samples produced a protein band recognised by 23/2 antibody.

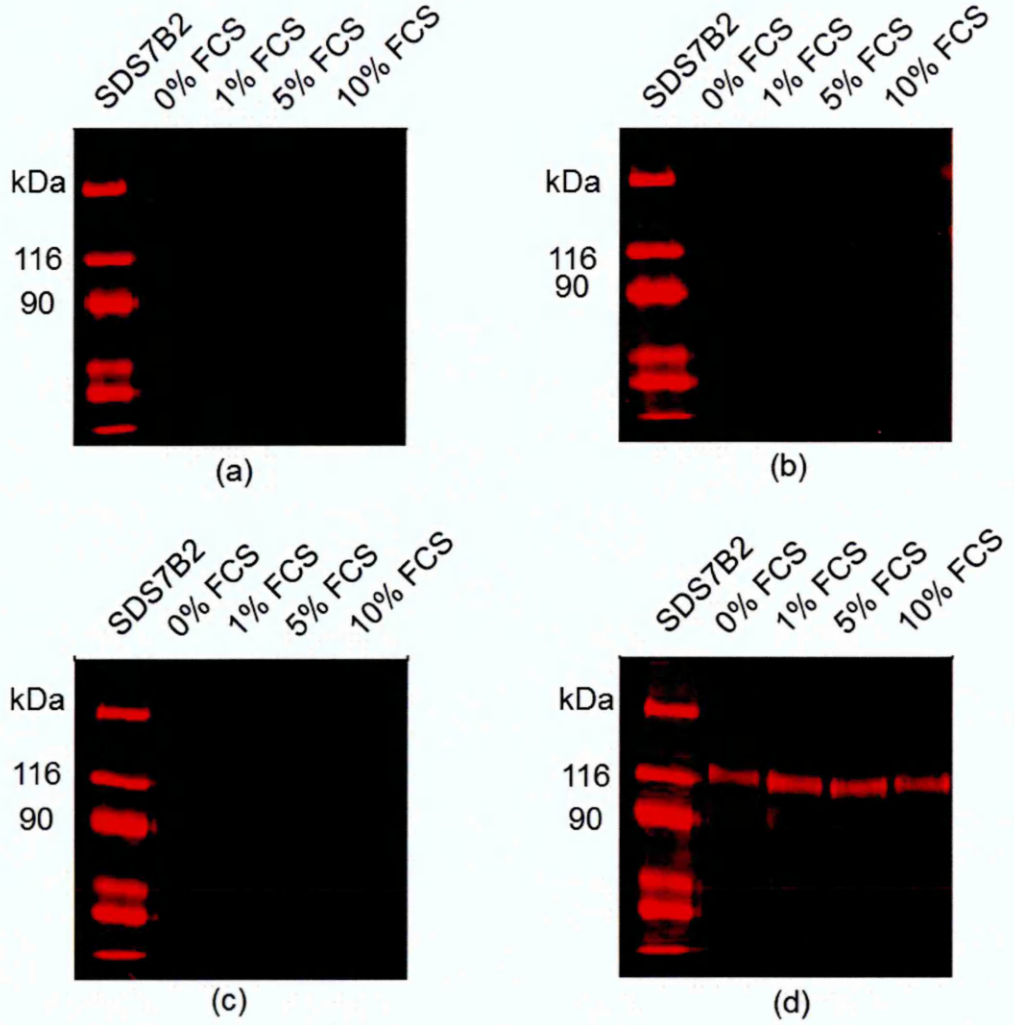

Figure 5.3.4 Protein analysis of APP secretion by HEK770.C6 cells which were cultured in medium containing varying concentrations of FBS: 0%, 1%, 5% and 10% over 24-hour period with four primary antibodies; (a) 1151, (b) 993, (c) 23/2 and (d) DE2. All culture medium contained different amount of FBS produced protein bands recognised by all four antibodies and the protein bands were approximately 120 kDa which corresponds to the molecular weight of APP770.

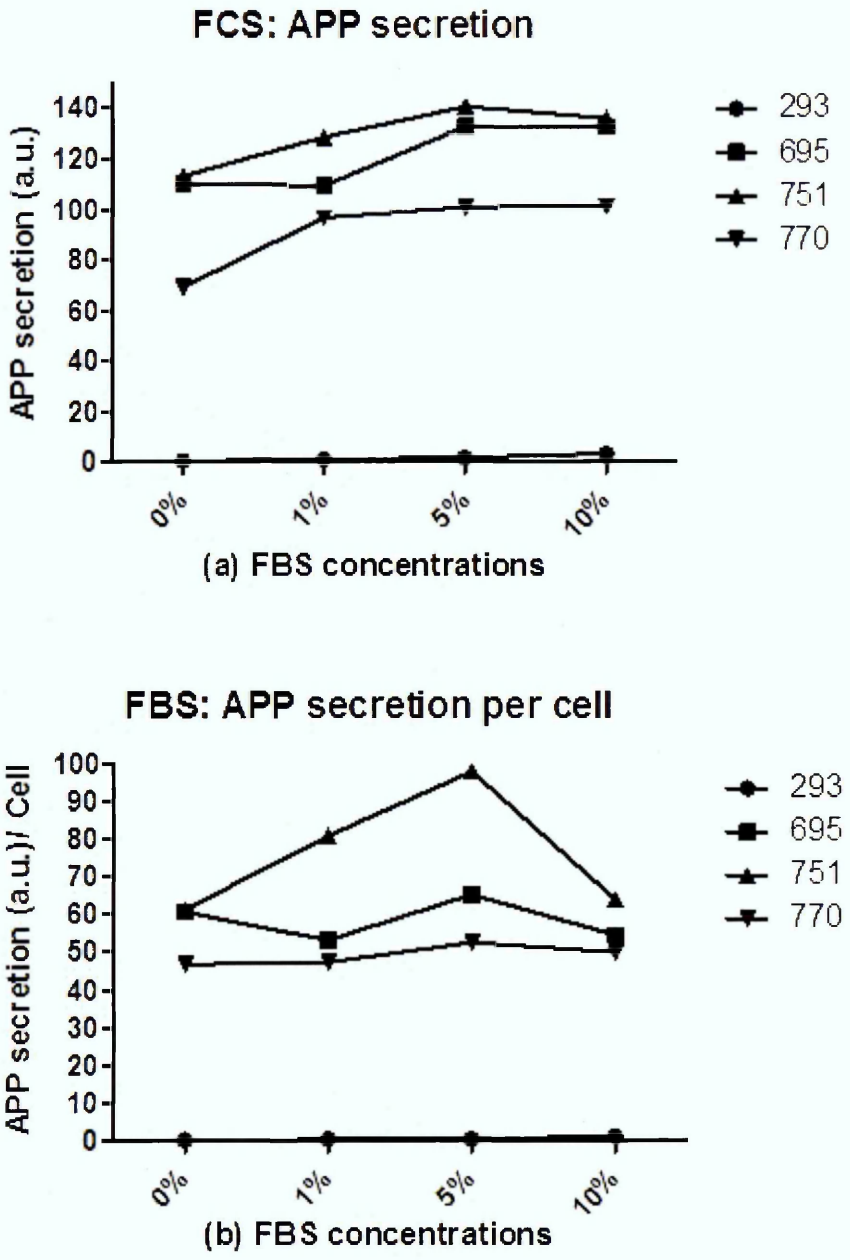

Figure 5.3.5 The APP secretion level as mean ± SEM. (a) the APP secretion (a.u.) of each cell type. All three clones shared the same pattern of APP secretion under the same FBS concentration: APP751> APP695> APP770. **(b) the APP secretion (a.u.) per cell of each cell type.** After the cell number was taken into account to calculate the APP secretion per cell, the same trend of APP secretion under the same FBS concentration was found: APP751> APP695> APP770.

Figure 5.3.6 The APP secretion level as mean ± SEM: cell types. Each graph represents each cell type; (a) non-transfected HEK293 cells, (b) HEK695.C5, (c) HEK751.C1 and (d) HEK770.C6 and consisted of four concentrations of FBS; 0%, 1%, 5% and 10%. The APP secretion of each cell type growing in culture medium containing 10% of FBS was as used as control. There were no significant changes in APP secretion within each cell type of non-transfected HEK293 cells, HEK695.C5, HEK751.C1 and HEK770.C6. However, the APP secretion trend was similar in each cell line; the APP secretion decreased as the FBS concentration decreased.

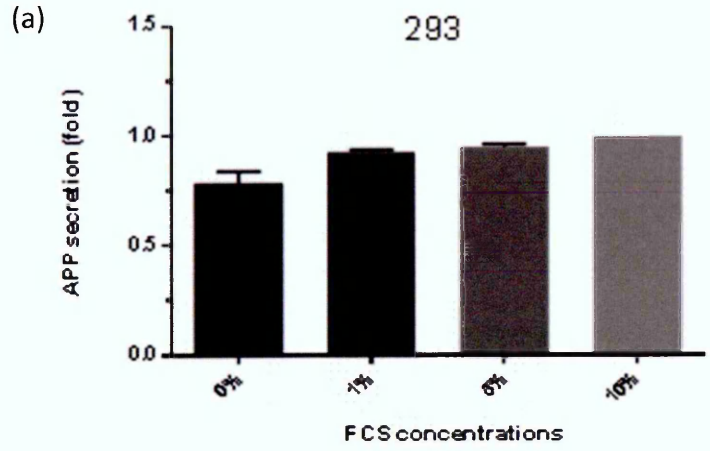
(a)
293
APP secration (fold)
1.5
1.0
0.5
0.0
0%
1%
5%
10%
FCS concentrations

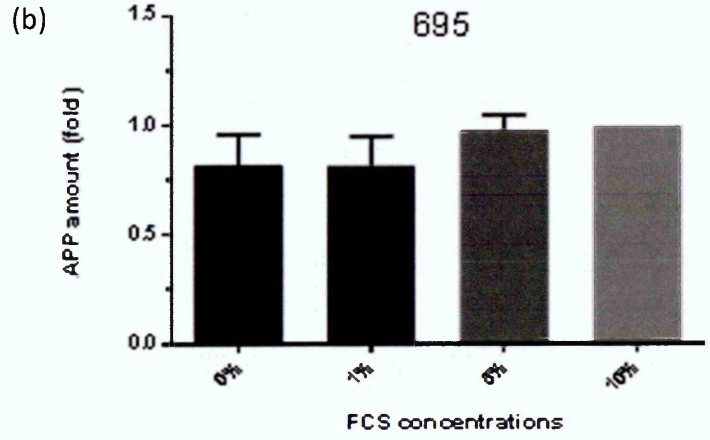
(b)
695
APP amount (fold)
1.5
1.0
0.5
0.0
0%
1%
5%
10%
FCS concentrations

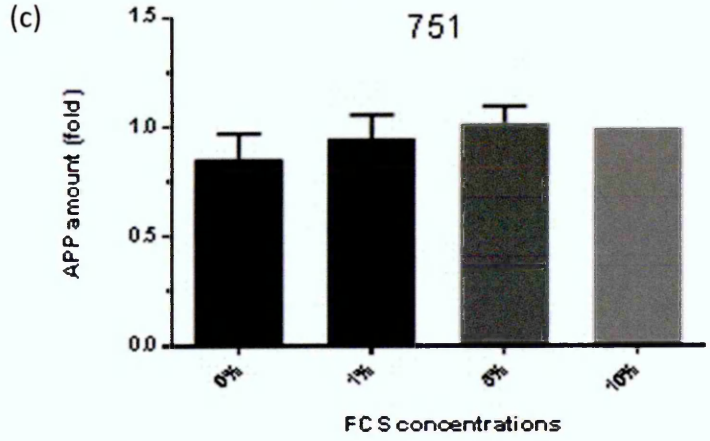
(c)
751
APP amount (fold)
1.5
1.0
0.5
0.0
0%
1%
5%
10%
FCS concentrations

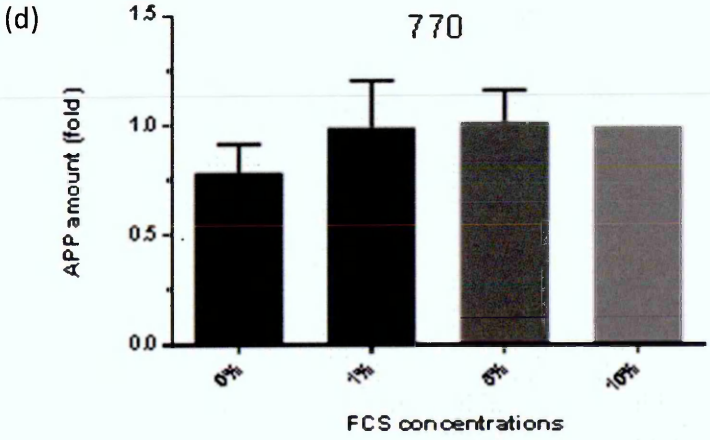
(d)
770
APP amount (fold)
1.5
1.0
0.5
0.0
0%
1%
5%
10%
FCS concentrations

Figure 5.3.7 The APP secretion level as mean ± SEM: concentration of FBS. Each graph represents each concentration of FCS; (a) 0%, (b) 1%, (c) 5% and (d) 10% and consisted of four cell types; non-transfected HEK293 cells, HEK695.C5, HEK751.C1 and HEK770.C6. The APP secretion of non-transfected HEK293 cells was used as a control. The APP secretion of HEK695.C5 increased significantly at all concentrations of FBS (0%: $p<0.01$; 1%, 5% and 10%: $p<0.05$) in comparison to the control. Also, the APP secretion of HEK751.C1 increased at all concentrations of FBS (0% and 5%: $p<0.01$; 1%, and 10%: $p<0.05$) in comparison to the control. The APP secretion of HEK770.C6 only showed significant increase in 0% and 1% FCS ($p<0.001$ for both concentrations of FBS) in comparison to the control. Moreover, there were no significant differences in APP secretion between cell types under the same conditions.

(a)

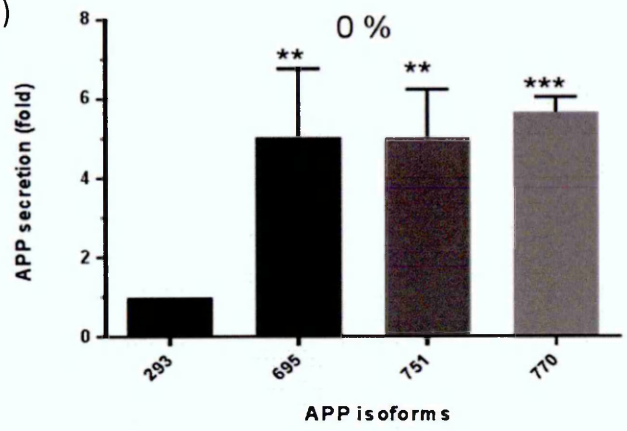
0 %
APP secretion (fold)
0
2
4
6
8
**
**
***
293
695
751
770
APP isoforms

(b)

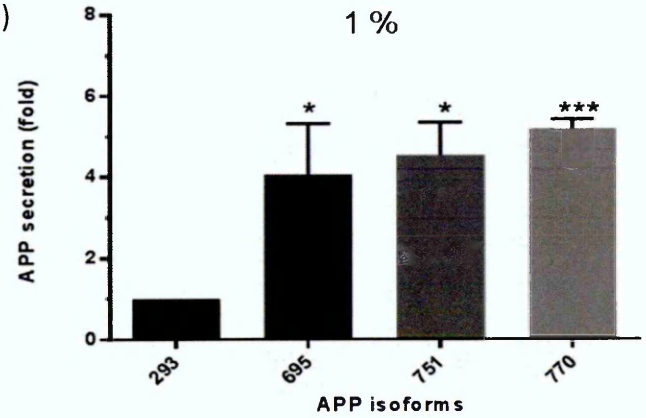
1 %
APP secretion (fold)
0
2
4
6
8
*
*
***
293
695
751
770
APP isoforms

(c)

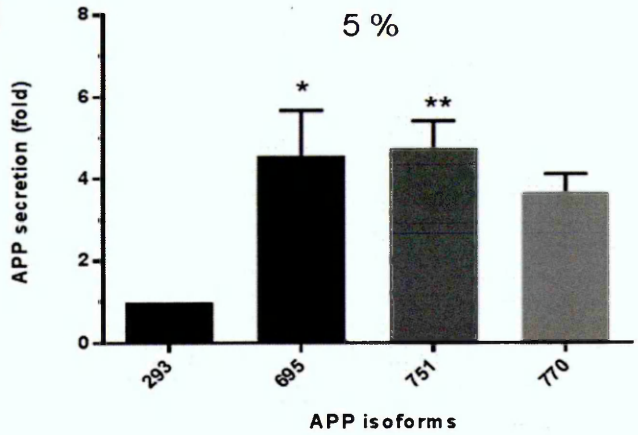
5 %
APP secretion (fold)
0
2
4
6
8
*
**
293
695
751
770
APP isoforms

(d)

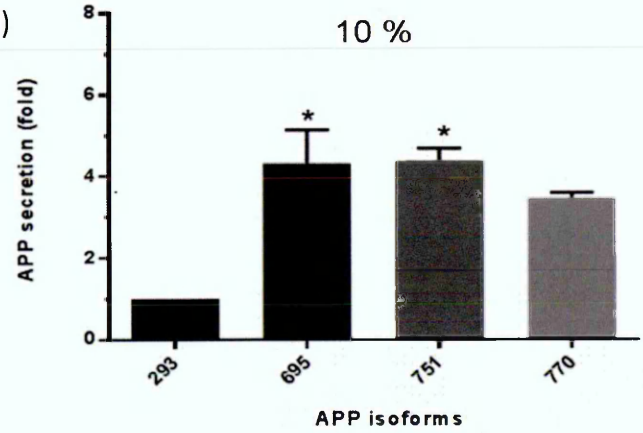
10 %
APP secretion (fold)
0
2
4
6
8
*
*
293
695
751
770
APP isoforms

5.4 Effects of FBS in cell culture medium on APP mRNA level

The final part of the investigation of FBS concentration in culture medium on APP production was to measure APP mRNA levels. Cells were plated out at 5 x 10^5 cells per well of 6-well plates and were cultured in culture medium containing various concentrations of FBS for 24 hours before cells were photographed and counted, and culture medium and cell pellets were collected.

5.4.1 Reference gene stability assessment

Before the determination of the mRNA level could be carried out, it is a common rule that one or more reference genes are selected to be used as normalizers.

The human geNorm™ Reference Gene Selection kit (PrimerDesign), which is a set of primers for 12 candidate reference genes was purchased. The 12 reference genes: ERCC6, UBE2D2, UBE4A, ENOX2, PRDM4, SCLY, TYW1, RNF20, CHO14ORF, ACTB, GAPDH and 18S were tested for their expression stability between non-transfected HEK293 and selected clones of HEK293 transfected with APP isoforms, also the stability of reference genes in all experimental conditions; variation in FBS concentrations and the addition of 2-Deoxy-D-glucose. Therefore, the obtained reference genes are suitable for normalization of the mRNA level in real-time RT-PCR. As mentioned in Section 2.25, the expression stability values were obtained using GeNorm software based on reference gene removal according to calculations of pair-wise correlation, which results in the M-value and the ideal reference genes should have an M-value less than 1.5.

The three separate sets of cell pellets were collected from; (1) untreated non-transfected HEK293, APP695.C5, APP751.C1 and APP770.C6: (2) non-transfected HEK293, APP695.C5, APP751.C1 and APP770.C6 which were cultured in culture medium contained various concentrations of FCS (0%, 1%, 5% and 10%) for 24 hours and (3) non-transfected HEK293, APP695.C5, APP751.C1 and APP770.C6 which were cultured in culture medium contained various amount of 2-Deoxy-D-glucose (5, 25 and 50 mM). Cell pellets were prepared according to the procedure stated in Sections 2.20 to 2.22 before proceeding with real-time RT-PCR (see Section 2.23). In short, total RNA from cell pellets were obtained using RNeasy Mini Kit following by RNA quantification

using NanoDrop ND-1000 UV-VIS spectrophotometer before conversion to cDNA using RT-PCR. Then the cDNA from each cell pellet sample was plated out in triplicate before adding master mix and subjected to the real-time RT-PCR procedure. Also, the gene stability assessment was carried out in triplicate. The obtained ΔC_t value from each sample in each experiment was subjected to analysis by GeNorm software and the results are shown in Figures 5.4.1 (a) and (b).

Figure 5.4.1 (a) shows the M-value of all 12 reference genes; the least stable reference gene located at the left of the graph, the average stability of genes were positioned due to an increase in stability and the most stable reference gene located on the right of the graph. The GeNorm software not only generated a graph representing the stability of reference genes but it also generated a pair-wise variation value (V). The V-value was used as a guideline to determine the minimum number of reference genes required for normalization in each of the determination of mRNA level experiment and the V-value at 0.15 was use as a cut-off point. Figure 5.4.1 (b) showed the V-value as $V_{n/n+1}$ and on $V_{2/3}$ column had a V-value of less than 0.15 which means the determination of mRNA level experiment required a minimum of two reference genes. Therefore SCLY and TYW1 were the two reference genes which were selected using M-value and V-value parameters.

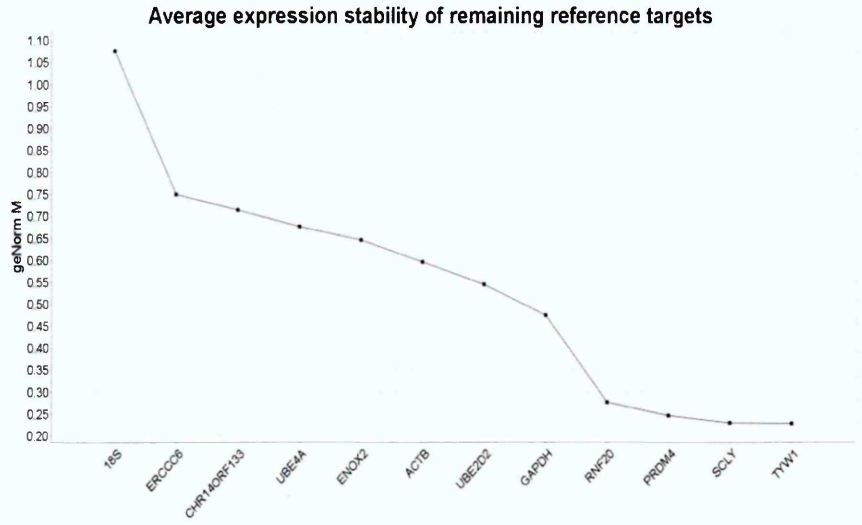

(a)

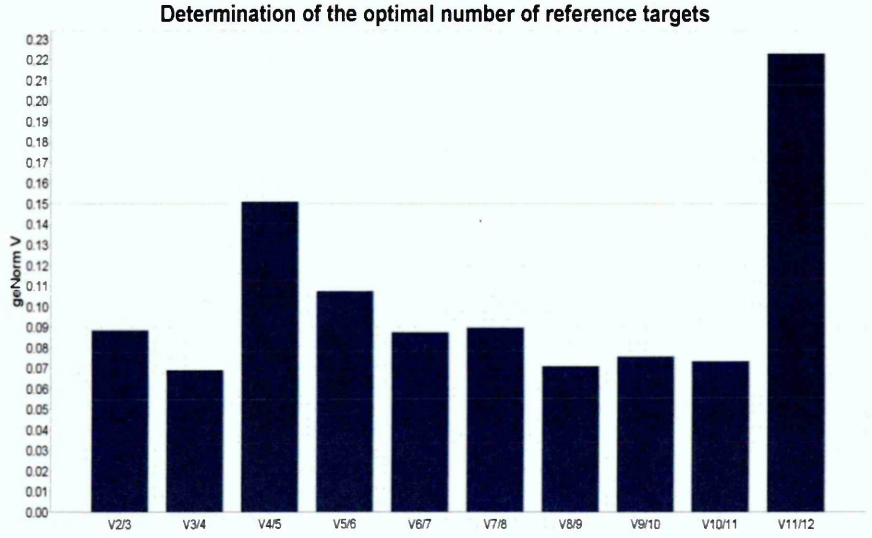

(b)

Figure 5.4.1 The reference genes transcript stability assessments. (a) Average expression stability: M-value of 12 reference genes. The least stable reference gene was located on the left side of the graph and the most stable reference gene was located on the right side of the graph. (b) Determination of the optimal number of reference genes required in the mRNA level determination experiments: V-value which is displayed as Vn/n+1. If Vn has a V-value less than 0.15, there was no need to introduce an additional reference gene. Therefore, the minimum number of reference genes required for each of the determination of mRNA level experiment was two reference genes; SCLY and TWY1.

5.4.2 Primer efficiency

As previously mentioned in Section 2.27, there are two models frequently used to determine relative quantification; one model takes the efficiency of the primers into account during the calculation while the other one does not. Also, the latter model is only used when primer efficiency is within an acceptable range due to a presumption made on primer efficiency during the calculation; $E_{sample} = E_{reference} = 2$. Therefore, it is crucial to determine primer efficiency before proceeding to the determination of mRNA level experiments. Once reference genes were selected, there were three pairs of primers which were assessed for efficiency; primers for APPs, primers for SCLY and TYW1. The primer efficiency assessment was carried out by diluting cDNA converted from the extracted total RNA of cell pellets obtained from non-transfected HEK293, APP695.C5, APP751.C1 and APP770.C6 into four dilutions: 1:5, 1:10, 1:50 and 1:100. The cDNA was diluted by adding an appropriate volume of RNAse/ DNAse-free water before 1 µl of each diluted cDNA was added into MicroAmp® Optical 96-Well Reaction Plate in triplicate. Then, 9 µl of master mix of each set of primers was added and the reaction plate was sealed before placing in the StepOnePlus™ Real-Time PCR System. The amplification conditions were carried out according to the standard procedure in Section 2.24.

The C_t values gained during the amplification stages were plotted on a semi-log graph between C_t value and log dilution of cDNA and a linear trend line was added later. According to Section 2.26, the percentage of primer efficiency and primer efficiency were obtained using the formulas below:

$$\% \text{ Efficiency} = [(10^{-(1/\text{slope})})-1] \times 100$$

$$\text{Efficiency (E)} = 10^{-(1/\text{slope})}$$

Slope is acquired from the plotted graph using data obtained from cDNA dilutions.

Figure 5.4.2 shows the semi-log graphs between C_t value and log dilution of cDNA obtained from non-transfected HEK293. The slopes obtained from the trend lines were -3.302 and R^2 value of 0.999 for APP primers, -3.224 and R^2 value of 0.9924 for SCLY, and -3.156 and R^2 value of 0.9999 for TYW1. As a consequence, the percentage of

primer efficiency or E value of APP, SCLY and TYW1 were 101%, 104% and 107% or 2.00, 2.04 and 2.07, respectively.

The C_t value obtained from APP695.C5 cDNA was plotted against log dilution of cDNA and the semi-log graphs are shown in Figure 5.4.3. According to the trend lines of the graphs, the slopes and R^2 value of APP primers, SCLY primers and TYW1 primers were -3.306 and 0.9984, -3.109 and 0.9976 and -2.988 and 0.9964, respectively. The percentage of primer efficiency for APP, SCLY and TYW1 primers were 100%, 110% and 116%, respectively, followed by efficiency of three primers; 2.01, 2.10 and 2.16, accordingly.

Figure 5.4.4 shows semi-log graphs between log dilution of cDNA on X-axis and C_t values gained from APP751.C1 cDNA on Y-axis. The slopes and R^2 values obtained from the graphs were as followed -3.324 and 0.9979 for APP primers, -3.062 and 0.9978 for SCLY and -3.103 and 0.9996 for TYW1. Subsequently, the slopes were applied to formulas mentioned above to generate the percentage of primer efficiency and E; APP (100% and 2.00), SCLY (112% and 2.12) and TWY1 (110% and 2.10).

As the C_t values gained using cDNA from APP770.C6 were plotted against log dilution of cDNA and shown as semi-log graphs in Figure 5.4.5, the slopes and R^2 values of APP, SCLY and TYW1 primers were generated as a result; -3.342 and 0.9992, -2.975 and 0.9976, and -3.292 and 0.9992, respectively. By applying the slopes to the formulas mentioned above, the percentage of primer efficiency and efficiency of primers were obtained; APP (100% and 2.00), SCLY (117% and 2.17) and TYW1 (101% and 2.01).

In order to make the results obtained from primer efficiency assessments easier to understand, these values and numbers of each primers and semi-log graphs are summarized in Figure 5.4.6.

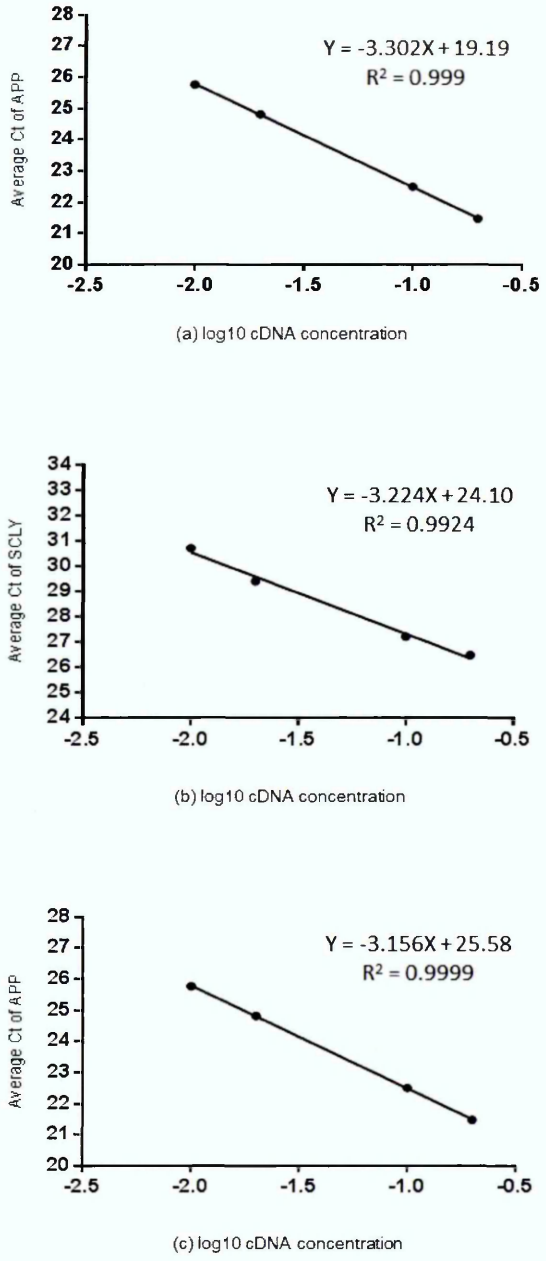

Figure 5.4.2 Standard curves of primer efficiency using diluted cDNA obtained from non-transfected HEK293. There were four dilutions: 1:5, 1:10, 1:50 and 1:100 which are plotted on semi-log graph against average Ct values gained from real-time RT-PCR by three different sets of primers; (a) APP, (b) SCLY and (c) TYW1. The slope of each graph was used in the primer efficiency calculation and the R^2 value which indicated correlation between data points. The percentage of primer efficiency and R^2 values were (a) 101% and 0.9999, (b) 104% and 0.9924 and (c) 107% and 0.9999.

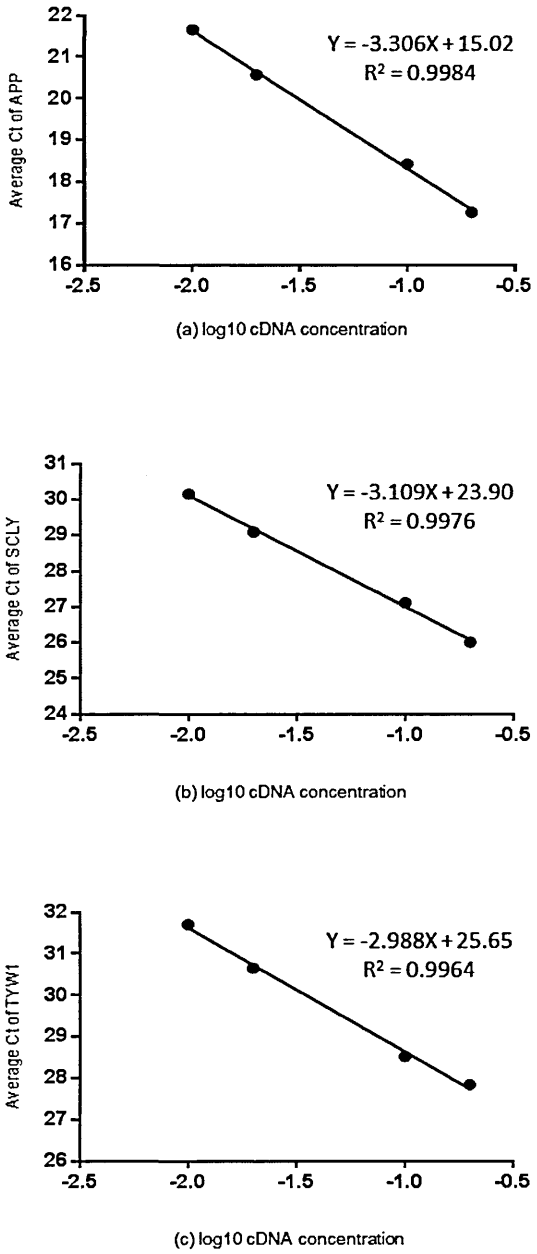

Figure 5.4.3 Standard curves of primer efficiency using diluted cDNA obtained from HEK695.C5. There were four dilutions: 1:5, 1:10, 1:50 and 1:100 which are plotted on semi-log graph against average C_t values gained from real-time RT-PCR by three different sets of primers; (a) APP, (b) SCLY and (c) TYW1. The slope of each graph was used in the primer efficiency calculation and the R^2 value which indicated correlation between data points. The percentage of primer efficiency and R^2 values were (a) 100% and 0.9984, (b) 110% and 0.9976 and (c) 116% and 0.9964.

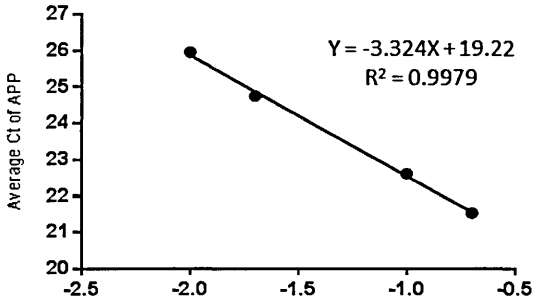

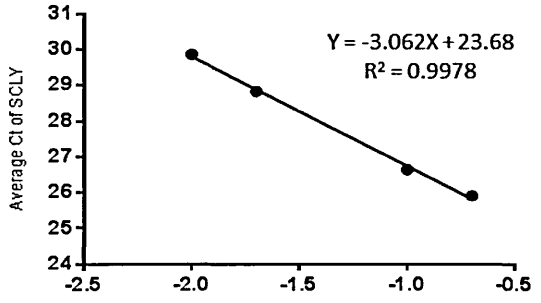

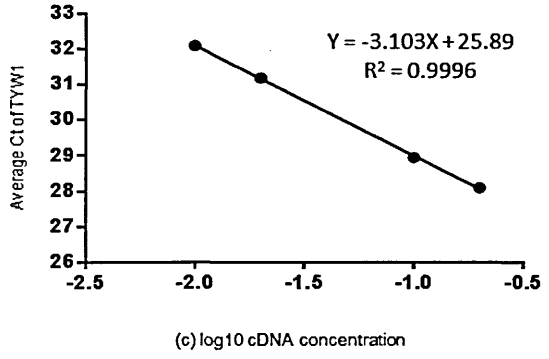

Figure 5.4.4 Standard curves of primer efficiency using diluted cDNA obtained from HEK751.C1. There were four dilutions: 1:5, 1:10, 1:50 and 1:100 which are plotted on semi-log graph against average C_t values gained from real-time RT-PCR by three different sets of primers; (a) APP, (b) SCLY and (c) TYW1. The slope of each graph was used in the primer efficiency calculation and the R^2 value which indicated correlation between data points. The percentage of primer efficiency and R^2 values were (a) 100% and 0.979, (b) 112% and 0.9978 and (c) 110% and 0.9996.

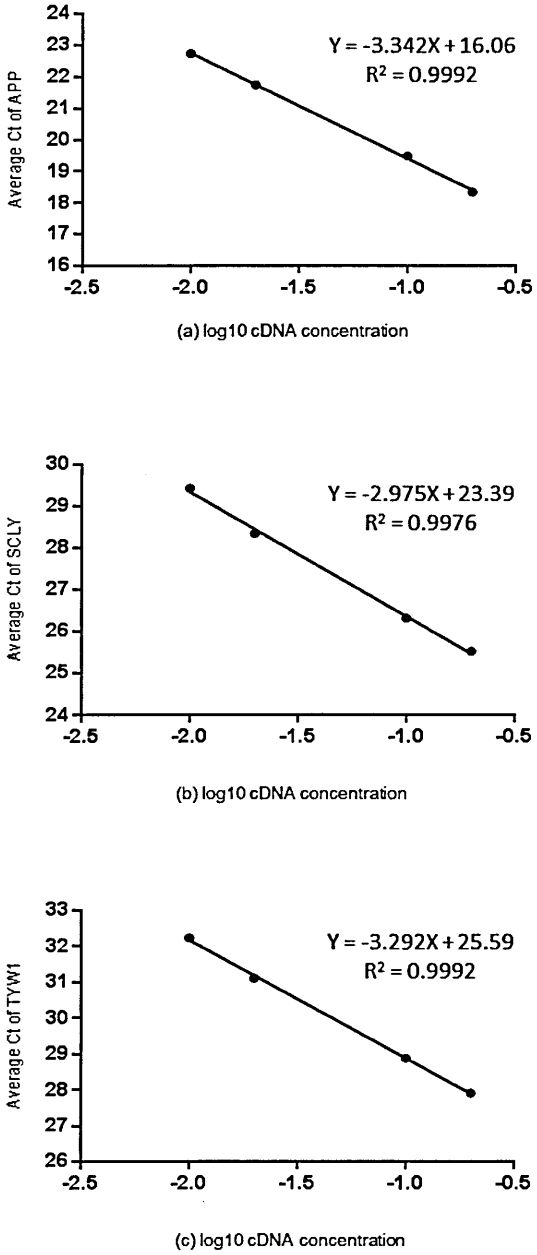

Figure 5.4.5 Standard curves of primer efficiency using diluted cDNA obtained from HEK770.C6. There were four dilutions: 1:5, 1:10, 1:50 and 1:100 which are plotted on semi-log graph against average C_t values gained from real-time RT-PCR by three different sets of primers; (a) APP, (b) SCLY and (c) TYW1. The slope of each graph was used in the primer efficiency calculation and the R^2 value which indicated correlation between data points. The percentage of primer efficiency and R^2 values were (a) 100% and 0.9992, (b) 117% and 0.9976 and (c) 101% and 0.9992.

Sample	Primers	R^2 value	Slope	Primer Efficiency (E) Efficiency (E) = $10^{-(1/slope)}$	Percentage of primer efficiency (%) % Efficiency= $[(10^{-(1/slope)})-1] \times 100$
Non-transfected HEK293	APP	0.9990	-3.302	2.00	101
	SCLY	0.9924	-3.224	2.04	104
	TYW1	0.9999	-3.156	2.07	107
Clone number 5 of APP695 transfected HEK293 (APP695.C5)	APP	0.9984	-3.306	2.01	100
	SCLY	0.9976	-3.109	2.10	110
	TYW1	0.9964	-2.988	2.16	116
Clone number 1 of APP751 transfected HEK293 (APP751.C1)	APP	0.9979	-3.324	2.00	100
	SCLY	0.9978	-3.062	2.12	112
	TYW1	0.9996	-3.103	2.10	110
Clone number 6 of APP770 transfected HEK293 (APP770.C6)	APP	0.9992	-3.342	2.00	100
	SCLY	0.9976	-2.975	2.17	117
	TYW1	0.9992	-3.292	2.01	101

Figure 5.4.6 Summary of R^2 values and slopes from semi-log graphs using data obtained from real-time RT-PCR. R^2 value showed a correlation between data points and the R^2 value higher than 0.99 was considered sufficient. The slope was applied to formulae: Efficiency (E) = $10^{-(1/slope)}$ and % Efficiency= $[(10^{-(1/slope)})-1] \times 100$ to gain Primer Efficiency (E) and Percentage of primer efficiency (%), respectively. The E and %E were also used to determine the relative quantification models used in data analysis.

5.4.3 Effects of FBS on APP mRNA level

After obtaining appropriate reference genes (SCLY and TYW1) and having determined the efficiency of each pair of primers, assessing the effects of FBS on APP mRNA level was then undertaken.

Methods in brief

The experiment began with plating 5 x 10^5 cells per well of 6-well plates. Cells were allowed to settle and adhere for at least 6 hours before the culture medium was discarded and 2 ml of fresh medium which contained varying concentrations of FBS was added. Twenty-four hours later cells were photographed using the XLI cap program and culture medium was collected for APP secretion analysis followed by cell counting and cell pellet harvesting. The cell count data was analysed and the results are shown in Section 5.2 while the culture medium was immunoprecipitated and analysed as the results showed in Section 5.3 along with photographs of the cells. The cell pellet was processed last. Total RNA was extracted from cell pellets (Section 2.20) using RNeasy Mini Kit before quantification using NanoDrop ND-1000 UV-VIS Spectrophotometer (Section 2.21). The RNA was converted into cDNA using QuantiTect Reverse Transcription Kit according to the procedure stated in Section 2.22 which at this point the cDNA of each sample was ready to be amplified by the described real-time RT-PCR technique. A complete list of real-time PCR component and procedure were mention in Section 2.24.

The real-time RT-PCR reactions were set up in MicroAmp® Optical 96-Well Reaction Plates and each reaction consisted of 1 µl of cDNA, 0.5 µl of TaqMan® assay probe, 5 µl of TaqMan® Fast Universal Master Mix and 3.5 µl of RNAse/DNAse free water. Also, 1 µl of cDNA sample obtained from the reverse transcriptase reaction containing no reverse transcriptase, 1 µl reaction without RNA and 1 µl RNAse/DNAse free water were used as negative controls. The MicroAmp® Optical 96-Well Reaction Plate was set up and each sample was loaded in triplicate before the reaction plate was sealed then placed in the StepOnePlus™ Real-Time PCR Systems and the amplification conditions were started.

The data from each amplification condition of each sample was gained as C_t value and as each sample was carried out in triplicate per reaction, therefore the mean of triplicate C_t values was use in the relative quantification of the mRNA level. The chosen relative quantification model was the one that takes the slope of primer efficiency into account. The model is shown as followed:

$$\text{Fold difference} = E_{sample}^{\Delta Ct\ sample} / E_{reference}^{\Delta Ct\ reference}$$

Where E_{sample} is the primer efficiency of the gene of interest; $E_{reference}$ is the primer efficiency of a reference gene; $\Delta C_{t\ sample}$ is the difference of the means of C_t between the control and the gene of interest; $\Delta C_{t\ reference}$ is the difference of mean of C_t between the reference gene of control and reference gene of sample.

The two-way ANOVA with 95% confidence interval was coupled with Bonferroni's multiple comparison test to evaluate any possible effects of the concentration of FBS in culture medium on APP mRNA level in non-transfected HEK293 and clones of APP transfected HEK293. The data are presented as graphs between independent factors (X-axis) and fold differences of mRNA level (Y-axis). The data were also analysed based on the two independent factors; (1) the concentration of FBS in culture medium and (2) the differences in the isoform of APP.

Results

The APP mRNA level of the cells incubated in culture medium which contained varying concentrations of FBS was shown in Figure 5.4.7: the effects of the FBS concentration in culture medium on APP mRNA level and Figure 5.4.8: the effect of the isoforms of APP on APP mRNA level in each concentration of FBS. The statistical analysis revealed that cell types and concentrations of FBS affected APP mRNA levels significantly ($p=0.0120$ and 0.0095, respectively) but both factors were independent from each other ($p>0.05$).

Figure 5.4.7 shows the graph of the mRNA level which the same cells growing in culture medium containing 10% FCS was used as controls. The statistical analysis revealed that the APP mRNA level of non-transfected HEK293 cells and HEK751.C1 were reduced in culture medium containing 0%, 1% and 5% of FBS but the reductions were not statistically significant. The APP mRNA level of HEK695.C5 was reduced in

culture medium containing 0% and 5% of FCS while it was slightly increased in the culture medium containing 1% of FCS. However, the changes occurred with APP mRNA level of HEK695.C5 were not significant. In contrast, the level of APP mRNA of HEK770.C6 was elevated in culture medium containing 0%, 1% and 5% of FCS but only the elevation of APP mRNA level in culture medium containing 0% FCS was statistically significant ($p<0.05$).

Figure 5.4.8 shows the graphs of the mRNA level data which contained all four cell types and each graph represented each concentration of FBS in culture medium: 0%, 1%, 5% and 10%. The non-transfected HEK293 cells growing in each concentration of FBS were used as controls. The statistical analysis revealed that there were changes due to the differences in cell type which significantly affected the APP mRNA level ($p<0.05$). In the culture medium containing 0% FBS, the APP mRNA level of HEK695.C5 and HEK770.C6 were reduced significantly in comparison to non-transfected HEK293 cells ($p<0.05$), whereas the APP mRNA level of HEK751.C1 appeared to be slightly increased though it was not statistically significant. In addition, all cell types which were cultured in culture medium containing 1% and 5% FBS shared the same pattern of APP mRNA level in comparison to non-transfected HEK293; the APP mRNA level of HEK695.C5 and HEK770.C6 were reduced significantly ($p<0.05$), and APP mRNA level of HEK751.C1 was reduced slightly. All cell types which were cultured in medium containing 10% FBS showed a similar pattern of the APP mRNA level to the culture medium containing 1% and 5% FBS: the level of APP mRNA of HEK695.C5, HEK751.C1 and HEK770.C6 were reduced though only APP mRNA level of HEK695.C5 was significantly reduced ($p<0.05$).

Figure 5.4.7 The APP mRNA level results as mean ± S.E.M.: cell types. The X-axis: concentration of FBS and Y-axis: fold difference of APP mRNA level. The same cell type incubated in complete culture medium containing 10% FBS were used as controls. There were four cell types; (a) non-transfected HEK293, (b) APP695.C5, (c) APP751.C2 and (d) APP770.C6. The APP mRNA level of non-transfected HEK293 cells and HEK751.C1 were reduced in culture medium containing 0%, 1% and 5% of FBS but the reductions were not statistically significant. The APP mRNA level of HEK695.C5 was reduced in culture medium containing 0% and 5% of FCS while it was slightly increased in the culture medium containing 1% of FCS. However, the changes which occurred to levels of APP mRNA of HEK695.C5 were not significant. In contrast, the level of APP mRNA of HEK770.C6 was elevated in culture medium containing 0%, 1% and 5% of FCS but only the elevation of APP mRNA level in culture medium containing 0% FCS was statistically significant ($p<0.05$).

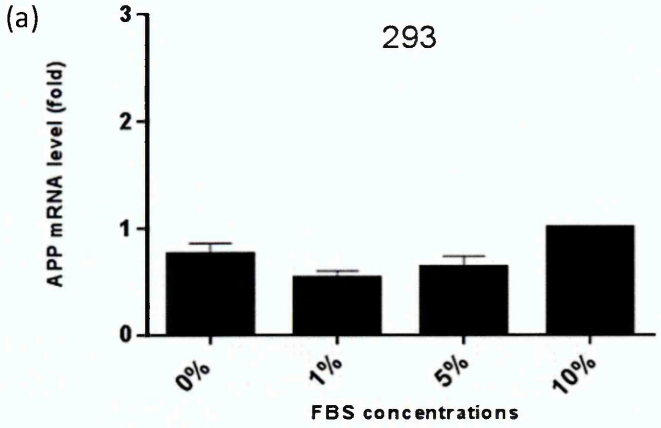
(a)
293
APP mRNA level (fold)
3
2
1
0
0%
1%
5%
10%
FBS concentrations

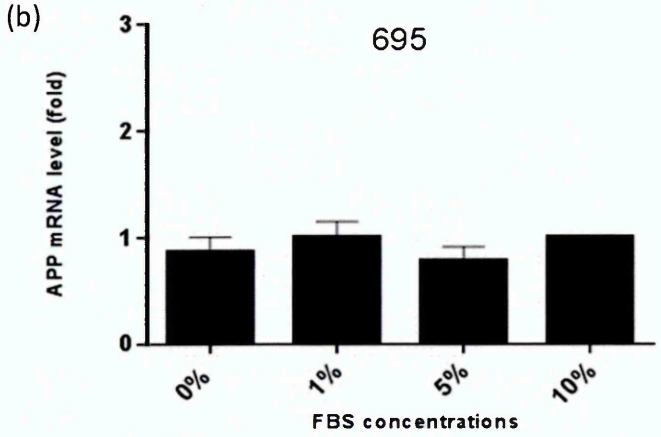
(b)
695
APP mRNA level (fold)
3
2
1
0
0%
1%
5%
10%
FBS concentrations

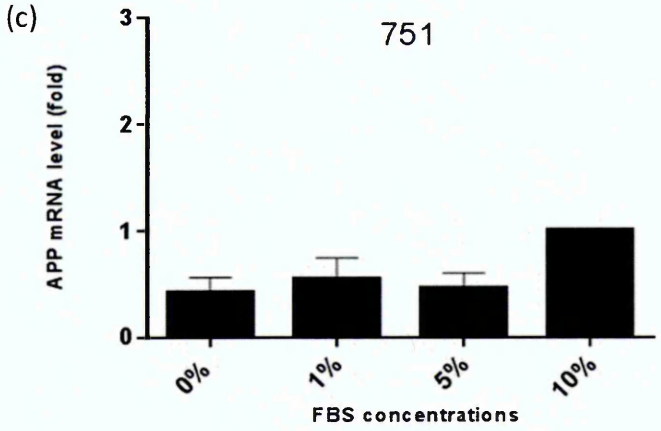
(c)
751
APP mRNA level (fold)
3
2
1
0
0%
1%
5%
10%
FBS concentrations

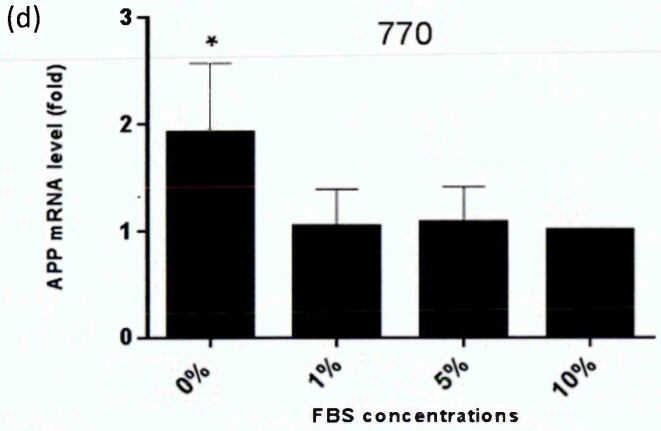
(d)
770
*
APP mRNA level (fold)
3
2
1
0
0%
1%
5%
10%
FBS concentrations

Figure 5.4.8 The APP mRNA level results as mean ± S.E.M.: concentrations of FBS. The X-axis: isoforms of APP and Y-axis: fold difference of APP mRNA level. The non-transfected HEK293 cells growing in each concentration of FBS were used as controls. There were four concentrations of FBS; (a) 0%, (b) 1%, (c) 5% and (d) 10%. In comparison to non-transfected HEK293 cells the APP mRNA level of HEK695.C5 was reduced significantly in all four concentrations of FBS ($p<0.05$), HEK751.C1 was slightly reduced in culture medium containing 1%, 5% and 10% FBS but the level of APP mRNA was slightly elevated in the absence of FBS in the culture medium, and HEK770.C6 was significantly reduced in culture medium containing 0%, 1% and 5% FBS ($p<0.05$).

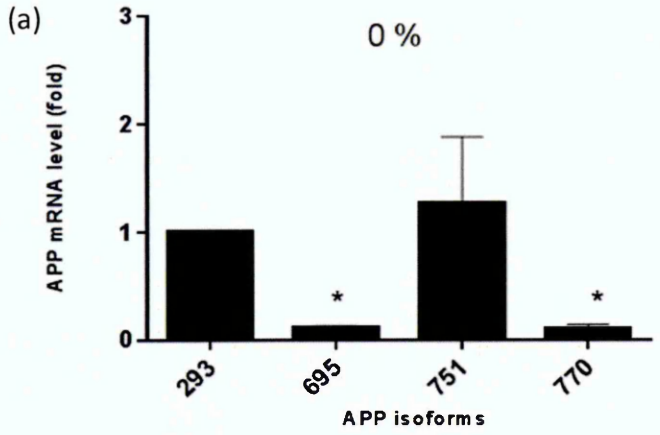
(a)
0 %
APP mRNA level (fold)
3
2
1
0
*
*
293
695
751
770
APP isoforms

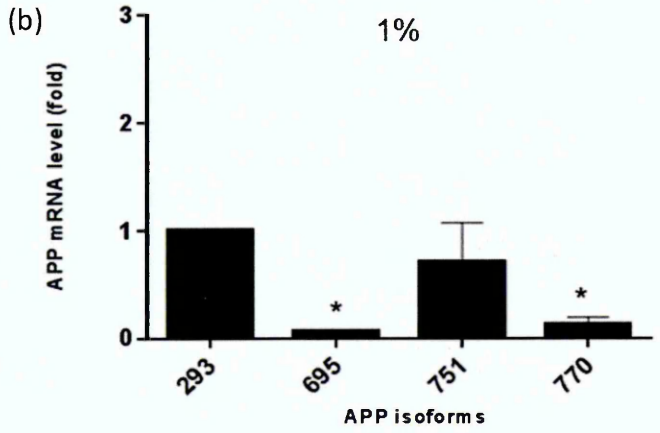
(b)
1%
APP mRNA level (fold)
3
2
1
0
*
*
293
695
751
770
APP isoforms

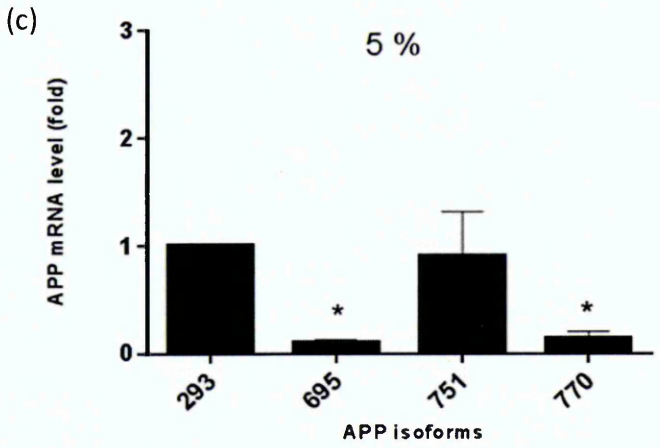
(c)
5 %
APP mRNA level (fold)
3
2
1
0
*
*
293
695
751
770
APP isoforms

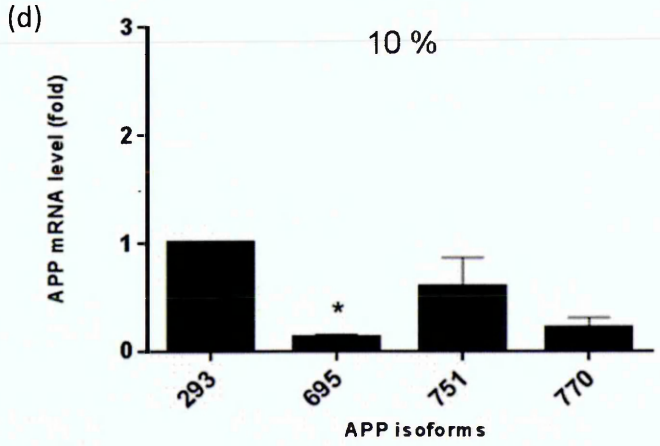
(d)
10 %
APP mRNA level (fold)
3
2
1
0
*
293
695
751
770
APP isoforms

5.5 mRNA: protein ratio

It was reported that there was a strong correlation between secreted APP and the APP mRNA level in the brains of patients with AD (Matsui et al. 2007). The translational efficiency is the rate of conversion from mRNA into proteins which could be determined using measured protein and mRNA level, as follows:

$$\text{mRNA: Protein} = [\text{mRNA/cell}] / [\text{Protein/cell}]$$

The statistics revealed that the HEK751.C1 is the least efficient in translating APP mRNA into APP while HEK695.C5 and HEK770.C6 are the most efficient. The lower the ratio the higher the translation and efficiency. The complete analysis of mRNA:Protein ratio is as follows:

- HEK695.C5: 0% FBS (0.04±0.04)> 1% FBS (0.03±0.02)= 5% FBS (0.03±0.02)
- HEK751.C1: 0% FBS (0.26±0.13)> 5% FBS (0.18±0.09)> 1% FBS (0.15±0.09)
- HEK770.C6: 5% FBS (0.04±0.02)> 1% FBS (0.03±0.02)= 0% FBS (0.03±0.01)

5.6 Discussion

The three clones that stably expressed isoforms of APP at comparable levels; HEK695.C5, HEK751.C1 and HEK770.C6 were used as cellular models in an investigation into the effects of FBS in culture medium which was the fourth objective of this project.

It was hypothesised that selected clones secreting similar amounts of APP695, APP751 and APP770 into culture media under normal cultured conditions (culture medium containing 10% FBS and 25 mM glucose) would be the consequence of production of equal amounts of mRNA for each isoform. However, the mRNA level of each isoform of APP appeared to be different: APP751> APP770> APP695. On average, the mRNA level between APP751 was 4 fold higher than APP695. The differences in mRNA levels between isoforms of APP could have significant effects on APP secretion and, ultimately, Aβ peptide secretion.

FBS in culture medium presents advantages and disadvantages. The advantages of FBS include providing hormonal factors, transporter proteins, facilitating cellular adherence and maintaining the pH of culture medium. The disadvantages include composition inconsistency, batch-to-batch variation and increased risk of infection. Also, the presence of FBS might interfere with the experimental results; especially with protein purification or isolation studies (Brunner et al. 2010). Therefore the objectives of this investigation were; (1) to determine whether FBS concentration affects the cell number, APP secretion and APP mRNA level at various concentrations, and (2) to find out if the alteration of FBS affects each isoform of APP differently.

The investigation of the effects of FBS in the culture medium was carried out in three separate parts: cell number, APP secretion and APP mRNA level. The data gained from each part of an investigation was subjected to statistical analysis based on two independent factors; (1) the concentrations of FCS in culture medium (using culture medium containing 10% FCS as control) and (2) the differences in isoforms of APP (using non-transfected HEK293 cells as control). Also, prior to the cell counting procedure, cells were photographed in order to observe morphological changes.

Serum deprivation and serum restriction are two of several interchangeable terms used to describe cell culture procedures involving an alteration in the concentration of FBS (Pirkmajer and Chibalin 2011). To date, there have been numbers of researchers who have used FBS concentration alteration as a tool in their studies including protein degradation studies (Epstein, Elias-Bishko and Hershko 1975), cellular stress response studies (Levin et al. 2010), apoptosis studies (Terra et al. 2011) and imitation of pathological conditions (Hamabe, Fujita and Ueda 2005; Pirkmajer and Chibalin 2011; Yu et al. 2008). As components in FBS have not been completely identified, the removal of FBS from culture medium also removes the both known and unknown residues which might cause interferences in the experiment (Pirkmajer and Chibalin 2011). Nevertheless, serum deprivation is commonly used as an apoptotic trigger in neurodegenerative disease studies as it allows the researchers to study the morphology of the cells under stress or in malnutritional conditions as well as studying newly discovered anti-apoptotic agents (Fiorelli, Kirouac and Padmanabhan 2013; Xie et al. 2013).

Atk1, also known as protein kinase Bα (PKBα), is a serine/ threonine protein kinase (Filippa et al. 1999; Nicholson and Anderson 2002) and it has been suggested to play role as a regulator of apoptosis, cell growth and proliferation, cell differentiation and cell metabolism (Mulukutla et al. 2010; Nicholson and Anderson 2002). Atk1 is activated by an activation of phosphoinositide 3-kinase (PI3K) initiating a synthesis of phosphatidylinositol (3, 4, 5)-triphosphate (PIP3) which facilitates the localization, phosphorylation and activation of Atk1. One of several ways which PI3K can be activated is autophosphorylation of kinase by ligands including growth factors and amino acids (Fayard et al. 2005; Filippa et al. 1999; Nicholson and Anderson 2002; Scheid and Woodgett 2003). Once the Atk1 is activated, it subsequently initiates protein translation/synthesis and cell growth via the mammalian target of rapamycin complex 1 (mTORC1).

Under growth factor and amino acid insufficiency mimicked by FBS concentration alteration, it was hypothesised that the cell number would decrease along with a decreased concentration of FBS as a result of an Atk1 inactivation. However, the cell count data presented in this Chapter (Figure 5.2.1) revealed that there is no significant reduction of cell number between concentrations of FBS in culture medium. Previous

studies have reported that the earliest which the changes in cell population culturing under serum deprived condition could be detected is 48 hours (Deorosan and Nauman 2011; Fiorelli, Kirouac and Padmanabhan 2013). The role of Atk1 in apoptosis regulation has been supported by a study demonstrating an inhibition of apoptosis signalling-regulating kinase-1 (ASK1) by activated Atk1 (Milosch et al. 2014). The activated Atk1 has been proposed to inhibit apoptosis by regulating the expression or phosphorylation of a series of pro-apoptotic proteins leading to inactivation of these proteins (Mulukutla et al. 2010; Scheid and Woodgett 2003). However the morphology of the cells as shown in Figure 5.2.2-5.2.5, which were cultured in culture medium containing various amounts of FBS, have shown the resemblance to cells undergoing apoptosis. These characters included cluster formation, shrinkage, blebbling and echinoid spike, all of which have been observed by several studies (Bottone et al. 2013; Fiorelli, Kirouac and Padmanabhan 2013; LeBlanc 1995; Steiger-Barraissoul and Rami 2009; Xie et al. 2013).

Not only does mTORC1 function, downstream of Akt1, as a regulator of cell growth but is also responsible for an increase of protein and ribosomal synthesis once activated (Kim et al. 2011; Li et al. 2014). Therefore it could be assumed that an inactivation of Akt1 by reducing growth factors and amino acids, provided by FBS in culture medium, ultimately inactivates mTORC1 thereby reducing protein synthesis (Mulukutla et al. 2010; Ueki et al. 1998). Hence it was hypothesised that culturing the cells with reduced FBS would essentially reduce APP synthesis thereby reducing APP secretion (only sAPPα has been measured in this experiment). Indeed, the APP secretion data (Figure 5.3.5-5.3.7) has revealed that the APP secretion has decreased with the concentration of FBS in culture medium, apart from cells which were cultured in complete culture medium containing 10% FBS. This could be the result of cell-cell contact inhibition which occurs in confluent culture and fast growing cell lines (Levine et al. 1965; Wieser and Oesch 1986; Puliafito et al. 2010).

As there was a decrease of the APP secretion level, it was hypothesised that the APP mRNA level should have decreased as well. Once the protein synthesis process is inhibited it would consequently inactivate the ribosomal synthesis (Kim et al. 2011; Ladevaia et al. 2012). However, the APP mRNA data (Figure 5.4.7-5.4.8) has revealed that the APP mRNA level remains at the similar level between concentrations of FBS

instead of reflecting the level of APP secretion. Since the secreted APP and the APP mRNA level were found to be correlated in human brains, the ratio between these two parameters was used to determine the efficiency of protein translation (Matsui et al. 2007). The efficiency of protein translation (shown as mRNA:protein ratio ± S.E.M.) revealed that HEK695.C5 and HEK770.C6 are the most efficient in APP secretion with the average ratio of 0.03±0.03 and 0.03±0.02 while the HEK751.C1 is the least efficient in APP secretion with the average ratio of 0.20±0.12.

In conclusion, the different isoforms of APP and the different concentration of FBS in culture medium did not affect the cell number, APP secretion and the APP mRNA level. This meant the FBS could be used in further experiments.

Chapter 6: Effects of 2-Deoxy-D-glucose on APP secretion in HEK293 cells transfected with APP isoforms

6.1 Introduction

The effect of FBS in culture medium on APP production was established in Chapter 5 on cellular models of APP; APP695.C5, APP751.C1 and APP770.C6. There were four experimental aspects which were taken into consideration; cell morphology, cell number, amount of secreted APP in culture medium and APP mRNA level. These aspects were also used to assess the effect of 2-deoxy-D-glucose (2DG) on APP transfected HEK293. This was the fifth and final objective of this project.

Glucose is a vital and main source of energy for living organisms, including humans. Although the brain only accounts for 2% of the body weight, it requires nearly 20% of all energy derived from glucose. Also, neuronal cells in the adult human brain have the highest demand for energy and require a constant supply of glucose from blood. The physiological functions of the brain are maintained through an ability to generate adenosine triphosphate (ATP), facilitate cellular maintenance and produce neurotransmitters from glucose, (Mergenthaler et al. 2013). Studies have shown that the functions and survival of neurons depended on the efficiency of energy metabolism from the main source of energy in the brain; glucose (Demitrius and Driver 2013). For example, when the blood glucose level is below 2-3 mM (blood glucose at normal fasting level), the brain shows certain cognitive impairments. Also, cells which use glucose as their primary source (such as neurons) are unlikely to be affected by stress in comparison to the cells that use other energy sources and undergo glycolysis as a consequence (Dwyer 2002).

In order to maintain the structure of the brain and its optimal function, the brain relies crucially on oxidative metabolism. ATP is one of many end-products obtained from the tricarboxylic acid cycle during oxidative metabolism of glucose. ATP is essential for cellular and molecular functions such as protein synthesis, ion homeostasis and

maintaining suitable pH conditions for the endoplasmic reticulum (ER) and Golgi apparatus. As ATP is mainly gained from glucose, then any impairment occurring in neuronal glucose oxidative metabolism results in glycation and accumulation of its product within neurons which made the neurons susceptible to degeneration (Hoyer 2004).

It was reported that the cellular and molecular functions in the brain of AD patients were disrupted due to abnormal activities during glucose metabolism. For example, $A\beta_{1-40}$ and $A\beta_{1-42}$ are believed to be the cause of a reduction in glucose metabolism by not only decreasing insulin binding to its receptor but also reducing insulin receptor autophosphorylation. If the shortage of neuronal glucose only occurs partly and temporarily, the brain is able to compensate for the loss of ATP from glucose by utilizing other available substrates in the brain such as amino acids and fatty acids. The glucoplastic amino acids are the amino acids that could be converted into glucose through the gluconeogenesis process and are commonly utilized; especially glutamate to make up for the lost ATP. As a result of the utilization of glutamate, neurotoxic ammonia is produced which later inhibits mitochondria dehydrogenases. In late onset or sporadic AD, the severe disruption of glucose metabolism occurs at early stages of the disease and worsens as clinical manifestations progress. As a consequence, the ATP production from glucose reduces by 50% (de la Monte 2012; Hoyer 2004). Moreover, several studies showed that early stages of AD are characterised by a shortage of glucose in the brain due to disruption of glucose metabolism especially in the temporal, parietal and frontal lobes of AD patients (Furst et al. 2012; Gasparini et al. 1997; Solano et al. 2000; Vassar et al. 2009). Also, the progression of the clinical manifestations of AD corresponded to worsen shortages of brain glucose (de la Monte 2012). Not only was cognitive decline linked to the reduction in glucose metabolism in the frontal and temporo-parietal lobes of the brain (Furst et al. 2012) but also a reduction in brain glucose metabolism was found in patients with mild cognitive impairment (Valliquette, O'Conner and Vassar 2005).

In vitro, the shortage of glucose can be mimicked by using a glucose antagonist such as 2-deoxy-D-glucose (2DG). 2DG shares the same structure with glucose apart from the replacement of a hydroxyl group with hydrogen at the second carbon atom (Aft, Zhang and Gius 2002) which means 2DG is transported into cells by glucose transporters.

Under normal conditions glucose is transported into the cell and phosphorylated by hexokinase to produce glucose-6-phosphate (G6P), before being subjected to conversion by phosphoglucose isomerase and entry into the glycolytic pathway; or being metabolized by glucose-6-phosphate dehydrogenase prior to entry into the pentose phosphate pathway (PPP), as shown in Figure 6.1.1. Regardless, the end product gained from both pathways is the same; pyruvate (Mergenthaler et al. 2013). So far, there are three proposed mechanisms of action of 2DG; (1) the 2DG inside the cell binds to hexokinase but cannot be phosphorylated (Yao et al. 2011), (2) 2DG is phosphorylated by hexokinase but due to hydrogen replacement at the 2-hydroxy group, is inhibited from further glucose metabolic processes (Aft, Zhang and Gius 2002), and (3) 2DG inhibits hexokinase and phosphoglucose-isomerase activities (Ralser et al. 2008). The consequences of these mechanisms of action are interference in glucose metabolism and sudden inhibition of cell growth.

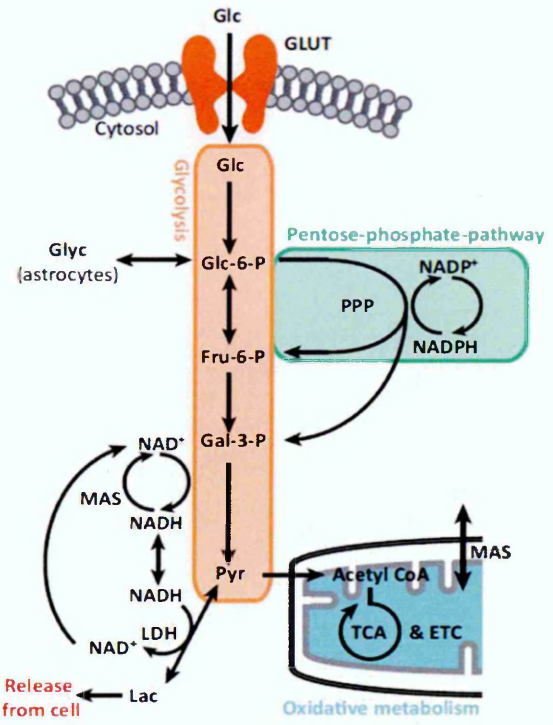

Figure 6.1.1 A simplified overview of glucose metabolism pathways. Glucose is transported into the cell and phosphorylated by hexokinase; obtaining glucose-6-phosphate (Glc-6-P). The phosphorylation process is not reversible. Glc-6-P could either continue along the glycolytic pathway or enter the pentose phosphate pathway (PPP). In the glycolytic pathway, Glc-6-P is converted by a series of enzymes; glucose-6-phosphate dehydrogenase, phosphofrucktokinase and glyceraldehye-3-phosphate dehydrogenase before yielding pyruvate as the end product of this pathway. While, glucose entering the PPP generates NADPH (used in oxidative stress management) before re-entering glycolytic pathway in the manner mentioned above (Adapted from Mergenthaler et al. 2013).

The objectives of this investigation were; (1) to find out how each isoform of APP responded to different levels of stress caused by various concentrations of 2DG and (2) to compare the responses between different isoforms of APP under the same stress level caused by the same concentration of 2DG. In addition, the investigation of the effect of 2DG in culture medium on APP was carried out by measuring these parameters; cell number, APP secretion into culture medium and APP mRNA level. Also, prior to cell counting, cells were photographed in order to observe the morphological changes due to the effect of 2DG in the culture medium.

6.2 Effects of 2DG in cell culture medium on cell number

In a similar manner to the investigation of the effects of FBS on HEK293 stably transfected APP cells, the first part of an investigation of the effect of 2-deoxy-D-glucose (2DG) on APP production was to examine the effect of 2DG on cell number. All three selected clones of HEK293 transfected APP isoforms; APP695.C5, APP751.C1 and APP770.C6 and non-transfected HEK293 were cultured according to the cell culture procedures described in Section 2.11.

Methods in brief

The experiments were carried out in 6-well plates and performed independently in triplicate. Also, there were three chosen concentrations of 2DG: 5 mM, 25 mM and 50 mM which were prepared with complete medium. The concentrations of 2DG were chosen on the basis on the range of the amount of glucose in culture medium (5mM-55mM or 1 g/L-10 g/L) and available publications (Aft, Zhang and Gius 2002; Chang et al. 2011; Domingues et al. 2007; Kaplan et al. 1990; Keenan, Liang and Clynes 2004; Mattson, Guo and Geiger 1999; Ralser et al. 2008; Shi, Xiang and Simpkins 1997; Solano et al. 2000). Each well contained approximately the same starting number of live cells: 5×10^5 cells in 2 ml of complete culture medium. Cells were allowed to settle and adhere for at least 6 hours before the culture medium was discarded and fresh medium which contained the appropriate concentration of 2DG was added. Twenty-four hours later, cells were photographed using the XLI cap program and culture medium was collected for APP secretion analysis followed by cell counting and cell pellet harvesting.

Cell counting was carried out three times per concentration of 2DG for each cell type. Briefly, 10 µl of cells suspension and 10 µl of 0.4% Trypan blue were combined thoroughly before 10 µl of the mixture was pipetted into the Countess® Cell Counting Chamber Slides and counted by using Countess® Automated Cell Counter. Each reading obtained from the cell counter machine measured total cell number, live cell number, dead cell number per ml of cell suspension and percentage of cell viability.

Results

The cell count data are shown as mean ± SEM. The two-way ANOVA with 95% confidence interval was coupled with Bonferroni's multiple comparisons test to evaluate any possible effect of 2DG on cell number. The data were analysed based on two independent factors; (1) the concentration of 2DG in culture medium on cell number, and (2) the differences in the isoform of APP. Moreover, the statistical analysis revealed that both the different concentrations of 2DG and the isoforms of APP had significant effects on cell number ($p<0.0001$ and $p<0.0001$, respectively). However, the interaction between both independent factors showed statistical significance ($p<0.01$) therefore the data gained from both independent factors were interpreted simultaneously, meaning that both factors have a dependable effect on cell number.

The cell count data were analysed using the same cells cultured in standard complete medium containing 25 mM glucose as the control. The data are sub-grouped according to cell type; non-transfected HEK293, HEK695.C5, HEK751.C1 and HEK770.C6 and there are three concentrations of 2DG (5 mM, 25 mM and 50 mM) in the culture medium and one control which contained 25 mM of glucose. Figure 6.2.1 shows that in the culture medium containing 5 mM 2DG the cell number of all three APP transfected HEK293 clones decreased significantly ($p<0.01$, $p<0.0001$ and $p<0.05$, respectively) while there was a significant increase in cell number of non-transfected HEK293 ($p<0.05$). The reduction in cell number occurred in all four cell types grown in culture medium containing 25 mM 2DG, however only the reductions in cell number of HEK695.C5, HEK751.C1 and HEK770.C6 were statistically significant ($p<0.0001$, $p<0.0001$ and $p<0.005$, respectively). In addition, the cell number of all cell types appeared to decrease significantly ($p<0.005$) in the culture medium containing 50 mM of 2DG.

The other way to analyse the cell count data was to use non-transfected HEK293 cells cultured in culture medium containing the same concentration of 2DG; 5 mM, 25 mM and 50 mM as controls. The data are sub-grouped according to the concentration of 2DG in the culture medium. In Figure 6.2.2, all three APP transfected HEK293 clones shared the same pattern of the cell number in all concentrations of 2DG; cell number

of HEK695.C5, HEK751.C1 and HEK770.C6 significantly decreased when cells were cultured in culture medium containing all three different concentrations of 2DG ($p<0.0001$). However, there was no significant reduction of cell number between different isoforms of APP.

Each cell type in culture medium containing various concentrations of 2DG was photographed at the end of 24-hour incubation period. The photographs of the cells are shown in Figure 6.2.3 to Figure 6.2.6

Figure 6.2.3 shows the photographs of the non-transfected HEK293 cells which were cultured in medium containing various concentrations of 2DG. It showed that cells grew at the minimal rate and majority of the cells adhered to the bottom of the well. The number of dead cells increased with an increase in concentration of 2DG; the cells started to detach themselves and died when they were cultured in the culture medium which contained 25 mM 2DG. Also, the majority of the cells showed the round and pebble-like morphology.

Figure 6.2.4 shows the photographs of HEK695.C5 cells which were cultured in culture medium containing various concentrations of 2DG. It appeared that not only did the cells grow extremely slowly, or did not grow at all, but also the live cells which were plated out originally appeared unhealthy i.e. as they showed round morphology and became detached from the wells.

Figure 6.2.5 shows the photographs of HEK751.C1 cells which were cultured in the culture medium containing various concentrations of 2DG. The majority of the cells adhered to the bottom of the well and they showed differentiation in character in the culture medium containing 25 mM and 50 mM 2DG whereas in the culture medium containing 5 mM 2DG the cells appeared flat and full. There were only a few cells which showed the round morphology indicating lesser numbers of dead.

Figure 6.2.6 shows the photographs of HEK770.C6 cells which were cultured in the culture medium containing various concentrations of 2DG. The cells did not appear to grow in any of the concentrations of 2DG. Many live cells, which were plated out originally, died as they detached from the wells when they were cultured in culture medium containing 25 mM and 50 mM 2DG. Also, in the culture medium containing 50

mM 2DG some cells were in a state of vacuolation. Moreover, there were only a small number of dead cells in 5 mM concentration of 2DG and the live cells showed pronounced apoptotic morphology, including elongation.

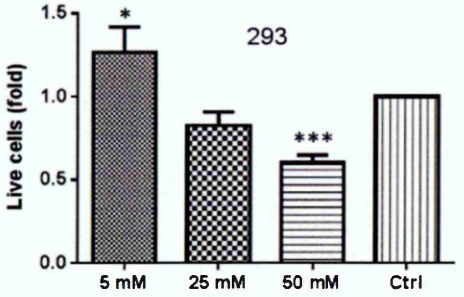

(a) 2DG concentrations

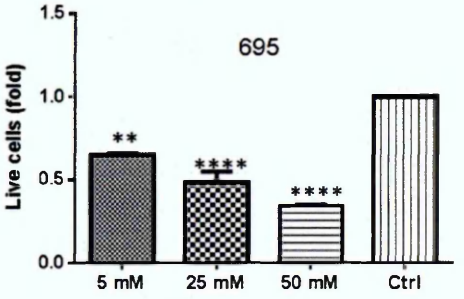

(b) 2DG concentration

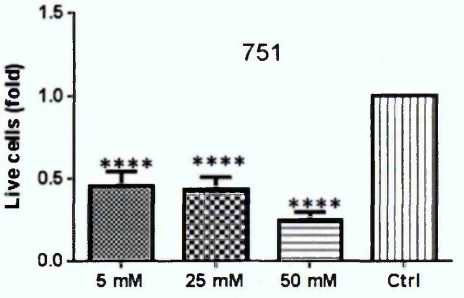

(c) 2DG concentration

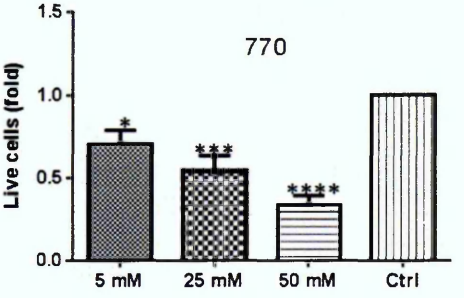

(d) 2DG concentration

Figure 6.2.1 Cell count data as mean ± SEM. Each graph illustrated each concentration of 2DG in culture medium; (a) 5 mM, (b) 25 mM and (c) 50 mM. Also, cell count data were sub-grouped according to cell type and statistical analysis was carried out using the same cell type growing in complete culture medium as the control. Statistical significance description: **p-value<0.05*, ***p-value<0.01*, ****p-value<0.005* and *****p-value<0.0001*

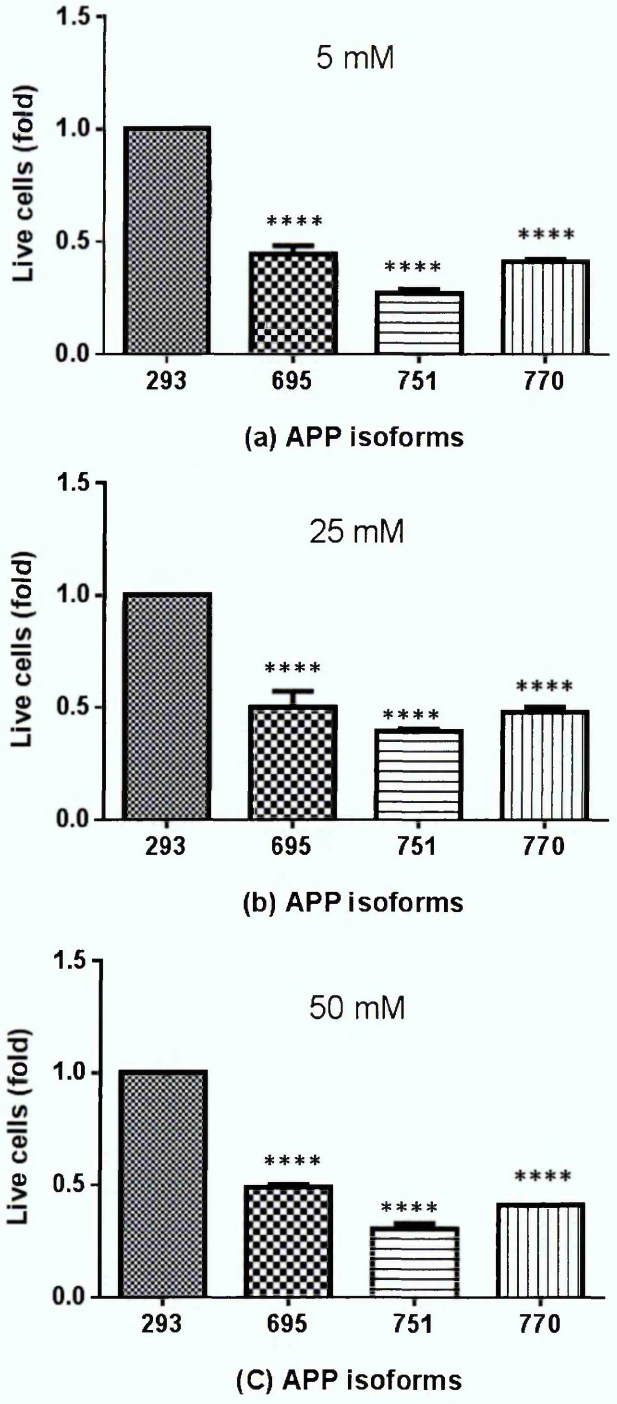

Figure 6.2.2 Cell count data as mean ± SEM. Each graph illustrated each concentration of 2DG in culture medium; (a) 5 mM, (b) 25 mM and (c) 50 mM. Also, cell count data were sub-grouped according to concentration of 2DG and statistical analysis was carried out using non-transfected HEK293 cells grown at same concentration of 2DG as control. It was clearly showed that there was significant reduction in all HEK293 transfected APP isoforms in every concentration of 2DG. Statistical significance description: ****$p\text{-value}<0.0001$.

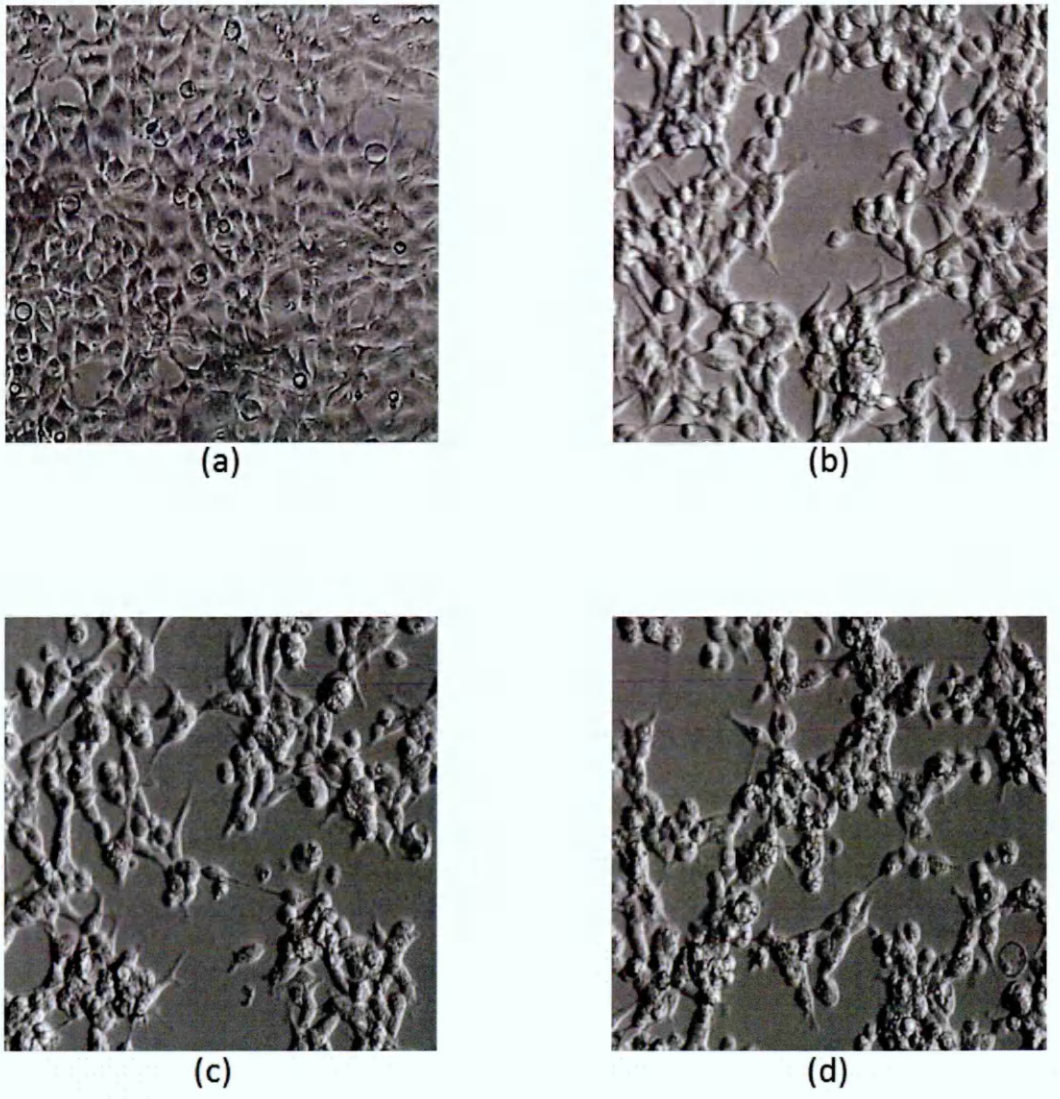

Figure 6.2.3 Photographs of non-transfected HEK293 cells which were cultured in culture medium containing various concentrations of 2DG; (a) control, (b) 5 mM, (c) 25 mM and (d) 50 mM. Cells grew at the minimal rate and majority of the cells adhered to the bottom of the well. The number of dead cells increased with an increase in concentration of 2DG; the cells started to detach themselves and died when they were cultured in the culture medium contain 25 mM 2DG. Also, the majority of the cells showed the round, pebble-like morphology. (magnification 200x)

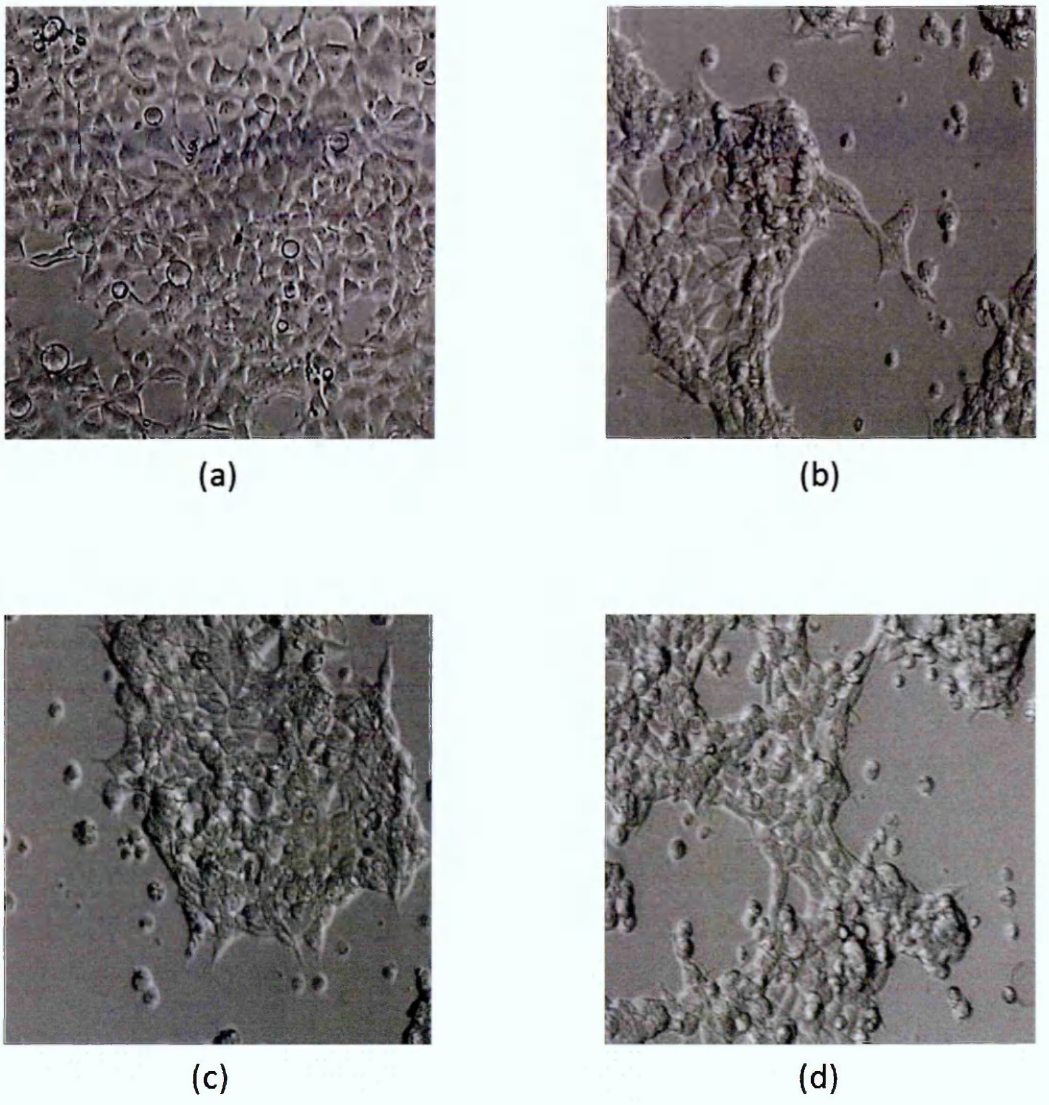

Figure 6.2.4 Photographs of HEK695.C5 cells which were cultured in culture medium containing various concentrations of 2DG; (a) control, (b) 5 mM, (c) 25 mM and (d) 50 mM. It appeared that not only did cells grow extremely slowly or did not grow at all but also 50% of the live cells which were plated out originally appeared unhealthy and dead; as shown by the round shape and detachment from the wells. The number of unhealthy and dead cells increased as the concentration of 2DG increased in culture medium. (magnification 200x)

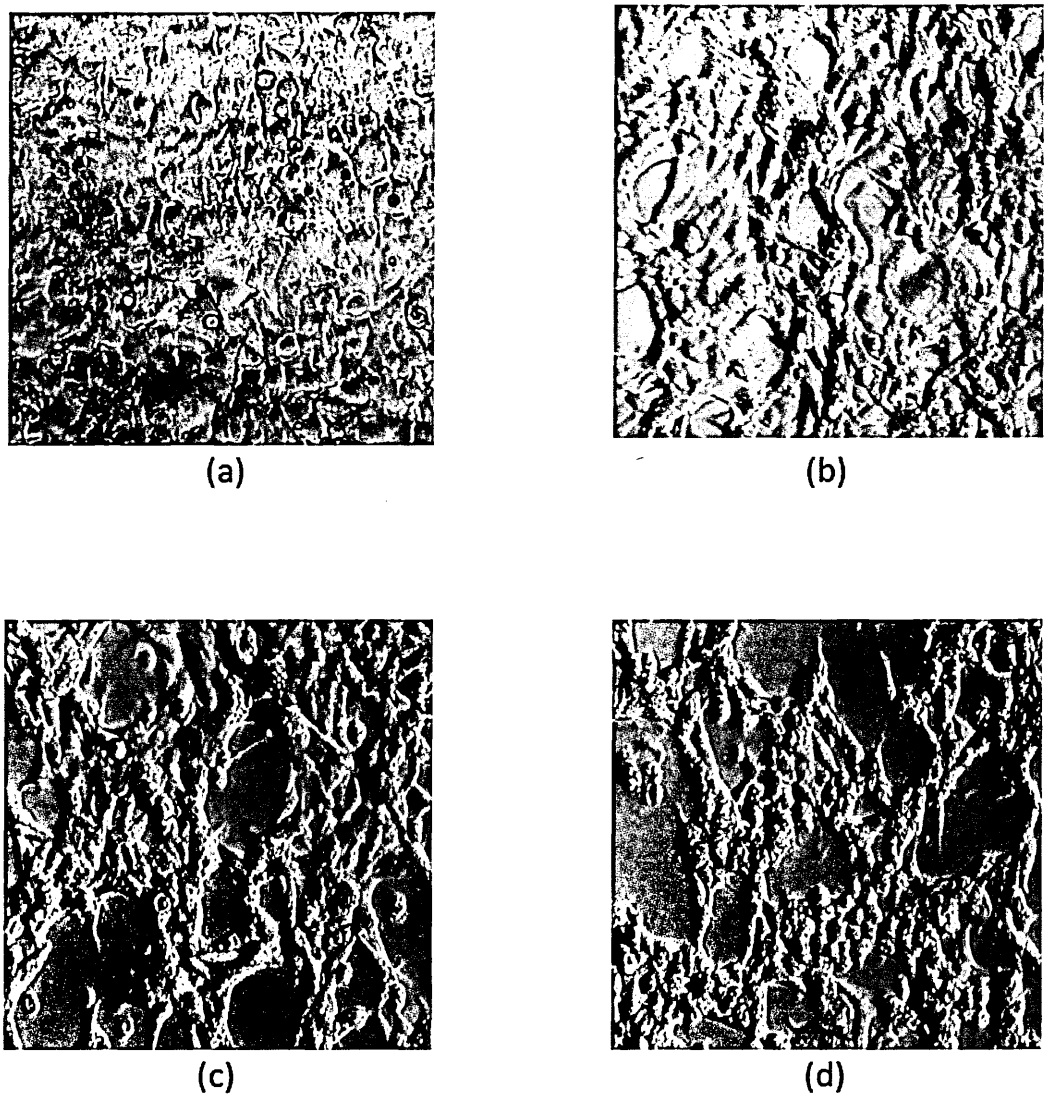

Figure 6.2.5 Photographs of HEK751.C1 cells which were cultured in the culture medium containing various concentrations of 2DG; (a) control, (b) 5 mM, (c) 25 mM and (d) 50 mM. The majority of the cells adhered to the bottom of the well and they showed a differentiated character in culture medium containing 25 mM and 50 mM 2DG whereas in the culture medium containing 5 mM 2DG the cells appeared flat and full. There were only a few cells which showed round morphology indicating lesser numbers of dead cells in each concentration. (magnification 200x)

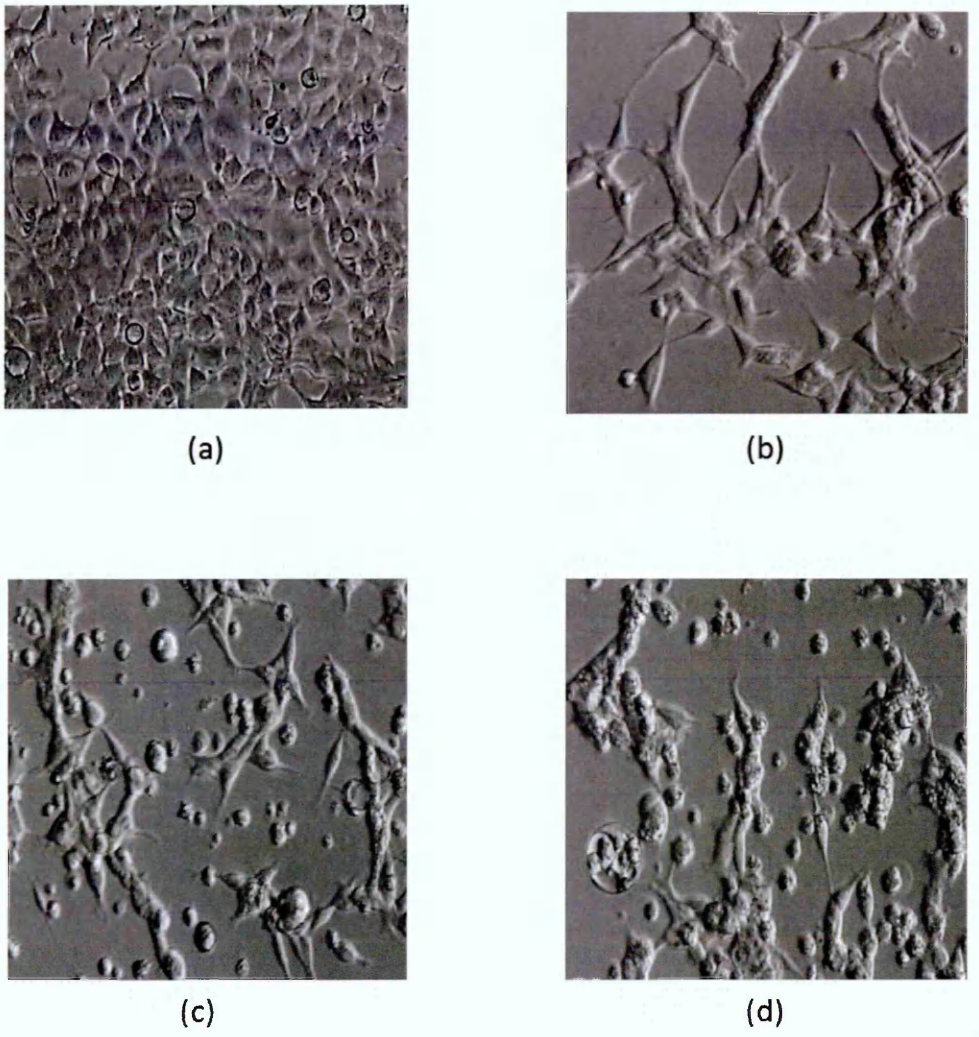

Figure 6.2.6 Photographs of HEK770.C6 cells which were cultured in the culture medium containing various concentrations of 2DG; (a) control, (b) 5 mM, (c) 25 mM and (d) 50 mM. The cells did not appear to grow in any of the concentrations of 2DG. Many live cells which were plated out originally died as they detached from the wells when they were cultured in culture medium containing 25 mM and 50 mM 2DG. Also, in the culture medium containing 50 mM 2DG some cells were in a state of vacuolation. Moreover, there were only a small number of dead cells in 5 mM of 2DG and the live cells showed pronounced a differentiated morphology as the cells started to elongate. (magnification 200x)

6.3 Effects of 2DG in cell culture medium on APP secretion

The second part of the investigation of the effect of 2DG in culture medium on APP production was to determine the amount of APP which was secreted into culture medium. It was previously mentioned that the majority of APP is processed through the secretory pathway. In brief, APP located either at the cell membrane or trans-Golgi network (TGN) is cleaved by a series of secretases before being transported to the extracellular space.

Methods in brief

The culture medium was collected prior to cell counting and then immunoprecipitated using DE2 antibody followed by reduction and alkylation of disulphide bonds. These samples prepared from collected culture medium were run on 6% SDS-PAGE gels before proceeding to protein expression analysis by immunoblotting (complete procedure: see Sections 2.16-2.19). Four primary antibodies and two secondary antibodies used during immunoblotting procedure were listed in Chapter 2 (Figure 2.19.1).

Results

Figure 6.3.1 shows the immunoblotting results obtained from immunoprecipitated culture medium containing various concentrations of 2DG collected from non-transfected HEK293. None of the samples produced the protein band against 1151, 993, 23/2 and DE2 antibodies however the control (non-transfected HEK293 cells grown in complete culture medium) produced a faint protein band against 993, 23/2 and DE2 antibody. The protein bands were approximately 120 kDa in size and most likely to be the result from bovine APP in the culture medium.

The immunoblotting results obtained from immunoprecipitated culture medium containing various concentrations of 2DG collected from HEK695.C5 is shown in Figure 6.3.2. All culture medium contained different amounts of 2DG produced protein bands against 1151 and DE2 primary antibodies and the approximate size of the protein band was 115 kDa which correspondened to the molecular weight of APP695. The protein bands produced against DE2 antibody were stronger than 1151 antibody possibly due

to bovine APP in the culture medium. Also, none of the samples produced protein bands against 993 and 23/2 antibodies.

The immunoblotting results obtained from immunoprecipitated culture medium containing various concentrations of 2DG collected from HEK751.C1 are displayed in Figure 6.3.3. All culture medium contained different amounts of 2DG produced clear protein bands against 1151, 993 and DE2 antibodies which was approximately 118 kDa in size corresponding to the molecular weight of APP751. Also, none of the samples produced a protein band against 23/2 antibody.

The final set of immunoblotting results obtained from immunoprecipitated culture medium containing various concentrations of 2DG collected from HEK770.C6 is shown in Figure 6.3.4. All culture medium contained different amounts of 2DG produced protein bands against all four antibodies and the protein band was approximately 120 kDa which corresponded to the molecular weight of APP770.

The APP obtained from cells grown in complete medium (CM) containing 10% FBS and 25 mM D-glucose was referred back to data collected in Chapter 5. Figure 6.3.5 (a) shows that the clones shared the same APP secretion trend in each concentration of 2DG; APP751 produced more APP than APP695 and APP770. After the number of live cells was taken into account in the determination of the amount of APP secretion per cell, the same trend of APP secretion was also found as shown in Figure 6.3.5 (b). The mean ± S.E.M. of the results of APP secretion (a.u.) per cell are as follows:

- CM: APP751 (34.69±7.13 a.u./cell)> APP695 (27.37±3.09 a.u./cell)> APP770 (16.04±9.26 a.u./cell).
- 5 mM: APP751 (76.58±0.3 a.u./cell)> APP695 (42.61±2.12 a.u./cell)> APP770 (32.48±9.51 a.u./cell).
- 25 mM: APP751 (85.41±3.07 a.u./cell)> APP695 (62.10±7.35 a.u./cell)> APP770 (42.71±14.08 a.u./cell).
- 50 mM: APP751 (149.5±7.93 a.u./cell)> APP695 (83.66±0.92 a.u./cell)> APP770 (74.99±18.67 a.u./cell).

The level of secreted APP per cell was calculated using the following formula: APP secretion level (a.u.) per cell = (fluorescence intensity x 10^6)/ cell number; where a.u. stands for Arbitrary unit.

The amount of secreted APP was statistically analysed using two-way ANOVA with 95% confidence interval and Bonferroni's multiple comparison test. Also, these data were analysed based on two independent factors; the concentrations of 2DG in culture medium and the differences in the isoform of APP. The statistical analysis revealed that each factor affected the APP secretion independently ($p>0.05$) and significantly; the type of cell ($p=0.0182$) and the different concentration of 2DG ($p=0.0019$). The changes in the APP secretion were presented as mean of fold change ± S.E.M. to the control.

Figure 6.3.6 shows the APP secretion level (mean of fold change ± S.E.M.) of each cell type compared with the same cells growing in the complete medium containing 25 mM of D-glucose, in order to compare the APP secretion of each cell type under different concentration of 2DG. The fold of APP secretion of non-transfected HEK293 were lower than the control at all concentrations of 2DG. The fold increase of APP695 and APP751 were similar to the control while the fold increases of APP770 were higher than control. The average changes in APP secretion are as follows:

- Non-transfected HEK293: 5 mM (0.85±0.08)> 25 mM (0.83±0.09)> 50 mM (0.80±0.1).
- APP695: 25 mM (1.09±0.15)> 50 mM (1.07±0.12)> 5 mM (1.03±0.09).
- APP751: 25 mM (1.07±0.05)> 50 mM (1.05±0.06)> 5 mM (1.01±0.04).
- APP770: 50 mM (2.25±0.89)> 5 mM (1.94±0.63)> 25 mM (1.9±0.63).

Each graph in Figure 6.3.6 represents each cell type; (a) non-transfected HEK293 cells, (b) HEK695.C5, (c) HEK751.C1 and (d) HEK770.C6 consisting of data from three concentrations of 2DG; 5 mM, 25 mM, 50 mM and control. There were no significant changes in APP secretion within each cell type of non-transfected HEK293 cells, HEK695.C5 and HEK751.C1, where the cells were cultured in the culture medium containing various concentrations of 2DG. However, the APP secretion of HEK770.C6 in culture medium containing 50 mM 2DG showed a significant increase in comparison to control ($p<0.05$).

Figure 6.3.7 shows the APP secretion level (mean of fold change ± S.E.M.) of each clone after subtraction of endogenous APP from non-transfected HEK293 in order to compare the APP secretion between isoforms of APP. All three isoforms of APP share the same trend of increases of APP secretion in the presence of 2DG; APP751 had higher fold increase than APP695 and APP770. The average results of fold of APP secretion are as follows:

- CM: APP751 (4.73±0.82)> APP695 (4.33±0.97)> APP770 (1.7±0.48).
- 5 mM: APP751 (5.47±0.40)> APP695 (4.99±0.52)> APP770 (3.32±0.53).
- 25 mM: APP751 (5.94±0.29)> APP695 (5.37±0.06)> APP770 (3.510.95).
- 50 mM: APP751 (6.11±0.63)> APP695 (5.53±0.37)> APP770 (4.01±0.83).

Each graph in Figure 6.3.7 represents each concentration of 2DG; (a) 5 mM, (b) 25 mM and (c) 50 mM and consists of four cell types; non-transfected HEK293 cells, HEK695.C5, HEK751.C1 and HEK770.C6. The APP secretion of HEK695.C5 and HEK751.C1 increased significantly at all concentrations ($p<0.001$ and $p<0.001$, respectively). Also, the APP secretion of HEK770.C6 increased greatly at all concentrations (5 mM: $p<0.05$; 25 mM: $p<0.05$ and 50 mM: $p<0.05$). Moreover, the APP secretion of HEK751.C1 was significantly greater than HEK770.C6 at the same concentration of 2DG (5 mM: $p<0.05$; 25 mM: $p<0.05$ and 50 mM: $p<0.05$).

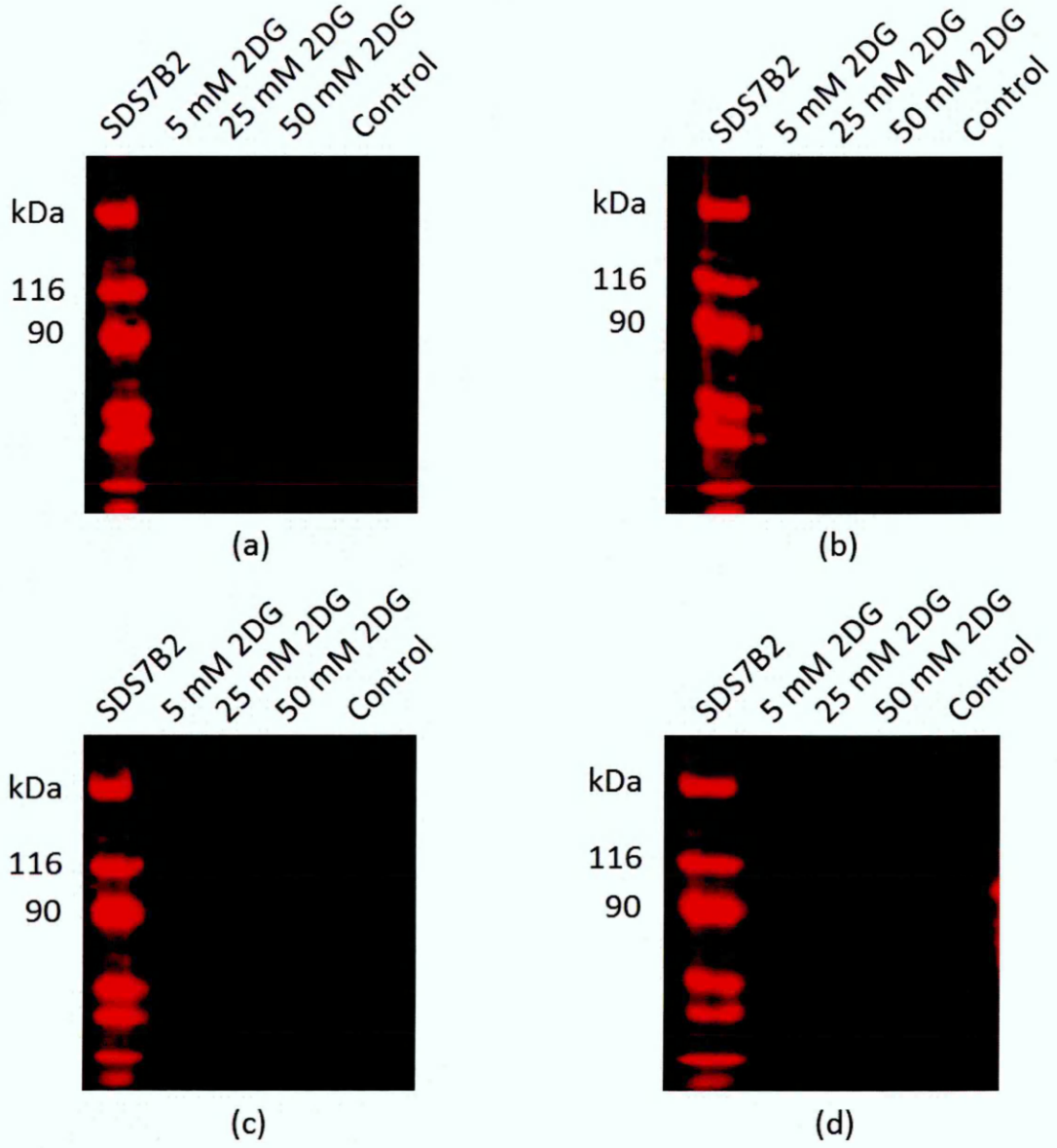

Figure 6.3.1 Protein analysis of secreted APP by non-transfected HEK293 cells which were cultured in culture medium containing various concentrations of 2DG; 5 mM, 25 mM and 50 mM over 24-hour period with four primary antibodies; (a) 1151, (b) 993, (c) 23/2 and (d) DE2. None of the samples produced a protein band recognised by any primary antibodies. However, the control sample (non-transfected HEK293 cells) produced a faint protein band recognised by all four primary antibodies which could be the result of bovine APP as the band was approximately 120 kDa in size.

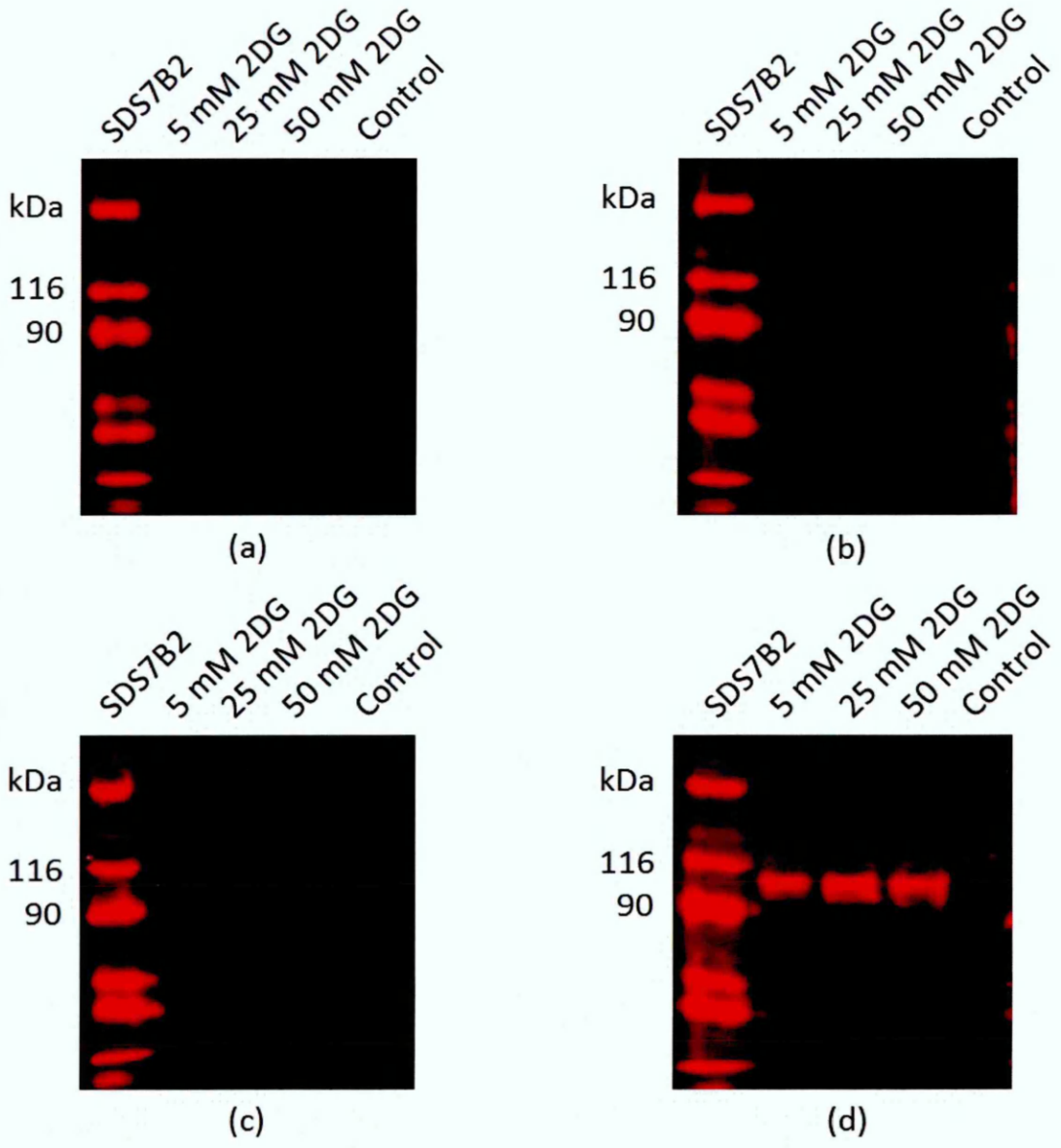

Figure 6.3.2 Protein analysis of secreted APP by HEK695.C5 which were cultured in culture medium containing various concentration of 2DG; 5 mM, 25 mM and 50 mM over 24-hour period with four primary antibodies; (a) 1151, (b) 993, (c) 23/2 and (d) DE2. Culture media contained different amounts of 2DG produced a protein band recognised by 1151 and DE2 primary antibodies and the approximate size of the protein band was 115 kDa which corresponded to the molecular weight of APP695. The produced protein band was recognised by DE2 antibody and was stained more strongly than 1151 antibody possibly due to bovine APP in culture medium. Also, none of the samples produced protein band recognised by 993 and 23/2 antibodies.

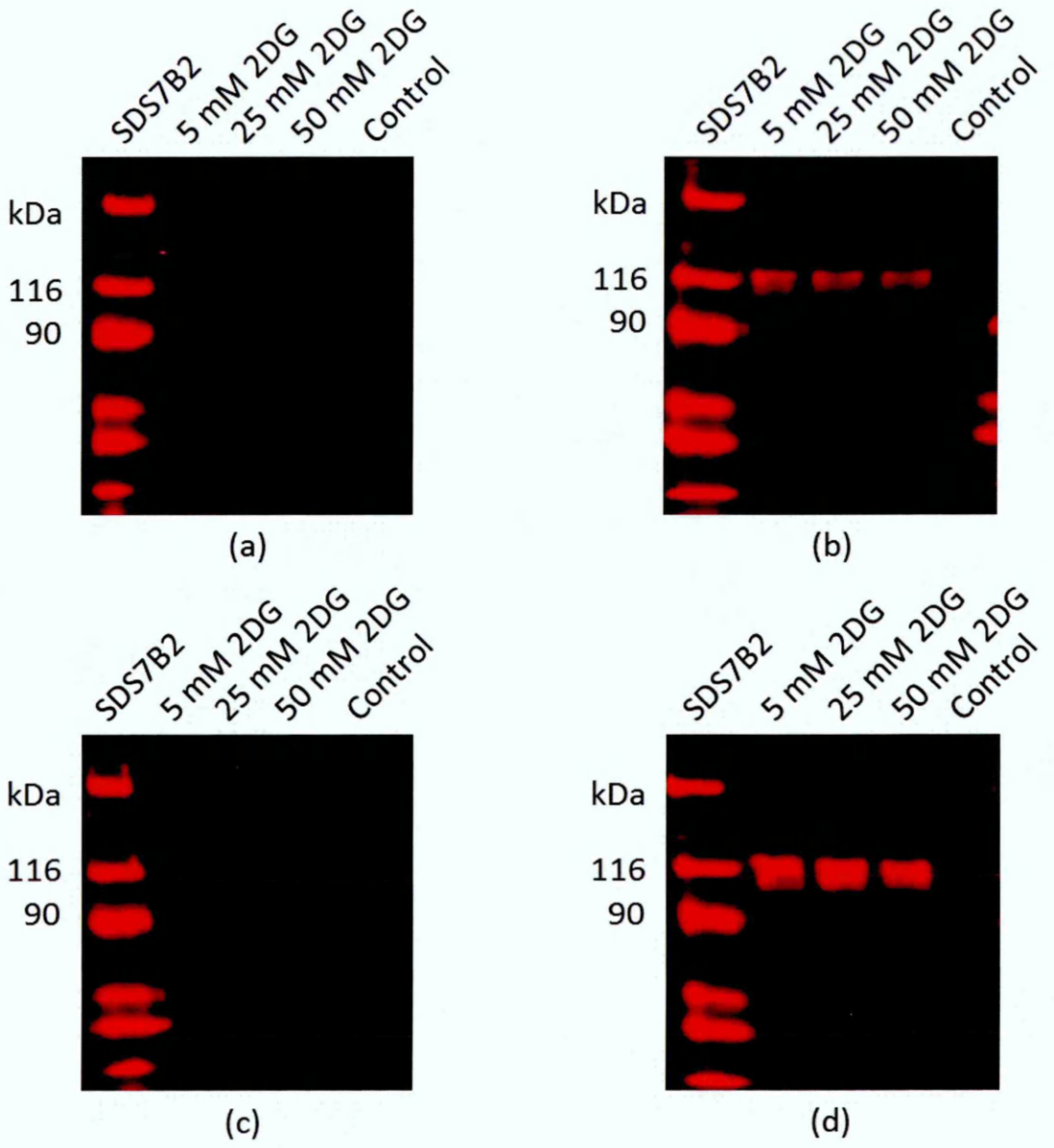

Figure 6.3.3 Protein analysis of secreted APP by HEK751.C1 which was cultured in culture medium containing various concentrations of 2DG; 5 mM, 25 mM and 50 mM over 24-hour period with four primary antibodies; (a) 1151, (b) 993, (c) 23/2 and (d) DE2. Culture media contained different amounts of 2DG produced clear protein band recognised by 1151, 993 and DE2 antibodies which was approximately 118 kDa in size which corresponded to the molecular weight of APP751. Also, none of the samples produced protein band against 23/2 antibody.

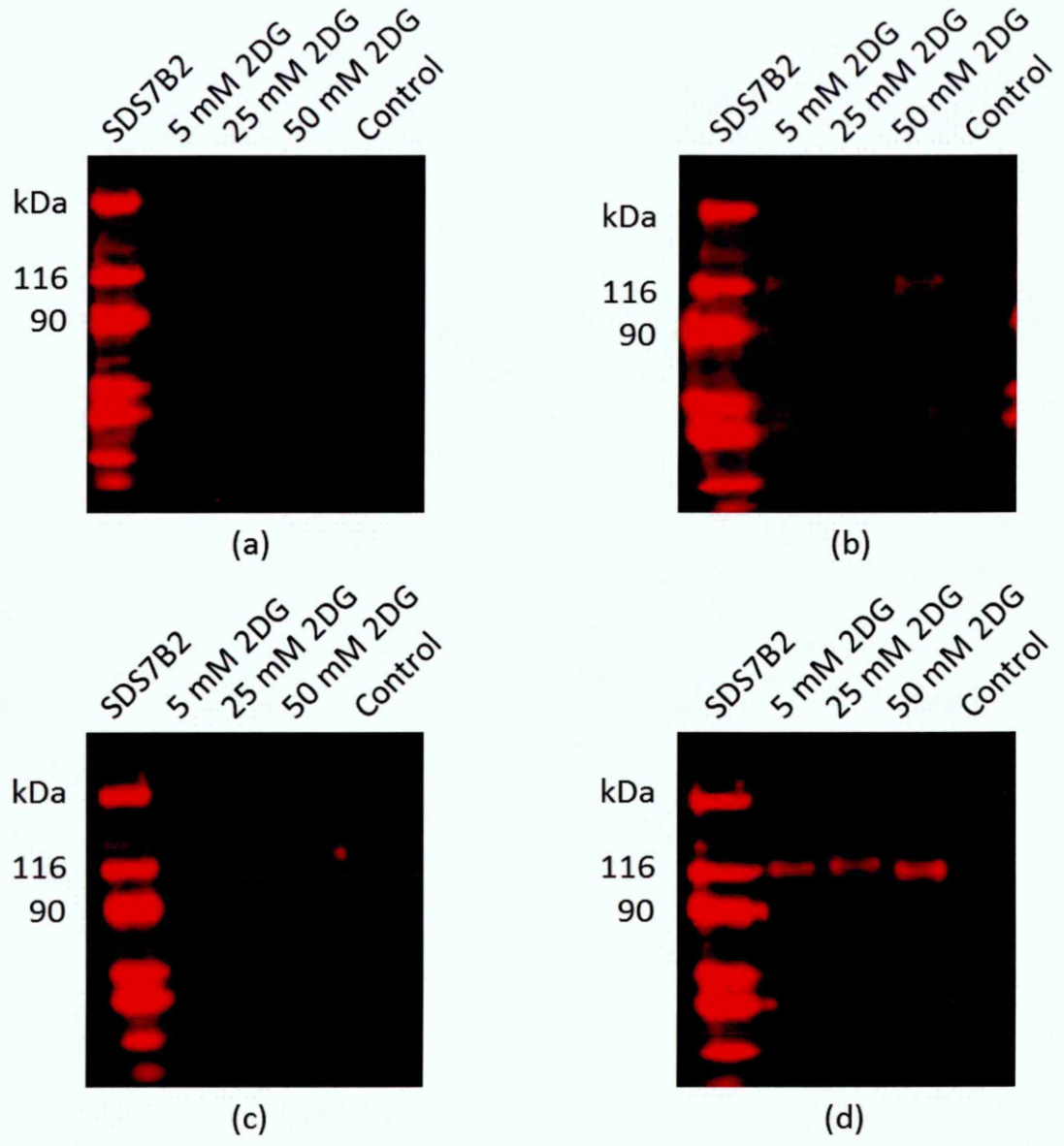

Figure 6.3.4 Protein analysis of secreted APP by HEK770.C6 which was cultured in culture medium containing various concentrations of 2DG; 5 mM, 25 mM and 50 mM over 24-hour period with four primary antibodies; (a) 1151, (b) 993, (c) 23/2 and (d) DE2. Culture medium contained different amounts of 2DG produced protein band recognised by all four antibodies and the protein band was approximately 120 kDa which corresponded to the molecular weight of APP770.

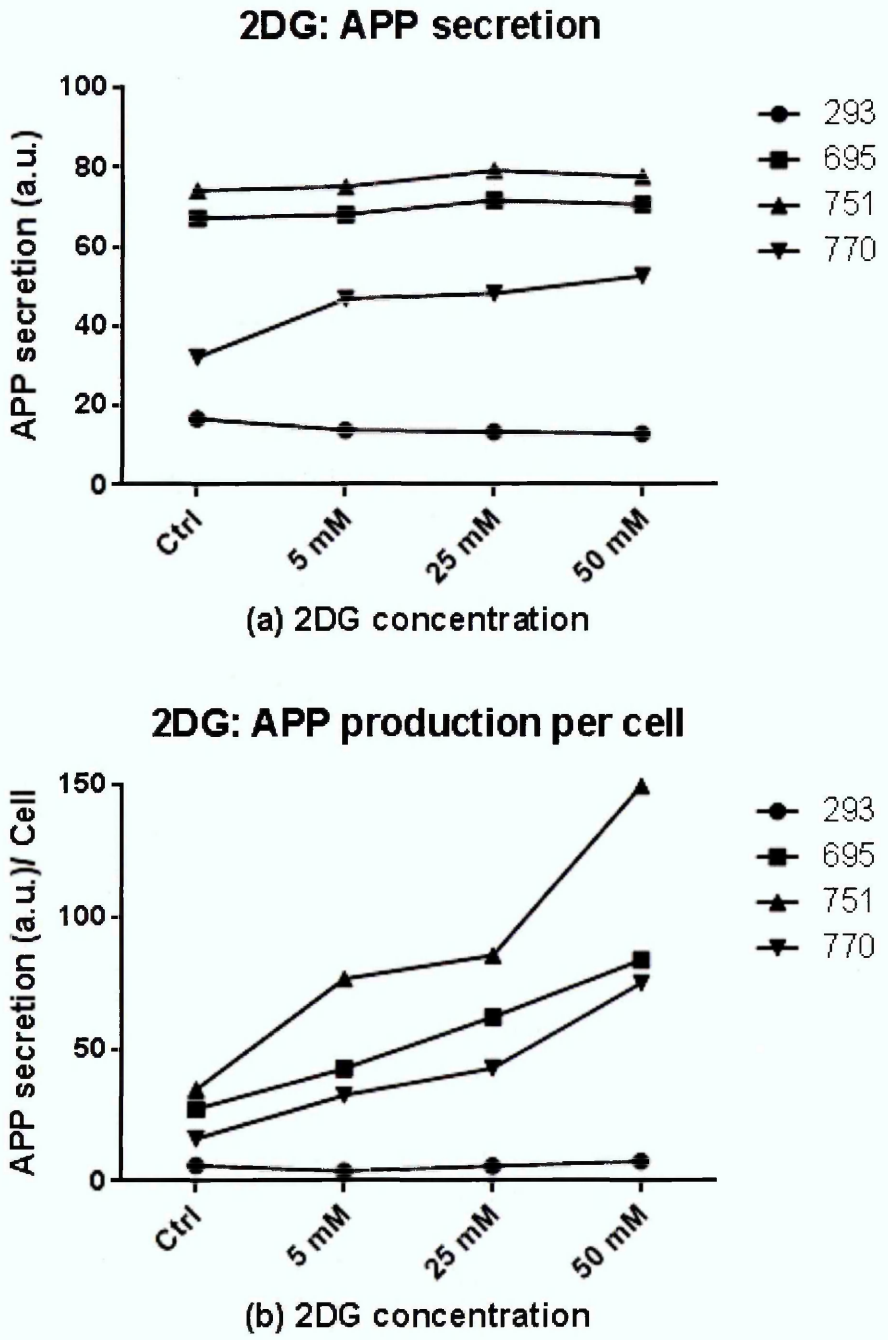

Figure 6.3.5 The APP secretion level as mean ± SEM. (a) the APP secretion (a.u.) of each cell type. All three clones shared the same pattern of APP secretion under the same concentration of 2DG: APP751> APP695> APP770. **(b) the APP secretion (a.u.) per cell of each cell type.** After the cell number was taken into account to calculate the APP secretion per cell, the same trend of APP secretion under the same concentration of 2DG was found: APP751> APP695> APP770.

Figure 6.3.6 The APP secretion level as mean ± S.E.M.: cell type. Each graph represents each cell type; non-transfected HEK293 cells, HEK695.C5, HEK751.C1 and HEK770.C6 and consists of three concentrations of 2DG; 5mM, 25 mM and 50 mM. The APP secretion of each cell type grown in culture medium containing 25 mM glucose was as used as a control. There were no significant changes in APP secretion within each cell type of non-transfected HEK293 cells, HEK695.C5 and HEK751.C1, where the cells were cultured in the culture medium containing various concentrations of 2DG. However, the APP secretion of HEK770.C6 in culture medium containing 50 mM 2DG showed a significant increase in comparison to the control ($p<0.05$).

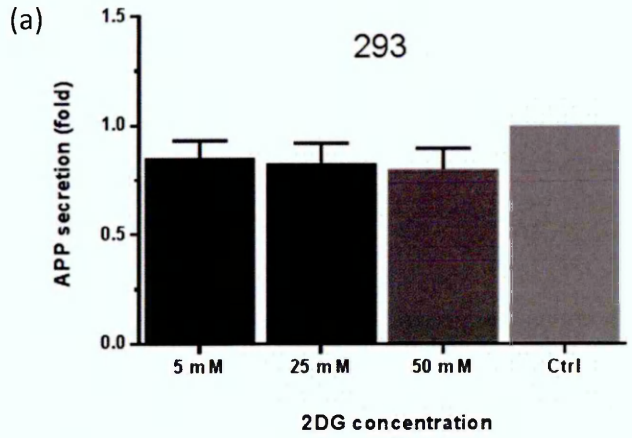
(a)
293
APP secretion (fold)
1.5
1.0
0.5
0.0
5 mM
25 mM
50 mM
Ctrl
2DG concentration

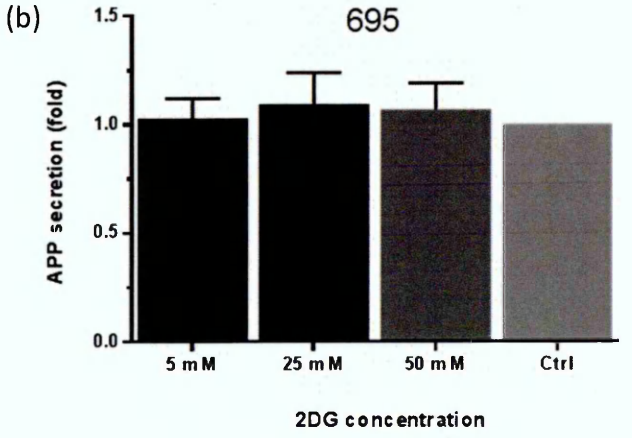
(b)
695
APP secretion (fold)
1.5
1.0
0.5
0.0
5 mM
25 mM
50 mM
Ctrl
2DG concentration

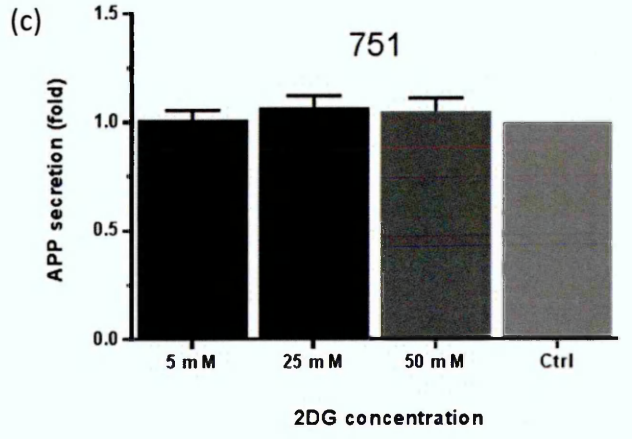
(c)
751
APP secretion (fold)
1.5
1.0
0.5
0.0
5 mM
25 mM
50 mM
Ctrl
2DG concentration

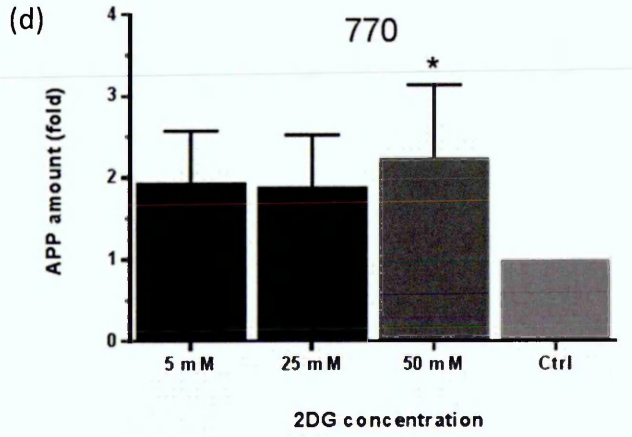
(d)
770
*
APP amount (fold)
4
3
2
1
0
5 mM
25 mM
50 mM
Ctrl
2DG concentration

Figure 6.3.7 The APP secretion level as mean ± S.E.M.: concentrations of 2DG. Each graph represents different concentration of 2DG; (a) 5 mM, (b) 25 mM and (c) 50 mM and consists of four cell types; non-transfected HEK293 cells, HEK695.C5, HEK751.C1 and HEK770.C6. The APP secretion of non-transfected HEK293 cells was used as the control. The APP secretion of HEK695.C5 and HEK751.C1 increased significantly at all concentrations ($p<0.001$ and $p<0.001$, respectively). Also, the APP secretion of HEK770.C6 increased greatly at all concentrations (5 mM: $p<0.05$; 25 mM: $p<0.05$ and 50 mM: $p<0.01$). Moreover, the APP secretion of HEK751.C1 was significantly greater than HEK770.C6 at the same concentration of 2DG (5 mM: $p<0.05$; 25 mM: $p<0.05$ and 50 mM: $p<0.05$).

(a)

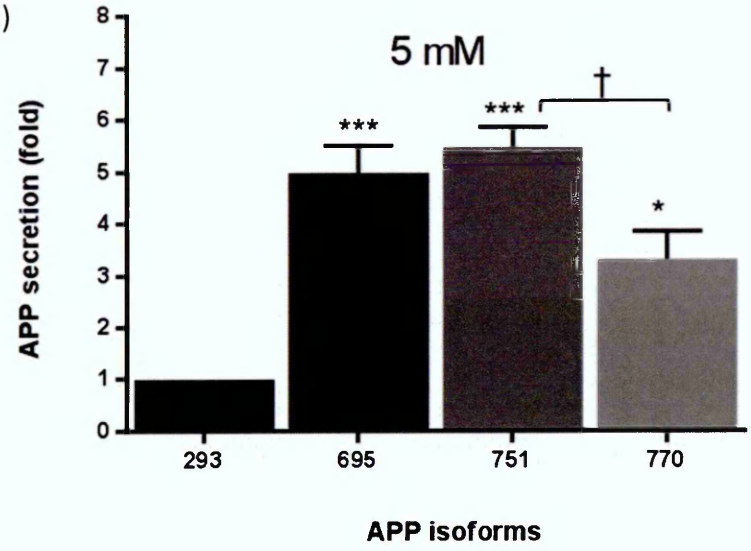
5 mM
APP secretion (fold)
0
1
2
3
4
5
6
7
8
***
***
†
*
293
695
751
770
APP isoforms

(b)

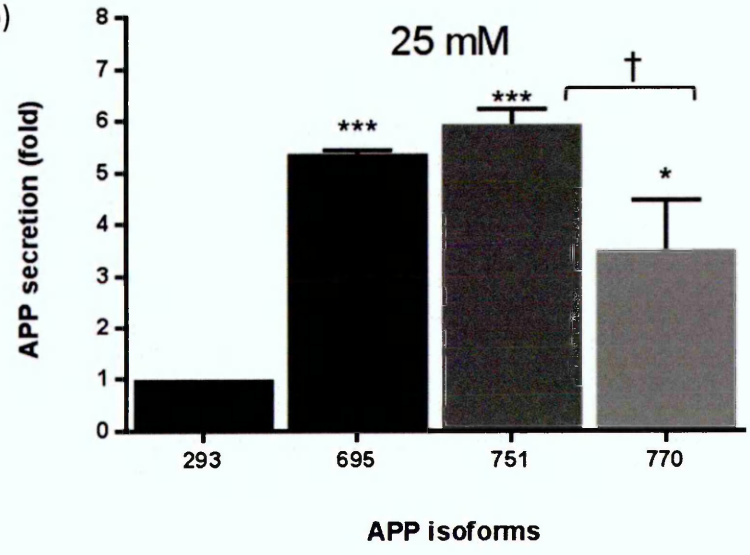
25 mM
APP secretion (fold)
0
1
2
3
4
5
6
7
8
***
***
†
*
293
695
751
770
APP isoforms

(c)

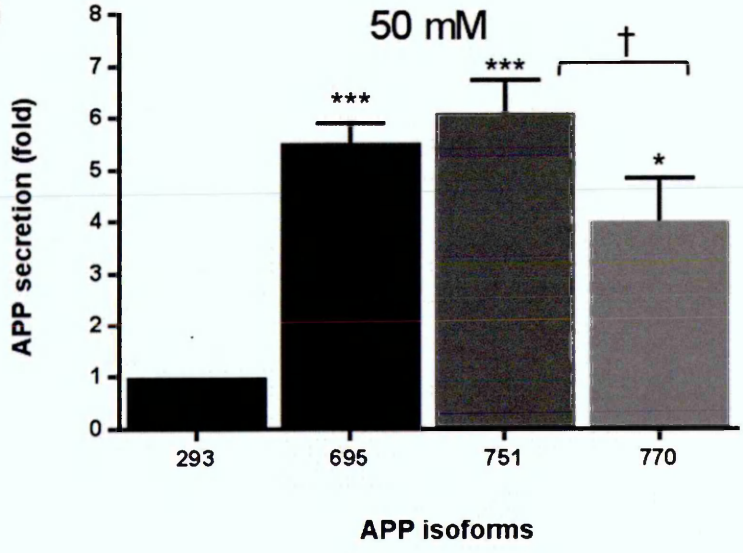
50 mM
APP secretion (fold)
0
1
2
3
4
5
6
7
8
***
***
†
*
293
695
751
770
APP isoforms

6.4 Effects of 2DG in cell culture medium on APP mRNA level

The last part of the investigation of the effects of 2DG on HEK293 transfected APP isoforms was to evaluate the levels of APP mRNA.

It is obligatory that appropriate reference genes are selected before the beginning of the determination of mRNA level experiments. As reference genes are to be used as a normaliser during the determination of mRNA level experiments, the most stable reference genes across the different experimental conditions were selected. The reference gene stability assessment was demonstrated in Chapter 5. In short, the 12 reference genes were tested for their expression stability between non-transfected HEK293 cells and selected clones of each HEK293 transfected APP isoforms under untreated and all experimental conditions; including the variation of 2DG concentrations in complete culture medium. The reference gene expression stability values (M-value) and the minimum number of reference genes required for normalisation (V-value) in the experiments were obtained using GeNorm software. As a result of the GeNorm software analysis, at least two reference genes were required in the determination of mRNA level analysis and SCLY and TYW1 were selected.

Methods in brief

After obtaining appropriate reference genes (SCLY and TYW1) and the efficiency of each pair of primers, measuring the determination of the effects of 2DG on APP mRNA levels was then carried out. The experiment began by plating approximately 5×10^5 of live cells per well in 6-well plates. Cells were allowed to settle and adhere for at least 6 hours before culture medium was discarded and fresh complete medium which contained varying concentrations of 2DG was added. Twenty-four hours later, cells were photographed using the XLI cap program and culture medium was collected for APP secretion analysis followed by cell counting and cell pellet harvesting. The cell count data was analysed as described in Section 6.2 including photographs of the cells. The culture medium was analysed and the results described in Section 6.3. Finally, the total RNA was extracted from the cell pellets according to the procedure described in Section 2.20 using RNeasy Mini Kit before quantification using NanoDrop ND-1000 UV-VIS Spectrophotometer (Section 2.21). The RNA was converted into cDNA using QuantiTect Reverse Transcription Kit as described in Section 2.23. At this point the

cDNA of each sample was ready to be amplified under real-time RT-PCR conditions. A complete list of real-time PCR components and procedures are described in Section 2.28.

The data from each amplification condition of each sample was obtained as the C_t value. Each sample was carried out in triplicate per reaction, therefore the mean of triplicate C_t values was used in relative quantification of the mRNA level. The chosen relative quantification model was the one that takes the slope of primer efficiency into account. The model is as followed:

$$\text{Fold difference} = E_{sample}^{\Delta Ct\ sample} / E_{reference}^{\Delta Ct\ reference}$$

Where E_{sample} is primer efficiency of gene of interest; $E_{reference}$ is primer efficiency of a reference gene; $\Delta C_{t\ sample}$ is the difference of mean of C_t between control and gene of interest; $\Delta C_{t\ reference}$ is the difference of the mean of C_t between the reference gene of control and the reference gene of sample.

The two-way ANOVA with 95% confidence interval was coupled with Bonferroni's multiple comparison test to evaluate any possible effect of 2DG at various concentrations in culture medium on APP mRNA level of non-transfected HEK293 cells and clones of APP transfected HEK293: HEk695.C5, HEK751.C1 and HEK770.C6. The APP mRNA level data are presented as graphs between independent factors on the X-axis and the fold difference of mRNA level on the Y-axis. Also, the data were analysed based on two independent factors; the concentration of 2DG and the differences in the isoform of APP.

Results

The statistical analysis showed that both isoforms of APP and the concentration of 2DG had significant effects on APP mRNA level ($p=0.0003$ and $p<0.0001$, respectively) but both dependent factors were independent from each other ($p>0.05$).

Figure 6.4.1 shows the graph of the APP mRNA level which contained all three concentrations of 2DG in culture medium and each graph represented each of the cell types: (a) non-transfected HEK293, (b) HEK695.C5, (c) HEK751.C1 and (d) HEK770.C6.

The same cells growing complete culture medium containing 25 mM of glucose were used as the controls. Overall, the APP mRNA level of all four cell types increased in comparison to controls but there were only a few changes which were significant. The statistical analysis revealed that the APP mRNA level of non-transfected HEK293 at 50 mM 2DG increased significantly in comparison to control ($p<0.05$). The APP mRNA level of HEK695.C5 increased significantly at all concentrations of 2DG (5 mM: $p<0.05$; 25 mM: $p<0.001$ and 50 mM: $p<0.001$) and there was a significant decrease in APP mRNA level at 5 mM 2DG in comparison to 50 mM 2DG ($p<0.001$). The APP mRNA level of HEK751.C1 at 25 mM and 50 mM 2DG increased significantly in comparison to controls ($p<0.01$).

Figure 6.4.2 shows the graph of APP mRNA level which contained four cell types and each graph represented each concentration of 2DG in culture medium: (a) 5 mM, (b) 25 mM and (c) 50 mM. The non-transfected HEK293 growing in each concentration of 2DG was used as controls. There was an increase in the APP mRNA level of four cell types and the changes between each concentration shared the same pattern: the mRNA of APP695 has the highest increase and the increase of mRNA of APP770 is greater than APP751. The APP mRNA level of HEK695.C5 increased significantly at all concentrations of 2DG (5 mM: $p<0.05$; 25 mM: $p<0.001$ and 50 mM: $p<0.001$). Also, the APP mRNA level of HEK751.C1 and HEK770.C6 significantly decreased in comparison to HEK695.C5 at all concentrations (at least $p<0.05$).

Figure 6.4.1 The APP mRNA level as mean ± S.E.M.: cell types. The X-axis: the concentrations of 2DG and the Y-axis: fold difference of APP mRNA level. The same cell type cultured in complete culture medium was used as a control. Each graph represents each cell type; (a) non-transfected HEK293 cell, (b) HEK695.C5, (c) HEK751.C1 and (c) HEK770.C6 treated with three 2DG concentrations; 5 mM, 25 mM and 50 mM. Each cell type cultured in culture medium containing 25 mM glucose was used as the control. The APP mRNA level of non-transfected HEK293 at 50 mM 2DG increased significantly in comparison to the control ($p<0.05$). The APP mRNA level of HEK695.C5 increased significantly at all concentrations of 2DG (5 mM: $p<0.05$; 25 mM: $p<0.001$ and 50 mM: $p<0.001$) and there was a significant decrease in APP mRNA level at 5 mM 2DG in comparison to 50 mM 2DG ($p<0.001$). The APP mRNA level of HEK751.C1 at 25 mM and 50 mM 2DG increased significantly in comparison to controls ($p<0.01$).

(a)

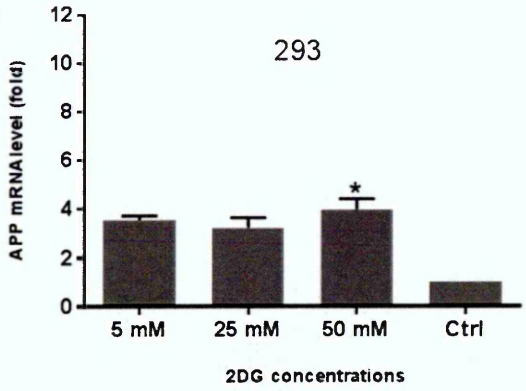
293
APP mRNA level (fold)
12
10
8
6
4
2
0
*
5 mM
25 mM
50 mM
Ctrl
2DG concentrations

(b)

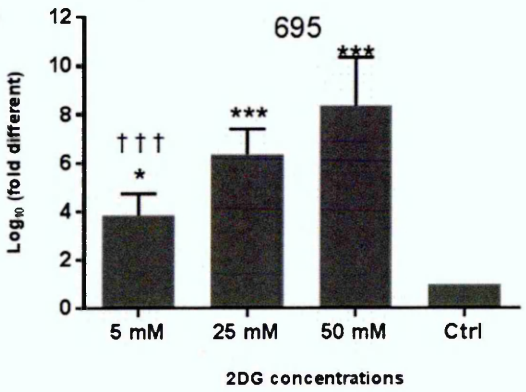
695
Log10 (fold different)
12
10
8
6
4
2
0
†††
*
***
***
5 mM
25 mM
50 mM
Ctrl
2DG concentrations

(c)

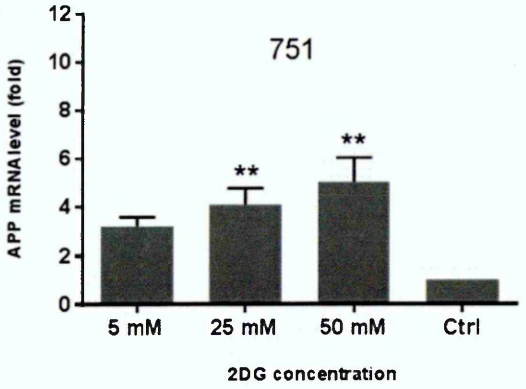
751
APP mRNA level (fold)
12
10
8
6
4
2
0
**
**
5 mM
25 mM
50 mM
Ctrl
2DG concentration

(d)

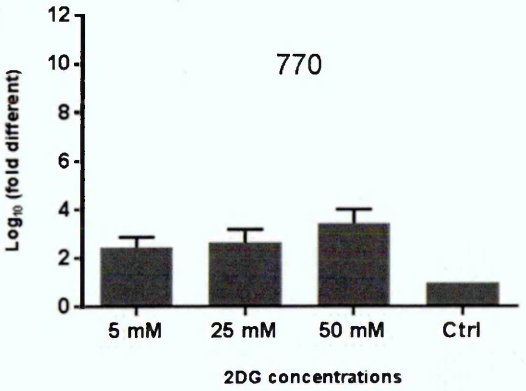
770
Log10 (fold different)
12
10
8
6
4
2
0
5 mM
25 mM
50 mM
Ctrl
2DG concentrations

Figure 6.4.2 The APP mRNA level as mean ± S.E.M.: concentrations of 2DG. The X-axis: cell types and the Y-axis: fold difference of APP mRNA level. The non-transfected HEK293 was used as a control. Each graph represents each concentration of 2DG; (a) 5 mM, (b) 25 mM and (c) 50 mM consisted of four cell types; non-transfected HEK293 cell, HEK695.C5, HEK751.C1 and HEK770.C6. The APP mRNA level of HEK695.C5 increased significantly at all concentrations of 2DG (5 mM: $p<0.01$; 25 mM: $p<0.001$ and 50 mM: $p<0.001$). Also, the APP mRNA level of HEK751.C1 and HEK770.C6 significantly decreased in comparison to HEK695.C5 at all concentrations (†; $p< 0.05$, ††; $p<0.01$, †††; $p<0.001$).

(a)

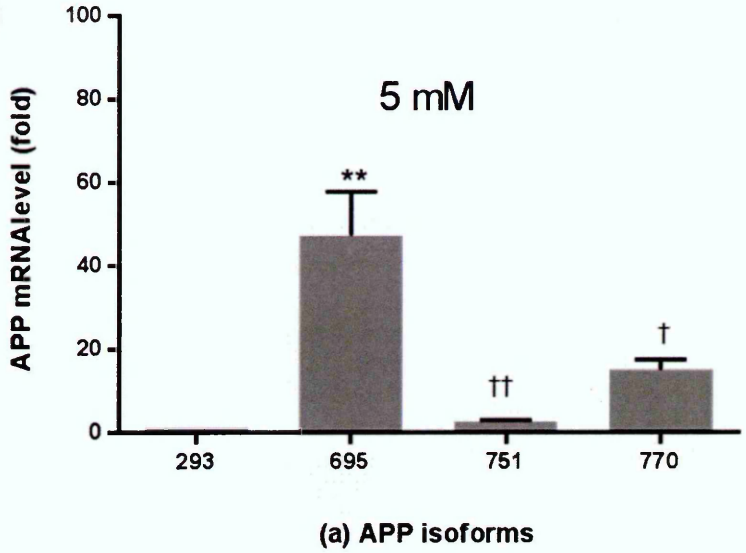

(a) APP isoforms

(b)

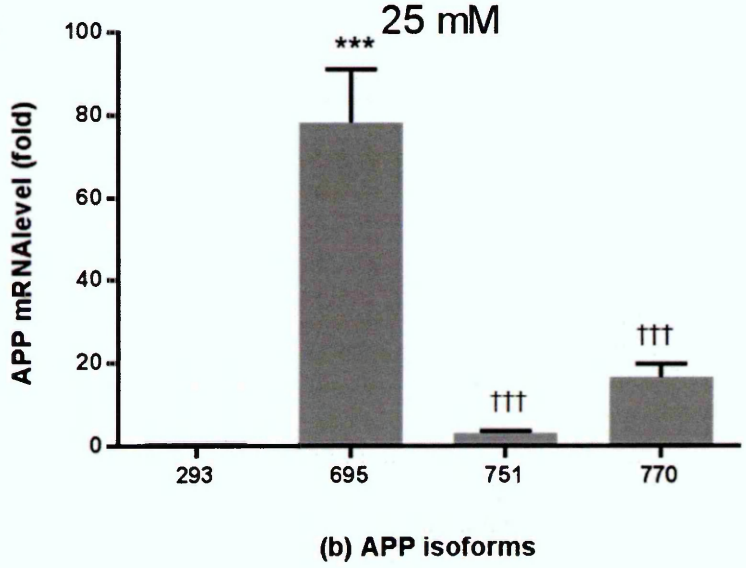

(b) APP isoforms

(c)

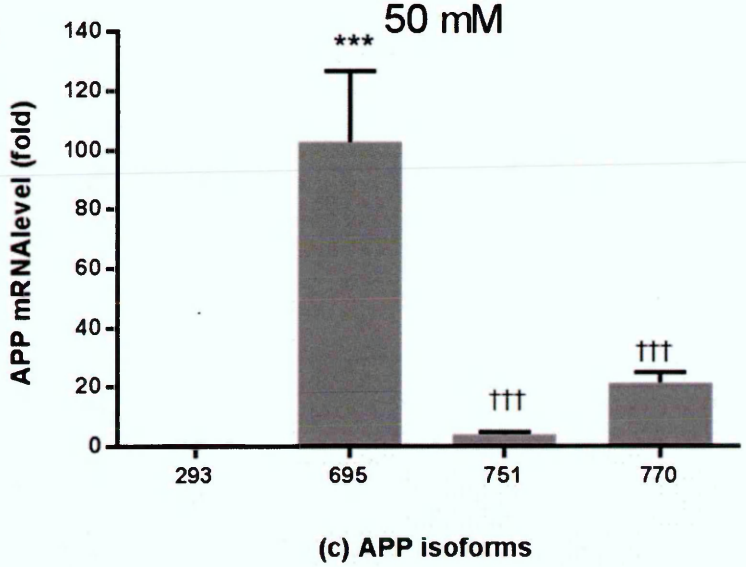

(c) APP isoforms

6.5 mRNA: protein ratio

It was reported that there was a strong correlation between secreted APP and the APP mRNA level in the brains of patients with AD (Matsui et al. 2007). The translational efficiency is the rate of conversion from mRNA into proteins which could be determined using measured protein and mRNA level, as follows:

mRNA: Protein = [mRNA/cell] / [Protein/cell]

The statistics revealed that the HEK751.C1 is the most efficient in translating APP mRNA into APP following by HEK770.C6 and HEK695.C5. The complete analysis of mRNA:Protein ratio is as follows:

- HEK695.C5: 50 mM (18.17±4.65)> 25 mM (14.55±3.16)> 5mM (9.37±1.93)
- HEK751.C1: 50 mM (0.65±0.09)> 25 mM (0.54±0.09)> 5mM (0.48±0.04)
- HEK770.C6: 50 mM (6.09±3.01)> 25 mM (5.78±3.48)> 5mM (4.97±2.27)

6.6 Discussion

The objectives of this investigation were; (1) to find out how each isoform of APP responded to different levels of stress caused by various concentrations of 2DG and (2) to compare the response between different isoforms of APP under the same stress level caused by the same concentration of 2DG. In addition, the investigation of the effect of 2DG in culture medium on APP was carried out in three main parts; cell number, APP secretion into culture medium and APP mRNA level. Also, prior to the cell counting procedure, cells were photographed in order to observe morphological changes due to the effects of 2DG in culture medium.

Impaired cerebral glucose metabolism has become a consistent pathophysiological feature of Alzheimer's disease (Chen and Zhong 2013). Since the brain has high energy consumption rate and the brain's energy is predominantly gained from glucose metabolism, the brain is susceptible to impaired glucose metabolism; both hypoglycaemia and hyperglycaemia (Hoyer 2004; Mergenthaler et al. 2013). Not only could cerebral glucose impairment enhance amyloid plaque deposition and tau phosphorylation but also affect the downstream pathological pathways including oxidative stress, mitochondrial dysfunction, inflammation and apoptosis (Chen and Zhong 2013).

The glucose antagonist, 2-deoxy-D-glucose (2DG) was used to initiate the glucose impairment *in vitro* by mimicking glucose shortage. The 2DG inhibits glycolysis at the same equimolar concentration as glucose by inhibiting hexokinase and the inhibition can be reversed by further addition of glucose (Barban and Schulze 1961; Mulukutla et al. 2010). Since 2DG shares a similar structure to glucose, it could be transported into the cell by glucose transporters and it can be phosphorylated by hexokinase at the first step of glycolysis. However, it cannot be processed further due to the substitution of the hydrogen at the second carbon atom. As a result, phosphorylated 2DG is trapped within the cell leading to intracellular phosphate depletion and an increase of the AMP: ATP ratio (Aft, Zhang and Gius 2002).

The increase of AMP: ATP ratio during cellular phosphate depletion activates the AMP-activated protein kinase (AMPK) which is one of the metabolic regulators (Laderoute et al. 2006; Mulukutla et al. 2010). The activated AMPK inactivates mammalian target of

rapamycin complex 1 (mTORC1) which essentially inhibits cell growth (Li et al. 2014; Mulukutla et al. 2010).

Previous studies have demonstrated that culturing cells in glucose deprived culture medium, with or without the presence of 2DG, has led to cell cycle and cell proliferation arrest whereas the viability of the cells was not affected (Aft, Zhang and Gius 2002; Jelluma et al. 2006; Webster et al. 1998). The cell count data presented in this Chapter have confirmed that while the cell viability remains constant at all concentrations of 2DG, the proliferation of the cell has slowed down at the lowest concentration of 2DG and stopped or decreased at the highest concentration of 2DG (Figure 6.2.1-Figure 6.2.2). The cell cycle arrest under glucose deprivation condition could be a result of phosphorylation of p53 by AMPK (Mulukutla et al. 2010).

Also, glucose metabolism has been strongly linked to apoptosis (Caro-Maldonado et al. 2010; King and Gottlieb 2009). One of several roles of glucose metabolism is to minimise cellular reactive oxygen species (ROS) levels by promoting glucose-6-phosphate (G6P) to the pentose phosphate pathway (PPP) which ultimately generates the reduced form of glutathione (GSH) as a consequence (King and Gottlieb 2009). It was suggested that 2DG is more likely to cause apoptotic cell death via the activation of caspase 3 and poly ADP ribose polymerase (PARP) (Aft, Zhang and Gius 2002). Cells undergoing apoptosis could be morphologically characterised by nuclear condensation, DNA fragmentation, membrane budding, cytoplasm elongation, shrinkage and forming clusters (Bottone et al. 2013; Fiorelli, Kirouac and Padmanabhan 2013; King and Gottlieb 2009; LeBlanc 1995; Steiger-Barraissoul and Rami 2009; Xie et al. 2013). The morphological changes of the cells cultured in culture medium containing 2DG resemble apoptosis. It has been proposed that under glucose deprivation conditions, the apoptotic process is initiated via stress-response pathways such as mitogen-activated protein kinases (MAPK) (Mulukutla et al. 2010).

The AMPK activation enhances the energy-generating processes, including glucose metabolism, to generate more ATP and suppresses several anabolic processes, including protein synthesis, to conserve ATP (Laderoute et al. 2006; Li et al. 2014; Mulukutla et al. 2010). The suppression of anabolic processes occurs via the inactivation of mTORC1 which is responsible for synthesising macromolecules such as

protein under normal nutrient and ATP-level conditions (Dibble and Manning 2013). Hence it was hypothesised that culturing the cells with 2DG would reduce APP synthesis thereby reducing the APP secretion (only sAPPα has been measured in this experiment). However, the APP secretion data has revealed that the APP secretion has increased as the concentration of 2DG increased in culture medium (Figure 6.3.5 – Figure 6.3.7). This could be because of a protective property of sAPPα which has been demonstrated by several studies (Corrigan et al. 2011; Corrigan et al. 2014; Milosch et al. 2014; Smith-Swintosky et al. 1994; Steinbach et al. 1998; Young-Pearse et al. 2008).

As there is an increase of the APP secretion level, it was hypothesised that the APP mRNA level should increase as well. Once the protein synthesis process is activated, it would promptly activate the translation-associated components which increase the translation of the existing mRNA (translational efficiency) as a consequence (Ladevaia et al. 2012). As expected, the level of APP mRNA reflects the level of secreted APP: there is an increase of APP mRNA level with the concentration of 2DG in the culture medium. Since the secreted APP and the APP mRNA level were found to be correlated in human brain, the ratio between these two parameters was used to determine the efficiency of protein translation (Matsui et al. 2007). The efficiency of protein translation (shown as mRNA:protein ratio±S.E.M.) revealed that HEK751.C1 is the most efficient in APP secretion with the average ratio of 0.56±0.07 following by HEK770.C6 with the average ratio of 5.61±0.47. Although, protein production efficiency decreased as the concentration of 2DG increased, the mRNA:protein ratio of these two clones did not vary significantly. The HEK695.C5 appeared to be the most efficient in producing protein (ratio of 9.37) in the medium containing 5 mM 2DG and the least efficient in the medium containing 50 mM 2DG with the ratio of 18.17.

In conclusion, the different isoforms of APP showed the ability to tolerate the stress equally which is indicated by the similarity of cell number under the stressed condition. Under the same level of stress APP751 appeared to secrete APP the most and have the most efficient in producing APP whereas APP695 appeared to have the highest APP mRNA level and the least efficient in producing APP. This could suggest that under glucose deprivation condition APP751 might be responsible for an increase of APP and its metabolites, such as Aβ peptide.

Chapter 7: General discussion

The aim of this project was to investigate the hypothesis that one of the APP isoforms (APP695, APP751 and APP770) is more likely to be the source of Aβ in Alzheimer's disease under stress-induced conditions.

7.1 To provide an appropriate model of APP processing for pathological study of Alzheimer's disease.

Despite the commonly used animal model in pathological studies of Alzheimer's disease, the animal models have several drawbacks. For example, there are 17 amino acid differences between rodent APP and human APP, and three of them are located in the Aβ domain: rodent -> human (Gly601-> Arg, Phe606-> Tyr and Arg609-> His) (De Strooper et al. 1995). These three amino acids were responsible for the small amount of Aβ peptide produced in rodent model experiments and the low susceptibility of amyloid aggregation (Fraser et al. 1992). Hence it would be appropriate to select an alternative model; a human cellular model for pathological studies of the disease.

Prior to testing the proposed hypothesis, the cellular models overexpressing APP695, APP751 and APP770 were established. Firstly, the expression vector pIREShyg2 containing human APP770 cDNA was provided by Professor Nigel Hooper. It was used to generate the expression vector pIREShyg2 containing human APP751 and human APP695 using molecular biology techniques consisting of conventional PCR, touchdown PCR and Overlap extension PCR. These expression vectors were then transfected into Chinese Hamster Ovary (CHO) cells in order to generate stably expressing clones which expressed APP at a similar level. After several unsuccessful attempts of trying to stably express the isoforms of APP in CHO, only the original expression vector pIREShyg2 containing human APP770, was successful, albeit with difficulty. The sequencing results of the expression vector pIREShyg2 containing APP751 and APP695 confirmed that the sequence of both APP isoforms were intact yet failed to express in CHO. It has been suggested that the pIREShy2 vector has an effect on the mRNA of the inserted DNA, resulting in suppression of the protein of interest expression in mammalian cells

(Shikama et al. 2010). Also, the mammalian cells were able to selectively silence the gene of interest which resulted in no or low expression of the protein of interest yet the cells still are able to survive the antibiotic selection. The in-house construct expression vectors could be more sensitive to post-translational modification as CHO cells are glycosylation abundant (Stanley 1988).

In order to carry on further with the project, three synthetic expression vectors, pcDNA3.1 containing human APP695, APP751 and APP770, were obtained and expressed in CHO cells to generate stably expressing clones which expressed APP at similar levels. As the new synthetic expression vectors were shown to be successful in CHO cells, these vectors were expressed in Human Embryonic Kidney 293 (HEK293) cells in order to more closely reflect the situation of Alzheimer's disease. Also, HEK293 is an ideal candidate as a host cell for studies of APP expression and processing because it allows the gene of interest in the expression vector to integrate into the host cell genome. HEK293 expresses signalling pathways, four neurofilament subunits and it has high rate of protein synthesis in comparison to CHO (Thomas and Smart 2005). One out of ten clones stably expressed each APP isoform at comparable levels and was selected as the cellular models overexpressing human APP695, APP751 and APP770.

7.2 To confirm the use of novel antibodies for the detection of secreted human APP expression.

The media of HEK293 cells expressing human APP695, APP751 and APP770 were subjected to antibodies testing to determine the utility of these antibodies. Four antibodies were used; 1151, 993, 23/2 and DE2. Each antibody recognises a different epitope of the APP sequence. The 1151 recognises the amino acid at the N – terminal of all three APP isoforms and is recognised by anti-rabbit antibody. The DE2 recognises the Aβ domain of all three APP isoforms and is recognised by anti-mouse antibody. The 993 antibody recognises the KPI domain on the APP sequence of APP751 and APP770 and is recognised by anti-rabbit antibody. The 23/2 antibody recognises the OX2 domain on the APP sequence of APP770 and is recognised by anti-rabbit antibody. Also, 1151 and 23/2 did not recognise bovine APP which typically exists in complete

medium. It was demonstrated throughout the project that not only could the different antibodies can be used to distinguish the isoform of APP, but also could be used in APP quantification with fluorescence detection.

7.3 Efficiency of mRNA translation by each isoform of APP

Several isoforms of APP ranging from 365 to 770 amino acid residues resulted from the alternative splicing of the APP transcript, three of which are the most relevant in Alzheimer's disease: APP695, APP751 and APP770, as shown in Figure 1.3.1, Chapter1 (Zheng and Koo 2011). Also, APP695 is the predominant isoform in the brain while APP751 and APP770 are mainly expressed in non-neuronal tissues (O'Brien and Wong 2011).

Prior to this study, it was hypothesised that when selected clones that secreted similar amounts of APP695, APP751 and APP770 into culture media under normal cultured conditions (culture medium containing 10% FBS and 25 mM glucose) would be the consequence of equal amounts of mRNA for each isoform.

There is approximately 10% difference in amino acid content among these isoforms of APP isoforms. Since under normal culture conditions the APP secretion from each isoform of APP was at a comparable level, it was then hypothesised that the mRNA levels would also be at comparable levels. However, the mRNA level of each isoform of APP appeared to be at different levels: APP751> APP770> APP695 (as reported in Chapter 5, Section 5.4). On average, the mRNA level between APP751 was 4 fold higher than APP695. The differences in mRNA levels between isoforms of APP could have significant effects on APP secretion and, ultimately, Aβ peptide secretion. As APP751 has the highest average level of mRNA resulting in the lowest protein production efficiency, it is hypothesised that APP751 translation might be subjected to a cellular "brake" system on protein conversion which slowed down mRNA translation into protein. If true, then in AD, reduction in the "brake" may lead to over production of APP751, leading to the greater secretion of Aβ peptide. Nevertheless, these observations are based on a single clone for each isoform of APP. Therefore this experiment requires repeating with more clones representing each isoform of APP.

The outcome of further experiments with more clones of each isoform of APP could provide the evidences for one of the following three scenarios. The first scenario (as shown in Figure 7.3.1) is that the new clones of each isoform of APP produce similar mRNA:protein ratios to the previous clone which indicates that APP751 is the least efficient in the mRNA-protein translation process while APP695 is the most efficient.

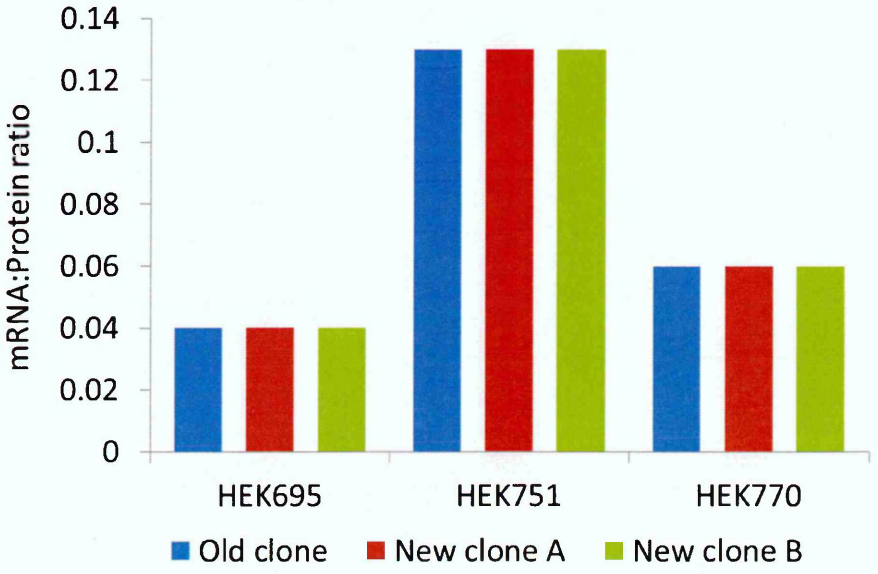

Figure 7.3.1 The first possible outcome of the further experiments with new clones. The new clones of each isoforms of APP would produce a similar outcome to the previous clone.

The second scenario (as shown in Figure 7.3.2) is that the new clones of HEK695 and HEK770 produce similar mRNA: protein ratios to the previous clones while the new clones of HEK751 produce different mRNA:protein ratios to the previous clone. This scenario would suggest that there are other factors other than the mRNA levels which affect the translational and post-translational process of APP in relation to AD pathogenesis besides the isoform of APP.

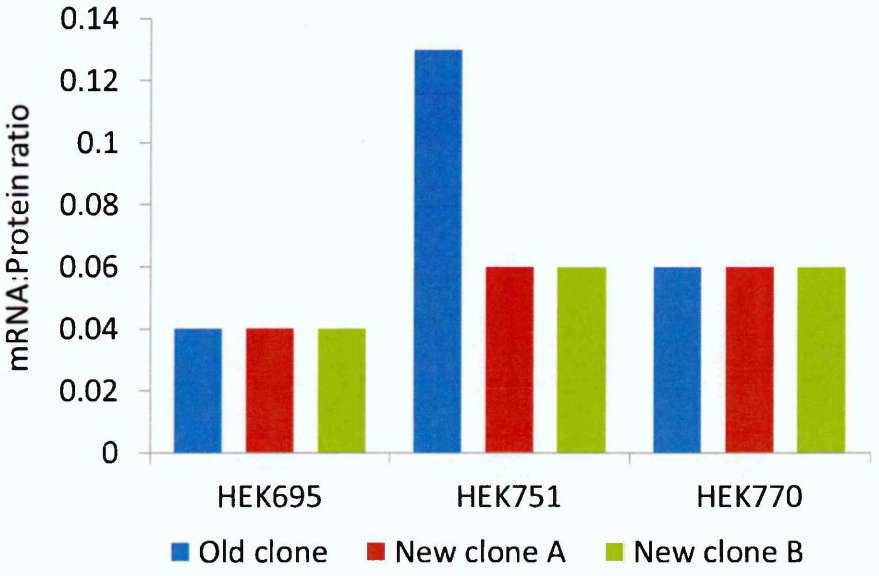

Figure 7.3.2 The second possible outcome of the further experiments with new clones. The new clones of HEK695 and HEK770 produce a similar outcome to the previous clones while the new clones of HEK751 produce a different outcome to the previous clone.

The third and final scenario (as shown in Figure 7.3.3) is that there is considerable variability in mRNA:protein ratios between clones, both previous and new clones, of each isoform of APP. This scenario would suggest that the results are more difficult to interpret but which could be due to multiple factors.

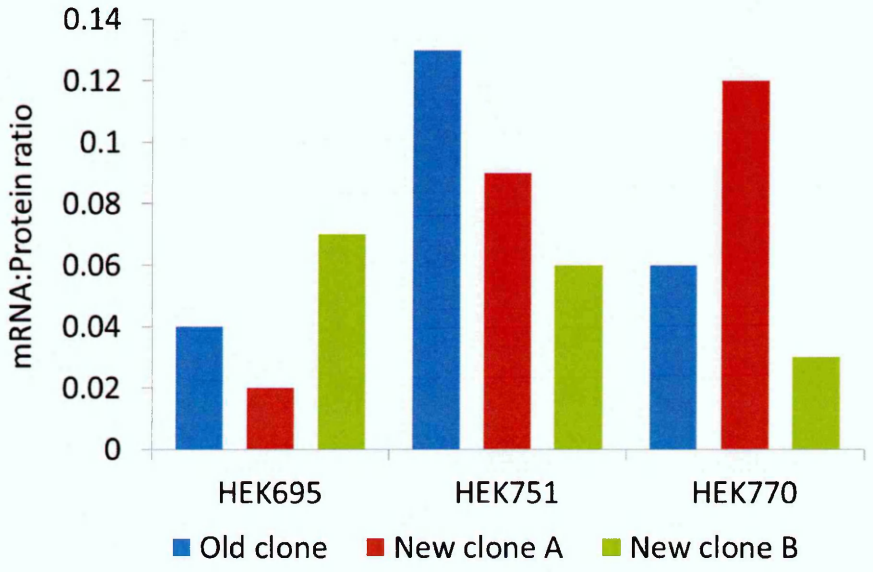

Figure 7.3.3 The third possible outcome of the further experiment with new clones. The outcome from all clones; both previous and new clones do not show any similarity between each clone of each isoform.

7.4 To investigate the hypothesis that APP secretion of one of these APP isoforms (APP695, APP751 and APP770) is more likely to be affected by stress.

One of several ways that cells respond to stress is to undergo the apoptotic pathway (Fulda et al. 2010). Also, it has been reported that apoptosis plays an essential role in neurodegenerative mechanism in AD (Alberghina and Colangelo 2006) as the Aβ was found to have induced apoptosis in both cell culture and animal models. However the soluble APP produced from APP processing was found to be advantageous to the

neuron (Araki and Wurtman 1998). Therefore, it was hypothesised that APP secretion of one of these APP isoforms; APP695, APP751 and APP770 would be more affected under stress-induced conditions; alteration of FBS concentration and energy deprivation using 2-deoxy-D-glucose (2DG). Also, one of these APP isoforms could be the source of Aβ in AD.

The basic survival strategy of cells is based on the regulation of extracellular nutrients and intracellular metabolites (Yuan, Xiong and Guan 2013). Under normal physiological conditions, the mammalian target of rapamycin complex 1 (mTORC1) combines the signals from nutrients (both growth factors and amino acids) and energy sufficiency in order to regulate cell growth (Roux et al. 2007) by activating anabolic processes which convert nutrients and energy into macromolecules such as protein and lipid (Dibble and Manning 2013). mTORC1 is a conserved serine/threonine kinase which is known as a nutrient-energy responsive regulator (Mulukutla et al. 2010; Roux et al. 2007). Also, mTORC1 plays a significant role in autophagy which is an essential housekeeping process in order to maintain the cellular functions and structure by balancing between anabolic and catabolic processes (Glick, Barth and Macleod 2010; Kim et al. 2011). Autophagy is activated by starvation which put cells under survival mode until the nutrients are available again (Glick, Barth and Macleod 2010).

It has been reported that Atk1 (also known as protein kinase B α, PKBα) is responsive to growth factors and amino acids while AMP-kinase (AMPK) is responsive to cellular energy. However, these two kinases have the same downstream target; mTORC1. The Figure 7.4.1 shows the relationship of Atk1, AMPK and mTORC1.

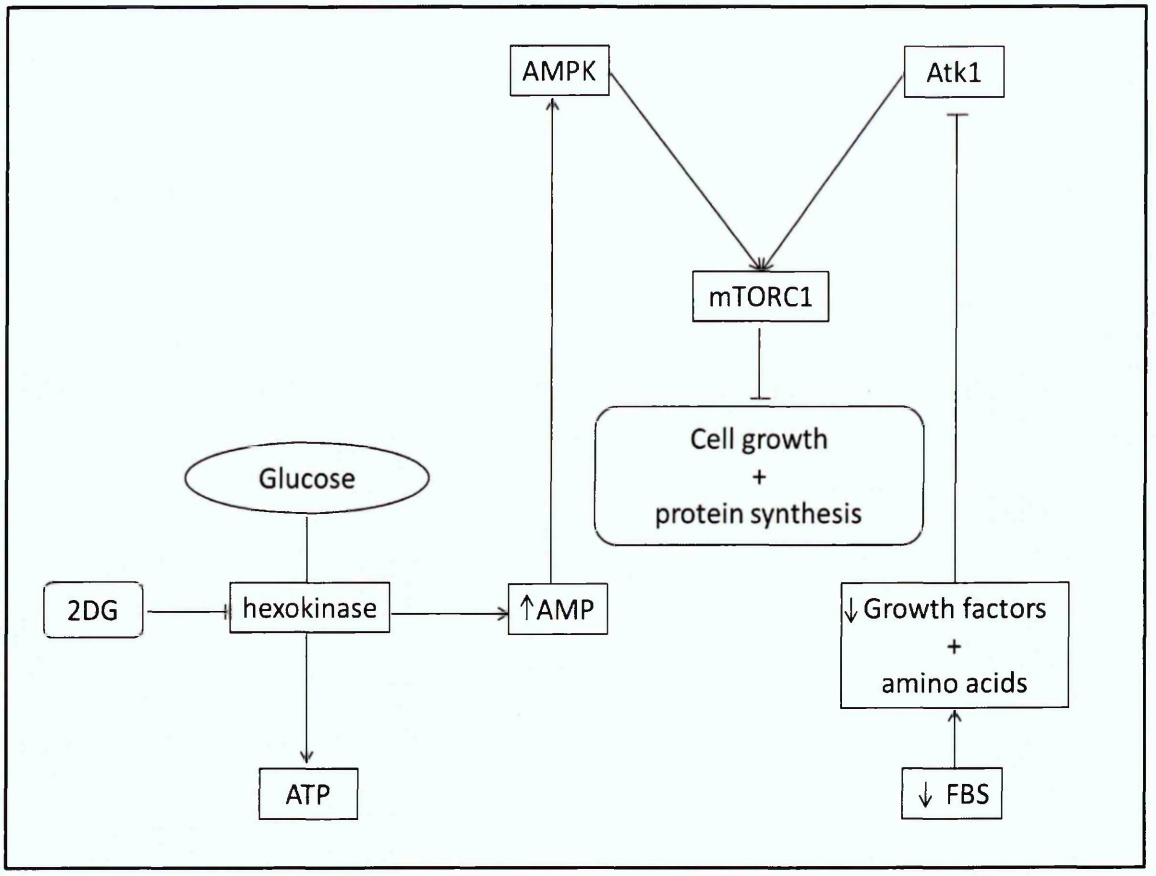

Figure 7.4.1 The possible mechanism of effects of FBS alteration and 2DG. By reducing the concentration of FBS in culture medium the available growth factors and amino acids are effectively reduced which possibly inactivated Atk1 thereby activating mTORC1 and inhibiting cell growth and protein synthesis. 2DG inhibits glucose metabolism by inhibiting hexokinase leading to ATP reduction and increased AMP. The increased AMP activates AMPK thereby activating mTORC1 and inhibiting cell growth and protein synthesis.

Atk1 play role as a regulator of apoptosis, cell growth and proliferation, cell differentiation and cell metabolism (Mulukutla et al. 2010; Nicholson and Anderson 2002) and can be activated by activation of phosphoinositide 3-kinase (PI3K) initiating synthesis of phosphatidylinositol (3, 4, 5)-triphosphate (PIP3) which facilitates the localization, phosphorylation and activation of Atk1. One of several ways which PI3K can be activated is autophosphorylation of kinase by ligands including growth factors and amino acids (Fayard et al. 2005; Filippa et al. 1999; Nicholson and Anderson 2002; Scheid and Woodgett 2003). As shown in Figure 7.4.1 once the Atk1 is activated, it subsequently initiates protein translation/synthesis and cell growth via the mammalian

target of rapamycin complex 1 (mTORC1). In order to mimic nutrient starvation the concentration of FBS containing both growth factors and amino acids was altered. It was hypothesised that the cell number, APP secretion as a consequence of APP production and the APP mRNA level would decrease with the decreased concentration of FBS due to Atk1 inactivation thereby inhibiting mTORC1. The data in this project have shown that there is no change in cell number, APP secretion and APP mRNA level which suggests that the Atk1 might not be inactivated, possibly due to the short incubation period (Deorosan and Nauman 2011; Fiorelli, Kirouac and Padmanabhan 2013). Also, the different isoforms of APP and the different concentrations of FBS in culture medium did not affect the cell number, APP secretion and the APP mRNA level. This mean the FBS could be used in further experiments where required without causing statistical variation on the APP related factors.

AMPK plays role as a metabolic regulator which once activated would inactivate mTORC1 and thereby inhibit cell growth (Laderoute et al. 2006; Li et al. 2014; Mulukutla et al. 2010). As shown in Figure 7.4.1, the AMPK can be activated when there is an increase of AMP: ATP ratio during cellular phosphate depletion (Laderoute et al. 2006; Mulukutla et al. 2010). The glucose antagonist, 2-deoxy-D-glucose (2DG) was used to initiate the glucose impairment *in vitro* by mimicking glucose shortage. The 2DG inhibits glycolysis at the same equimolar concentration as glucose and the inhibition can be reversed by further addition of glucose (Barban and Schulze 1961). Since 2DG shares the similar structure to glucose, it could be transported into the cell by glucose transporters and it can be phosphorylated by hexokinase at the first step of glycolysis. However, it cannot be processed further due to the substitution of the hydrogen at the second carbon atom. As a result, phosphorylated 2DG is trapped within the cell leading to intracellular phosphate depletion and an increase of the AMP: ATP ratio (Aft, Zhang and Gius 2002). Therefore it was hypothesised that the cell number, APP secretion as a consequence of APP production, and the APP mRNA level would decrease as the concentration of 2DG increased due to AMPK activation thereby inhibiting mTORC1. The data in this project have shown that there is a decrease in cell number and there is an increase in both APP secretion and mRNA level which suggest that the AMPK is activated but might be offset by a protective property of sAPPα

(Corrigan et al. 2011; Corrigan et al. 2014; Milosch et al. 2014; Smith-Swintosky et al. 1994; Steinbach et al. 1998; Young-Pearse et al. 2008).

7.5 Future work

Although the morphological changes of the cells cultured in both stress-induced conditions: FBS alteration and 2DG, resemble apoptosis, further experiments are still required to confirm this observation. These experiments include measuring plasma membrane alteration, mitochondrial dysfunction and AMP: ATP ratio, chromatin condensation and DNA fragmentation.

The cellular models of APP695, APP751 and APP770 could be used in further experiments to determine whether a cellular "brake" system exists and how it is modulated in relation to AD pathogenesis. The proposed experiments would enable the first step towards the clarification process of the cellular "brake" system through measurement of heat shock protein (HSP) since HSP is not only associated with aging and stress conditions but also the main mitochondrial stress proteins (e.g. HSP10 or HSP60). Also these cellular models should be treated with other stress-inducing substances and conditions such as reactive oxygen species, transition metals and hypoxic condition. This could be carried out in serum free media to avoid the contamination of known and unknown substances including transition metals. Also, it was shown in this project that the presence or absence of FBS in culture medium did not affect the APP production and secretion levels. These treatments along with the complete profile of APP metabolites and HSP level would provide further understanding regarding the pathogenesis of AD which might enable the therapeutic discovery or prevention for AD.

Since an impaired glucose metabolism has been shown as an important feature of AD these cellular models could be used in testing herbal extracts such as charatin and allicin which have indications for lowering blood glucose and enhancing the sensitivity of beta cells as well as maintaining insulin production leading to stable glucose metabolism. One leading hypothesis might be the stable level of Aβ peptide production as regulated by controlled glucose metabolism as a direct consequence of

the use of these herbal extracts. The longer term ambition for future work would be to compare clinical monitoring for blood and brain glucose metabolism with APP metabolites as well as cognitive function when using these herbal extracts as directed by completion of the cell model studies.

7.6 Final conclusion

The data described in this project has shown no significant effects of short term stress, in term of nutrient deprivation, on the APP mRNA level and secretion when compared to the three main isoforms of APP: APP695, APP751 and APP770. This suggests that mTORC1 inhibition via Atk1 might require other effectors and take longer than 24 hours under starvation conditions. A significant finding, however, is that a difference between APP751 on one hand and APP695 and APP770 on the others, with the former consistently showing a lower efficiency of conversion of mRNA to protein under normal culture condition. This may result from APP751 being subjected to a cellular "braking" system. Pathological changes in AD occur over numbers of year, so a small change in the "braking" system give the relatively high levels of APP751 mRNA which could result in the considerable changes in APP secretion as shown when culturing in 2DG containing medium. Not only does this confirm the importance of glucose as a source of energy but also suggest the possible relationship between glucose metabolism and pathogenesis of AD. Ultimately, this could also be the source of Aβ peptide and hence the pathogenesis of AD.

Bibliography

AFT, R. L., ZHANG, F. W. and GIUS, D. (2002). Evaluation of 2-deoxy-D-glucose as a chemotherapeutic agent: mechanism of cell death. *British Journal of Cancer*, **87** (7), 805-812.

ALBERGHINA, L. and COLANGELO, A. M. (2006). The modular systems biology approach to investigate the control of apoptosis in Alzheimer's disease neurodegeneration. *BCM Neuroscience*, **7** (Suppl1), S2.

ALLINSON, T. M. J., et al. (2003). ADAMs family members as amyloid precursor protein alpha-secretases. *Journal of Neuroscience Research*, **74**, 342-352.

ALZHEIMER'S DISEASE INTERNATIONAL (2014). *Dementia statistics*. [online]. Last accessed 15 June. http://www.alz.co.uk/research/statistics

ALZHEIMER'S SOCIETY (2014). *Drug treatments for Alzheimer's disease*. [online]. http://alzheimers.org.uk/site/scripts/documents_info.php?documentID=147

ALZHEIMER'S SOCIETY (2015). *Statistic*. [online]. Last accessed 15 June. http://www.alzheimers.org.uk/statistics

ANDERSON, J. P., et al. (1991). Exact cleavage site of Alzheimer amyloid precursor in neuronal PC-12 cells. *Neuroscience Letters*, **128** (1), 126-128.

ANDERSON, O. M., et al. (2005). Neuronal sorting protein-related receptor sorLA/LR11 regulates processing of the amyloid precursor protein. *Proceedings of the National Academy of Sciences of the United States of America*, **102** (38), 13461-13466.

AN, Y., et al. (2005). A rapid and efficient method for multiple-site mutagenesis with a modified overlap extension PCR. *Applied Genetics and Molecular Biotechnology*, **68** (6), 774-778.

ANNAERT, W. and DE STROOPER, B. (2002). A CELL BIOLOGICAL PERSPECTIVE ON ALZHEIMER'S DISEASE. *Annual Review of Cell and Developmental Biology*, **18**, 25-51.

APPLIED BIOSYSTEMS (2014). *Applied Biosystems*. [online]. http://www.lifetechnologies.com/uk/en/home/brands/applied-biosystems.html

ARAKI, W. and WURTMAN, R. J. (1998). Increased expression of amyloid precursor protein and amyloid precursor-like protein 2 during trophic factor withdrawal-induced death of neuronal PC12. *Molecular Brain Research*, **56** (1-2), 169-177.

ARVANITAKIS, Z., et al. (2011). Cerebral Amyloid Angiopathy Pathology and Cognitive Domains in Older Persons. *Annals of Neurology*, **69** (2), 320-327.

ATTEMS, J., et al. (2011). Review: Sporadic cerebral amyloid angiopathy. *Neuropathology and Applied Neurobiology*, **37** (1), 75-93.

AXELSEN, P. H., KOMATSU, H. and MURRAY, I. V. J. (2011). Oxidative Stress and Cell Membranes in the Pathogenesis of Alzheimer's Disease. *Physiology*, **26** (1), 54-69.

BARBAN, S. and SCHULZE, H. O. (1961). The effects of 2-Deoxyglucose on the Growth and Metabolism of Cultured Human Cells. *The Journal of Biological Chemistry*, **236** (7), 1887-1890.

BASUN, H., et al. (2008). Clinical and neuropathological features of the Arctic APP mutation causing early onset Alzheimer's disease. *Archives of Neurobiology*, **65** (4), 499-505.

BAYER, T. A. and WIRTHS, O. (2010). Intracellular accumulation of amyloid-beta – a predictor for synaptic dysfunction and neuron loss in Alzheimer's disease. *Frontiers in Aging Neuroscience*, **2** (8),.

BEECH, J. S., et al. (2007). The MHP36 line of murine neural stem cells expresses functional CXCR1 chemokine receptors that initiate chemotaxis in vitro. *Journal of Neuroimmunology*, **184** (1), 198-208.

BELYAEV, N. D., et al. (2010). The Transcriptionally Active Amyloid Precursor Protein (APP) Intracellular Domain Is Preferentially Produced from the 695 Isoform of APP in a β-Secretase-dependent Pathway. *The Journal of Biological Chemistry*, **285** (53), 41443-41454.

BHATIA, N. and HALL, G. F. (2013). Untangling the role of tau in Alzheimer's disease: A unifying hypothesis. *Translational Neuroscience*, **4** (2), 115-133.

BIFFI, A. and GREENBERG, S. M. (2011). Cerebral Amyloid Angiopathy: A Systematic Review. *Journal of Clinical Neurology*, **7** (1), 1-9.

BLOCHLINGER, K. and DIGGELMANN, H. (1984). Hygromycin B Phosphotransferase as a Selectable Marker for DNA Transfer Experiments with Higher Eucaryotic Cells. *MOLECULAR AND CELLULAR BIOLOGY*, **4** (12), 2929-2931.

BOCHKOV, Y. A. and PALMENBERG, A. C. (2006). Translational efficiency of EMCV IRES in bicistronic vectors is dependent upon IRES sequence and gene location. *Biotechniques*, **41** (3), 283-4, 286, 288.

BORDJI, K., et al. (2010). Activation of extrasynaptic, but not synaptic, NMDA receptors modifies amyloid precursor protein expression pattern and increases amyloid-ß production. *The Journal of Neuroscience*, **30** (47), 15927-15942.

BOROVINSKAYA, M. A., et al. (2008). Structural basis for hygromycin B inhibition of protein biosynthesis. *RNA*, **14** (8), 1590-1599.

BOTTONE, M. G., et al. (2013). Morphological Features of Organelles during Apoptosis: An Overview. *Cells*, **2** (2), 294-305.

BROUWERS, N., SLEEGERS, K. and VAN BROECKHOVEN, C. (2008). Molecular genetics of Alzheimer's disease: an update. *Annals of Medicine*, **40** (8), 562-583.

BRUGG, B., et al. (1995). Inflammatory processes induce beta-amyloid precursor protein changes in mouse brain. *Proceedings of the National Academy of Sciences of the United States of America*, **92** (7), 3032-3035.

BRUNDEN, K. R., et al. (2010). The characterization of microtuble-stabilizing drugs as possible therapeutic agents for Alzheimer's disease and related tauopathies. *Pharmacological Research*, **63** (4), 341-351.

BRUNNER, D., et al. (2010). Serum-free Cell Culture: The Serum-free Media Interactive Online Database. *ALTEX*, **27** (1), 53-62.

BRYKSIN, A. V. and MATSUMURA, I. (2010). Overlap extension PCR cloning: a simple and reliable way to create recombinant plasmids. *Biotechniques*, **48** (6), 463-465.

BUTTERFIELD, D. A. and POCERNICH, C. B. (2003). The Glutamatergic System and Alzheimer's Disease. *CNS Drugs*, **17** (9), 641-652.

CAO, X. and SUDHOF, T. C. (2001). A Transcriptively Active Complex of APP with Fe65 and Histone Acetyltransferase Tip60. *Science*, **293** (5527), 115-120.

CAPPAI, R. (2014). Making sense of the amyloid precursor protein: its tail tells an interesting tale. *Journal of Neurochemistry*, **130** (3), 325-327.

CARO-MALDONADO, A., et al. (2010). Glucose deprivation induces an atypical form of apoptosis mediated by caspase-8 in Bax-, Bak-deficient cells. *Cell Death and Differentiation*, **17** (8), 1335-1344.

CASTELLANI, R. J., ROLSTON, R. K. and SMITH, M. A. (2010). Alzheimer Disease. *Disease-a-Month*, **56** (9), 484-546.

CAUSEVIC, M., et al. (2011). β-Amyloid precursor protein and tau protein levels are different;y regulated in human cerebellum compared to brain regions vunerable to Alzheimer's type neurodegeneration. *Neuroscience Letter*, **485** (3), 162-166.

CHANG, H., et al. (2011). High glucose alters apoptosis and proliferation in HEK293 cells by inhibition of cloned BK Ca channel. *Journal of Cellular Physiology*, **226** (6), 1660-1675.

CHARLES, I., et al. (2005). Serum Deprivation Induces Apoptotic Cell Death of Transformed Rat Retinal Ganglion Cells via Mitochondrial Signaling Pathway. *Investigative Opthalmology & Visual Science*, **46** (4), 1330-1338.

CHASSEIGNEAUX, S., et al. (2011). Secreted Amyloid Precursor Protein β and Secreted Amyloid Precursor Protein α Induce Axon Outgrowth In Vitro through Egr1 Signaling Pathway. *PLoS One*, **6** (1), e16301.

CHECLER, F. and VINCENT, B. (2002). Alzheimer's and prion diseases: distinct pathologies, common proteolytic denominators. *Trends in Neuroscience*, **25** (12), 616-620.

CHEN, Z. and ZHONG, C. (2013). Decoding Alzheimer's disease from perturbed cerebral glucose metabolism: implications for diagnostic and therapeutic strategies. *Progress in Neurobiology*, **108**, 21-34.

CHING, J. K., et al. (2010). A role for AMPK in increased insulin action after serum starvation. *American Journal of Physiology*, **299** (5), C1171-C1179.

CHOW, V. W., et al. (2010). An Overview of APP Processing Enzymes and Products. *NeuroMolecular Medicine*, **12** (1), 1-12.

CHUA, L-M, LIM, M-L and WONG, B-S (2013). The Kunitz-protease inhibitor domain in amyloid precursor protein reduces cellular mitochondrial enzyme expression and function. *Biochemical and Biophysical Research Communications*, **437**, 642-647.

COLORADO'S DEMENTIA NEWS AND RESOURCE CENTER (2014). *The plaques and tangles of Alzheimer's.* [online]. http://coloradodementia.org/tag/neurofibrillary-tangles/

CONTESTABILE, A. (2011). The history of the cholinergic hypothesis. *Behavioural Brain Research*, **221** (2), 334-340.

CORRIGAN, F., et al. (2010). The neuroprotective domains of the amyloid precursor protein, in traumatic brain injury, are located in the two growth factor domains. *Brain Research*, **1378**, 137-143.

CORRIGAN, F., et al. (2011). The neuroprotective domains of the amyloid precursor protein, in traumatic brain injury, are located in the two growth factor domains. *Brain Research*, **1378**, 137-143.

CORRIGAN, F., et al. (2014). The neuroprotective activity of the amyloid precursor protein against traumatic brain injury is mediated via the heparin binding site in residues 96-110. *Journal of Neurochemistry*, **128** (1), 196-204.

CRAIG, L. A., HONG, N. S. and MCDONALD, R. J. (2011). Revisiting the cholinergic hypothesis in the development of Alzheimer's disease. *Neuroscience & Biobehavioural Reviews*, **35** (6), 1397-1409.

CRENTSIL, V. (2004). The pharmacogenomics of Alzheimer's disease. *Ageing Research Review*, **3** (2), 153-169.

CRUTS, M., THEUNS, J. and VAN BROECKHOVEN, C. (2012). Locus-specific mutation databases for neurodegenerative brain diseases. *Human Mutation*, **33** (9), 1340-1344.

DAWKINS, E. and SMALL, D. H. (2014). Insights into the physiological function of the β-amyloid precursor protein: beyond Alzheimer's disease. *Journal of Neurochemistry*, **129** (5), 756-769.

DE LA MONTE, S. M. (2012). Contributions of Brain Insulin Resistance and deficiency in Amyloid-Related Neurodegeneration in Alzheimer's disease. *Drugs*, **72** (1), 49-66.

DE PAULA, V. de J. R., et al. (2009). Neurobiological pathways to Alzheimer's disease: Amyloid-beta, TAU protein or both? *Dementia & Neuropsychologia*, **3** (3), 188-194.

DE SILVA, R., et al. (1997). Cell-specific expression of beta-amyloid precursor protein isoform mRNAs and proteins in neurons and astrocytes. *Molecular Brain Research*, **47** (1-2), 147-156.

DE STROOPER, B. (2007). Loss-of-function presenilin mutations in Alzheimer's disease. Talking Point on the role of presenilin mutations in Alzheimer's disease. *EMBO reports*, **8** (2), 141-146.

DE STROOPER, B., IWATSUBO, T. and WOLFE, M. S. (2012). Presenilins and γ-Secretase: Structure, Function, and Role in Alzheimer Disease. *Cold Spring Harbor Perspectives in Medicine*, **2** (1), 1-19.

DE STROOPER, B., et al. (1995). Production of intracellular amyloid-containing fragments in hippocampal neurons expressing human amyloid precursor protein and protection against amyloidogenesis by subtle aminoacid substitutions in the rodent sequence. *The EMBO Journal*, **14** (20), 4932-4938.

DEMITRIUS, L. A. and DRIVER, J. (2013). Alzheimer's as a metabolic disease. *Biogerontology*, **14** (6), 641-649.

DEOROSAN, B. and NAUMAN, E. A. (2011). The Role of Glucose, Serum and Three-Dimensional Cell Culture on the Metabolism of Bone Marrow-Derived Mesenchymal Stem Cells. *Stem Cells Internation*, 1-12.

DIBBLE, C. C. and MANNING, B. D. (2013). Signal integration by mTORC1 coordinates nutrient input with biosynthetic output. *Nature Cell Biology*, **15** (6), 555-564.

DICKSON, D. W. (2004). Apoptotic mechanism inAlzheimer's neurofibrillary degeneration: cause or effect? *The Journal of Clinical Investigation*, **14** (1), 23-27.

DOMINGUES, S. C. T. S., et al. (2007). Altered Subcellular Distribution of the Alzheimer's Amyloid Precursor Protein Under Stress Conditions. *Annals of the New York Academy of Sciences*, **1096** (1), 184-195.

DWYER, D. S. (2002). *Glucose Metabolism in the Brain*. vol.51. illustrated ed., Academic Press.

EPSTEIN, D., ELIAS-BISHKO, S. and HERSHKO, A. (1975). Requirement for Protein Synthesis in the Regulation of Protein Breakdown in Culture Hepatoma Cells. *Biochemistry*, **14** (23), 5199-5204.

EUSTICE, D. C. and WILHELM, J. M. (1984). Mechanisms of action of aminoglycoside antibiotics in eucaryotic protein synthesis. *Antimicrobial Agents and Chemetherapy*, **26** (1), 53-60.

FAYARD, E., et al. (2005). Protein kinase B/Akt at a glance. *Journal of Cell Science*, **118** (24), 5675-5678.

FERRI, C. P., et al. (2005). Global prevalence of dementia: a Delphi consensus study. *The Lancet*, **366** (9503), 2112-2117.

FILIPPA, N., et al. (1999). Mechanism of Protein Kinase B Activation by Cyclic AMP-Dependent Protein Kinase. *Molecular and Cellular Biology*, **19** (7), 4989-5000.

FIORELLI, T., KIROUAC, L. and PADMANABHAN, J. (2013). Altered Processing of Amyloid Precursor Protein in Cells Undergoing Apoptosis. *PLOS ONE*, **8** (2), 1-12.

FORSTL, H. and KURZ, A. (1999). Clinical features of Alzheimer's disease. *European Archives of Psychiatry and Clinical Neuroscience*, **249** (6), 288-290.

FRANCIS, P. T., et al. (1999). The cholinergic hypothesis of Alzheimer's disease: a review of progress. *Journal of Neurology, Neurosurgery & Psychiatry*, **66** (2), 137-147.

FRASER, P. E., et al. (1992). Fibril formation by primate, rodent, and Dutch-hemorrhagic analog of Alzheimer amyloid beta-protein. *Biochemistry*, **31** (44), 10716-10723.

FULDA, S., et al. (2010). Cellular Stress Responses: Cell Survival and Cell Death. *Internation Journal of Cell Biology*, **2010** (Article ID: 214074), 1-23.

FURST, A. J., et al. (2012). Cognition, glucose metabolism and amyloid burden in Alzheimer's disease. *Neurobiology of Aging*, **33** (2), 215-255.

GASPARINI, L., et al. (1997). Effect of energy shortage and oxidative stress on amyloid precursor protein metabolism in COS cells. *Neuroscience letter*, **231** (2), 113-117.

GELLA, A. and DURANY, N. (2009). Oxidative stress in Alzheimer disease. *Cell Adhesion & Migration*, **3** (1), 88-93.

GHISO, J., et al. (2010). CEREBRAL AMYLOID ANGIOPATHY AND ALZHEIMER'S DISEASE. *Hirosaki Igaku*, **61** (Suppl), S111-S124.

GLENNER, G. G. and WONG, C. W. (1984). Alzheimer's disease and Down's syndrome: Sharing of a unique cerebrovascular amyloid fibril protein. *Biochemical and Biophysical Research Communication*, **122** (3), 1131-1135.

GLICK, D., BARTH, S. and MACLEOD, K. F. (2010). Autophagy: cellular and molecular mechanisms. *The Journal of Pathology*, **221** (1), 3-12.

GOATE, A. and HARDY, J. (2012). Twenty years of Alzheimer's disease-causing mutations. *Journal of Neurochemistry*, **120** (Supplement S1), 3-8.

GOLDIN, A., et al. (2006). Advanced Glycation End Products: Sparking the Development of Diabetic Vascular Injury. *Circulation*, **114** (6), 597-605.

GOODSELL, D. S. (2002). The Molecular Perspective: Restriction Endonucleases. *The Oncologist*, **7** (1), 82-83.

GRAHAM, F. L., et al. (1977). Characteristics of a human cell line transformed by DNA from human adenovirus type 5. *Journal of General Virology*, **36** (1), 59-72.

GREENOUGH, M. A., CAMAKARIS, J. and BUSH, A. I. (2013). Metal dyshomeostasis and oxidative stress in Alzheimer's disease. *Neurochemistry international*, **62** (5), 540-555.

GSTRAUNTHALER, G. (2003). Alternative to the Use of Fetal Bovine Serum: Serum-free Cell Culture. *ALTEX*, **20** (4), 275-281.

GUERREIRO, R. J., GUSTAFSON, D. R. and HARDY, J. (2012). The genetic architecture of Alzheimer's disease: beyond APP, PSENs and APOE. *Neurobiology of Aging*, **33** (3), 437-456.

HAASS, C., et al. (1993). beta-Amyloid peptide and a 3-kDa fragment are derived by distinct cellular mechanisms. *The Journal of Biological Chemistry*, **268** (5), 3021-3024.

HAASS, C., et al. (2012). Trafficking and proteolytic processing of APP. *Cold Spring Harbor Perspectives in Medicine*, **2** (5),.

HAHN, P. and SCANLAN, E. (2010). Gene delivery into mammalian cells: an overview on existing approaches employed in vitro and in vivo. *Topics in Current Chemistry*, **296**, 1-13.

HAMABE, W., FUJITA, R. and UEDA, H. (2005). Insulin Receptor-Protein Kinase C gamma Signaling Mediates Inhibition of Hypoxia-Induced Necrosis of Cortical Neurons. *Journal of Pharmacology and Experiment Therapeutics*, **313** (3), 1027-1034.

HARDY, J. (2009). The amyloid hypothesis for Alzheimer's disease: a critical reapprasial. *Jounal of Neurochemistry*, **110** (4), 1129-1134.

HARDY, J. A. and HIGGINS, G. A. (1992). Alzheimer's Disease: The amyloid Cascade Hypothesis. *Science*, **256** (5054), 184-185.

HARDY, J. and SELKOE, D. J. (2002). The amyloid hypothesis of Alzheimer's disease: progress and problems on the road to therapeutics. *Science*, **297** (5580), 353-356.

HARTL, D. L. and JONES, E. W. (2005). DNA Structure and DNA Manipulation. In: WEAVER, Stephen L, et al. (eds.). *Genetics: Analysis of Genes and Genomes*. 6th ed., London, Jones & Bartlett Learning, 54-56.

HARTMANN, T. (1999). Intracellular biology of Alzheimer's disease amyloid beta peptide. *European archives of psychiatry and clinical neuroscience*, **249** (6), 291-298.

HENNECKE, M., et al. (2001). Composition and arrangement of genes define the strength of IRES-driven translation in bicistronic mRNAs. *Nucleic Acids Research*, **29** (16), 3327-3334.

HIGUCHI, R., KRUMMEL, B. and SAIKI, R. K. (1988). A general method of in vitro preparation and specific mutagenesis of DNA fragments: study of protein and DNA interactions. *Nucleic Acid Research*, **16** (15), 7351-7367.

HO, S. C. L., et al. (2013). Comparison of Internal Ribosome Entry Site (IRES) and Furin-2A (F2A) for Monoclonal Antibody Expression Level and Quality in CHO Cells. *PLoS One*, **8** (5), e63247.

HOYER, S. (2004). Glucose metabolism and insulin receptor signal transduction in Alzheimer disease. *European Journal of Pharmacology*, **490** (1-3), 115-125.

HYND, M. R., SCOTT, H. L. and DODD, P. R. (2004). Glutamate-mediated excitotoxicity and neurodegeneration in Alzheimer's disease. *Neurochemistry international*, **45** (5), 583-595.

IQBAL, K., et al. (2005). Tau pathology in Alzheimer disease and other tauopathies. *Biochimica et Biophysica Acta (BBA) - Molecular Basis of Disease*, **1793** (2-3), 198-210.

IQBAL, K., et al. (2010). Tau in Alzheimer Disease and Related Tauopathies. *Current Alzheimer Research*, **7** (8), 656-664.

JANKOWSKY, J., et al. (2004). Mutant presenilins specifically elevate the levels of the 42 residue β-amyloid peptide in vivo: evidence for augmentation of a 42-specific γ secretase. *Human Molecular Genetics*, **13** (2), 159-170.

JAYAPAL, K. P., et al. (2007). Recombinant Protein Therapeutics from CHO Cells -- 20 Years and Counting. *Chemical Engineering Progress*, 33-52.

JELLUMA, N., et al. (2006). Glucose withdrawal induces oxidative stress followed by apoptosis in glioblastoma cells but not in normal human astrocytes. *Molecular Cancer Research*, **4** (5), 319-330.

JOHNSON, J. W. and KOTERMANSKI, S. E. (2006). Mechanism of action of memantine. *Current Opinion in Pharmacology*, **6** (1), 61-67.

JOMOVA, K., BAROS, S. and VALKO, M. (2012). Redox active metal-induced oxidative stress in biological system. *Transition Metal Chemistry*, **37** (2), 127-134.

JOMOVA, K. and VALKO, M. (2011). Advances in metal-induced oxidative stress and human disease. *Toxicology*, **283** (2-3), 65-87.

KAPLAN, O., et al. (1990). Effects of 2-Deoxyglucose on Drug-sensitive and Drug-resistant Human Breast Cencer Cells: Toxicity and Magnetic Resonance Spectroscopy Studies of Metabolism. *Cencer Reasearch*, **50** (3), 544-551.

KAYED, R., et al. (2003). Common Structure of Soluble Amyloid Oligomers Implies Common Mechanism of Pathogenesis. *Science*, **300** (5618), 486-489.

KEENAN, J., LIANG, Y. and CLYNES, M. (2004). Two-deoxyglucose as an anti-metabolite in human carcinoma cell line RPMI-2650 and drug-resistant variants. *Anticancer Research*, **24** (2A), 433-440.

KHALIFA, N. B., et al. (2012). Structural features of KPI domain control APP dimerization, trafficking, and processing. *The Journal of the Federation of American Societies for Experimental Biology*, **26** (2), 855-867.

KIM, J., et al. (2011). AMPK and mTOR regulate autophagy through direct phosphorylation of Ulk1. *Nature Cell Biology*, **13**, 132-141.

KING, A. and GOTTLIEB, E. (2009). Glucose metabolism and programmed cell death: an evolutionary and mechanistic perspective. *Current Opinion in Cell Biology*, **21** (6), 885-893.

KOLAROVA, M., et al. (2012). Structure and Pathology of Tau Protein in Alzheimer Disease. *International Journal of Alzheimer's Disease*, **2012** (1), 1-13.

KOPAN, R. and ILAGAN, M. X. G. (2004). γ-Secretase: proteasome of the membrane? *Nature Reviews Molecular Cell Biology*, **5** (6), 499-504.

KORBIE, D. J. and MATTICK, J. S. (2008). Touchdown PCR for increased specificity and sensitivity in PCR amplification. *NATURE PROTOCOL*, **3** (9), 1452-1456.

KOZAK, M. (2005). A second look at cellular mRNA sequences said to function as internal ribosome entry sites. *Nucleic Acids Research*, **33** (20), 6593-6602.

KUMAR-SINGH, S., et al. (2002). In Vitro Studies of Flemish, Dutch, and Wild-Type β-Amyloid Provide Evidence for Two-Staged Neurotoxicity. *Neurobiology of Disease*, **11** (2), 330-340.

LADEROUTE, K. R., et al. (2006). 5'-AMP-Activated Protein Kinase (AMPK) Is Induced by Low-Oxygen and Glucose Deprivation Conditions Found in Solid-Tumor Microenvironments. *Molecular and Cellular Biology*, **26** (14), 5336-5347.

LADEVAIA, V., et al. (2012). Roles of the mammalian target of rapamycin, mTOR, in controlling ribosome biogenesis and protein synthesis. *Biochemical Society Transactions*, **40** (1), 168-172.

LEBLANC, A. (1995). Increased production of 4 kDa amyloid beta peptide in serum deprived human primary neuron cultures: possible involvement of apoptosis. *The Journal of Neuroscience*, **15** (12), 7837-7846.

LEE, J., et al. (2008). Adaptor protein sorting nexin 17 regulates amyloid precursor protein trafficking and processing in the early endosomes. *The Journal of Biological Chemistry*, **283** (17), 11501-11508.

LEVINE, E. M., et al. (1965). CONTACT INHIBITION, MACROMOLECULAR SYNTHESIS, AND POLYRIBOSOMES IN CULTURED HUMAN DIPLOID FIBROBLASTS. *Proceeding of the National Academy of Sciences of the United States of America*, **53** (2), 350-356.

LEVIN, V. A., et al. (2010). Different Changes in Protein and Phosphoprotein Levels result from Seum Starvation of High-Grade Glioma and Adenocarcinoma Cell Lines. *Journal of Proteome Research*, **9** (1), 179-191.

LI, X. and GREENWALD, I. (1998). Additional evidence for an eight-transmembrane-domain topology for Caenorhabditis elegans and human presenilins. *Proceedings of the National Academy of Sciences of the United States of America*, **95** (12), 7109-7114.

LI, H., et al. (2014). AMPK activation prevents excess nutrient-induced hepatic lipid accumulation by inhibiting mTORC1 signaling and endoplasmic reticulum stress

response. *Biochimica et Biophysica Acta (BBA) - Molecular Basis of Disease*, **1842** (9), 1844-1854.

LINDEBERG, J. and EBENDAL, T. (1999). Use of an internal ribosom entry site for bicistronic expression of Cre recombinase or rtTA transactivator. *Nucleic Acids Research*, **27** (6), 1552-1554.

LING, Y., MORGAN, K. and KALSHEKER, N. (2003). Amyloid precursor protein (APP) and the biology of proteolytic processing: relevance to Alzheimer's disease. *The International Journal of Biochemistry & Cell Biology*, **35**, 1505-1535.

LIU, F., et al. (2003). Regulation of amyloid precursor protein expression and secretion via activation of ERK1/2 by hepatocyte growth factor in HEK293 cells transfected with APP751. *Experimental Cell Research*, **287** (2), 387-396.

LI, D. and WANG, M. (2012). Construction of a bicistronic vector for the co-expression of two genes in Caenorhabditis elegans using a newly identified IRES. *Biotechniques*, **53** (3), 173-176.

LUKIW, W. J. (2012). Amyloid beta (Abeta) peptide modulators and other current treatment stratgies for Alzheimer's disease (AD). *Expert opinion on Emerging Drugs*, **17** (1), 43-60.

MACCIONI, R. B., et al. (2010). The Revitalized Tau Hypothesis on Alzheimer's Disease. *Archives of Medical Research*, **41** (3), 226-231.

MALENKA, R. C. and MANILOW, R. (2011). Alzheimer's disease: Recollection of lost memories. *Nature*, **469** (7382), 44-45.

MATSUI, T., et al. (2007). Expression of APP pathway mRNAs and proteins in Alzheimer's disease. *Brain Research*, **1161**, 116-123.

MATTSON, M. P., GUO, Z. H. and GEIGER, J. D. (1999). Secreted form of amyloid precursor protein enhances basal glucose and glutamate transport and protects against oxidative impairment of glucose and glutamate transport in synaptosomes by a cyclic GMP-mediated mechanism. *Journal of Neurochemistry*, **73** (2), 532-537.

MAYEUX, R. and STERN, Y. (2012). Epidemiology of Alzheimer Disease. *Cold Spring Harbor Perspectives in Medicine*, **2**, 1-18.

MCKHANN, G. M., et al. (2011). The diagnosis of dementia due to Alzheimer's disease: recommendations from the National Institute on Aging-Alzheimer's Association workgroups on diagnostic guidelines for Alzheimer's disease. *Alzheimer's & Dementia*, **7** (3), 1-7.

MERGENTHALER, P., et al. (2013). Sugar for the brain: the role of glucose in physiological and pathological brain function. *Trends in Neurosciences*, **36** (10), 587-597.

MILNE, G. L., MUSIEK, E. S. and MORROW, J. D. (2005). F2-Isoprostanes as markers of oxidative stress in vivo: An overview. *Informa Healthcare*, **10** (1), 10-23.

MILOSCH, N., et al. (2014). Holo-APP and G-protein-mediated signaling are required for sAPPα-induced activation of the Akt survival pathway. *Cell Death and Disease*, **5** (e1391),.

MOHANDAS, E., RAJMOHAN, V. and RAGHUNATH, B. (2009). Neurobiology of Alzheimer's disease. *Indian Journal of Psychiatry*, **51** (1), 55-61.

MOIR, R. D., et al. (1998). Relative Increase in Alzheimer's Disease of Soluble Forms of Cerebral Aβ Amyloid Protein Precursor Containing the Kunitz Protease Inhibitory Domain. *The Journal of Biological Chemistry*, **273** (9), 5013-5019.

MOKREJS, M. and POSPISEK, M. (2015). *IRESite: The database of experimentally verified IRES structures.* [online]. Last updated 24 Sept. http://iresite.org/IRESite_web.php?page=search&search_type=fulltext

MOKREJS, M., et al. (2006). IRESite: the database of experimentally verified IRES structures (www.iresite.org). *Nucleic Acids Research*, **34** (Database), D125-D130.

MOLOFSKY, A. V., et al. (2012). Astrocytes and disease: a neurodevelopmental perspective. *Genes & Development*, **26**, 891-907.

MULUKUTLA, B. C., et al. (2010). Glucose metabolism in mammalian cell culture: new insights for tweaking vintage pathways. *Trends in Biotechnology*, **28** (9), 476-484.

MURRAY, M. E., et al. (2011). Neuropathologically defined subtypes of Alzheimer's disease with distinct clinical characteristics: a retrospective study. *THE LANCET Neurology*, **10** (9), 785-796.

NALIVAEVA, N. and TURNER, A. J. (2013). The amyloid precursor protein: A biochemical enigma in brain development, function and disease. *FEBS Letters*, **587** (13), 2046-2054.

NG, H. K. and CHAN, W. Y. (1993). The pathology of Alzheimer's disease. *Journal of The Hong Kong Medical Association*, **45** (1), 33-39.

NICHOLSON, K. M. and ANDERSON, N. G. (2002). The protein kinase B/Akt signalling pathway in human malignancy. *Cellular Signalling*, **14** (5), 381-395.

NITSCH, R. M., et al. (1992). Release of Alzheimer amyloid precursor derivatives stimulated by activation of muscarinic acetylcholine receptors. *Science*, **258** (5080), 304-307.

NUNOMURA, A., et al. (2009). RNA oxidation in Alzheimer disease and related neurodegenerative disorders. *Acta Neuropathologica*, **118** (1), 151-166.

O'BRIEN, R. J. and WONG, P. C. (2011). Amyloid Precursor Protein Processing and Alzheimer's Disease. *Annual Review of Neuroscience*, **34**, 185-204.

OBULESU, M., VENU, R. and SOMASHEKHAR, R. (2011). Tau Mediated Neurodegeneration: An Insight into Alzheimer's Disease Pathology. *Neurochemical Research*, **36** (8), 1329-1335.

OVERMYER, M., et al. (1999). Reactive microglia in aging and dementia: an immunohistochemical study of postmortem human brain tissue. *Acta Neuropathologica*, **97** (4), 383-392.

PALOP, J. J. and MUCKE, L. (2010). Amyloid-beta-induced neuronal dysfunction in Alzheimer's disease: from synapses toward neural networks. *Nature Neuroscience*, **13** (7), 812-818.

PANEGYRES, P. K., ZAFIRIS-TOUFEXIS, K. and KAKULAS, B. A. (2000). Amyloid precursor protein gene isoforms in Alzheimer's disease and other neurodegenerative disorders. *Journal of the Neurological Sciences*, **173** (2), 81-92.

PARENT, M. J., et al. (2013). Cholinergic Depletion in Alzheimer's Disease Shown by [18F]FEOBV Autoradiography. *International Journal of Molecular Imaging*, **2013** (Article ID 205045), 1-6.

PARSON, C. G., STOFFLER, A. and DANYSZ, W. (2007). Memantine: a NMDA receptor antagonist that improves memory by restoration of homeostasis in the glutamatergic system - too little activation is bad, too much is even worse. *Neuropharmacology*, **53** (6), 699-723.

PERL, D. P. (2010). Neuropathology of Alzheimer's Disease. *Mount Sinai Journal of Medicine: A Journal of Translational and Personalized Medicine*, **77** (1), 32-42.

PERRY, H. V., CUNNINGHAM, C. and HOLMES, C. (2007). Systemic infections and inflammation affect chronic neurodegeneration. *Nature Review Immunology*, **7** (2), 161-167.

PESCHON, J. J., et al. (1998). An Essential Role for Ectodomain Shedding in Mammalian Development. *Science*, **282** (5392), 1281-1284.

PFAFFL, M. W. (2001). A new mathematical model for relative quantification in real-time RT–PCR. *Nucleic Acids Research*, **29** (9), 2002-2007.

PFAFFL, M. W., et al. (2004). Determination of stable housekeeping genes, differentially regulated target genes ad sample integrity: BestKeeper-Exel_based tool using pair-wise correlations. *Biotechinology Letters*, **26**, 509-515.

PIERANDREI-AMALDI, P., et al. (1999). Understanding the Translation Regulatory Mechanisms to Improve the Efficiency and the Specificity of Protein Production by the Cell Factory. *Cell Engineering*, **1**, 1-37.

PIMPLIKAR, S. W. (2008). Reassessing the Amyloid Cascade Hypothesis of Alzheimer's Disease. *The International Journal of Biochemistry & Cell Biology*, **41** (6), 1261-1268.

PIRKMAJER, S. and CHIBALIN, A. V. (2011). Serum starvation: caveat emptor. *American Journal of Physiology - Cell Physiology*, **301** (2), C272-C279.

PORTELIUS, E., et al. (2008). Targeted Proteomics in Alzheimer's Disease: Focus on Amyloid-Beta. *Expert Review of Proteomics*, **5** (2), 225-237.

POSTINA, R., et al. (2004). A disintegrin-metalloproteinase prevents amyloid plaque formation and hippocampal defects in an Alzheimer disease mouse model. *The Journal of Clinical Investigation*, **113** (10), 1456-1464.

PRATICO, D. (2008). Evidence of Oxidative Stress in Alzheimer's Disease Brain and Antioxidant Therapy. *Annals of the New York Academy of Sciences: Mitochondria and Oxidative Stress in Neurodegenerative Disorders*, **1147**, 70-78.

PREECE, P., et al. (2004). Amyloid precursor protein mRNA levels in Alzheimer's disease brain. *Molecular Brain Research*, **122** (1), 1-9.

PRINCE, M., PRINA, M. and GUERCHET, M. (2013). *World Alzheimer Report 2013: Journey of Caring*. Annual report, London, Alzheimer's Disease International (ADI).

PULIAFITO, A., et al. (2010). Collective and single cell behavior in epithelial contact inhibition. *Proceedings of the National Academy of Sciences of the United States of America* , **109** (3), 739-744.

QIAO QIU, W., et al. (1995). Cell-surface beta-amyloid precursor protein stimulates neurite outgrowth of hippocampal neurons in an isoform-dependent manner. *The Journal of Neuroscience*, **15** (3), 2157-2167.

RALSER, M., et al. (2008). A catabolic block does not sufficiently explain how 2-deoxy-d-glucose inhibits cell growth. *Proceedings of the National Academy of Sciences of the United States of America*, **105** (46), 17807-17811.

RESINK, A. A. M., et al. (2003). Pathogenesis of cerebral amyloid angiopathy. *Brain Research Review*, **43** (2), 207-223.

RICHTER, J. D. and SONENBERG, N. (2005). Regulation of cap-dependent translation by eIF4E inhibitory proteins. *Nature*, **433** (7025), 477-480.

RING, S., et al. (2007). The secreted beta-amyloid precursor protein ectodomain APPs alpha is sufficient to rescue the anatomical, behavioral, and electrophysiological abnormalities of APP-deficient mice. *Neurobiology of Disease*, **27** (29), 7817-7826.

ROBERT, B. R., et al. (2012). The role of metallobiology and amyloid-β peptides in Alzheimer's disease. *Journal of neurochemistry*, **120** (Suppl), 149-166.

ROUX, P. P., et al. (2007). RAS/ERK signaling promotes site-specific ribosomal protein S6 phosphorylation via RSK and stimulates cap-dependent translation. *The Journal of biological chemistry*, **282** (19), 14056-14064.

ROUX, P. P., et al. (2007). RAS/ERK Signaling Promotes Site-specific Ribosomal Protein S6 Phosphorylation via RSK and Stimulates Cap-dependent Translation. *The Journal of bioloigical chemistry*, **282** (19), 14056-14064.

RUBIO-PEREZ, J. M. and MORILLAS-RUIZ, J. M. (2012). A Review: Inflammatory Process in Alzheimer's Disease, Role of Cytokines. *The Scientific World Journal*, **2012**, 1-15.

SACHS, A. B. (2000). Cell Cycle–Dependent Translation Initiation: IRES Elements Prevail. *Cell*, **101** (3), 243-245.

SALMINEN, A., et al. (2009). ER stress in Alzheimer's disease: a novel neuronal trigger for inflammation and Alzheimer's pathology. *Journal of Neuroinflammation*, **6** (41),.

SALOMONE, S., et al. (2011). New pharmacological strategies for treatment of Alzheimer's disease: focus on disease modifying drugs. *British Journal of Clinical Pharmacology*, **73** (4), 504-517.

SAMBROOK, J. and RUSSELL, D. W. (2001). Blunt-end Cloning of PCR Product. In: *Molecular Cloning: A Laboratory Manual, Volume 1*. third ed., New York, CSHL Press, 8.32-8.34.

SCHEID, M. P. and WOODGETT, J. R. (2003). Unravelling the activation mechanisms of protein kinase B/Akt. *FEBS Letters*, **546** (1), 108-112.

SCHELLENBERG, G. D. and MONTINE, T. J. (2012). The Genetics and Neuropathology of Alzheimer's Disease. *Acta Neuropathologica*, **124** (3), 305-323.

SCHLONDORFF, J., BECHERER, D. J. and BLOBEL, C. P. (2000). Intracellular maturation and localization of the tumour necrosis factor α convertase (TACE). *The Biochemical Journal*, **347** (1), 131-138.

SCHOCHETMAN, G., OU, C-Y and JONES, W. K. (1988). Polymerase Chain Reaction. *The Journal of Infectious Diseases*, **158** (6), 1154-1157.

SEALS, D. F. and COURTNEIDGE, S. A. (2003). The ADAMs family of metalloproteinases: multidomain proteins with multiple functions. *Genes and Developments*, **17**, 7-30.

SHIKAMA, Y., et al. (2010). Transcripts expressed using a biscistronic vector pIREShyg2 are sensitized to nonsense-mediated mRNA decay. *BMC Molecular Biology*, **11** (42), 1-9.

SHIMOHAMA, S. (2000). Apoptosis in Alzheimer's disease-an update. *Apoptosis*, **5** (1), 9-16.

SHI, J., XIANG, Y. and SIMPKINS, J. W. (1997). Hypoglycemia enhances the expression of mRNA encoding β-amyloid precursor protein in rat primary cortical astroglial cells. *Brain Research*, **772** (1-2), 247-251.

SINGH, R., et al. (2001). Advanced glycation end-products: a review. *Diabetologia*, **44** (2), 129-146.

SINGHRAO, S. K., et al. (1999). Differential expression of individual complement regulators in the brain and choroid plexus. *Laboratory Investigation; a Journal of Technical Methods and Pathology*, **79** (10), 1247-1259.

SISODIA, S. S. (1992). Beta-amyloid precursor protein cleavage by a membrane-bound protease. *Proceeding of the National Academy of Sciences of the United States of America*, **89** (13), 6075-6079.

SISODIA, S. S., et al. (1990). Evidence that beta-amyloid protein in Alzheimer's disease is not derived by normal processing. *Science*, **248** (4954), 492-495.

SLOMNICKI, L. P. and LESNIAK, W. (2008). A putative role of the Amyloid Precursor Protein Intracellular Domain (AICD) in transcription. *Acta Neurobiologiae Experimentalis*, **68** (2), 219-228.

SMALL, D. H. and CAPPAI, R. (2006). Alois Alzheimer and Alzheimer's disease: a centennial perspective. *Journal of Neurochemistry*, **99** (3), 708-710.

SMALL, D. H., KLAVER, D. W. and FOA, L. (2010). Presenilins and the γ-secretase: still a complex problem. *Molecular Brain*, **3** (7), 1-6.

SMITH-SWINTOSKY, V. L., et al. (1994). Secreted Forms of β-Amyloid Precursor Protein Protect Against Ischemic Brain Injury. *Journal of Neurochemistry*, **63** (2), 781-784.

SOLANO, D. C., et al. (2000). Insulin regulates soluble amyloid precursor protein release via phosphatidyl inositol 3 kinase-dependent pathway. *The Federation of American Societies for Experimental Biology*, **14** (7), 1015-1022.

SRIKANTH, V., et al. (2011). Advanced glycation enproducts and their receptor RAGE in Alzheimer's disease. *Neurobiology of Aging*, **32** (5), 763-777.

STANLEY, P. (1988). Chinese Hamster Ovary Cell Mutants with Multiple Glycosylation Defects for Production of Glycoproteins with Minimal Carbohydrate Heterogeneity. *Molecular and Cellular Biology*, **9** (2), 377-383.

STEIGER-BARRAISSOUL, S. and RAMI, A. (2009). Serum deprivation induced autophagy and predominantly an AIF-dependent apoptosis in hippocampal HT22 neurons. *Apoptosis*, **14** (11), 1274-1288.

STEINBACH, J. P., et al. (1998). Hypersensitivity to seizures in bold beta-amyloid precursor protein deficient mice. *Cell Death and Differentiation*, **5** (10), 858-866.

SUDOH, S., KAWAKAMI, H. and NAKAMURA, S. (1996). Serum deprivation alters the expression and the splicing at exons 7, 8 and 15 of the beta-amyloid precursor protein in the C6 glioma cell line. *Molecular Brain Research*, **39** (1-2), 12-22.

SULTANA, R. and BUTTERFIELD, A. D. (2010). Role of oxidative stress in the progression of Alzheimer's disease. *Journal of Alzheimer's disease*, **19** (1), 341-353.

SWOMLEY, A. M., et al. (2013). Abeta, oxidative stress in Alzheimer disease: Evidence based on proteomics studies. *Biochimica et biophysica acta. Molecular basis of disease*, **1832** (9), 1361-1462.

TABNER, B. J., MAYES, J. and ALLSOP, D. (2011). Hypothesis: Soluble Aβ Oligomers in Association with Redox-Active Metal Ions Are the Optimal Generators of Reactive Oxygen Species in Alzheimer's Disease. *International Journal of Alzheimer's Disease*, **2011** (1), 1-6.

TERRA, L. F., et al. (2011). Recombinant human prolactin promotes human beta cell survival via inhibition of extrinsic and intrinsic apoptosis pathways. *Diabetologia*, **54** (6), 1388-1397.

THINAKARAN, G. and KOO, E. H. (2008). Amyloid Precursor Protein Trafficking, Processing, and Function. *The Journal of Biological Chemistry*, **283** (44), 29615-29619.

THOMAS, P. and SMART, T. G. (2005). HEK293 cell line: a vehicle for the expression of recombinant proteins. *Journal of Pharmacological and Toxicological Methods*, **51** (3), 187-200.

TURNER, P. R., et al. (2003). Roles of amyloid precursor protein and its fragments in regulating neural activity, plasticity and memory. *Progress in Neurobiology*, **70**, 1-32.

UEKI, K., et al. (1998). Potential Role of Protein Kinase B in Insulin-induced Glucose Transport, Glycogen Synthesis, and Protein Synthesis. *Journal of Biological Chemistry*, **273** (9), 5315-5322.

URBAN, A., NEUKIRCHEN, S. and JAEGER, K-E (1997). A rapid and efficient method for site-directed mutagenesis using one-step overlap extension PCR. *Nucleic Acids Research*, **25** (11), 2227-2228.

VALLIQUETTE, R. A., O'CONNER, T. and VASSAR, R. (2005). Energy Inhibition Elevates β-Secretase Levels and Activity and Is Potentially Amyloidogenic in APP Transgenic Mice: Possible Early Events in Alzheimer's Disease Pathogenesis. *The Journal of Neuroscience*, **25** (47), 10874-10883.

VANDESOMPELE, J., et al. (2002). Accurate normalization of real-time quantitative RT-PCR data by geometric averaging of multiple internal control genes. *Genome Biology*, **3** (7), 1-12.

VASSAR, R., et al. (1999). β-Secretase Cleavage of Alzheimer's Amyloid Precursor Protein by the Transmembrane Aspartic Protease BACE. *Science*, **286** (5440), 735-741.

VASSAR, R., et al. (2009). The β-Secretase Enzyme BACE in Health and Alzheimer's Disease: Regulation, Cell Biology, Function, and Therapeutic Potential. *The Journal of Neuroscience*, **29** (41), 12787-12794.

VENUGOPAL, C., et al. (2008). Beta-secretase: Structure, Function, and Evolution. *CNS & Neurological Disorders - Drug Targets*, **7** (3), 278-294.

VETRIVEL, K. S. and THINAKARAN, G. (2010). Membrane rafts in ALzheimer's disease beta-amyloid production. *Biochimica et Biophysica Acta*, **1810**, 860-867.

WALKER, E. S., et al. (2005). Presenilin 2 familial Alzheimer's disease mutations result in partial loss of function and dramatic changes in Aβ 42/40 ratios. *Journal of Neurochemistry*, **92** (2), 294-301.

WANG, Y. and HA, Y. (2004). The X-ray structure of an antiparallel dimer of the human amyloid precursor protein E2 domain. *Molecular Cell*, **15** (3), 343-353.

WANG, Y. P., et al. (2004). Effect of amyloid peptides on serum withdrawal-induced differentiation and cell viability. *Cell Research*, **14** (6), 467-472.

WANG, J-Z, et al. (2012). Abnormal Hyperphosphorylation of Tau: Sites, Regulation, and Molecular Mechanism of Neurofibrillary Degeneration. *Journal of Alzheimer's Disease*, **33** (Supplement 1/2013), S123-S139.

WANG, J-Z, et al. (2013). Abnormal Hyperphosphorylation of Tau: Sites, Regulation, and Molecular Mechanism of Neurofibrillary Degeneration. *Journal of Alzheimer's Disease*, **33** (Supplement 1/2013), S123-S139.

WEBSTER, M-T, et al. (1998). The effect of perturbed energy metabolism on the processing of amyloid procursor protein in PC12 cells. *Journal of Neural Transmission*, **105** (8-9), 839-853.

WIESER, R. J. and OESCH, F. (1986). Contact inhibition of growth of human diploid fibroblasts by immobilized plasma membrane glycoproteins. *Journal of Cell Biology*, **103** (2), 361-367.

WIMO, A. and PRINCE, M. (2010). *World Alzheimer Report 2010: The Global Economic Impact of Dementia*. Annual report, Alzheimer's Disease International (ADI).

WURM, F. M. and HACKER, D. (2011). First CHO genome. *Nature Biotechnology*, **29** (8), 718-720.

WYSS-CORAY, T. and ROGERS, J. (2012). Inflammation in Alzheimer Disease—A Brief Review of the Basic Science and Clinical Literature. *Cold Spring Harb Perspect Medicine*, **2** (1), 1-23.

XIE, L., et al. (2013). Methylene blue induces macroautophagy through 5' adenosine monophosphate-activated protein kinase pathway to protect neurons from serum deprivation. *Frontiers in Cellular Neuroscience*, **7** (1), 1-9.

XU, W., FERRARI, C. and WANG, H-X (2013). Epidemiology of Alzheimer's disease. In: ZERR, Inga (ed.). *Understanding Alzheimer's Disease*. InTech, 329-358.

YAO, J., et al. (2011). 2-Deoxy-D-Glucose Treatment Induces Ketogenesis, Sustains Mitochondrial Function, and Reduces Pathology in Female Mouse Model of Alzheimer's Disease. *PLoS ONE*, **6** (7),.

YATES, D. and MCLOUGHLIN, D. M. (2007). The molecular pathology of Alzheimer's disease. *Psychiatry*, **7** (1), 1-5.

YEN, S-H, et al. (1995). Alzheimer Neurofibrillary Lesions: Molecular Nature and Potential Roles of Different Component. *Neurobiology of Aging*, **16** (3), 381-387.

YIANNOPOULOU, K. G. and PAPAGEORGIOU, S. G. (2013). Current and future treatments for Alzheimer's disease. *Therapeutic Advance in Neurological Disorders*, **6** (1), 19-33.

YOUNG-PEARSE, T. L., et al. (2008). Secreted APP regulates the function of full-length APP in neurite outgrowth through interaction with integrin beta1. *Neural Development*, **3** (15),.

YUAN, H-X, XIONG, Y. and GUAN, K-L (2013). Nutrient sensing, metabolism, and cell growth control. *Molecular Cell*, **49** (3), 379-387.

YU, S., et al. (2008). Neuroprotective Effects of Salidroside in the PC12 Cell Model Exposed to Hypoglycemia and Serum Limitation. *Cellular and molecular neurobiology*, **28** (8), 1067-1078.

ZHANG, H., et al. (2012). Proteolytic processing of Alzheimer's β-amyloid precursor protein. *Journal of Neurochemistry*, **120**, 9-21.

ZHENG, H. and KOO, E. H. (2011). Biology and pathophysiology of the amyloid precursor protein. *Molecular Neurodegeneration*, **6** (27), 1-16.

ZOTOVA, E., et al. (2010). Inflammation in Alzheimer's disease: relevance to pathogenesis and therapy. *Alzheimer's Research & Therapy*, **2** (1), 1-9.